

Investigation of mammalian cell metabolism by quantification of key metabolic enzyme activities

Dissertation

zur Erlangung des akademischen Grades

Doktoringenieur

(Dr.-Ing.)

von: Dipl.-Ing. Robert Janke

geb. am: 07.03.1983 in Dresden

genehmigt durch die Fakultät für Verfahrens- und Systemtechnik der Otto-von-Guericke-Universität Magdeburg

Promotionskommission: Prof. Dr.-Ing. Andreas Seidel-Morgenstern

Prof. Dr.-Ing. Udo Reichl

Prof. Dr.-Ing. Ralf Takors

Dr.-Ing. Aljoscha Wahl

eingereicht am: 20.06.2012

Promotionskolloquium am: 07.12.2012

Danksagung

Diese Arbeit wurde während meiner Tätigkeit als wissenschaftlicher Mitarbeiter in der Bioprozesstechnik-Gruppe des Max-Planck-Instituts für Dynamik komplexer technischer Systeme in Magdeburg angefertigt. Ich danke allen herzlichst, die zum Gelingen der Arbeit beigetragen haben, insbesondere:

Herrn Prof. Dr.-Ing. Udo Reichl für die Möglichkeit in seiner Arbeitsgruppe mitzuwirken und unter exzellenten Forschungsbedingungen zu promovieren. Die dabei mir zugestandenen Freiräume während meiner Studien sowie die stetige Diskussionsbereitschaft habe ich sehr geschätzt.

Herrn Prof. Dr.-Ing. Ralf Takors sowie Herrn Dr.-Ing. Aljoscha Wahl danke ich vielmals für die Begutachtung der vorliegenden Arbeit. Herrn Prof. Dr.-Ing. Andreas Seidel-Morgenstern danke ich für die Übernahme des Prüfungsvorsitzes.

Frau Dr. rer. nat. habil. Yvonne Genzel danke ich sehr für ihre Betreuung und Unterstützung meiner Arbeiten sowie die anregenden Diskussionen und Ratschläge bei der Gestaltung und beim Verfassen der wissenschaftlichen Beiträge.

Herrn Prof. Dr. Mark Stitt, Herrn Dr. Yves Gibon und Herrn Dr. John Lunn der Abteilung Metabolische Netzwerke (Systemregulation) des Max-Planck-Instituts für molekulare Pflanzenphysiologie in Potsdam/Golm danke ich sehr für die aktive Unterstützung beim Wissens- und Methodentransfer im Rahmen der Plattform für Enzymaktivitätsmessungen.

Allen technischen AssistentInnen, insbesondere Ilona Behrendt, Claudia Best, Susanne König und Nancy Wynserski sei herzlich gedankt für die stets gute Zusammenarbeit und ihre Hilfe bei der Durchführung der Analysen und Kultivierungen im Labor.

Besonders danke ich Christine Rühmkorf, Peter Schäfer, Janine Seidemann, Nadine Händel und Maria Wetzel für ihr Engagement im Rahmen ihrer Abschlussarbeiten und den damit verbundenen Beiträgen zu dieser Arbeit.

Allen Kollegen in der Bioprozesstechnik-Gruppe, insbesondere Björn Heynisch, Marc Rüger, Jana Rödiger und Susann Freund danke ich vielmals für die freundliche Arbeitsatmosphäre und die zahlreichen Anregungen.

Dem BMBF danke ich für die finanzielle Unterstützung im Rahmen des FORSYS-Projekts „Systemanalyse von Signal- und Regulationsnetzwerken“ (FKZ: 0313922).

Der größte Dank gilt meiner lieben Familie.

Meinen Eltern

Kurzfassung

Bei der Kultivierung von Säugerzellen in glutaminhaltigen Medien werden große Mengen an Laktat und Ammonium in den Kulturüberstand ausgeschieden. Diese toxischen Nebenprodukte können sich nicht nur negativ auf die Zellvitalität und die Produktivität auswirken, sondern auch das Wachstum zu hohen Zelldichten verhindern. Verschiedene Produktionszelllinien, die für die Herstellung von biopharmazeutischen Produkten eingesetzt werden, können zum Beispiel auch mit Pyruvat (Pyr) anstelle von Glutamin (Gln) im Kulturmedium wachsen. Als Folge verbrauchen diese Zellen nicht nur weniger Glucose (Gluc), sie produzieren auch signifikant weniger Laktat und kein Ammonium.

Eine Möglichkeit, den Zellstoffwechsel und die zugrunde liegenden zellulären regulatorischen Mechanismen näher zu untersuchen, stellen Enzymaktivitätsstudien dar. Obwohl die Analyse von Enzymen relativ komplex ist und Hochdurchsatztechnologien für Enzymaktivitäten nicht überall zur Verfügung stehen, kann deren Messung wertvolle Informationen über Flussraten im Stoffwechselweg liefern, die für das Verständnis von metabolischen Netzwerken von großer Bedeutung sind. Darüber hinaus können Datensätze zu Enzymaktivitäten zusammen mit Proteom- und Metabolomdaten im Sinne eines systembiologischen Ansatzes in mathematische Modelle zum Zellmetabolismus integriert werden. Solche Modelle können Informationen über Stoffwechselwege liefern, die wichtig für die Optimierung von Zelllinien und Kulturmedien sind.

Die Zielsetzung der vorliegenden Studie bestand im Wesentlichen in der Charakterisierung der Wirkung von verschiedenen Kultivierungsbedingungen auf die Aktivitäten von Schlüsselenzymen des Zentralstoffwechsels der Madin-Darby canine kidney (MDCK)-Produktionszelllinie. Auf Basis einer Hochdurchsatzplattform für Enzymaktivitätsmessungen in Pflanzenzellextrakten sollte zunächst eine effiziente Analyseplattform zur Bestimmung von Enzymaktivitäten in Säugerzellen entwickelt werden. Eine geeignete Gruppierung von verschiedenen Enzymen sollte es ermöglichen, deren Aktivitäten mit einer gemeinsamen Messmethode nachzuweisen.

Der erste Abschnitt dieser Arbeit befasste sich mit der Etablierung von sensitiven und auf Mikroplattenbasierenden Assays zur Messung von 28 Enzymen des zentralen Kohlenstoff- und Gln-Metabolismus in Säugerzellen. Die neue Hochdurchsatzplattform zur Bestimmung von Enzymaktivitäten bestand aus vier verschiedenen Cycling-Assays. Der Vorteil bei der Verwendung von enzymatischen Cycling-Assays und 96-Well Mikrotiterplatten lag in der

hohen Sensitivität bei der Produktbestimmung (0,025 bis 0,4 nmol) und im Probanddurchsatz. Aufgrund des Fehlens von Zellwänden in Säugerzellen war die Generierung von Proben im Vergleich zur Plattform für Pflanzenzellen einfacher. Zudem können kontinuierliche Zelllinien leicht unter kontrollierten Bedingungen wachsen. Auch waren entsprechende Versuche weit weniger zeitaufwendig als Experimente mit Pflanzen. Zellextrakte konnten stark verdünnt werden, so dass eventuelle Interferenzen durch andere Komponenten im Extrakt verringert sowie Über- und Unterschätzungen der tatsächlichen Enzymaktivität vermieden wurden. Da Substratkonzentrationen im Assay durchgehend auf einem annähernd konstanten Niveau gehalten werden konnten, wurden ferner mögliche Enzyminhibierungen durch zu hohe Produktkonzentrationen unterbunden. Um eine Inhibierung des zu untersuchenden Enzyms durch zu hohe Substratlevel zu vermeiden, wurde die maximal mögliche Substratkonzentration verwendet, bei der keine Inhibierung beobachtet wurde. Alle Enzymassays wurden mit MDCK-Zellextrakt optimiert und validiert.

Im Zuge der Entwicklung der Assay-Plattform für Säugerzellen wurde im zweiten Schritt der Arbeit ein wichtiges Kopplungsenzym für die Anwendung in sensitiven Glycerol-3-Phosphat (G3P)-Assays produziert, welches auch für zukünftige Studien zum Zellstoffwechsel Verwendung finden kann. Dazu wurde eine Glycerokinase (GK) aus *Pichia farinosa* mit einem 5-L Bioreaktor rekombinant in *Pichia pastoris* hergestellt. Das Enzym wurde anschließend mit einer Kombination aus Nickel-Affinitäts- und Anionenaustauschchromatographie aufgereinigt. Die spezifische Aktivität des finalen Produkts lag bei etwa 200 Units pro mg an Protein. Das pH- und Temperaturoptimum lag bei 7,0 beziehungsweise 45 °C. Der effektivste Phosphatdonor für die Umwandlung von Glycerol in G3P war ATP, wobei auch ITP, UTP, GTP oder CTP genutzt werden konnte. Das Enzym zeigte mit UTP, GTP und CTP das Phänomen der negativen Kooperativität und konnte erfolgreich für die Messung der Pyruvatkinase-Aktivität in MDCK Zellen verwendet werden.

Im dritten Teil der Studie wurde die entwickelte Assay-Plattform für die Untersuchung der Wirkung von Medienwechsel auf Enzymaktivitäten des Gluc- und Gln-Metabolismus von adhären MDCK-Zellen genutzt. Dabei wurden die Zellen in Sechs-Well-Platten mit Gln- oder Pyr-haltigem GMEM-Medium bis zur exponentiellen und stationären Wachstumsphase kultiviert und die Aktivitäten von 28 metabolischen Enzymen in Zellextrakten untersucht. Vorangegangene Studien zu Stoffflussanalysen in MDCK-Zellen vermuteten unter anderem, dass dem Medium zugesetztes extrazelluläres Pyruvat direkt in den Citratsäurezyklus eingeht. Während des exponentiellen Wachstums in Pyr-haltigem Medium waren die Enzym-

aktivitäten des Pentosephosphatweges insgesamt höher, was auf einen erhöhten Fluss von Glucose-6-Phosphat in den oxidativen Teil dieses Stoffwechselweges hindeutete. Darüber hinaus zeigten die anaplerotischen Enzyme Pyruvatcarboxylase und Pyruvatdehydrogenase höhere zellspezifische Aktivitäten mit dem Pyr-haltigen Medium. Gesteigerte Aktivitäten wurden ebenfalls bei der NAD^+ -abhängigen Isocitratdehydrogenase, Glutamatdehydrogenase und Glutaminsynthetase in MDCK-Zellen mit Pyr als Kohlenstoff- und Energiequelle gefunden. Es liegt die Vermutung nahe, dass der Anstieg in den Enzymaktivitäten höchstwahrscheinlich für die Kompensierung des Energiebedarfs der Zelle und zur Auffüllung des Gln-Pools benötigt wurde. Zudem waren die Aktivitäten der glutaminolytischen Enzyme Aspartat- und Alanintransaminase, Phosphoenolpyruvat-Carboxykinase und des NADP^+ -abhängigen Malatenzyms (ME) geringer, was auf einen verminderten Gln-Stoffwechsel in mit dem Pyr-haltigen Medium kultivierten Zellen vermuten ließ.

Der letzte Teil dieser Arbeit befasste sich mit der Virus-Wirtszell-Interaktion und der Zellantwort während der frühen Virusinfektion von adhärennten MDCK-Zellen. Frühere Studien zu Infektionsexperimenten mit Influenzaviren zeigten deutliche Änderungen im Proteom sowie im Verlauf von intra- und extrazellulären Metaboliten während der späten Infektionsphase in MDCK-Zellen. Konfluente Zellen wurden in der vorliegenden Studie mit einem Influenza-A-Virus (H1N1) bei einer hohen Infektionsmultiplizität infiziert und hinsichtlich Aktivitätsänderungen von Enzymen des Zentralstoffwechsels untersucht. Virusinfizierte Zellen zeigten eine Hochregulierung einzelner Schlüsselenzyme, die für die Produktion des Reduktionsäquivalents NADPH (Glucose-6-Phosphat-Dehydrogenase, 6-Phosphogluconat-Dehydrogenase und ME) und Acetyl-CoA (Citratlyase und Acetat-CoA-Ligase), ein wichtiger Vorläufermetabolit für die Lipid- und Cholesterolsynthese, verantwortlich sind. Da sich Viren unter Mitnahme von Zellmembranbestandteilen (Lipidhülle) von der Wirtszelloberfläche ablösen, scheint die Synthese von Fettsäuren und Cholesterin eine wichtige Rolle bei der Replikation von Influenzaviren in MDCK-Zellen zu spielen.

Zusammenfassend konnte eine Hochdurchsatzplattform für die Bestimmung von Enzymaktivitäten in Säugerzellen etabliert werden, mit der metabolische Zustände von Produktionszellen näher charakterisiert werden können. Dies kann anschließend dazu verwendet werden, um zelluläre Prozesse besser zu verstehen und Zelllinien und Kulturmedien zu optimieren. Darüber hinaus können die Datensätze zu Enzymaktivitäten zusammen mit Daten zu intra- und extrazellulären Metabolitkonzentrationen für die Erstellung und Validierung von mathematischen Modellen zum Zellstoffwechsel von Nutzen sein.

Abstract

During growth of mammalian cells in glutamine-containing media, large amounts of lactate and ammonia are secreted into the culture supernatant. These toxic by-products not only affect cell viability and productivity but often also prevent growth to high cell densities. However, different production cell lines typically used for manufacturing of biopharmaceuticals and viral vaccines can also grow on pyruvate (Pyr) instead of glutamine (Gln) in the culture medium. As a consequence, these cells not only release no ammonia but glucose (Gluc) consumption and lactate production are also reduced significantly.

One possibility to better understand cell metabolism and the cellular regulatory mechanisms that govern cell growth is to perform enzyme activity studies. Although the analysis of enzymes is more complex and high-throughput technologies for enzyme activities are not commonly available, enzyme activities provide information on pathway flux rates, which is important for the understanding of metabolic networks. Furthermore, the integration of enzyme activity data into mathematical models of cell metabolism together with proteome and metabolome data by systems biology approaches will significantly contribute towards a better understanding of metabolic pathways relevant for cell line and media optimization.

The objective of this thesis was to characterize the effect of different culture conditions on key enzyme activities of central metabolic pathways in the Madin-Darby canine kidney (MDCK) production cell line. On the basis of a high-throughput platform for measuring enzyme activities in plant cell extracts, the work first involved the development of a platform to determine enzyme activities in mammalian cells including grouping of various enzymes that share a common detection method.

The first part of this work addressed the establishment of sensitive microplate-based assays to measure the activities of 28 enzymes involved in central carbon and Gln metabolism of mammalian cells. The new high-throughput platform for enzyme activity measurements consisted of four different cycling assays. The use of enzymatic cycling methods combined with the application of 96-well microplates allowed a more sensitive (0.025 to 0.4 nmol product) and faster determination of enzyme activities than most of the existing assays. Compared to the platform for plant cells, sample preparation steps were less laborious for mammalian cell lines as disruption of cell walls was not required. Furthermore, continuous cell lines can be easily grown under controlled conditions and studies were not as time-consuming as experiments using plant cells. Cell extracts could be highly diluted, which

reduced possible interferences caused by other components of the extract and additionally minimized under- or overestimation of the actual enzyme activity. Furthermore, possible enzyme inhibition by high concentration of a product was prevented since substrate concentrations could be maintained at a near constant level throughout the assay. Enzyme inhibition by high substrate levels was avoided by using the maximum possible substrate concentration at which no inhibition was observed. All enzyme assays were validated and optimized with extracts from adherent MDCK cells.

Within the development of the assay platform for mammalian cells, the second step of this work was comprised of the production of an important coupling enzyme to exploit all the benefits of the glycerol 3-phosphate (G3P) cycle. Therefore, a glycerokinase (GK) from *Pichia farinosa* was produced recombinantly in *Pichia pastoris* using a 5-L stirred-tank bioreactor. The enzyme was purified by a combination of nickel affinity chromatography and anion exchange chromatography. The specific activity of the final preparation was approximately 200 units per mg protein. The pH and temperature optimum was determined as 7.0 and 45 °C, respectively. Although the most effective phosphoryl group donor tested was ATP, GK from *P. farinosa* could also utilize ITP, UTP, GTP, or CTP to produce G3P. The kinetic properties of the enzyme with respect to UTP, GTP, and CTP suggested that GK exhibited negative cooperativity as double reciprocal plots showed a biphasic response to increasing nucleoside triphosphate concentrations. Finally, the homogeneous enzyme preparation was successfully applied to measure the specific activity of pyruvate kinase (PK) in MDCK cell extracts by coupling the PK-induced ATP production to the formation of G3P.

In the third stage of this thesis, the developed assay platform was used to investigate the impact of media changes on Gluc and Gln metabolism of adherent MDCK cells. Therefore, the cells were grown to stationary and exponential phases in six-well plates in GMEM supplemented with Gln or Pyr, and 28 key metabolic enzyme activities of cell extracts were analyzed. Previous studies on MDCK cell metabolism focused, for example, on the measurement of intracellular metabolites or on metabolic flux models. Evaluation of flux distributions suggested that the additional extracellular Pyr enters the TCA cycle directly, whereas most of the consumed Gluc is excreted as lactate in MDCK cells. During exponential cell growth in Pyr-containing medium, the overall activity of the pentose phosphate pathway was up-regulated, which suggested that more glucose 6-phosphate was channeled into the oxidative branch. Furthermore, the anaplerotic enzymes pyruvate carboxylase and pyruvate dehydrogenase showed higher cell-specific activities with Pyr.

Increased specific activities were also found for NAD⁺-dependent isocitrate dehydrogenase, glutamate dehydrogenase and glutamine synthetase in MDCK cells grown with Pyr. It could be assumed that the increase in enzyme activities was most likely required to compensate for the energy demand and to replenish the Gln pool. Moreover, the activities of the glutamolytic enzymes aspartate transaminase, alanine transaminase, malic enzyme (ME) and phosphoenolpyruvate carboxykinase were decreased in MDCK cells grown with Pyr, which seemed to be related to a decreased Gln metabolism.

The last part of this work dealt with the investigation of virus-host cell interactions and the cell response during early virus infection in adherent MDCK cells. Previous infection experiments with influenza viruses clearly showed proteome alterations as well as changes in intra- and extracellular metabolites during late virus infection in MDCK cells. In this study, confluent cells were infected with an influenza A (H1N1) virus at a high multiplicity of infection, and key metabolic enzyme activities of cell extracts were analyzed. Virally infected cells showed an up-regulation of some key enzymes producing the reducing equivalent NADPH (glucose-6-phosphate dehydrogenase, 6-phosphogluconate dehydrogenase, and ME) and acetyl-CoA (citrate lyase and acetate-CoA ligase), a precursor needed for lipid and cholesterol biosynthesis. It seemed that the synthesis of fatty acids and cholesterol plays a crucial role for the replication of influenza viruses in adherent MDCK cells as they acquire lipid envelopes from their host cells (specific regions of the apical membrane) during budding.

Taken together, a high-throughput platform for the measurement of enzyme activities in mammalian cells was established where metabolic states of production cell lines can now be further characterized. This can then be used to improve the understanding of metabolic pathways relevant for cell line and media optimization. Furthermore, valuable datasets on enzyme activities together with data on intra- and extracellular metabolite concentrations will support the validation of mathematical models of cellular metabolism in systems biology approaches.

Table of Contents

1	<i>Introduction</i>	1
2	<i>Background and Theory</i>	6
2.1	Metabolism in mammalian cell culture	6
2.1.1	Glucose metabolism: glycolysis and pentose phosphate pathway.....	7
2.1.2	Glutamine metabolism: glutaminolysis	11
2.1.3	Metabolic waste products of <i>in vitro</i> cultured cell lines.....	13
2.1.3.1	Ammonium and lactate.....	13
2.1.3.2	Measures to reduce toxic by-product formation during cultivation	15
2.1.4	Cell metabolism under stress conditions: viral infection.....	16
2.1.5	Analytical tools to measure cell metabolism	19
2.2	Measuring enzyme activities in mammalian cells.....	23
2.2.1	The Michaelis-Menten equation	24
2.2.2	Graphical determination of K_m and V_{max}	26
2.2.3	Key enzymes and metabolic fluxes	28
2.2.4	Determination of maximum enzyme activities.....	31
2.2.4.1	Overview on available assay procedures	31
2.2.4.2	Continuous and discontinuous assay systems.....	32
2.2.4.3	Increasing the sensitivity by enzymatic cycling	33
2.2.4.4	Coupling enzymes	36
2.3	The <i>Pichia pastoris</i> expression system	37
3	<i>Materials and Methods</i>	39
3.1	Cell line and culture media.....	39
3.2	Cell culture	39
3.3	Virus culture	40
3.4	Analytical techniques	40
3.4.1	Cell concentration and cell viability	40
3.4.2	Extracellular metabolites	41
3.4.3	Virus titer	41
3.4.4	Protein concentration	42
3.5	Specific growth rate, doubling time and yield coefficient	42
3.6	Intracellular enzyme activity measurements	43
3.6.1	Preparation of cell-free crude extract.....	43
3.6.2	Pipetting scheme for enzyme assays.....	44
3.6.2.1	Indirect assays with enzymatic cycling	44
3.6.2.2	Direct assays.....	45
3.6.3	Enzyme activity assays	46

3.6.3.1	Citrate synthase (CS: EC 2.3.3.1).....	46
3.6.3.2	Citrate lyase (CL: EC 2.3.3.8).....	47
3.6.3.3	NAD ⁺ -dependent isocitrate dehydrogenase (NAD-ICDH: EC 1.1.1.41).....	47
3.6.3.4	Fumarase (FUM: EC 4.2.1.2).....	47
3.6.3.5	Glutamate dehydrogenase (GLDH: EC 1.4.1.2).....	48
3.6.3.6	Alanine transaminase (AlaTA: EC 2.6.1.2).....	48
3.6.3.7	Aspartate transaminase (AspTA: EC 2.6.1.1).....	48
3.6.3.8	Phosphoenolpyruvate carboxykinase (PEPCK: EC 4.1.1.32).....	49
3.6.3.9	Acetate-CoA ligase (ACoAL: EC 6.2.1.1).....	49
3.6.3.10	Hexokinase (HK: EC 2.7.1.1).....	50
3.6.3.11	Glucose-6-phosphate dehydrogenase (G6PDH: EC 1.1.1.49).....	50
3.6.3.12	6-Phosphogluconate dehydrogenase (6PGDH: EC 1.1.1.44).....	50
3.6.3.13	NADP ⁺ -dependent isocitrate dehydrogenase (NADP-ICDH: EC 1.1.1.42).....	51
3.6.3.14	Malic enzyme (ME: EC 1.1.1.40).....	51
3.6.3.15	Phosphofructokinase (PFK: EC 2.7.1.11).....	51
3.6.3.16	Fructose-1,6-bisphosphate aldolase (FBPA: EC 4.1.2.13).....	52
3.6.3.17	Glyceraldehyde-3-phosphate dehydrogenase (GAPDH: EC 1.2.1.12).....	52
3.6.3.18	Pyruvate kinase (PK: EC 2.7.1.40).....	52
3.6.3.19	Transketolase (TK: EC 2.2.1.1).....	53
3.6.3.20	Transaldolase (TA: EC 2.2.1.2).....	53
3.6.3.21	Glycerokinase (GK: EC 2.7.1.30).....	54
3.6.3.22	Glutaminase (GLNase: EC 3.5.1.2).....	54
3.6.3.23	Glutamine synthetase (GS: EC 6.3.1.2).....	54
3.6.3.24	Lactate dehydrogenase (LDH: EC 1.1.1.27).....	55
3.6.3.25	Malate dehydrogenase (MDH: EC 1.1.1.37).....	55
3.6.3.26	Phosphoglucose isomerase (PGI: EC 5.3.1.9).....	55
3.6.3.27	Triose-phosphate isomerase (TPI: EC 5.3.1.1).....	56
3.6.3.28	Pyruvate dehydrogenase (PDH: EC 1.2.4.1).....	56
3.6.3.29	Pyruvate carboxylase (PC: EC 6.4.1.1).....	56
3.6.4	Cycling assay reagents.....	57
3.6.4.1	NAD ⁺ cycling assay.....	57
3.6.4.2	NADP ⁺ cycling assay.....	57
3.6.4.3	G3P cycling assay.....	58
3.6.4.4	Glu cycling assay.....	58
3.6.5	Expression of results.....	59
3.7	Cloning, expression, purification, and characterization of <i>Pichia farinosa</i> glycerokinase.....	59
3.7.1	Strains, plasmids, enzymes and reagents.....	59
3.7.2	Construction of the expression vector.....	60
3.7.3	Transformation of <i>Pichia pastoris</i>	61
3.7.4	Production of <i>Pichia farinosa</i> glycerokinase by <i>Pichia pastoris</i>	62
3.7.5	Purification of His ₆ -tagged recombinant glycerokinase.....	63
3.7.6	Protein analysis.....	64
3.7.7	Determination of glycerol and methanol.....	64

3.7.8	Enzymatic characterization of recombinant His ₆ -tagged GK.....	65
4	Results.....	66
4.1	Development of an enzymatic assay platform for mammalian cells	66
4.1.1	Optimization of extraction and reaction conditions for enzymes from mammalian cells.....	67
4.1.2	Establishment of a new glutaminase assay	72
4.1.2.1	Optimization of cycling reagent concentrations	73
4.1.2.2	Calibration curve with standard liquid samples.....	74
4.1.2.3	Confirmation with cell extract.....	75
4.1.3	Validation of the remaining enzyme assays	77
4.1.4	Application of the established enzyme platform on MDCK cells.....	85
4.2	Production of <i>Pichia farinosa</i> glycerokinase for the application in sensitive cycling assays.....	89
4.2.1	Construction of expression vector for His ₆ -tagged glycerokinase.....	90
4.2.2	Glycerokinase production by exponential feeding of methanol	91
4.2.3	Purification of recombinant glycerokinase	92
4.2.4	Biochemical characterization of glycerokinase	95
4.2.5	Use of the recombinant glycerokinase as a coupling enzyme	97
4.3	Central metabolic enzymes in MDCK cells under different cultivation conditions	98
4.3.1	Cell growth in six-well plates in glutamine and pyruvate-containing medium..	98
4.3.1.1	Cell densities	99
4.3.1.2	Extracellular metabolites	100
4.3.1.3	Cellular protein concentration	103
4.3.2	Maximum enzyme activities in glutamine- and pyruvate-containing medium	104
4.3.2.1	Glycolysis	107
4.3.2.2	Pentose phosphate pathway	108
4.3.2.3	Tricarboxylic acid cycle	109
4.3.2.4	Glutaminolysis.....	111
4.4	Influence of influenza virus infection on key metabolic enzyme activities in MDCK cells.....	113
4.4.1	Cell numbers and virus replication	113
4.4.2	Maximum enzyme activities in influenza infected cells.....	114
5	Discussion.....	119
5.1	Development of an enzymatic assay platform for mammalian cells	119
5.1.1	Development of 28 enzyme assays.....	121
5.1.2	Advantages and disadvantages of enzymatic cycling assays.....	123
5.1.3	Enzyme activities in confluent MDCK cells	124

5.2 Production of <i>Pichia farinosa</i> glycerokinase: “missing enzyme” for PK analysis in G3P cycling assay	127
5.2.1 Biochemical characterization of glycerokinase	129
5.2.2 Use of the recombinant glycerokinase as a coupling enzyme	130
5.3 Effect of different cultivation conditions on central metabolic enzymes in MDCK cells.....	131
5.3.1 Glucose metabolism.....	132
5.3.2 Glutamine metabolism.....	135
5.4 Influence of influenza virus infection on key metabolic enzyme activities in MDCK cells.....	138
6 Conclusions	143
7 Outlook	147
List of Figures and Tables	149
References.....	152
Appendix	169

List of Abbreviations and Symbols

Abbreviations

2-OG	2-oxoglutarate
1,3BPG	1,3-bisphosphoglycerate
3PG	3-phospho-D-glycerate
6PG	6-phospho-D-gluconate
6PGDH	6PG dehydrogenase
6PGL	6-phospho-D-glucono-1,5-lactone
A549	human lung adenocarcinoma cell line
AcCoA	acetyl-CoA
ACoAL	acetate-CoA ligase
ADH	alcohol dehydrogenase
AGPase	ADP-glucose pyrophosphorylase
AGS	human gastric adenocarcinoma cell line
Ala	L-alanine
AlaTA	Ala transaminase
Amm	ammonium
<i>AOX1</i>	alcohol oxidase 1 gene
<i>AOX2</i>	alcohol oxidase 2 gene
Asp	L-aspartate
AspTA	Asp transaminase
ATG	sequence of adenine-thymine-guanine bases (start codon)
ATPase	adenosine triphosphatase
AU	arbitrary unit
BHK	baby hamster kidney
BMG	buffered minimal glycerol
BMM	buffered minimal methanol
BSM	basal salts medium
BV	bed volume
CHO	Chinese hamster ovary
CK	creatine kinase
CL	citrate lyase
CS	citrate synthase
CV	coefficient of variation
cycl	cycling
DAP	dihydroxyacetone phosphate
DCW	dry cell weight
DTNB	5,5'-dithiobis(2-nitrobenzoic acid)
DTT	dithiothreitol
E4P	D-erythrose 4-phosphate
EB	extraction buffer
E	enzyme
ES	enzyme-substrate
ESI	electrospray ionization
F6P	D-fructose 6-phosphate
FBP	D-fructose 1,6-bisphosphate
FBPA	FBP aldolase
FCS	fetal calf serum
FeCS	ferric chloride solution
<i>FLDI</i>	formaldehyde dehydrogenase gene
FUM	fumarase
G3P	sn-glycerol 3-phosphate

G3PDH	G3P dehydrogenase
G3POX	G3P oxidase
G1P	D-glucose 1-phosphate
G6P	D-glucose 6-phosphate
G6PDH	G6P dehydrogenase
GAP	D-glyceraldehyde 3-phosphate
<i>GAP</i>	glyceraldehyde-3-phosphate dehydrogenase gene
GAPDH	GAP dehydrogenase
GExp	exponential growth phase of GMEM-Gln
γ GH	L- γ -glutamyl hydroxamate
GK	glycerokinase
GLDH	glutamate dehydrogenase
Gln	L-glutamine
GLNase	glutaminase
Glu	L-glutamate
Gluc	glucose
GMEM-Gln	Glasgow minimum essential Medium containing 2 mM glutamine
GMEM-Pyr	GMEM without glutamine but with additional 10 mM pyruvate
GRAS	generally recognized as safe
GS	glutamine synthetase
GStat	stationary growth phase of GMEM-Gln
<i>GUT1</i>	GK gene
HA	hemagglutinin
HCMV	human cytomegalovirus
<i>HIS4</i>	histidinol dehydrogenase gene
HK	hexokinase
hpi	hours post infection
Lac	lactate
LDH	lactate dehydrogenase
LOD	limit of detection
LOQ	limit of quantitation
M1	matrix protein
M2	ion channel protein
MALDI	matrix assisted laser desorption/ionization
MCS	multiple cloning site
MD	minimal dextrose
MDCK	Madin-Darby canine kidney
MDH	malate dehydrogenase
ME	malic enzyme
α -MF	<i>Saccharomyces cerevisiae</i> mating factor alpha
MFA	metabolic flux analysis
MM	minimal methanol
MOI	multiplicity of infection
MPI	Max Planck Institute
MS	mass spectrometry
MTT	thiazolyl blue tetrazolium bromide
Mut ⁺	methanol utilization fast
Mut ^S	methanol utilization slow
n/a	not applicable
NA	neuraminidase
NAD-ICDH	NAD ⁺ -dependent isocitrate dehydrogenase
NADP-ICDH	NADP ⁺ -dependent ICDH
NMR	nuclear magnetic resonance
NTP	nucleoside triphosphate
NP	nucleoprotein

NS1	non-structural protein 1
NS2	non-structural protein 2
OAA	oxaloacetate
OMP	orotidine 5'-phosphate
ox	oxidized
PBS	phosphate-buffered saline
PDH	pyruvate dehydrogenase
PC	pyruvate carboxylase
PCR	polymerase chain reaction
PEP	phosphoenolpyruvate
PEPCK	PEP carboxykinase
PES	phenazine ethosulfate
PExp	exponential growth phase of GMEM-Pyr
PFK	phosphofructokinase
PGI	phosphoglucose isomerase
PGK	phosphoglycerate kinase
PK	pyruvate kinase
PMSF	phenylmethylsulfonyl fluoride
PP	pentose phosphate
PStat	stationary growth phase of GMEM-Pyr
PTM ₁	<i>Pichia pastoris</i> trace metals 1
Pyr	pyruvate
R5P	ribose 5-phosphate
red	reduced
rgt	reagent
RNP	ribonucleoprotein
RKI	Robert Koch Institute
RPMI	Roswell Park Memorial Institute
RT	room temperature
Ru5P	D-ribulose 5-phosphate
S7P	D-sedoheptulose 7-phosphate
SD	standard deviation
SOP	standard operating procedure
TA	transaldolase
TCA	tricarboxylic acid
TCID ₅₀	50 % tissue culture infectious dose
TNB	5-thio-2-nitrobenzoic acid
TK	transketolase
TPI	triose-phosphate isomerase
UDPGal	UDP-galactose
UDPGlc	UDP-glucose
UDP-Gal PPase	galactose-1-phosphate uridylyltransferase
UDP-Glc PPase	glucose-1-phosphate uridylyltransferase
VMM	virus maintenance medium
X5P	D-xylulose 5-phosphate

Symbols

ρ_S	density of the feed solution	(g L ⁻¹)
μ	cell-specific growth rate	(h ⁻¹)
μ_{\max}	maximum cell-specific growth rate	(h ⁻¹)
μ_{set}	desired specific growth rate	(h ⁻¹)
$\epsilon_{340 \text{ nm}}$	extinction coefficient at a wavelength of 340 nm	(mM ⁻¹ cm ⁻¹)
$\epsilon_{570 \text{ nm}}$	extinction coefficient at a wavelength of 570 nm	(mM ⁻¹ cm ⁻¹)
E	enzyme	(mM)
E_0	total amount of enzyme	(mM)
ES	enzyme-substrate complex	(mM)
F(t)	feeding rate	(L h ⁻¹)
ΔG	Gibbs free energy change	(J mol ⁻¹)
ΔG^0	standard state free energy change	(J mol ⁻¹)
ΔG^\ddagger	activation energy	(J mol ⁻¹)
G_S	average free energy for the reactant S	(J mol ⁻¹)
G_P	average free energy for the product P	(J mol ⁻¹)
k_{cat}	turnover number	(min ⁻¹)
K_{eq}	equilibrium constant	-
k_1	association rate constant of ES binding	(mM ⁻¹ min ⁻¹)
k_{-1}	rate constant of the ES complex releasing E and S	(min ⁻¹)
k_2	rate constant of the ES complex releasing E and P	(min ⁻¹)
K_m	Michaelis constant, substrate concentration where $v = V_{\max}/2$	(mM)
$M_S(t)$	mass feeding rate	(g h ⁻¹)
m_S	specific maintenance coefficient	(g g ⁻¹ h ⁻¹)
P	product	(mM)
P_0	product concentration at the beginning of cultivation	(mM)
P_{end}	product concentration at the end of cultivation	(mM)
S	substrate	(mM)
S_0	substrate concentration at the beginning of cultivation	(mM)
S_{end}	substrate concentration at the end of cultivation	(mM)
S_F	substrate concentration in the feeding solution	(g L ⁻¹)
t_0	time point $t=0$	(h)
t_1	time point t_1	(h)
t_2	time point t_2	(h)
t_d	doubling time	(h)
$t-t_0$	time span since starting of the feed	(h)
U	unit	($\mu\text{mol min}^{-1}$)
v	catalytic activity	(U)
V_0	culture volume at the start of feeding	(L)
V_{\max}	maximum reaction rate	(nmol min ⁻¹ (10 ⁶ cells) ⁻¹) or (U (mg protein) ⁻¹)
X	cell concentration	(cells well ⁻¹)
X_0	biomass concentration at the start of feeding	(g L ⁻¹)
X_1	cell concentration at time point t_1	(cells well ⁻¹)
X_2	cell concentration at time point t_2	(cells well ⁻¹)
$Y_{P/S}$	yield coefficient of any product/substrate pair	(mM mM ⁻¹)
$Y_{X/S}$	yield coefficient of biomass/substrate	(g g ⁻¹)

1 Introduction

Over the past 20 years, biotechnology emerged as one of the most important technologies leading to a rise in developing new production processes for a wide variety of biopharmaceuticals such as monoclonal antibodies (Chotteau et al., 2007; Kunert et al., 2000; Rüker et al., 1991), recombinant proteins (Baker et al., 2001; Gaillet et al., 2007; Negro et al., 1994), and viral vaccines (Aunins, 2000; Buckland, 2005; Doroshenko and Halperin, 2009; Genzel et al., 2010; Lohr et al., 2009; Shen et al., 2012). These biologicals are mainly produced using human and animal cell lines such as the Chinese hamster ovary (CHO) cell line for antibody manufacturing. Appropriate folding and post-translational modifications (i.e., glycosylation) of the product are generally not properly performed using other microbial systems (e.g., yeasts and bacteria). However, most cell lines display an inefficient metabolic phenotype characterized by up-regulation of glycolytic and glutaminolytic fluxes during the cultivation in glutamine (Gln)-containing media, which results in the release of incompletely oxidized intermediates such as lactate (Lac) and ammonia into the culture broth. These toxic by-products often not only affect cell viability and productivity but also can prevent growth to high cell densities (Genzel et al., 2005; Glacken, 1988; Hassell et al., 1991; Ozturk et al., 1992). For example, ammonia in culture medium, which is mainly resulting from Gln degradation, was shown to decrease the growth rate of Madin-Darby canine kidney (MDCK) cells at levels exceeding 7 mM by about 50 % (Glacken et al., 1986), and the accumulation of more than 2 mM ammonia resulted in growth inhibition of baby hamster kidney (BHK) cells (Butler and Spier, 1984). Lac as the second major waste product arises from anaerobic glycolysis, and Lac levels higher than 20 mM were shown to inhibit growth as well as recombinant protein and antibody production of BHK and hybridoma cells, respectively (Cruz et al., 2000; Glacken, 1988; Ozturk et al., 1992).

Different measures can be taken to better understand the metabolic interactions relevant for cell growth and product formation, and to increase cell densities and process yields. These include not only optimization of cultivation conditions such as advanced feeding strategies, but also design of media or modification of specific properties of cells by molecular biology approaches. For example, by introducing a cytosolic yeast pyruvate carboxylase (PC) gene into the BHK-21A and HEK-293 cell line, glucose (Gluc) uptake, Gln consumption, Lac production and ammonia formation could be markedly reduced (Henry and Durocher, 2011; Irani et al., 1999). Another approach was presented by Genzel et al. (2005) who found that the replacement of Gln by pyruvate (Pyr) supported growth of different production cells

(MDCK, BHK, CHO) without reduction in specific growth rate in serum-containing and serum-free media. For MDCK cells, the addition of Gln or Pyr to cell culture media resulted in distinct differences in extra- and intracellular metabolite concentrations as well as in metabolic fluxes in glycolysis and tricarboxylic acid (TCA) cycle (Genzel et al., 2005; Sidorenko et al., 2008; Wahl et al., 2008). In Pyr-containing (Gln-free) medium, MDCK cells grew to comparable cell densities without the need of a long adaptation process. Furthermore, Gluc uptake and Lac release were significantly reduced, and the cells produced no ammonia during growth. Evaluation of flux distributions suggested that the additional extracellular Pyr enters the TCA cycle directly, whereas most of the consumed Gluc is excreted as Lac in MDCK cells (Sidorenko et al., 2008). However, the calculation of flux distributions from extracellular concentrations was only possible under certain assumptions, and some open questions remained. For example, the flux of Gluc carbon through the oxidative branch of the pentose phosphate pathway was assumed to be insignificant and set to zero for both cultivations considered (Gln and Pyr-containing conditions). Furthermore, the flux through the anaplerotic reaction to the TCA cycle via carboxylation of Pyr (catalyzed by PC) was assumed to be negligible under both conditions. Finally, fluxes through metabolic pathways not only depend on metabolite concentrations but also on activities of enzymes as well as regulatory mechanisms. Therefore, key enzyme activity measurements could give further insights into primary energy metabolism and precursor pools required for product formation (Newsholme and Crabtree, 1986).

Early work on metabolism in animal cells focused only on Gluc and Gln metabolism by measuring specific maximum activities of regulatory enzymes involved in glycolysis and glutaminolysis (Board et al., 1990; Fitzpatrick et al., 1993; Neermann and Wagner, 1996; Vriezen and van Dijken, 1998a). The simplest methods used for determination of enzyme activities are direct assays in which the enzyme-catalyzed reaction is monitored by measuring product accumulation or substrate uptake over time (Fitzpatrick et al., 1993; Madej et al., 1999; McClure, 1969; Neermann and Wagner, 1996; Vriezen and van Dijken, 1998b; Yallop et al., 2003; Zammit and Newsholme, 1976). In case changes in product or substrate concentrations cannot be observed directly, it is a common practice to use one or more coupling enzymes to generate a detectable product (Bergmeyer et al., 1978; Kotzé, 1967). An advantage of these continuous assays is that the progress of reaction is immediately measured and initial rates can be directly checked for linearity. Therefore, continuous assays are generally preferred compared to stop-time assays because they give more information during

the measurement, for instance on substrate depletion, product inhibition or enzyme stability. However, this assay principle does not allow amplification of the signal because the amount of product accumulating depends on the activity of the enzyme under study in the sample preparation. Additionally, if the enzyme activity is very low, only small quantities of a product can be formed in a certain time interval resulting in low signal intensities. Therefore, several enzymatic cycling systems have been developed and applied for the quantitative determination of low levels of an enzyme (Chi et al., 1988; Gibon et al., 2004; Lowry et al., 1978; Lowry et al., 1983; Sulpice et al., 2007) or a metabolite (Gibon et al., 2002; Khampha et al., 2004; Valero and Garcia-Carmona, 1998; Valero et al., 1995). For example, Gibon et al. (2004) developed a robot-based platform to measure enzyme activities of central carbon and nitrogen metabolism in plant cell extracts using a set of cycling assays. In such a cycling system, a target metabolite is regenerated by two enzymes acting in opposite directions. This leads to a constant concentration of the recycling substrate, while other products of the enzymatic reactions are accumulated at each turn of the cycle. As a result, the amount of product accumulated is directly proportional to the original amount of metabolite in the sample (Lowry, 1980). This technique significantly increases the sensitivity of enzymatic assays. The indirect assays require additional steps such as the preincubation of the sample with a substrate of the enzyme and the stopping of the reaction by pH extremes or heat before measuring the amount of accumulated product. However, low detection limits for metabolites allow high extract dilution, which minimizes interferences by other components of the sample extract and reduces unwanted side reactions by other interfering enzymes (Gibon et al., 2004; Lowry, 1980).

The aim of the present work was to better characterize the cell metabolism by quantitative analysis of key enzymes in mammalian cells under specific cultivation conditions. The focus was on the determination of maximum enzyme activities involved in the central carbon metabolism (glycolysis, pentose phosphate pathway, TCA cycle, and glutaminolysis) of adherent MDCK cells to better understand growth and product formation of cells under different cultivation conditions. Although the analysis of enzymes is more complex and high-throughput technologies for enzyme activities are not commonly available, enzyme activities provide valuable information on pathway flux rates (Newsholme and Crabtree, 1986), which is important for the understanding of metabolic networks. Furthermore, the integration of enzyme activity data into mathematical models of cell metabolism together with proteome and metabolome data by systems biology approaches will significantly contribute towards a

better understanding of metabolic pathways relevant for product formation, cell line and media optimization.

Accordingly, the task of this work was to establish and validate a new enzyme assay platform for mammalian cells and to subsequently analyze enzyme activities during cell growth and product formation. The new assay platform should provide valuable information regarding available metabolic pathways of mammalian cells under specific cultivation conditions, on interactions between metabolic pathways, and on mechanisms of enzyme control. Therefore, 17 different cycling assays used in plant metabolomics were adapted to monitor enzyme activities in mammalian cells. In addition, the platform was extended to 11 new enzyme assays for reactions relevant in central carbon and Gln metabolism of mammalian cells. The method is based on a high-throughput platform established for measuring enzyme activities in plant cell extracts that uses three cycling systems to determine $\text{NAD}^+(\text{H})$, $\text{NADP}^+(\text{H})$, and glycerol 3-phosphate (G3P) or dihydroxyacetone phosphate (DAP) (Gibon et al., 2004; Sulpice et al., 2007).

Furthermore, the newly established enzyme platform for mammalian cells had to be extended with a special enzyme that not only allowed for measuring pyruvate kinase (PK) activity in extracts of MDCK cells but also provided the flexibility needed (e.g., to analyze UTP-generating enzymes) for future studies on cell metabolism. The glycerokinase (GK) from *Pichia farinosa*, for example, is not specific for ATP and can use different nucleoside triphosphates (e.g., GTP and UTP) for the phosphorylation of glycerol to G3P. Therefore, this enzyme was produced with an adequate expression system, purified to homogeneity, and applied as an additional coupling enzyme to exploit all the benefits of the G3P cycling system (Gibon et al., 2002).

Subsequently, the aim of the present study was to apply the established enzyme platform for monitoring of enzyme activities in MDCK cells. As an example, maximum enzyme activities should be measured in these cells under different cultivation conditions. It could be previously shown that Pyr in the culture medium can support growth of different production cell lines in the absence of Gln (Genzel et al., 2005). For a better understanding of the metabolic switch from Gln-containing to Gln-free (Pyr) medium, new data on enzyme activities of the central carbon and Gln metabolism of MDCK cells had to be generated. The results obtained should give useful information to check assumptions concerning the activity of critical enzymes in metabolic pathways required for metabolic flux analysis (Sidorenko et al., 2008; Wahl et al., 2008). Together with datasets on intracellular and extracellular

metabolites obtained in previous studies with MDCK cells (Genzel et al., 2004b; Genzel et al., 2005; Ritter, 2010; Ritter et al., 2008), these new measurements of the central metabolic enzymes should contribute towards a better understanding of the general effect of Gln substitution by Pyr on enzyme activities and towards a better understanding of cell metabolism in general.

Finally, metabolic activity of key enzymes had to be analyzed in MDCK cells infected with a human influenza A virus. For the manufacturing of influenza vaccines, cell culture-based technology is nowadays thought to be more efficient and allows a more flexible production compared to the traditionally used virus propagation in embryonated hens' eggs. Adherent MDCK cells have been shown to replicate influenza strains to sufficient titer and are already used as a cell substrate for influenza vaccine production (Brands et al., 1999; Doroshenko and Halperin, 2009; Genzel et al., 2004a; Genzel et al., 2010; Genzel and Reichl, 2009; Liu et al., 2009). In general, the cultivation of anchorage-dependent MDCK cells in stirred tank bioreactors or in a Wave Bioreactor[®] (Wave Biotech, Tagelswangen, Switzerland) requires microcarriers to provide a surface for cell growth and this can be performed in serum-free cell culture media (Genzel et al., 2006a; Genzel et al., 2006b). However, like all viruses, influenza relies on the host's metabolic network to provide energy and macromolecular precursors for viral replication. Influenza viruses bud from the apical host plasma membrane with an envelope containing lipid rafts enriched in cholesterol and glycosphingolipids (Nayak et al., 2009; Scheiffele et al., 1999; Zhang et al., 2000). For example, it has been shown that enveloped viruses directly alter the central carbon and lipid metabolism of their host cell during the infection process, e.g., by increasing the Gluc consumption, Lac release, and intracellular metabolite concentrations of the upper part of glycolysis in influenza infected MDCK cells compared to mock-infected cells after 12 h post infection (Ritter et al., 2010) or by up-regulating various genes involved in cholesterol biosynthesis and genes associated with lipid metabolism in, for example, human immunodeficiency virus and hepatitis C virus infected cells (reviewed in Chan et al., 2010). Therefore, newly obtained data on key enzyme activities should improve the understanding of virus-host cell interaction and cell response during early influenza virus infection, and help to overcome limitations such as slow virus replication and low virus yields in cell culture-derived influenza vaccine production.

2 Background and Theory

The Bioprocess Engineering group of the Max Planck Institute (MPI) for Dynamics of Complex Technical Systems in Magdeburg aims at the investigation and optimization of cell culture derived influenza vaccine production processes. One emphasis is on the analysis of cellular metabolism of different production cell lines, such as MDCK and Vero cells. Among the basic concepts of kinetic analysis of enzymes, the following chapters address some aspects and properties of cell metabolism.

2.1 Metabolism in mammalian cell culture

Primary cells are isolated directly from tissues or organs of apparently healthy animals or humans that can be expanded by appropriate cell culture techniques. Although widely used for a variety of research and medical purposes, these cells do have one major drawback. They have been shown to exhibit only a finite replicative capacity *in vitro*, meaning that a specific cell type can undergo only a limited number of maximum 50 ± 10 doublings before reaching a non-proliferated state termed cellular senescence (Hayflick and Moorhead, 1961; Passos et al., 2009). The industrial production of, e.g., diagnostic and therapeutic proteins or viral vaccines, however, usually necessitates a group of morphologically uniform cells that can be propagated for an indefinite period of time in culture. The most established method to extend the cellular life span is to inactivate tumor suppressor genes (e.g., p53 and Rb) that can induce a replicative senescent state (Münger et al., 1989; Scheffner et al., 1990; Wazer et al., 1995). This can be achieved by *in vitro* immortalization using viral oncogenes, including human papillomavirus E6 and E7 (Kiyono et al., 1998), Simian virus 40 large and small T antigen (Yuan et al., 2002), adenovirus E1A and E1B (Shay et al., 1991), and Epstein-Barr virus latent membrane protein 1 (Mainou et al., 2005). However, cells with an extended life capacity can also be generated by spontaneous mutation (Madin and Darby, 1958). Such modified cells are most suitable for the large-scale production of various biologicals and are referred to as permanent or continuous cell lines. However, continuous cell lines show a change in central carbon metabolism, which results in an increased glycolytic rate and in the production of high amounts of Lac even under aerobic conditions (Donnelly and Scheffler, 1976; Häggström, 2000). Furthermore, most immortalized cells have a high demand for Gln as the major energy and carbon source and excrete high amounts of incompletely oxidized intermediates (e.g., ammonium, Lac, alanine, and/or aspartate) into the culture medium.

These waste-products (mainly Lac and ammonium) can be toxic and, therefore, negatively affect cell growth and product formation. The following two chapters give a summary of the most important metabolic pathways that provide building blocks, cofactors and energy for cell growth, and enzymes involved in Gluc and Gln degradation.

2.1.1 Glucose metabolism: glycolysis and pentose phosphate pathway

Gluc is a main carbon and energy source for cultured mammalian cells in most cases, and culture media for *in vitro* cultivation of primary and continuous cell lines typically contain 5 to 25 mM Gluc. The degradation of Gluc takes place in the cell's cytoplasm via glycolysis and the pentose phosphate pathway. Several precursor metabolites, such as glucose 6-phosphate (G6P), fructose 6-phosphate (F6P), DAP, and 3-phosphoglycerate (3PG) are produced in the glycolytic pathway (Figure 2.1).

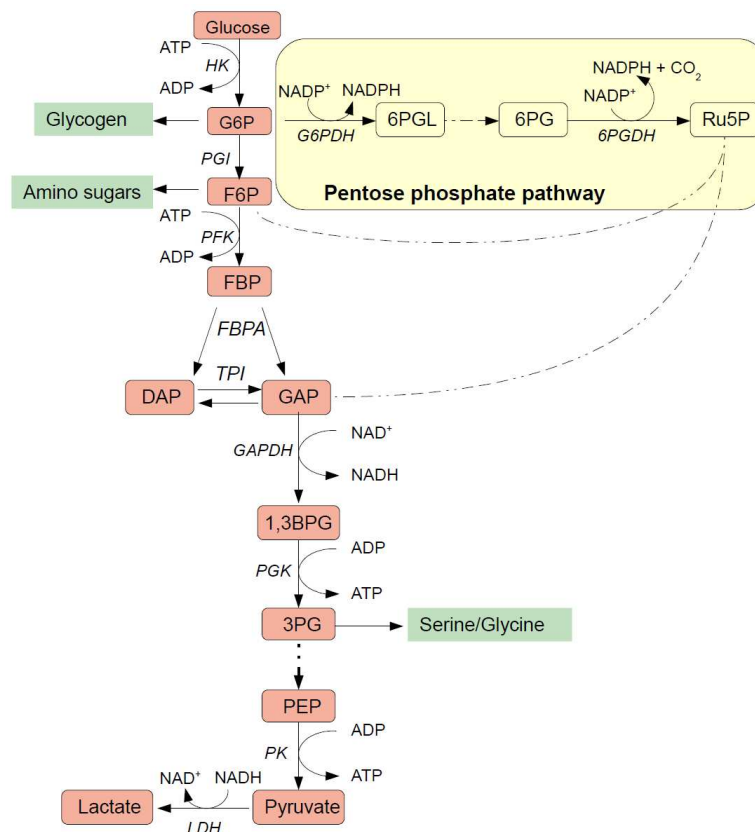


Figure 2.1: Schematic overview of glucose metabolism (modified from Häggström, 2000). Metabolites of glycolysis are highlighted in red and possible products from glycolytic precursor metabolites are shown in green. The oxidative branch of the pentose phosphate pathway is highlighted in yellow. For names of enzymes and metabolites see abbreviation list.

The first step of Gluc degradation in mammalian cells is catalyzed by the key enzyme hexokinase (HK), which transfers a terminal phosphate group from ATP to Gluc. The HK

reaction is regulated by feedback inhibition by its product to prevent accumulation of large amounts of G6P in the cell. Due to the relatively low specific activity in different cell lines, the HK reaction is thought to be a limiting step in glycolysis (Neermann and Wagner, 1996; Nelson et al., 2008). After the isomerization of G6P to F6P via the phosphoglucose isomerase (PGI) follows a second activation reaction, in which ATP is used to produce fructose 1,6-bisphosphate (FBP) from F6P. This reaction step is essentially irreversible and is catalyzed by the action of phosphofructokinase (PFK). The PFK is a highly regulated, allosteric enzyme in all types of cells (Nelson et al., 2008; Voet et al., 2002). Because the activity of this key regulatory enzyme is affected by a variety of metabolites (reviewed in Dunaway, 1983), it controls not only fluxes but also the direction of the glycolytic pathway. Most notably, the activators AMP and fructose 2,6-bisphosphate and the inhibitors ATP, citrate and various fatty acids are considered to be important effectors in the regulation of PFK (Ramadoss et al., 1976; Reddy and Ramaiah, 1984; Tejwani, 1978; Van Schaftingen et al., 1981). After the hydrolysis of FBP into the two three-carbon units DAP and glyceraldehyde 3-phosphate (GAP) by fructose-1,6-bisphosphate aldolase (FBPA), the products can be reversibly interconverted by the triose-phosphate isomerase (TPI).

The subsequent reactions of Gluc catabolism represent the energy-yielding steps that produce ATP and NADH in the cell. At first, the glyceraldehyde-3-phosphate dehydrogenase (GAPDH) catalyzes the reversible NAD^+ -dependent oxidation and phosphorylation of GAP to 1,3-bisphosphoglycerate (1,3BPG) and NADH. The energy-rich intermediate 1,3BPG is then used to form ATP and 3PG via the phosphoglycerate kinase (PGK). Until now, two moles of ATP per mole of Gluc are produced, which compensate for the cost of energy used for the upper part of glycolysis. The two subsequent reactions are aimed at converting 3PG to a higher energy form (phosphoenolpyruvate, PEP) catalyzed by phosphoglycerate mutase and phosphopyruvate hydratase/enolase.

The final step in aerobic glycolysis is catalyzed by the regulated PK enzyme, which converts the essentially irreversible reaction from PEP to Pyr and transfers the high-energy phosphate group from PEP to ADP, thus generating ATP. Four different types of PK have been found in mammalian tissues: M1 (in muscles and brain), M2 (in kidney, adipose tissue and lungs), L (in liver), and R (in red blood cells) (reviewed in Munoz and Ponce, 2003). These isoenzymes have different kinetic properties that reflect the different metabolic requirements of the tissues (Carbonell et al., 1973; Munoz and Ponce, 2003; Nowak and Suelter, 1981). For example, type L PK shows distinct sigmoidal kinetics with respect to the concentration of

PEP, is allosterically inhibited by ATP and alanine (Ala), and activated by FBP (Carbonell et al., 1973). One theory for the energetically inefficient metabolism (e.g., secretion of high amounts of Lac) is that the isoenzyme composition of PK shifts from the tissue-specific to the M2 type in immortal cells (Mazurek et al., 2005). This isoenzyme (M2-PK) can switch between a nearly inactive dimeric form (low affinity for its substrate PEP) and a highly active tetrameric form (high PEP affinity), thus regulating the flux through the downstream-part of the glycolytic pathway (Gupta and Bamezai, 2010; Spoden et al., 2009). The tetramer/dimer ratio of M2-PK is regulated by certain oncoproteins and the glycolytic phosphometabolite FBP, which at high levels induces the association of two dimers to the tetrameric form (Ashizawa et al., 1991; Eigenbrodt et al., 1992; Mazurek and Eigenbrodt, 2003). An increase in FBP levels is induced by high levels of dimeric M2-PK. Consequently, when the tetrameric form predominates, Gluc is converted to Lac with production of energy (ATP) until FBP concentrations drop below a certain level. Accordingly, the tetrameric form dissociates to the inactive dimeric form and the intermediates of the upper part of glycolysis accumulate and are available as precursors for biosynthetic processes (Mazurek, 2012). Another allosteric activator of M2-PK is serine (synthesized from 3PG, see Figure 2.1), which increases the affinity of M2-PK to its substrate PEP. Inhibitors of M2-PK are other amino acids that are linked to the glutaminolytic pathway (e.g., Ala and proline, see Figure 2.2) as well as fatty acids (Mazurek and Eigenbrodt, 2003; Mazurek et al., 2001).

The last metabolite of aerobic glycolysis, Pyr, can either be transported into the mitochondria, where it enters the TCA cycle and is further metabolized under aerobic conditions to produce reducing equivalents (NAD(P)H) and more energy (GTP, ATP) or Pyr is anaerobically reduced to Lac. Continuous cell lines, however, cannot completely oxidize Pyr via the TCA cycle to CO₂ and H₂O (plus ATP). These cells predominantly excrete the Gluc-derived three-carbon molecule as Lac into the culture broth. For example, Fitzpatrick et al. (1993) could demonstrate that only limited amounts of Gluc were metabolized by the TCA cycle in murine B-lymphocyte hybridoma cells grown in batch culture. Studies on maximum enzyme activities of key enzymes connecting glycolysis with the citrate cycle revealed that no or only very low activities of pyruvate dehydrogenase (PDH), pyruvate carboxylase (PC), and phosphoenolpyruvate carboxykinase (PEPCK) are present in mammalian cell lines, which may partly explain the low amount of Gluc-derived carbon being shunted into the TCA cycle (Board et al., 1990; Neermann and Wagner, 1996; Vriezen and van Dijken, 1998a; Yallop et al., 2003). Typically, over 90 % of Gluc taken up by continuous cell lines is broken down to

Lac via the lactate dehydrogenase (LDH) (Fitzpatrick et al., 1993; Wagner, 1997). In this way, only two moles of ATP can be produced per mole Gluc metabolized to Pyr compared to approximately 30 (if NADH from glycolysis is transported by the glycerol 3-phosphate shuttle) to 32 (malate-aspartate shuttle) moles of ATP during complete Gluc oxidation in the TCA cycle (Garrett and Grisham, 2010; Glacken, 1988; Häggström, 2000). Glycolysis also releases two moles of NADH per mole Gluc converted to Pyr. However, NAD^+ must be regenerated to drive the glycolytic pathway. This is mainly done by the reduction of Pyr via LDH in permanent cell lines rather than transporting NADH into mitochondria via shuttle mechanisms (e.g., malate-aspartate shuttle) (Häggström, 2000; Wagner, 1997). The abnormal metabolic behavior in continuous cell lines (release of large amounts of Lac during growth) may be partly explained by the very high activity of LDH in these cells compared to the limited activity of different shuttle systems that compete for reducing equivalents.

The intermediate metabolite G6P can also be metabolized via the pentose phosphate pathway, which major role is the biosynthesis of NADPH used as reducing equivalent for anabolic processes (e.g., fatty acid and cholesterol synthesis), and ribose 5-phosphate (R5P) for synthesis of nucleotides and nucleic acids (Häggström, 2000; Wagner, 1997). The two key enzymes of the oxidative branch are glucose-6-phosphate dehydrogenase (G6PDH) and 6-phosphogluconate dehydrogenase (6PGDH), which each produce one mole of NADPH. Additionally, G6PDH converts G6P to 6-phosphogluconolactone (6PGL), and 6PGDH catalyzes the oxidative decarboxylation of 6-phosphogluconate (6PG) to ribulose 5-phosphate (Ru5P). In the case that the cell needs more NADPH in reductive biosyntheses than Ru5P for nucleotides, Ru5P can be further converted to intermediates of glycolysis (F6P and GAP) catalyzed by non-oxidative branch enzymes, such as transaldolase (TA) and transketolase (TK) (Nelson et al., 2008). The pentose phosphate pathway only seems to play a minor role in continuous cell lines, as only about 3 % of Gluc were metabolized via this route in murine B-lymphocyte hybridoma cells (Fitzpatrick et al., 1993). In HeLa cells, however, it was shown that an increase in the Gluc concentration reduced the flux of Gluc-derived carbon through the pentose phosphate pathway while simultaneously the flux of Gluc carbon through the glycolytic pathway to Lac increased (Reitzer et al., 1979).

Finally, Gluc can be synthesized from non-carbohydrate sources such as amino acids and fatty acids. However, this metabolic pathway, known as gluconeogenesis, plays only a minor role at sufficient substrate supply during the cultivation of continuous cell lines (Häggström, 2000), and is not considered in the following.

2.1.2 Glutamine metabolism: glutaminolysis

Gln can be considered to be a key amino acid and the major energy source in cultured mammalian cells since it provides typically 30 to 98 % of the cell energy (Fitzpatrick et al., 1993; Glacken, 1988; Reitzer et al., 1979; Zielke et al., 1978). Furthermore, Gln provides important carbon precursors for *de novo* peptide and protein synthesis and its nitrogen serves as a donor for several biosynthetic reactions (e.g., purines, pyrimidines, and amino sugars) (Hägström, 2000). The Gln metabolism in mammalian cell cultures (Figure 2.2), which comprises parts of the TCA cycle machinery and the malate-aspartate shuttle, is termed glutaminolysis (McKeehan, 1982).

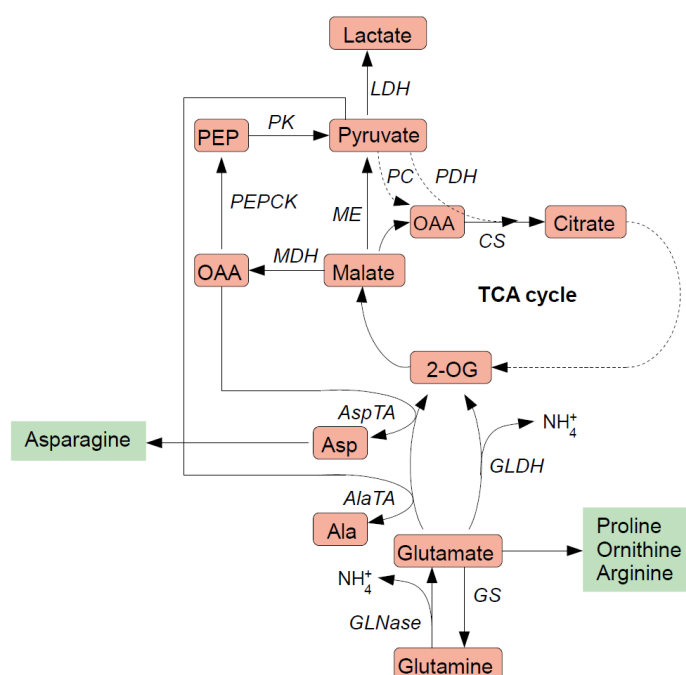


Figure 2.2: Schematic overview of Gln metabolism (modified from Hägström, 2000).

Metabolites involved in glutaminolysis are highlighted in red and possible products from glutaminolytic precursor metabolites are shown in green. For names of enzymes and metabolites see abbreviation list.

The first step in glutaminolysis is initiated by the mitochondrial enzyme glutaminase (GLNase), which catalyzes the deamination of Gln to glutamate (Glu) and ammonia/ammonium (NH_4^+). Glu is the direct precursor of both proline and ornithine, and Glu is a major donor of amino groups in several biosynthetic pathways (Hägström, 2000). The next step of Gln degradation involves the enzymes glutamate dehydrogenase (GLDH), alanine transaminase (AlaTA), and aspartate transaminase (AspTA). In all cases, the TCA cycle intermediate 2-oxoglutarate (2-OG) is formed, whereas the reversible GLDH reaction is additionally characterized by the release of a second ammonia (Amm) ion using NAD^+ as

coenzyme. The formation of 2-OG from Glu in the transaminase pathways, however, is stoichiometrically coupled to the transamination of Pyr and oxaloacetate (OAA) to Ala and aspartate (Asp), respectively (Häggsström, 2000). 2-OG can then be completely oxidized in the TCA cycle to CO₂ and H₂O, which is rather unlikely in *in vitro* cultivated continuous cells. However, 2-OG can also be converted to Lac where the key enzymes malic enzyme (ME) and/or phosphoenolpyruvate carboxykinase (PEPCK) are involved (Ardawi and Newsholme, 1982).

The complete Gln oxidation to CO₂ (and H₂O) via the GLDH pathway yields a maximum of 27 moles of ATP per mole Gln compared to only 9 moles of ATP during the incomplete oxidation to Lac or to the amino acids Ala and Asp via the transaminase pathways (Glacken, 1988; Häggsström, 2000). However, cultured mammalian cells mainly use the transaminase pathways for energy production, which was confirmed by NMR studies of Gln and nitrogen metabolism (Martinelle et al., 1998; Street et al., 1993). The more energy efficient pathway involving GLDH appears to be only used at limiting substrate supply. For example, it could be shown that the flux via GLDH (and GLNase) in fructose-grown hybridoma cells and in Gluc-starved myeloma cells significantly increased with a concomitant increase of Gln uptake and Amm release as compared to cells with sufficient supply of Gluc (Martinelle et al., 1998). This behavior may be partly explained by the complex allosteric regulation of the responsible key enzymes (Schoolwerth et al., 1980; Snodgrass and Lund, 1984). The reaction product 2-OG, for instance, which accumulates in cells with high transaminase activity, is a competitive inhibitor of GLDH (Schoolwerth et al., 1980).

Glutamine synthetase (GS) is an important key enzyme that catalyzes the biosynthesis of Gln via the ATP-dependent condensation of Glu and ammonia. The catalytic properties and the regulation of GS have been reported to vary markedly between different mammalian tissues (reviewed in Eisenberg et al., 2000). For example, the liver enzyme has been shown to be inhibited by, e.g., Ala and carbamoyl phosphate, and activated by 2-OG and citrate (Tate and Meister, 1971). Several continuous cell lines can grow in culture media devoid of Gln where the Gln needed for protein synthesis was supplied by the action of GS. This was shown for CHO and BHK cells when the Gln concentration in the medium was decreased or the medium was supplemented with Glu instead of Gln, respectively (Christie and Butler, 1999; Sanfeliu and Stephanopoulos, 1999). This finding was also demonstrated by label incorporation of ¹⁵N from ¹⁵NH₄Cl into the amide position of Gln in CHO cells expressing high levels of GS (Street et al., 1993). Additionally, Street et al. (1993) showed that HeLa

cells possessed GS activity when cells were adapted to a medium containing low Gln concentrations. An increase in GS activity was also observed for murine B-lymphocyte hybridoma cells in the stationary phase (limiting Gln concentrations) of the cultures (Fitzpatrick et al., 1993). These results indicate that GS activity is up-regulated at low Gln concentrations in the medium and down-regulated in the presence of exogenous Gln. However, mammalian cells, which do not express sufficient GS to survive without added Gln, can be transfected with a GS gene to permit growth in a Gln-free medium (Bell et al., 1995).

2.1.3 Metabolic waste products of *in vitro* cultured cell lines

Mammalian cell lines grown under batch conditions are characterized by high rates of glycolysis and glutaminolysis (Warburg, 1956). As a result, these cells often show inefficient use of nutrients for growth, leading to the accumulation of inhibitory by-products, such as Lac and ammonia/Amm. This often not only affects cell viability, productivity, and product quality but can also prevent growth to high cell densities when large amounts are secreted into the culture medium (Glacken, 1988; Hassell et al., 1991; McQueen and Bailey, 1990a; Ozturk et al., 1992).

2.1.3.1 Ammonium and lactate

Free Amm accumulating in cell culture is either derived directly from the Gln in the medium by temperature-dependent degradation (Tritsch and Moore, 1962) or results from cellular metabolism via GLDH and/or GLNase pathways (glutaminolysis). For example, Amm concentration at levels exceeding 2 mM in culture was shown to decrease the growth rate of BHK cells (Butler and Spier, 1984), and an accumulation of more than 7 mM ammonia resulted in growth inhibition of MDCK cells (Glacken et al., 1986). One proposed mechanism of ammonia/Amm toxicity is through changes in intracellular pH that can alter the activity of different metabolic enzymes (Martinelle and Häggström, 1993; McQueen and Bailey, 1990b; McQueen and Bailey, 1990c; Ozturk et al., 1992). Formation of mitochondrial ammonia/Amm essentially results in cytoplasmic acidification (decrease in intracellular pH). The regulation of intracellular pH in response to the formation of ammonia/Amm by the cell and the transport mechanisms are complex (Martinelle and Häggström, 1993). For example, Amm can be transported across the cytoplasmic membrane via certain transport proteins (e.g., the Na⁺/K⁺-ATPase transporter) (Post et al., 1960). The influence of different Amm

concentrations on cell growth and productivity of hybridoma cells (mainly; see reference) is summarized in Table 2.1.

Table 2.1: Influence of different ammonium concentrations on cell growth and productivity (Wagner, 1997).

Ammonium concentration (mM)	Growth	Productivity	Reference
<2	no effect	no effect	(Glacken, 1988) (Cruz et al., 2000)
2-5	inhibition	no effect	(Glacken et al., 1988) (McQueen and Bailey, 1990a) (Newland et al., 1990) (Ozturk et al., 1992)
>5	inhibition	inhibition	(Glacken et al., 1986) (Glacken, 1988)

Lac is mainly generated from Gluc degradation via the enzyme LDH. When secreted into the culture medium, Lac can become inhibitory by lowering the pH of the medium generally at concentrations exceeding 20 mM (Glacken, 1988; Sanfeliu et al., 1996). This can be restricted by controlling the concentration of Gluc or the pH within an optimum range (Reuveny et al., 1986). However, Lac levels higher than 20 mM were shown to inhibit growth as well as recombinant protein and antibody production of BHK and hybridoma cells, respectively (Cruz et al., 2000; Glacken, 1988; Ozturk et al., 1992). The inhibitory effect of Lac most likely results from an increase in the osmolarity of the medium with increasing Lac concentrations (Hassell et al., 1991; Ozturk and Palsson, 1991; Ozturk et al., 1992). The influence of different Lac concentrations on cell growth and productivity of hybridoma cells (mainly; see reference) is shown in Table 2.2.

Table 2.2: Effect of different medium concentrations of lactate on cell growth and productivity at constant pH (Wagner, 1997).

Lactate concentration (mM)	Growth	Productivity	Reference
<20	no effect	no effect	(Wagner et al., 1988) (Miller et al., 1988) (Cruz et al., 2000)
20-40	no effect	inhibition	(Glacken et al., 1988)
>40-60	slight inhibition	inhibition	(Glacken et al., 1988) (Ozturk et al., 1992)
>60	inhibition	inhibition	(Glacken, 1988)

2.1.3.2 Measures to reduce toxic by-product formation during cultivation

Many efforts have been made to reduce the accumulation of Lac and ammonia in the culture medium, and, therefore, to increase the productivity of mammalian cell culture processes (reviewed in Schneider et al., 1996). A promising approach to optimize cultivation strategies is the use of perfusion systems. Here, cells are retained in the cultivation vessel and substrate as well as product concentrations can be maintained at a constant level by continuously feeding fresh and discarding waste medium (Merten et al., 1994). Another method to reduce the concentration of waste products was described for hybridoma cells. The cultivation was performed under Gluc and Gln-limited conditions in fed-batch mode and, as a consequence, the cells metabolized these substrates more efficiently (Ljunggren and Häggström, 1994). For high-density cultivation of adherent MDCK cells, a repeated fed-batch operation was established, which also reduced the concentration of unwanted by-products of the cellular metabolism by removal of medium after defined time intervals (Bock et al., 2010). Irani et al. (1999) presented a different approach to avoid ammonia accumulation. By introducing a cytosolic yeast PC gene into a BHK-21A cell line, Gln and Gluc utilization could be reduced by a factor of two and four, respectively. A similar approach was described by Bell et al. (1995) for a mouse hybridoma cell line. Here, the introduction of a vector containing the GS cDNA enabled growth in Gln-free medium and reduced the production of ammonia. However, unwanted by-product formation in production cells can also be dramatically decreased by deletion of specific genes (Chen et al., 2001; Zhou et al., 2011). For example, Chen et al. (2001) genetically manipulated the pathway of Lac synthesis in hybridoma cells, which significantly reduced the specific activity of LDH and Lac production. As a consequence, cell growth was improved in terms of cell density and cell viability. Finally, the substitution of one or several components in the culture medium can also lead to a reduction of ammonia in the medium (Butler and Christie, 1994). McDermott and Butler (1993) found that the replacement of Gln by Glu supported growth of McCoy cells with normal specific growth rates (doubling time of 20 h) after 2-3 passages in the medium. Furthermore, it was recently shown that Gln could be substituted by Pyr without reduction in specific growth rate of different adherent cell lines (MDCK, BHK21, CHO-K1) in serum-containing and serum-free media (Genzel et al., 2005). In Gln-free medium with Pyr as carbon source, MDCK cells grew to high cell densities without the need of a long adaptation process. Gluc consumption and Lac production was reduced significantly while cells released no ammonia during growth.

2.1.4 Cell metabolism under stress conditions: viral infection

Besides the superior capacity of continuous cell lines for large-scale manufacturing of a variety of medical and diagnostic biologicals, such as monoclonal antibodies (reviewed in Birch and Racher, 2006) or recombinant proteins (reviewed in Wurm, 2004), several cell lines are also accessible to viral infection and either considered or already used for industrial production of viral vaccines (Aunins, 2000; Barrett et al., 2009; Genzel and Reichl, 2009; Pérez and Paolazzi, 1997). For example, MedImmune (Santa Clara, CA, USA) and Novartis Vaccines (Marburg, Germany) developed new mammalian cell culture-based production processes for influenza virus vaccines (Aggarwal et al., 2011; Doroshenko and Halperin, 2009). However, although different human and animal cell lines can be employed for cell culture-based influenza vaccine production (reviewed in Genzel and Reichl, 2009; Hickling and D'Hondt, 2006), the manufacture of influenza vaccines is still predominantly performed in embryonated (fertilized) hen's eggs (Tree et al., 2001). Cells that are suitable as substrates for influenza virus propagation include the simian and canine kidney epithelium cell lines Vero and MDCK, respectively, (Doroshenko and Halperin, 2009; Kistner et al., 2010), the human embryonic retina cell line PER.C6[®] (Pau et al., 2001), the human embryonic kidney cell line HEK-293 (Le Ru et al., 2010), the avian embryonic retina cell line AGE1.CR[®] (Lohr et al., 2009; Sandig and Jordan, 2005), and the avian embryonic stem cell line EB66[®] (Brown and Mehtali, 2010). Among these cell lines, MDCK cells can be considered to be one of the most investigated and best characterized cell lines that possess optimal influenza replicating properties (Aggarwal et al., 2011). They have been shown to produce high quantities of influenza virus (Merten, 2002; Merten et al., 1996; Merten et al., 1999; Tree et al., 2001), and MDCK-derived vaccines showed similar or even slightly higher immunogenicity in young and elderly adults as compared to the control vaccine (egg-based) (Gregersen et al., 2011; Groth et al., 2009).

The influenza virus belongs to the family of *Orthomyxoviridae*, and like all viruses, influenza relies on the host's metabolic network to provide energy and macromolecular precursors for viral replication. The replication cycle of influenza viruses including entry, uncoating, genome transcription and replication, assembly and release (budding) has been extensively studied with type A strains (reviewed in Cox et al., 2010; Nayak et al., 2004; Rossman and Lamb, 2011). The influenza virus particle consists of three major parts: the ribonucleocapsid, the matrix protein M1, and the envelope, which is derived from the plasma membrane of the

host cell. The lipid bilayer of the viral envelope contains the ion channel protein M2 and the immunogenic glycoproteins hemagglutinin (HA) and neuraminidase (NA) (Figure 2.3).

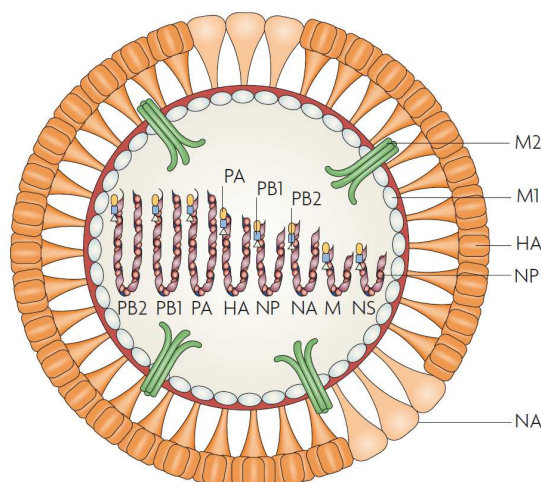


Figure 2.3: Schematic representation of an influenza A virus. Reprinted from Subbarao and Joseph (2007), with permission.

The lipid envelope of the influenza A virus particle is derived from the host cell membrane. Three viral proteins are embedded in the lipid bilayer (shown in red) of the viral envelope: the glycoproteins (HA and NA) and the ion channel protein M2. The inner side of the viral envelope is covered with a layer consisting of M1 matrix proteins and contains 8 different ribonucleoprotein (RNP) complexes. A RNP complex is composed of a negative sense single-stranded RNA molecule, which is encapsidated with nucleoprotein (NP) and associated with three polymerase proteins (PA, PB1, and PB2). The different RNA molecules encode for PA, PB1, PB2, HA, NA, NP, M (M1 and M2), and the non-structural proteins (NS1 and NS2).

The success of viral replication within the infected cell is directly linked to the ability of viruses to hijack host cell mechanisms. Influenza viruses bud from the apical host plasma membrane with an envelope containing lipid rafts, which are enriched in cholesterol and glycosphingolipids (Scheiffele et al., 1999; Zhang et al., 2000). Numerous studies indicate that enveloped viruses directly alter the lipid metabolism of their host cell during the infection process (reviewed in Chan et al., 2010). For example, it could be shown that the metabolic flux of citrate through the TCA cycle and its efflux to the pathway of fatty acid biosynthesis as malonyl-CoA increased in human cytomegalovirus (HCMV) infected MRC-5 fibroblasts (Munger et al., 2008). A more recent metabolite profiling study found significant changes in metabolite concentrations during influenza A virus replication in human lung adenocarcinoma A549 and human gastric adenocarcinoma AGS cells, indicating that influenza A virus altered fatty acid biosynthesis and cholesterol metabolism in these cell lines (Lin et al., 2010). Furthermore, it is known that hepatitis C virus enhances its replication by modulating host cell lipid metabolism (increased lipogenic activity), and inhibitors of

cholesterol/fatty acid biosynthetic pathways inhibit virus replication, maturation and secretion (Su et al., 2002; Syed et al., 2010; Yang et al., 2008).

Continuous cell lines with enhanced lipogenesis need to generate cytosolic acetyl-CoA, the building block for both cholesterol and fatty acid synthesis (Häggström, 2000). The cytosolic precursor originates from citrate formed from mitochondrial acetyl-CoA and OAA by citrate synthase (CS). The acetyl-CoA may either be derived from Gluc degradation or the consumption of amino acids (Sharfstein et al., 1994). However, OAA is likely to be formed by Gln metabolism in permanent cell lines lacking PDH and PC activities (Häggström, 2000). Mitochondrial citrate can be exported to the cytoplasm via the citrate/malate shuttle where it is cleaved by the key enzyme citrate lyase (CL) to cytosolic acetyl-CoA and OAA (Figure 2.4). Cytosolic OAA can then enter the mitochondria and be further metabolized in the TCA cycle after being converted to malate by MDH. However, malate may also be converted to Pyr via the mitochondrial ME and participate in the AlaTA reaction to yield 2-OG (and Ala).

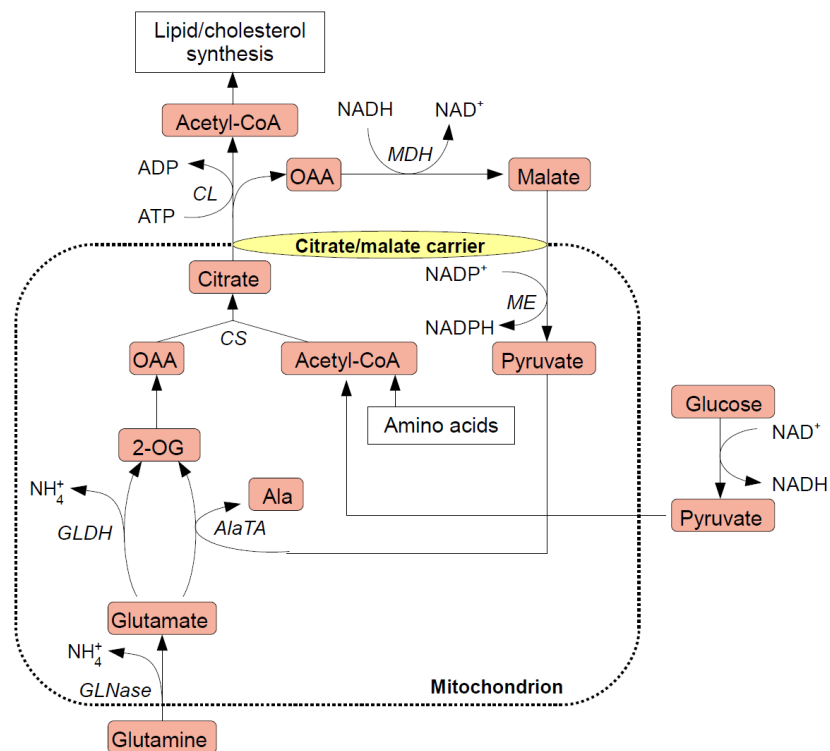


Figure 2.4: Schematic overview of Gln metabolism involving the lipid cycle (modified from Häggström, 2000).

Metabolites involved in Gln metabolism and the lipid cycle are highlighted in red. The citrate/malate carrier is shown in yellow. For names of enzymes and metabolites see abbreviation list.

2.1.5 Analytical tools to measure cell metabolism

There exist many different approaches for characterizing cell metabolism and the regulation of biochemical pathways in response to environmental influences, such as the global analysis of gene expression (transcriptomics), comprehensive protein analysis (proteomics), and the quantitative study of metabolites (metabolomics), which will be introduced in the following (Figure 2.5).

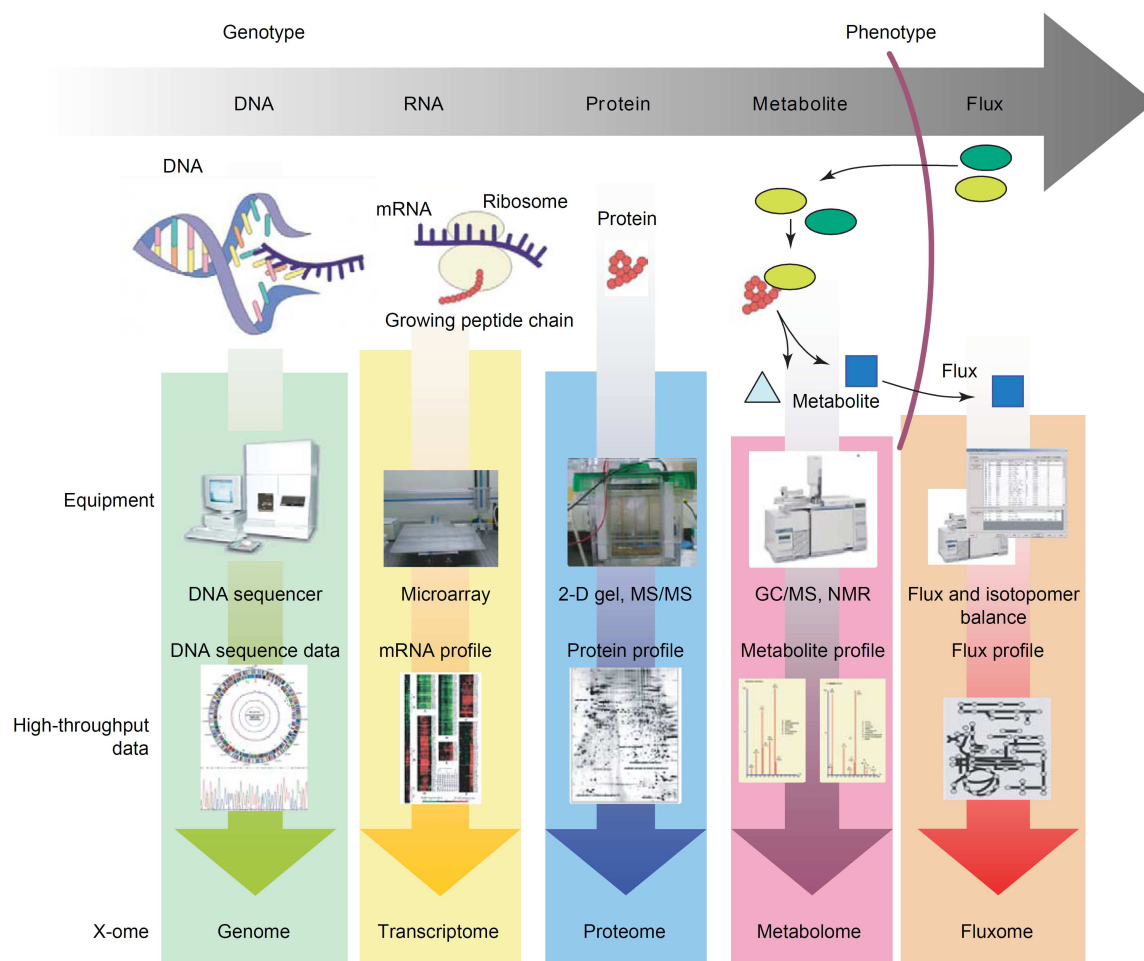


Figure 2.5: High-throughput “omics” research tools and technologies. Reprinted from Lee et al. (2005), with permission.

The majority of genome-wide mRNA expression profiling approaches in cell culture studies is based on DNA microarray methods that provide relative quantitative measurements of transcripts (mRNA) between samples being compared (Griffin et al., 2007). This analytical tool can simultaneously measure the expression of thousands of mRNAs and is used to characterize changes in biological processes such as responses to drugs or mutations, development stages, and disease states (Young, 2000). One major limitation of this high-

throughput technology can be seen in the restriction to species for which a large collection of gene sequences is available, e.g., the genomic sequence of the CHO-K1 cell line (Xu et al., 2011). Therefore, gene expression studies strongly depend on the availability of the transcript sequence for preparing DNA probe molecules that can be immobilized on the array surface (Griffin et al., 2007). Another drawback of this method is the limitation to measure only changes at the mRNA level. Although the expression of many genes is controlled at the transcriptional level, the cellular transcriptome is only predictive of protein expression and typically does not give information about post-transcriptional regulation mechanisms involving mRNA structure, mRNA stability and mRNA translation (Tian et al., 2004). Finally, the amount of datasets produced that need to be analyzed and correctly interpreted is another major problem evolved with this technique (Curtis et al., 2005). However, the microarray technique was successfully applied, for instance, to probe transcriptomic changes on the response to hypoxia in a myeloma NS0 cell line, which revealed the up-regulation of metabolic pathways such as glycolysis and the down-regulation of genes involved in purine/pyrimidine metabolism (Swiderek et al., 2008). Integrated analyses by using DNA microarrays together with protein expression profiling can, however, gain more information on regulatory mechanisms in cellular development or product formation (Krampe et al., 2008; Tian et al., 2004).

Proteome studies can be seen as a complement to transcriptome studies that aim at the large-scale analysis of proteins encoded by the genome. Proteomic technologies potentially offer information on protein isoforms, post-translational modifications, the structure of proteins, and the subcellular localization of proteins (Zhu et al., 2003). The most established practical approach for proteomic analysis is the two-dimensional separation of proteins by polyacrylamide gel electrophoresis, which relies on two characteristics of proteins: charge and molecular weight. This method allows for simultaneous separation of over a thousand different proteins and quantitative comparison of changes in protein profiles of cells (Klose, 1975; O'Farrell, 1975). Visualization of the separated proteins from complex mixtures is achieved by different staining techniques followed by image analysis, where identification and characterization is most commonly accomplished by using either matrix assisted laser desorption/ionization (MALDI) mass spectrometry (MS) or electrospray ionization (ESI) MS (reviewed in Garbis et al., 2005; Gevaert and Vandekerckhove, 2000). Although proteomic analysis is an effective investigative tool, it still suffers from significant technical limitations, such as the difficulty in the separation and identification of low-abundant proteins, the

extraction of integral membrane proteins (low solubility), and the visualization of highly basic proteins (Klein and Thongboonkerd, 2004). However, the application of the proteomic approach was shown to be an effective method for, e.g., the characterization of a recombinant monoclonal antibody production process using a GS-NS0 murine myeloma cell line (Dinnis et al., 2006; Smales et al., 2004). Furthermore, the analysis of cellular proteome alterations in virus infected cells can gain detailed insights into proteins involved in the host cell's stress response and the virus-induced apoptosis (van Diepen et al., 2010; Vester et al., 2009).

Metabolomic analysis is the complement for transcriptomic and proteomic measurements, and aims at comprehensively quantifying all small-molecule metabolites within a biological system. As metabolites are the end products of all regulation, metabolomics leads to a better characterization of physiological states and the cell's phenotypic behavior compared to other high-throughput studies (e.g., proteomics) (Dietmair et al., 2010). The analysis of metabolites in complex biological samples is generally accomplished by nuclear magnetic resonance (NMR) and MS (reviewed in Cuperlovic-Culf et al., 2010; Dettmer et al., 2007). To avoid metabolite degradation and alteration of the sample composition, special care has to be taken in quenching the cell metabolism (enzyme activities) as fast as possible.

Compartmentalization of cells and the enormous complexity of the metabolome (e.g., wide variety of compound classes, very diverse physical and chemical properties) create a major problem in the recovery of intracellular metabolites from the cells. Therefore, optimized sampling and extraction methods have been developed for reliable metabolite profiling, that are specific to the cells being analyzed (Dettmer et al., 2011; Dietmair et al., 2010; Ritter et al., 2008; Sellick et al., 2011). For the characterization of mammalian cell culture processes, a metabolite profiling approach was successfully applied to monitor changes of intracellular metabolite pools of central metabolic pathways during growth under different cultivation conditions (Ritter, 2010). A similar approach was used to investigate the metabolic effects of influenza virus infection on intracellular metabolite concentrations in MDCK cells (Ritter et al., 2010).

Another useful experimental method for analyzing cell culture metabolites involves stable isotope labeling, and either NMR or MS techniques are used to determine the labeling patterns. Together with metabolic flux analysis (MFA) (Quek et al., 2010), this approach allows tracing of the metabolic pathways and measurement of intracellular metabolic fluxes (Lin et al., 1993; Marin et al., 2004; Wittmann, 2007), which lead to an improved understanding of cell metabolism and regulatory mechanisms under different metabolic

states. Frequently used substrates for cell culture studies are ^{13}C -labeled Gluc and Gln, either uniformly labeled or position-specific labeled. For example, the investigation of CHO cell metabolism using isotopic tracers and MS revealed significant changes in energy and redox metabolism, oxidative pentose phosphate pathway and anaplerosis during different growth phases (Ahn and Antoniewicz, 2011). In particular, the glycolytic flux from Gluc to Lac and the rate of anaplerosis (from Pyr to OAA and from Glu to 2-OG) were increased at the exponential growth phase in CHO cells compared to the stationary phase. However, although MFA is a powerful tool to analyze cell metabolism, studies that are exclusively based on the known biochemistry and extracellular rates without knowledge of intracellular metabolite concentrations or details of the enzyme kinetics can be highly questionable, as several assumptions on, e.g., fluxes in cyclic metabolic pathways have to be made that not necessarily reflect the true *in vivo* situation of a cell under the specific conditions considered (Bonarius et al., 1996; Nadeau et al., 2000; Sidorenko et al., 2008; Wahl et al., 2008).

The metabolism of adherent MDCK cells during growth, product formation and under different cultivation conditions has been extensively studied at the Bioprocess Engineering group (MPI Magdeburg). Different analytical tools were developed to determine extra- and intracellular metabolite concentrations (Genzel et al., 2004b; Ritter et al., 2008), and MFA was used to analyze the cell metabolism (Sidorenko et al., 2008; Wahl et al., 2008). For example, previous work on MDCK cell metabolism revealed that the addition of Gln or Pyr to cell culture media resulted in distinct differences in extra- and intracellular metabolite concentrations as well as in metabolic fluxes in glycolysis and TCA cycle (Genzel et al., 2005; Sidorenko et al., 2008; Wahl et al., 2008). In particular, cells grew to similar cell densities without ammonia release when Pyr was added instead of Gln. Additionally, Gluc uptake and Lac release was lower. However, concerning the interpretation of experimental data, for example, measured changes in extracellular concentrations and calculated metabolic fluxes, still some open questions remained. Several assumptions were made for calculation of flux distributions from extracellular concentrations concerning the activity of critical enzymes in metabolic pathways required for MFA. For example, the flux of Gluc carbon through the anaplerotic pathway via carboxylation of Pyr (PC) was neglected and assumed to be zero in both cultivations (Gln and Pyr-containing conditions) (Sidorenko et al., 2008). For PDH a zero assumption for the flux was also made for Gln-containing medium, whereas for Pyr-containing medium a transport of Pyr into the mitochondria (TCA cycle) was found. Therefore, with regard to the dependence of maximum catalytic activities on certain enzymes

and to the maximum flux through metabolic pathways, key enzyme activity measurements could give further insights into primary energy metabolism and precursor pools required for product formation (Fitzpatrick et al., 1993; Newsholme and Crabtree, 1986; Vriezen and van Dijken, 1998b). Finally, label-free approaches based on measuring enzyme activities could avoid the need for ^{13}C -based MFA, and thus, the use of comparatively expensive substrates and equipment, and sophisticated data analysis tools.

2.2 Measuring enzyme activities in mammalian cells

The measurement of key metabolic enzyme activities using, e.g., enzymatic cycling assays is an additional analytical tool to assess metabolism in mammalian cell cultures. As enzymes play a key role in all metabolic processes (e.g., controlling biochemical pathways), the influence of key enzymes on metabolic fluxes and the measurement of enzyme activities in cell extracts will be described in the following (see chapters 2.2.3 and 2.2.4). However, another aim of this work was to produce and to biochemically characterize a coupling enzyme for the application in sensitive cycling assays. Therefore, the first parts of this chapter provide an overview of the basics of enzyme kinetics.

Enzymes are highly specific and efficient protein catalysts that mediate almost all of the biochemical reactions in a cell. They modify and dramatically increase the rate of a given reaction by lowering the activation energy needed to start the reaction without being consumed in the process (Figure 2.6).

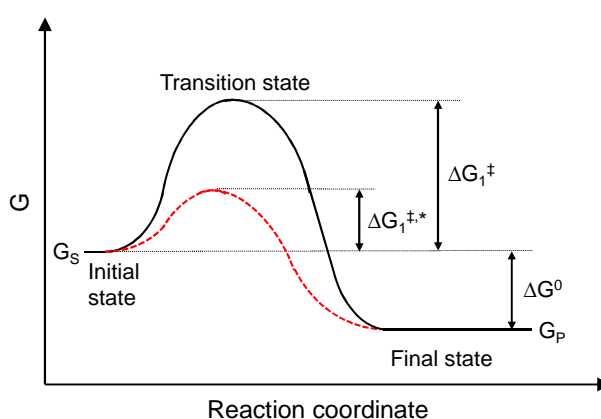


Figure 2.6: Free energy diagram according to the transition state theory for a simple unimolecular exothermic reaction ($S \rightarrow P$, indices) (modified from Rogers and Gibon, 2009). G_S and G_P represent the average free energies per mole for the reactant S and the product P, respectively. The ΔG^0 is the standard state free energy change for the reaction. Reactant S must pass the transition state in order to be transformed to product P. The ΔG_1^{\ddagger} and the $\Delta G_1^{\ddagger*}$ indicate the activation energy needed to perform this transition for the uncatalyzed (solid graph) and catalyzed (dashed, red graph) reactions, respectively.

The transition state theory suggests that a temporary species with high free energy ΔG_1 (activated complex) is formed when the reactant molecules come into contact with each other and the reaction proceeds (bonds are breaking and/or new bonds are forming) (Cornish-Bowden, 2004). The state of the reaction at which the free energy reaches a maximum is defined as the transition state. The important criterion is that colliding molecules must have sufficient energy to overcome this potential energy barrier, known as the activation energy (ΔG^\ddagger), to react. As mentioned above, enzymes function by lowering the activation energy of a particular reaction, thus accelerating reactions or even permitting a reaction that practically takes only place with a catalyst. For example, orotidine 5'-phosphate (OMP), the immediate biosynthetic precursor of UMP, decarboxylates with a half time of 78 million years in neutral aqueous solution at room temperature, whereas OMP decarboxylase enhances the reaction rate by a factor of 10^{17} (Radzicka and Wolfenden, 1995). An accepted model used to explain the enzymatic catalysis is the induced fit theory, where the enzyme binds its substrate to form an enzyme-substrate (ES) complex (Koshland, 1958). The substrate causes a change in the conformation of the active side, which brings the catalytic groups into the proper orientation for reaction. Furthermore, the conformation of the substrate can also be altered upon binding, and thereby reducing the amount of energy required for the conversion of the reactant into a product (Rogers and Gibon, 2009). However, most enzyme-catalyzed reactions are more complex than illustrated in Figure 2.6. Frequently, more substrates are involved, and the reaction consists of more steps with intermediates and multiple transition states (Cornish-Bowden, 2004).

2.2.1 The Michaelis-Menten equation

In 1913 Michaelis & Menten analyzed in their studies the hydrolysis of sucrose into Gluc and fructose by performing initial velocity measurements on the enzyme invertase, and showed that the rate of an enzyme-catalyzed reaction is proportional to the concentration of the ES complex predicted by the Michaelis-Menten equation (Johnson and Goody, 2011; Michaelis and Menten, 1913). This formulation was then further developed by Briggs & Haldane (1925) and is described in the following.

The mechanism of an irreversible reaction ($S \rightarrow P$) catalyzed by an enzyme E, where the first step in the reaction is the substrate binding and the second step is the catalytic conversion of the substrate into product, can be depicted as:



The k_1 ($\text{mM}^{-1} \text{min}^{-1}$) is the association rate constant of ES binding, and k_{-1} (min^{-1}) and k_2 (min^{-1}) are the rate constants of the ES complex releasing free enzyme E and substrate S or product P, respectively. With $[E]=[E_0]-[ES]$, where $[E_0]$ is the total amount of enzyme present and $[ES]$ the amount of enzyme in the ES complex, the following rate equation can be formulated:

$$\frac{d[ES]}{dt} = k_1 \cdot ([E_0] - [ES]) \cdot [S] - k_{-1} \cdot [ES] - k_2 \cdot [ES] \quad \text{(Equation 2.2)}$$

Briggs & Haldane (1925) assumed that the concentration of the ES complex will not change and $[ES]$ will rapidly approach a steady state under conditions $[S] \gg [E_0]$, thus $d[ES]/dt \sim 0$ (steady-state assumption). Therefore, equation 2.2 can be rearranged to:

$$[ES] = \frac{k_1 \cdot [E_0] \cdot [S]}{k_{-1} + k_2 + k_1 \cdot [S]} \quad \text{(Equation 2.3)}$$

The second step in this single-substrate reaction ($[ES] \rightarrow [E] + [P]$) is a simple first-order reaction. The rate of the reaction is directly proportional to the concentration of the ES complex ($[ES]$) at all values of $[S]$ and is given by $v = k_2 [ES]$ (Lineweaver and Burk, 1934), thus equation 2.3 can be represented as:

$$v = \frac{k_1 \cdot k_2 \cdot [E_0] \cdot [S]}{k_{-1} + k_2 + k_1 \cdot [S]} = \frac{k_2 \cdot [E_0] \cdot [S]}{\frac{k_{-1} + k_2}{k_1} + [S]} \quad \text{(Equation 2.4)}$$

The term $(k_{-1} + k_2)/k_1$ including the three rate constants can be written as K_m , known as the Michaelis constant, and the dissociation constant k_2 is generally denoted as k_{cat} , the turnover number of the enzyme:

$$v = \frac{k_{cat} \cdot [E_0] \cdot [S]}{K_m + [S]} \quad \text{(Equation 2.5)}$$

However, the true molar concentration of an enzyme ($[E_0]$) is often unknown. The problem is commonly avoided by combining k_{cat} and $[E_0]$ into a single constant V_{max} (the limiting maximum rate) (Cornish-Bowden, 2004), thus yielding the widely known Michaelis-Menten equation:

$$v = \frac{V_{\max} \cdot [S]}{K_m + [S]} \quad \text{(Equation 2.6)}$$

Because the enzyme molarity is usually unknown, the catalytic activity (v) is often defined as Unit (U), where 1 U is the amount of enzyme that can catalyze the conversion of 1 μmol of substrate (or the formation of 1 μmol of product) per minute under standard conditions (Cornish-Bowden, 2004).

Equation 2.6 contains two important parameters, V_{\max} and K_m , whose values can be used to assess the enzyme's properties. The V_{\max} is the limiting value of v at which the catalytic rate reaches its maximum (achieved at saturating $[S]$). In general, the Michaelis constant K_m is defined as the substrate concentration at which the catalytic rate of the reaction is at half the maximum ($v=V_{\max}/2$). Furthermore, as K_m is defined as $(k_{-1}+k_2)/k_1$, this value also provides an indication of the binding strength of the enzyme to its substrate (Rogers and Gibon, 2009). However, only if k_2 is much smaller than k_{-1} , does a low K_m indicate strong binding. On the other hand, a large K_m indicates a lower affinity of the enzyme for its substrate.

2.2.2 Graphical determination of K_m and V_{\max}

The hyperbolic relationship between the substrate concentrations and the rate of reaction for a simple enzyme-based reaction obeying the Michaelis-Menten equation is shown in Figure 2.7.

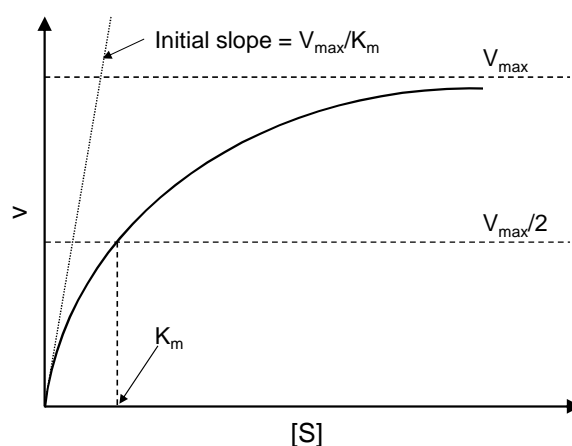


Figure 2.7: Relationship between the reaction rate (v) and substrate concentration ($[S]$) for an enzymatic reaction based on equation 2.6. The Michaelis constant (K_m) is equal to $[S]$ corresponding to one-half V_{\max} .

At very low substrate concentrations ($[S] \ll K_m$), the reaction rate (v) is directly proportional to $[S]$ (first-order dependence):

$$v = \frac{V_{\max} \cdot [S]}{K_m} \quad \text{(Equation 2.7)}$$

When $[S]$ is equal to K_m , equation 2.6 simplifies to:

$$v = \frac{V_{\max} \cdot [S]}{2 \cdot [S]} = \frac{V_{\max}}{2} \quad \text{(Equation 2.8)}$$

At very large values of $[S]$ ($[S] \gg K_m$), the reaction rate (v) is essentially independent to $[S]$ (zero-order dependence):

$$v = V_{\max} = k_{cat} \cdot E_0 \quad \text{(Equation 2.9)}$$

Although the best method for analyzing enzyme data is by fitting the experimentally acquired data directly to the Michaelis-Menten equation using nonlinear regression, the determination of K_m and V_{\max} is commonly achieved by using double-reciprocal plots. For example, Lineweaver & Burk (1934) introduced an analysis of enzyme kinetics based on the plotting of the reciprocals of v and $[S]$. Therefore, equation 2.6 can be transformed into:

$$\frac{1}{v} = \frac{K_m}{V_{\max}} \cdot \frac{1}{[S]} + \frac{1}{V_{\max}} \quad \text{(Equation 2.10)}$$

A plot of $1/v$ against $1/[S]$ gives a straight line with a slope of K_m/V_{\max} , and intercepts of $1/V_{\max}$ and $-1/K_m$ on the y-axis and on the x-axis, respectively (Figure 2.8 A). However, the reciprocals distort the experimental error, which means that small errors in v at low substrate concentrations produce large errors in $1/v$ and, hence, this could lead to large errors in the determination of K_m and V_{\max} (Cornish-Bowden, 2004).

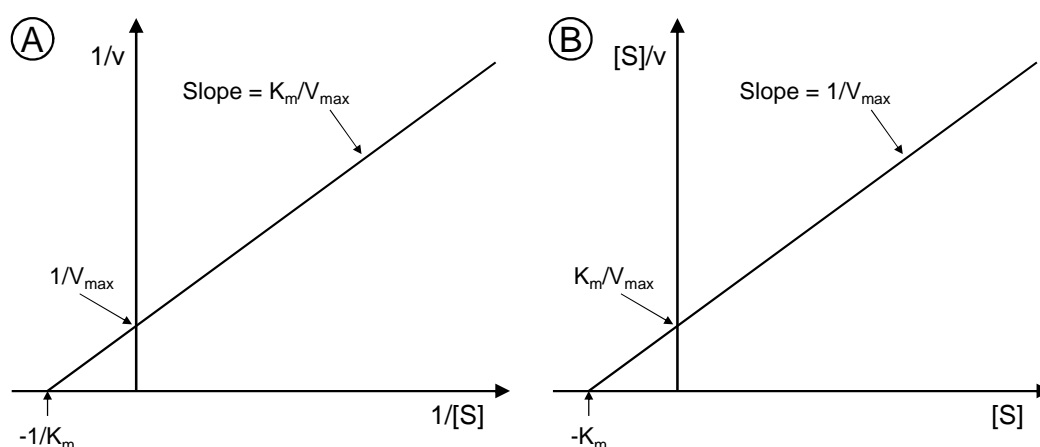


Figure 2.8: (A) Lineweaver-Burk plot (double-reciprocal plot of $1/v$ against $1/[S]$) and (B) the Hanes plot ($[S]/v$ against $[S]$) of the Michaelis-Menten equation (Hanes, 1932; Lineweaver and Burk, 1934).

Another plot, sometimes referred to as the Hanes plot, can be obtained by multiplying both sides of equation 2.10 by the substrate concentration (Hanes, 1932):

$$\frac{[S]}{v} = \frac{1}{V_{\max}} \cdot [S] + \frac{K_m}{V_{\max}} \quad \text{(Equation 2.11)}$$

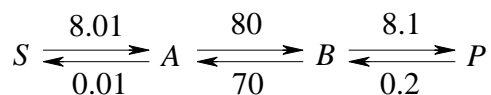
The Hanes plot ($[S]/v$ against $[S]$) is more reliable for the graphical visualization of enzyme data as the error is more evenly distributed over a wide range of $[S]$ (Cornish-Bowden, 2004). This plot gives a straight line with a slope of $1/V_{\max}$, and the intercepts on the y-axis and on the x-axis are K_m/V_{\max} and $-K_m$, respectively (Figure 2.8 B). However, the correlation coefficient R (widely used goodness-of-fit measure) is not applicable, as the independent variable $[S]$ also appears on the dependent axis.

The following chapter focuses on key enzymes, which are important for the regulation of the metabolism and how they can be used to assess fluxes through metabolic pathways.

2.2.3 Key enzymes and metabolic fluxes

In vitro studies on single enzyme reactions might not provide information on metabolic processes as they occur *in vivo*, but can give valuable information on the metabolic flux. The difficulty is to develop assays that truly mimic the *in vivo* physiological conditions (different cell compartments, metabolite concentrations, pH levels) for all enzymes under investigation. However, measurement of enzyme activity can identify the steps in a metabolic pathway that are likely to be rate-limiting and can provide the potential for alternative pathways under different cultivation conditions or in different cells.

The metabolic flux through a pathway depends not only on metabolite concentrations but is also closely related to the cellular amount of metabolic enzymes as well as to regulatory mechanisms (e.g., allosteric effects). Biochemical reactions in the metabolic network can be divided into two classes: near-equilibrium and non-equilibrium reactions. Newsholme and Crabtree (1986) described near-equilibrium reactions as those in which both the forward and the reverse catalytic process are much greater than the overall flux. Hence, the catalytic activity of the enzyme is high in relation to the activities of other enzymes in the metabolic pathway. Non-equilibrium reactions are potential control points in a metabolic pathway. The rate of the reverse reaction is much lower than the rate of the forward reaction (e.g., an enzyme catalyzes a reaction with comparatively low activity in the metabolic pathway). This is exemplarily shown in the following equation 2.12. The upper and lower numbers represent the rates of the forward and the reverse reaction, respectively (Newsholme et al., 1979):



(Equation 2.12)

The reactions $S \rightarrow A$ and $B \rightarrow P$ are therefore non-equilibrium. The reaction $A \rightarrow B$ is near-equilibrium ($\Delta G \sim 0$) as the difference in the rates of the forward and the reverse reaction is only 10 % and the rate of the forward reaction is 10-fold higher than the overall flux through the hypothetical pathway.

If an enzyme catalyzes a non-equilibrium reaction in a metabolic pathway under substrate-saturating conditions, the catalytic rate of the reaction only depends on the amount of produced enzyme (zero-order dependence; see equation 2.9) and the reaction is known as the “flux-generating step” for the pathway. In a steady state, this reaction step initiates a defined flux ($S \rightarrow A$) to which all other reactions in the pathway must adjust (Newsholme and Crabtree, 1986; Newsholme et al., 1979). On the basis of this concept, a metabolic pathway can be defined as an enzyme-catalyzed reaction series that is initiated by a flux-generating step and ends with the loss of products to a metabolic sink (e.g., lipids) or to the surrounding environment (e.g., Lac and Ala). Alternatively, the end-product(s) can serve as pathway substrate(s) for key-enzymes that initiate rate-limiting steps in other metabolic pathways (Newsholme and Crabtree, 1986).

The assumption that the rate of a metabolic pathway is controlled by only one flux-generating step in the pathway seems to be rather unlikely. In fact, most metabolic enzymes work below their maximum capacities (low fractional saturation of total binding sites) *in vivo* to serve their physiological roles in the pathways (Suarez et al., 1997). This allows regulation by both substrate/product concentrations and modulation of binding affinity by allosteric effectors and covalent modifications (e.g., acetylation and phosphorylation) (Löffler, 2005; Suarez and Darveau, 2005). The glycolytic pathway, for instance, contains three potentially rate-limiting enzymes (HK, PFK, and PK; see chapter 2.1.1) that catalyze non-equilibrium reactions and are subjected to various forms of regulation (Dobson et al., 2002; Suarez et al., 1997). One could conclude that these key enzymes of glycolysis would be ideal candidates to control the metabolic flux through this pathway. Genetic engineering of cells using recombinant DNA technology allows increasing the amount of a certain enzyme activity through an increase in the respective gene copy number. However, an overexpression of one or several enzymes of glycolysis in, for example, the fermentative yeast *Saccharomyces cerevisiae* did not result in a significant effect on the glycolytic flux (Davies and Brindle, 1992; Niederberger et al., 1992; Schaaff et al., 1989; Smits et al., 2000). Thus, the central carbon metabolism of

S. cerevisiae is tightly regulated and robust towards most changes. It was suggested that only the simultaneous elevation of a group or all enzymes in a metabolic pathway could produce significant increase in the pathway flux (Niederberger et al., 1992). This is also proposed by the “metabolic control theory” (Heinrich and Rapoport, 1974; Kacser and Burns, 1973), which states that the flux through a linear pathway is controlled by multiple steps and analysis of the regulation of a metabolic pathway must consider the whole reaction chain. The metabolic control analysis was successfully applied to studies on physiological control of flux through various metabolic pathways (Fell, 1992; Fell, 1998; Fell and Thomas, 1995; Thomas et al., 1997). The authors revealed that the development of pathways with high flux rates requires the modulation of enzyme activities at multiple sites. A characteristic *in vivo* behavior of “multisite modulation” is the coordinate change in enzyme levels whose relative contribution can change in response to changes in physiological or environmental conditions (Fell and Thomas, 1995).

However, past studies showed that maximum activities (V_{\max}) of certain key enzymes (e.g., HK, PFK, and G6PDH) *in vitro* can provide a quantitative indication of the maximum flux through metabolic pathways *in vivo* (Ardawi and Newsholme, 1982; Blomstrand et al., 1983; Board et al., 1990; de Almeida et al., 1989; Newsholme et al., 1979; Newsholme et al., 1986). The maximum capacity for flux (V_{\max} , see equation 2.9) is a function of the total amount of enzyme/enzyme concentration ($[E_0]$) and catalytic efficiency (k_{cat}), and thus, V_{\max} values set theoretical upper limits to flux in metabolic pathways (see Figure 2.7). Furthermore, these values, when obtained under optimal (opposed to physiological) *in vitro* conditions, can be expressed in the same units as measured or calculated *in vivo* flux rates (Suarez et al., 1997). For instance, close matches between enzymatic flux capacities ($V_{\max, \text{HK}} \sim 40 \mu\text{mol/g/min}$) and maximum physiological flux rates (glycolytic flux rate $\sim 30 \mu\text{mol/g/min}$) were found in muscles of flying honeybees (Suarez et al., 1996). In combination with other data (e.g., intracellular metabolite concentrations), these rates (V_{\max} and *in vivo* flux) provide insights into enzyme function, and can be used to correlate capacities to physiological loads (Neermann and Wagner, 1996; Staples and Suarez, 1997; Suarez et al., 2009). Finally, enzyme data can be used to establish and improve mathematical models for, e.g., the selection of available pathways, the identification of optimal metabolic pathways or the prediction of metabolic flux distributions (De et al., 2008; Kurata et al., 2007; Rossell et al., 2011).

2.2.4 Determination of maximum enzyme activities

Most studies of enzymes, which involve the detection of their catalytic activity, rely on assays that were developed and optimized for the 96-well microplate format (Ashour et al., 1987; Gibon et al., 2004). Enzyme activity is determined by measuring the quantity of product formed or substrate consumed per unit time under specified experimental conditions (e.g., temperature, pH, and ionic strength). When the concentrations of enzymes are much smaller than their substrate concentrations ($[E_0] \ll [S]$, e.g., in highly diluted cell extracts), most enzymes obey the Michaelis-Menten kinetics (Segel, 1988). The maximum catalytic activity of an enzyme (V_{\max}) can then be measured in optimized assays where the conditions, including the substrate concentrations, are kept nearly constant so that the reaction rate solely depends on the concentration/amount of enzyme under investigation (pseudo-zero-order reaction, see equation 2.9) (Rogers and Gibon, 2009). However, although the equipment for enzyme activity assays is relatively inexpensive and these assays provide quantitative data, the large diversity of enzymes, which requires determination of specific assay conditions for each single enzyme under investigation, makes high-throughput studies difficult. A promising approach towards generating large datasets of enzyme activities under different conditions was presented by Gibon et al. (2004), where an efficient robot-based platform using 96-well microplates was developed. In this assay system, established for plant cells, subsets of enzymes could be grouped in modules that share a common detection method (e.g., for NADPH).

2.2.4.1 Overview on available assay procedures

The most widely used procedures for the measurement of enzyme activities are spectrophotometric (Bergmeyer et al., 1983; Bergmeyer et al., 1984), fluorometric (Castro and Fernández-Romero, 1991; Donato et al., 2004; Marx et al., 2001), and luminometric methods (Bessho et al., 1988; Ching, 1982; Hanocq-Quertier et al., 1988). Typically, this involves the monitoring of the change in absorbance at an accessible wavelength with a spectrophotometer. Many enzymatic reactions use the oxidized or reduced forms of $\text{NAD}^+(\text{P})$, where the reduced forms exploit large absorbance at a wavelength of 340 nm (Horecker and Kornberg, 1948). However, $\text{NAD}(\text{P})\text{H}$ can also be measured by using its fluorescent properties (Lohmann et al., 1988). In cases, where these two forms of dinucleotides are not directly involved, it may still be possible to couple the reaction of interest to detect a spectrophotometric change (see chapter 2.2.4.4).

Radiometric assays measure the rate of incorporation into substrates or release of radioactivity from labeled substrates and are generally more sensitive (Broschat et al., 2002; Johnson and Russell, 1975; Thorner and Paulus, 1971). However, these methods lack the convenience and safety needed for broad application in science and industry.

Furthermore, enzyme activities can also be assessed by amperometric assays or by MS methods. The first procedure involves, e.g., oxygen or hydrogen peroxide electrodes that measure signal intensities of enzymatic reactions as a function of the corresponding electric current (Gyurcsanyi et al., 2002; Sagi et al., 2006; Wallace et al., 1977). The second principle is based on mass differences between substrate and product peaks, and has the advantage that most natural substrates and/or products of enzymatic reactions can be detected directly, and thus, does not require chromophore or radiolabelling (Bothner et al., 2000; Greis, 2007; Rathore et al., 2010; Shen et al., 2004). Both amperometric and MS-based assay systems for the measurement of enzyme activities are evolving technologies and amenable to high-throughput mode, but require comparatively expensive and sophisticated equipment as well as highly trained personnel.

2.2.4.2 Continuous and discontinuous assay systems

Several continuous and discontinuous assays were developed for the measurement of enzyme activities. In a continuous assay system, the progress of an enzyme-catalyzed reaction is directly monitored by measuring product accumulation or substrate decrease over time, where the signal is usually being followed photometrically or fluorimetrically (Eisenthal and Danson, 2002). In case the changes in product or substrate concentrations cannot be observed directly, it is a common practice to use one or more coupling enzymes to generate a detectable product. An advantage of these continuous assays is that the progress of reaction is measured immediately and initial rates can be directly checked for linearity. Therefore, continuous assays are generally preferred over discontinuous approaches as they give more information during the measurement, for instance on substrate depletion, product inhibition or enzyme stability. During the progress of an enzymatic reaction, the amount of product accumulated is proportional to the amount of substrate converted. Therefore, the application of continuous methods may be restricted to purified enzymes (highly concentrated) or enzymes that are highly active in raw cell extracts.

In a discontinuous assay, the enzymatic reaction is stopped by addition of a strong acid/base or by heat after a defined time period and the product may then be measured with a second

specific reaction (Eisenthal and Danson, 2002; Rogers and Gibon, 2009). A potential disadvantage of this type of assay is that progress curves (enzymatic reactions) are not monitored directly, they are more time-consuming (more pipetting steps), and volume inaccuracies may be introduced. Furthermore, it has to be checked that the estimated rates are truly proportional to the enzyme concentration. However, these methods allow many enzyme assays to be run in parallel and different steps of the procedure can easily be automated (e.g., robotic pipetting platform) (Gibon et al., 2004). Furthermore, the first step in discontinuous assays (the enzymatic reaction) can be performed with low volumes (e.g., 20 μ L per well of a 96-well microplate), which can significantly decrease the cost of assays when expensive reagents are to be used. Finally, the analytical sensitivity of the enzyme assay can be increased significantly when the determination of the product (second step) is performed with tracer or kinetic methods (e.g., enzymatic cycling) (Lowry, 1980; Rogers and Gibon, 2009). This offers the possibility to measure enzymes from raw cell extracts that possess only low activity, and thus, only produce small quantities of a product in a certain time interval.

2.2.4.3 Increasing the sensitivity by enzymatic cycling

The method of enzymatic cycling allows the amplification of analytical sensitivity (see Figure 2.9) for a variety of biochemical substances and has been developed and applied, for instance, to quantitatively determine enzyme activities (Chi et al., 1988; Gibon et al., 2004; Lowry et al., 1978; Lowry et al., 1983; Sulpice et al., 2007) or the amount of metabolites (Gibon et al., 2002; Khampha et al., 2004; Valero and Garcia-Carmona, 1998; Valero et al., 1995). In such a cycling system, a target metabolite is regenerated by two enzymes acting in opposite directions, which leads to a constant concentration of the recycling substrate (Lowry, 1980; Passonneau and Lowry, 1993).

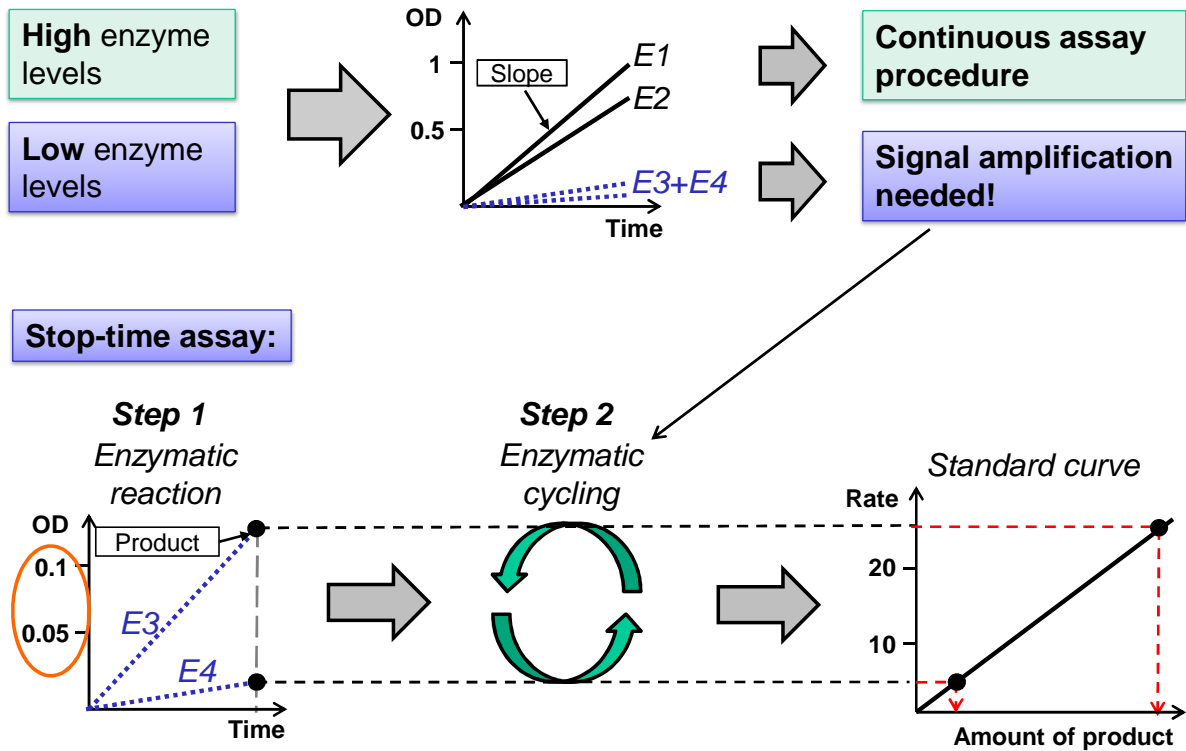


Figure 2.9: Choice of assay for determination of enzyme activity.

The enzyme activities E_1 and E_2 are high enough to be measured directly in a continuous assay. However, enzyme samples that were highly diluted to reduce interferences from other components in the cell extract (e.g., specific or non-specific activators or inhibitors) or enzymes that show low activities in cell extracts (E_3 and E_4 , in blue) are difficult to detect by a continuous assay procedure. Therefore, the signal from the enzymatic reaction (step 1) needs to be amplified, which can be done by an enzymatic cycling system (step 2).

The amplification of an enzymatic activity in a discontinuous (stop-time) assay using the enzymatic cycling method, where A and B is the substrate and the product of the enzyme to be measured (E_1), respectively, may be described as follows:



In equation 2.14, S_2 and B are the substrates for the cycle enzyme E_2 , and S_3 and C are the substrates for the cycle enzyme E_3 , where B and C are the recycling substrates. P_2 and P_3 are products of the enzymatic reactions that accumulate at each turn of the cycle.

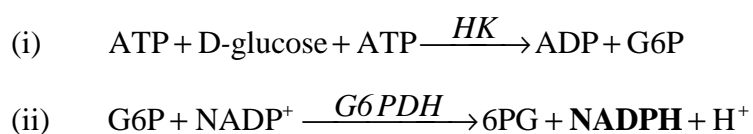
It is assumed, that the reaction rate v_1 of the first step (equation 2.13) remains constant (steady state), when the concentration of A is saturating or the consumption of A during the

reaction time is very low ($[A] \gg [E_1]$). The S_2 and S_3 concentrations of the second step (equation 2.14) are also assumed to be saturating or remain constant during the cycling reaction under conditions $[S_2] \gg [E_2]$ and $[S_3] \gg [E_3]$. Furthermore, the concentrations of B and C must be clearly lower than their respective Michaelis constants ($K_{m,B}$ and $K_{m,C}$ towards E_2 and E_3 , respectively) during the cycling, so that the reaction rates (v_2 and v_3) are proportional to their respective concentrations. Under these conditions, a small quantity of B produced by the enzymatic reaction of the first step can yield to the formation of many molecules of the products P_2 and P_3 . Thus, the cycling system acts as a chemical amplifier for the E_1 activity, when either P_2 or P_3 is measured. For detailed information on kinetic analyses of these systems, the reader is referred to the studies performed by Valero and García-Carmona (Valero and García-Carmona, 1996; Valero et al., 2004; Valero et al., 1997; Valero et al., 1995).

Discontinuous/indirect assays with enzymatic cycling provide a 100 to 10,000-fold higher analytical sensitivity compared to conventional (continuous/direct) assays. This has the advantage that interferences from raw cell extracts (e.g., unwanted reactions, unrelated optical absorbance, or turbidity) can be avoided or significantly reduced (Rogers and Gibon, 2009). Furthermore, enzymes with low catalytic activity can be determined precisely, and if the amplification achieved is still insufficient, sensitivity can be further increased by double cycling (Lowry, 1980). Many different cycling methods are described for the quantification of low amounts of a substance in the literature. However, the most suited cycling systems for the determination of enzyme activities are the G6P cycle (Gibon et al., 2002; Misaki, 1987), the NAD^+ cycle (Bernofsky and Swan, 1973), and the $NADP^+$ cycle (Nisselbaum and Green, 1969; Vilee, 1962). For example, enzymes belonging to the $NAD(P)^+$ -dependent dehydrogenase family can be assayed by a G6PDH/phenazine ethosulfate (PES) cycle or an alcohol dehydrogenase (ADH)/PES cycle (Gibon et al., 2004). As these cycling systems do not distinguish between oxidized and reduced forms, the excess pyridine nucleotide must be destroyed. When the product is an oxidized coenzyme, the enzymatic reaction can be stopped with HCl ($NAD(P)^+$ is stable at low pH and labile at high pH), otherwise, NaOH can be used to adjust the pH ($NAD(P)H$ is stable at high pH and destroyed at low pH).

2.2.4.4 Coupling enzymes

If an enzyme catalyzes a reaction, where the products can not be directly quantified or the enzymatic reaction under study has an unfavourable equilibrium constant (e.g., the forward reaction of GLDH; $K_{eq} = 3.87 \times 10^{-3}$ mM, Williamson et al., 1967), coupling enzymes can be included to the assay mixture to convert one of the reaction products to a measurable metabolite or displace the equilibrium, respectively (Cornish-Bowden, 2004). For example, the HK-catalyzed phosphorylation of Gluc can be assayed by coupling the production of G6P to the formation of NADPH using the G6PDH:



In a coupled assay, it is essential that the rate of the measured reaction is directly proportional to the concentration of the enzyme under investigation and does not become limiting. Thus, the coupling enzyme(s) must be present in sufficient excess in terms of activity. For the above reaction, the activity of the G6PDH coupling enzyme must be high enough to oxidize G6P as fast as it is produced, so that the rate of NADP^+ reduction corresponds to the rate of the HK reaction. However, high concentration of coupling enzyme can lead to complications because of unwanted side reactions (e.g., G6PDH can use Gluc as substrate) (Storer and Cornish-Bowden, 1974). Therefore, appropriate corrections for the measured rate must always be performed by recording the blank rate in the absence of substrate (e.g., ATP in the assay for HK).

If an important coupling enzyme is needed to detect the activity of an enzyme under study but is not commercially available or cannot be replaced by a similar enzyme from a different species as it has, e.g., different substrate affinities, it may be possible to produce this coupling enzyme recombinantly when the specific gene sequence is known. In the following chapter, a widely used expression system is presented, which is based on the yeast *Pichia pastoris*.

2.3 The *Pichia pastoris* expression system

Many different heterologous expression platforms can be used for the production of intracellular or secreted proteins (e.g., *Escherichia coli*, *S. cerevisiae*). However, the methylotrophic yeast *P. pastoris* as host species has been shown to be superior to other eukaryotic and prokaryotic expression systems due to its capacity for post-translational modifications (e.g., glycosylation) and ease of purification of secreted products (reviewed in Cregg et al., 2000; Li et al., 2007; Romanos et al., 1992).

P. pastoris is known as a Crabtree-negative organism, which does not show ethanol production followed by repression of respiratory enzymes when exposed to sugar excess (*P. pastoris* is more sensitive to changes in oxygen concentration than to variations in substrate levels) (Alexander and Jeffries, 1990; van Urk et al., 1989). Its preference to respiratory growth facilitates high cell density cultivation processes using low-cost chemically defined media, and its ability to metabolize methanol as a sole carbon source greatly prevents contamination with other microorganisms during the production process. *P. pastoris* can grow in a relatively broad pH range of 3 to 7 in a bioreactor (Cregg et al., 1993). Furthermore, *P. pastoris* can, to a certain degree, perform post-translational modifications on proteins, such as glycosylation, polypeptide folding, or disulphide bond formation. Another advantage of *P. pastoris* is its classification as GRAS (generally recognized as safe) because yeast cells do not have endotoxin and viral contamination problems associated with bacteria or with biologicals produced in mammalian cells, respectively (Cereghino and Cregg, 2000; Gellissen et al., 2005). Finally, the availability of the *P. pastoris* expression system as a “ready-to-use” kit including different strains and expression vectors facilitates the development of new processes for recombinant products (Invitrogen, 2002a; Invitrogen, 2002b).

Recombinant proteins can either be produced intracellularly or secreted into the culture medium. To ensure secretion of the product, the pre-pro leader sequence of *S. cerevisiae* mating factor alpha (α -MF) is often used (Cregg, 2007). The extracellular production of recombinant biomolecules, such as antibodies or peptides, is generally preferred (Tschopp et al., 1987b), as *P. pastoris* secretes only very low levels of native proteins, which simplifies the purification of the target product (Cregg et al., 2000; Romanos et al., 1992). However, if the product quality is negatively affected (e.g., unstable enzyme with rapidly decreasing activity in the culture broth due to adverse cultivation conditions, i.e., medium, pH and

temperature influences), intracellular expression might be the only method. Many different expression strains of *P. pastoris* with multiple genotypes and three phenotypes are available for research and industry purposes (Daly and Hearn, 2005). For example, the *P. pastoris* GS115 and KM71 strains are the most commonly used expression hosts and are defective in the histidinol dehydrogenase gene (*HIS4*), which allows transformants to be selected based on their ability to grow in histidin-free medium. The GS115 strain contains functional copies of both the alcohol oxidase 1 gene (*AOX1*) and the alcohol oxidase 2 gene (*AOX2*), where the *AOX1* promoter regulates 85 % of the alcohol oxidase production (Cregg et al., 1989). This strain grows on methanol at the wild-type rate and is therefore designated as Mut⁺. The KM71 strain, however, contains a deleted *AOX1* gene replaced with the *S. cerevisiae ARG4* (argininosuccinate lyase) gene (Cregg et al., 2000). As a result, this strain relies on the much weaker *AOX2* gene for alcohol oxidase and grows only slowly on methanol. The phenotype is therefore termed ‘methanol utilization slow’ (Mut^S). However, if both *AOX* genes are deleted, as it is the case for the expression host MC100-3 (Chiruvolu et al., 1997), this strain is totally unable to grow on methanol (Mut⁻).

Recombinant *P. pastoris* strains are generally generated in three steps (Cereghino and Cregg, 2000; Higgins, 2001): (i) insertion of the gene of interest into an expression vector, (ii) introduction of the plasmid into the genome, and (iii) identification of recombinants expressing the foreign gene product. Most *P. pastoris* expression vectors contain an origin of replication and an ampicillin resistance gene for plasmid replication and maintenance in *E. coli*, an expression cassette and one or more functional markers (e.g., *HIS4* and/or the kanamycin resistance gene). The expression cassette is often composed of the 5' promoter sequence of *AOX1* followed by a multiple cloning site (MCS) for insertion of the foreign gene and the transcription termination sequence from the *P. pastoris AOX1* gene that directs efficient 3' processing and polyadenylation of the mRNAs (Koutz et al., 1989; Li et al., 2007). The *P. pastoris* alcohol oxidase 1 promoter is tightly regulated: the expression is completely repressed under growth on Gluc or glycerol and strongly induced when the yeast is exposed to methanol (Tschopp et al., 1987a). However, in cases where the *AOX1* promoter is inappropriate for certain heterologous protein production processes, alternative promoters that are not (or not necessarily) induced by methanol, such as the *GAP* (glyceraldehyde-3-phosphate dehydrogenase gene) or the *FLDI* (formaldehyde dehydrogenase gene) promoters may be useful (Shen et al., 1998; Waterham et al., 1997).

3 Materials and Methods

All chemicals, consumables, equipment, and standard operating procedures (SOPs) used in this study can be found in the appendix. All SOPs were established in the Bioprocess Engineering group of the MPI for Dynamics of Complex Technical Systems (Magdeburg, Germany). Ultra-pure water from a Milli-Q system (Millipore, Billerica, MA, USA) was used for dissolving chemicals. All assay validations were performed using the validation template “temp_vali_AR_v1.8.xls” (version 1.8) of the Bioprocess Engineering group.

3.1 Cell line and culture media

Adherent Madin-Darby canine kidney (MDCK) cells obtained from the European Collection of Animal Cell Cultures (No. 84121903) were used in this study. Cell thawing and cell passaging were done according to the SOPs Z/02 and Z/04. The number of passages was limited to a maximum of 20 steps.

Under serum-containing conditions cells were grown in GMEM-Gln or GMEM-Pyr. The cell culture media were produced according to the SOPs M/03 and M/04. In brief, GMEM-Gln composition was GMEM (Gibco/Invitrogen, Carlsbad, CA, USA) containing 2 mM Gln supplemented with Gluc (Sigma, Taufkirchen, Germany, final concentration 30 mM), 10 % (v/v) fetal calf serum (FCS, Gibco) and 2 g/L peptone (International Diagnostics Group, autoclaved 20 % (w/v) solution) and 48 mM NaHCO₃ (Merck, Darmstadt, Germany), whereas GMEM-Pyr composition was GMEM without Gln (Sigma) supplemented as GMEM-Gln but with additional 10 mM Pyr (Sigma). Under serum-free conditions cells were grown in Episerf (Gibco) supplemented with Gluc (final concentration 30 mM), Gln (final concentration 2 mM) and Pyr (final concentration 2 mM). Before the experiments, cells were cultivated in the respective medium for at least two passages to adapt cells to the different growth conditions. For virus culture the medium composition was GMEM containing 2 mM Gln supplemented with Gluc (final concentration 30 mM), and 2 g/L peptone (autoclaved 20 % (w/v) solution) and 48 mM NaHCO₃ (referred to as virus maintenance medium, VMM).

3.2 Cell culture

Cells were routinely cultured in six-well plates (10 cm²) containing 4 mL of GMEM-based medium or Episerf medium in a CO₂ incubator at 37 °C and 5 % CO₂. Inoculation of the cell culture plates was done with approximately 4 to 5 x 10⁵ viable cells per well. Cells were

grown to exponential phases (~2 days of growth, 1.0 to 1.5×10^6 viable cells/well) with GMEM-Gln (referred to as GMEM-Gln^{exp}) and GMEM-Pyr (referred to as GMEM-Pyr^{exp}) or to stationary phases (~5 days of growth, 3.5 to 4.0×10^6 viable cells/well) with GMEM-Gln (referred to as GMEM-Gln^{stat}), GMEM-Pyr (referred to as GMEM-Pyr^{stat}), and Episerf (referred to as Episerf^{stat}). Before storing, cells were washed twice with ice-cold phosphate-buffered saline (PBS, 8.0 g/L NaCl, 0.2 g/L KCl, 0.2 g/L KH₂PO₄, 1.15 g/L Na₂HPO₄). The complete plate was snap-frozen in liquid nitrogen and stored at -80 °C until further use.

3.3 Virus culture

Adherent MDCK cells were cultured in six-well plates containing 4 mL of GMEM-based medium (2 mM Gln, 30 mM Gluc, 10 % (v/v) FCS, 2 g/L peptone, 48 mM NaHCO₃) in a CO₂ incubator at 37 °C and 5 % CO₂ to the stationary phase (~5 days of growth, 3.5 to 4.0×10^6 cells/well). Before infection, cells were washed twice with PBS. For virus culture, serum-free VMM containing $\sim 2.0 \times 10^{-6}$ U/cell porcine trypsin (Gibco) was used. MDCK cells were either mock-infected or infected with MDCK cell-adapted human influenza virus A/Puerto Rico/8/34 (H1N1) from the Robert Koch Institute (RKI, Berlin, Germany) at a multiplicity of infection (MOI) of 5 or 20 as described by the SOP V/03 (titer of seed virus was 3.18×10^9 virions/mL, which was estimated by the TCID₅₀ assay – SOP V/08 version 2.1). Cells were washed twice with ice-cold PBS 9 hours post infection (hpi), and the complete plate was then snap-frozen in liquid nitrogen and stored at -80 °C until further use.

3.4 Analytical techniques

3.4.1 Cell concentration and cell viability

Cell concentration and viability were determined for samples from six-well plates by counting at least three separate wells per sampling time point (the mean was used for further analysis). Cells were counted using the trypan blue exclusion method in an automated cell counter (Vi-CELL[®], Beckman Coulter, Krefeld, Germany; cell type MDCK100, SOP G/21 version 1.5). Cells were detached from the growth surface with trypsin, and diluted with PBS. Briefly, the cells were washed twice with PBS and detached by exposure to 0.5 g/L trypsin/0.2 g/L EDTA (0.5 mL). The trypsin activity was stopped by addition of an equal volume of FCS to the cell suspension.

For the quantification of MDCK cells, an assay validation with weighted linear regression analysis (inhomogeneous variances) for a range between 5.0×10^4 and 1.0×10^7 cells/mL was performed (08.08.08). The limit of detection (LOD) was 1.7×10^4 cells/mL, the limit of quantitation (LOQ) was 5.0×10^4 cells/mL, and the relative standard deviation (SD) of the method was 8.9 %.

3.4.2 Extracellular metabolites

The metabolite concentrations were determined for supernatants from six-well plates by measuring at least three separate wells per sampling time point. Gluc, Lac, Gln, Glu, and Amm in cell culture medium were measured with a Bioprofile 100 Plus (Nova Biomedical, Waltham, MA, USA) according to the SOP A/02 (version 1.0). The relative SDs of the validated method are given in Table 3.1. Extracellular Pyr was determined directly after dilution of the samples with water by anion exchange chromatography and conductivity detection (BioLC system with eluent generator, DX320, Dionex, Sunnyvale, CA, USA) as described by Genzel et al. (2005).

Table 3.1: The validated range, LOD, LOQ, and the relative and absolute SD of the method for Gluc, Lac, Gln, Glu, and Amm measured with a Bioprofile 100 Plus.

Metabolite	Concentration (mM)	LOD (mM)	LOQ (mM)	Relative SD of the method (%)	Absolute SD of the method (mM)
Glucose	1.11-41.07	0.650	1.859	10.97	0.194
Lactate	2.22-33.30	0.921	2.775	1.58	0.278
Glutamine	0.20-2.60	0.136	0.411	4.67	0.041
Glutamate	0.20-2.60	0.072	0.217	3.35	0.022
Ammonium	0.20-5.20	0.057	0.172	2.22	0.017

Note. An assay validation with weighted linear regression analysis (inhomogeneous variances) was performed for Gluc (10.05.11), Gln (20.04.11), Glu (20.04.11), and Amm (04.05.11) measurements. For Lac (15.04.11), an unweighted quadratic regression analysis (homogeneous variances) was used.

3.4.3 Virus titer

For the quantitation of influenza virus, HA (hemagglutinin) activity was determined as described by Kalbfuss et al. (2008). The assay procedure, as well as the preparation of internal standards and chicken-erythrocyte suspensions was done according to the SOPs V/05 (version 2.2) and V/07. The HA assay was used with a well to well dilution of $1:2^{0.5}$ and a chicken-erythrocyte solution of $\sim 2.0 \times 10^7$ cells/mL. HA titers were determined in 96-well microplates with a plate reader (Tecan, Männedorf, Switzerland) at 700 nm, and extinction data were evaluated after Boltzmann sigmoid fitting using Microsoft® Excel spreadsheets.

The HA titers are expressed as \log_{10} HA units/100 μL with a relative SD of the validated method of 9.3 %.

3.4.4 Protein concentration

Total protein concentration was determined by the BCA assay (Pierce, Rockford, IL, USA) according to the manufacturer's protocol (microplate procedure) using bovine serum albumin as a standard.

For the measurement of protein concentration in the working ranges of 20 to 2,000 $\mu\text{g/mL}$ (standard test tube protocol) and 5 to 250 $\mu\text{g/mL}$ (enhanced test tube protocol), two assay validations with unweighted quadratic regression analysis (homogeneous variances) were performed. For the "standard" assay validation (23.10.09), the LOD was 40.02 $\mu\text{g/mL}$, the LOQ was 121.28 $\mu\text{g/mL}$, and the absolute and relative SD of the method was 12.13 $\mu\text{g/mL}$ and 1.77 %, respectively. For the "enhanced" assay validation (21.08.08), the LOD was 3.73 $\mu\text{g/mL}$, the LOQ was 11.30 $\mu\text{g/mL}$, and the absolute and relative SD of the method was 1.13 $\mu\text{g/mL}$ and 1.49 %, respectively.

3.5 Specific growth rate, doubling time and yield coefficient

The metabolism of adherent MDCK cells during growth on different substrates was assessed by calculating the maximum specific growth rate, doubling time and the total molar yield coefficients.

The maximum cell-specific growth rate μ_{\max} (h^{-1}) was estimated during the exponential growth phase based on equation 3.1.

$$\frac{dX}{dt} = \mu \cdot X(t) \quad \text{(Equation 3.1)}$$

X	cell concentration	(cells well ⁻¹)
μ	cell-specific growth rate	(h ⁻¹)

After integration, equation 3.1 has the solution:

$$\ln\left(\frac{X_2}{X_1}\right) = \mu \cdot (t_2 - t_1) \quad \text{(Equation 3.2)}$$

X_1	cell concentration at time point t_1	(cells well ⁻¹)
X_2	cell concentration at time point t_2	(cells well ⁻¹)
t_1	time point t_1	(h)
t_2	time point t_2	(h)

The μ_{\max} value was then determined by linear regression of the exponential growth phase data (see Figure 4.21).

The doubling time t_d (h) of the cells was calculated according to equation 3.3.

$$t_d = \frac{\ln(2)}{\mu_{\max}} \quad \text{(Equation 3.3)}$$

t_d	doubling time	(h)
μ_{\max}	maximum cell-specific growth rate	(h ⁻¹)

The total molar yield coefficients $Y_{\text{Lac/Gluc}}$ and $Y_{\text{Amm/Gln}}$ were calculated by equation 3.4.

$$Y_{P/S} = \frac{P_{\text{end}} - P_0}{S_0 - S_{\text{end}}} \quad \text{(Equation 3.4)}$$

$Y_{P/S}$	yield coefficient of any product/substrate pair	(mM mM ⁻¹)
P_0	product concentration at the beginning of cultivation	(mM)
P_{end}	product concentration at the end of cultivation	(mM)
S_0	substrate concentration at the beginning of cultivation	(mM)
S_{end}	substrate concentration at the end of cultivation	(mM)

3.6 Intracellular enzyme activity measurements

All chemicals for the enzyme activity measurements were purchased from Sigma (see appendix), except acetyl-CoA, NAD⁺, NADP⁺, NADH, and NADPH (Roche, Mannheim, Germany). Enzymes for analysis were purchased from Roche, except glycerol-3-phosphate oxidase from *Streptococcus thermophilus*, aspartate transaminase from pig heart, citrate synthase from porcine heart, diaphorase, glutamate dehydrogenase from bovine liver, creatine kinase, phosphoglycerate kinase, and GK from *E. coli* (Sigma) and *P. farinosa* (see chapter 3.7).

3.6.1 Preparation of cell-free crude extract

After thawing, samples were extracted by sonification (USC600D, VWR, Darmstadt, Germany) on maximum power for 30 s with 1 mL extraction buffer (EB) and kept at 0 to 4 °C. The composition of the EB was similar to that reported for plant cells (Gibon et al., 2004) but adapted for mammalian cells with respect to the specific concentrations of each component (17 % (v/v) glycerol, 1 % (v/v) Triton X-100, 50 mM HEPES/KOH, pH 7.5, 10 mM MgCl₂, 1 mM EDTA, 1 mM EGTA, 1 mM benzamidine, 1 mM ε-aminocaproic acid, 20 mM leupeptin, 0.5 mM dithiothreitol (DTT), and 1 mM phenylmethylsulfonyl fluoride

(PMSF)). PMSF was added just prior to extraction. The samples were centrifuged at 16,000 g and 4 °C for 5 min to remove cell debris. The supernatant was used to measure the respective enzyme activities.

3.6.2 Pipetting scheme for enzyme assays

3.6.2.1 Indirect assays with enzymatic cycling

Enzyme activity analysis was performed as previously described with a few modifications (Gibon et al., 2004; Sulpice et al., 2007). A schematic overview of the assay procedure is presented in Figure 3.1. In brief, enzymes were assayed on flat bottom 96-well microplates with single- and multichannel Research[®] pro pipettes (Eppendorf, Hamburg, Germany). Per well of a 96-well microplate (0 to 4 °C), 2 µL of extract or standard were given. Then, the microplate was transferred to 37 °C and 18 µL of the specific assay mix with substrate (V_{\max}) or without substrate (V_{blank}) were added to start the reaction. Depending on the assay, plates were incubated with gentle shaking either for 20 or 40 min. To stop the reaction 20 µL of a stop solution (containing 0.5 M HCl in 100 mM Tricine/KOH, pH 9, or 0.5 M NaOH) were added and the plates were incubated for 10 or 20 min at room temperature or 70 °C, respectively. After cooling, 20 µL of a neutralizing solution and 50 µL of the cycling reagent were added to determine the concentration of product accumulated. Therefore, the reaction was immediately and continuously monitored by measuring the change in absorbance at 340 or 570 nm (depending on the assay) in an ELx808 (BioTek, Winooski, VT, USA) microplate reader kept at 37 °C. Typically, about 2 min were required to reach a linear rate. Then, the rate was constant for at least 30 min. The rates of reactions were calculated as the decrease or increase (depending on the assay) of the absorbance in mOD/min by using the Gen5 software (BioTek). All microplates included five standards and each measurement (V_{blank} and V_{\max}) was performed in three to four replicates. Microsoft[®] Excel spreadsheets were used to calculate the activity for each well on the microplate.

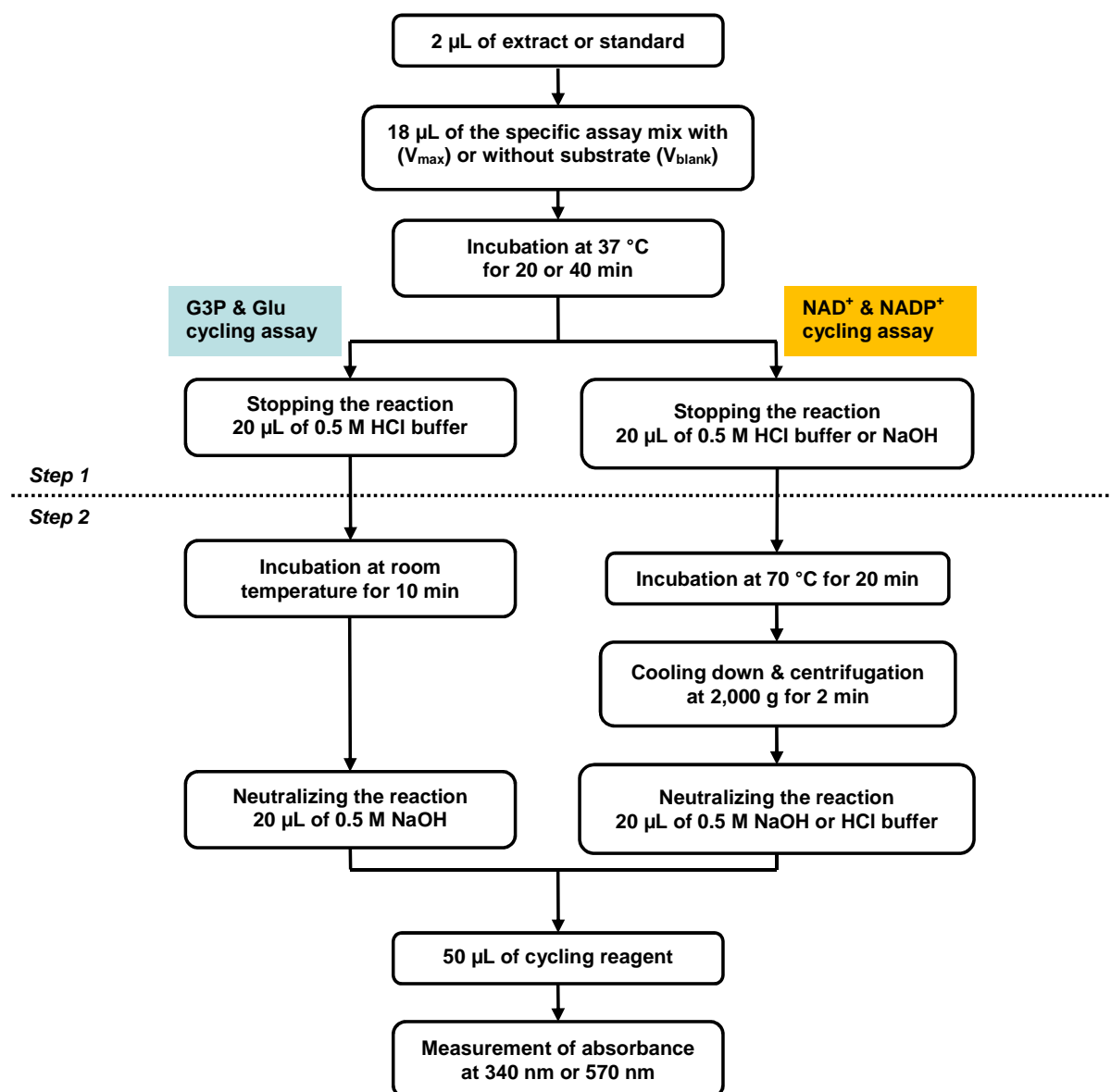


Figure 3.1: Flow chart of the procedure for the indirect assays with enzymatic cycling. The method for the G3P and Glu cycling assays is indicated in blue and for the NAD^+ and NADP^+ cycling assays in orange.

3.6.2.2 Direct assays

Extracts (5 μL) were dispensed into a flat bottom 96-well microplate (0 to 4 $^{\circ}\text{C}$). After adding 50 μL of specific assay mix, the microplate was transferred to 37 $^{\circ}\text{C}$, gently shaken, and preincubated for 1 min. Then, 45 μL of the appropriate starter solution with substrate (V_{max}) or without substrate (V_{blank}) were added to start the reaction, and the microplate was shaken again. The reaction was immediately and continuously monitored for change in absorbance at 340, 405 or 570 nm (depending on the assay) (ELx808 microplate reader, 37 $^{\circ}\text{C}$). Typically, about 2 min were required to reach a linear rate, which was then constant for at least 10 min. Determination of rates was performed according to the previous chapter (3.6.2.1). The

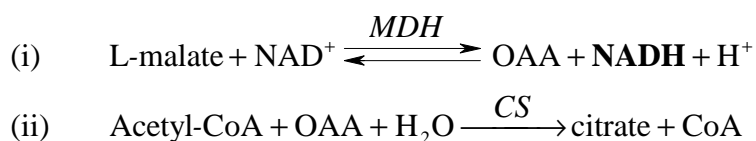
following molar extinction coefficients were used for the calculation of enzyme activity: 6.22 (NADH, NADPH), 12.8 (reduced DTNB), and 17 mM⁻¹ cm⁻¹ (reduced MTT).

3.6.3 Enzyme activity assays

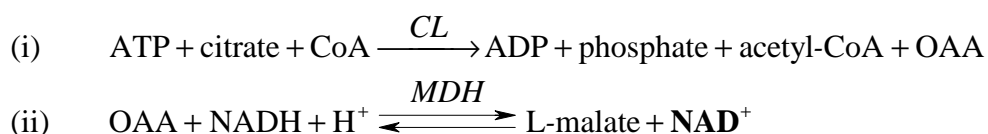
The determination of enzyme activities was based on zero-order kinetics meaning that the measured enzyme activity was independent of substrate concentration since the assays were carried out under relatively high substrate concentrations and low enzyme concentrations. For all enzyme assays, individual protocols and SOPs were prepared according to the standards of the Bioprocess Engineering group (MPI in Magdeburg), and all assays were validated as described in chapter 4.1.2. In all enzyme assay mixtures, 0.05 % (v/v) Triton X-100 was added to the assay system to complete the extraction of the enzymes. Cell extracts, as well as standards, were prepared in the EB (chapter 3.6.1). In all cases, blank determinations were carried out simultaneously, which typically contained similar reaction mixtures to the activity test, but with the “starting reagent” omitted.

In the following chapters (3.6.3.1 to 3.6.3.22), all assays are shortly described until the end of step 1 (see Figure 3.1). The simplified enzymatic reactions presented in the following are depicted as they would occur under physiological conditions in mammalian cells. However, the assay conditions were set to drive the reactions to the desired conversion (on the right-hand side). Step 2, the quantification of product (marked in bold letters in the reaction schemes) by addition of the cycling reagent is described under chapter 3.6.4.

3.6.3.1 Citrate synthase (CS: EC 2.3.3.1)



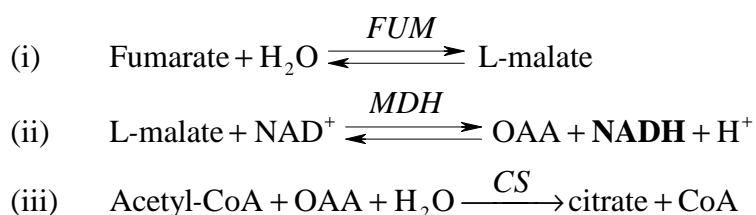
The assay is based on the coupled reaction given above. Activity was assayed in the forward direction by measuring the consumption of OAA. The concentrations used for malate, NAD⁺ and acetyl-CoA were chosen according to Shepherd & Garland (1969). Extracts, as well as NADH standards prepared in the EB and ranging from 0 to 200 μM, were incubated in a medium containing 100 mM Tricine/KOH, pH 8.5, 0.3 mM malate, 0.25 mM NAD⁺, and 5 U/mL malate dehydrogenase (MDH). The reaction was started by addition of acetyl-CoA to a final concentration of 0.2 mM (maximum activity). The blank was measured without acetyl-CoA. The reaction was stopped after 40 min with 20 μL of 0.5 M NaOH.

3.6.3.2 Citrate lyase (CL: EC 2.3.3.8)

Activity was assayed in conditions adapted from Ranganathan et al. (1980). Extracts, as well as OAA standards prepared in the EB and ranging from 0 to 200 μM , were incubated in a medium containing 100 mM Tricine/KOH, pH 8.5, 10 mM MgCl_2 , 10 mM KCl, 20 mM citrate, 0.2 mM NADH, 0.3 mM CoA, and 1 U/mL MDH. Before adding NADH, contaminating NAD^+ was removed from the NADH stock solution (20 mM in 100 mM NaOH) by heating for 10 min at 95 $^\circ\text{C}$. The reaction was started by addition of ATP to a final concentration of 5 mM (maximum activity). The blank was measured without ATP. The reaction was stopped after 20 min with 20 μL of 0.5 M HCl in 100 mM Tricine/KOH, pH 9.

3.6.3.3 NAD^+ -dependent isocitrate dehydrogenase (NAD-ICDH: EC 1.1.1.41)

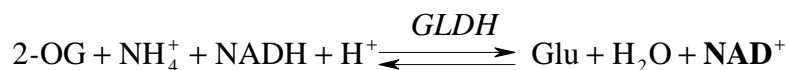
Activity was assayed in conditions adapted from Willson & Tipton (1980). Extracts, as well as NADH standards prepared in the EB and ranging from 0 to 200 μM , were incubated in a medium containing 100 mM MOPS, pH 7.5, 5 mM MgSO_4 , and 1 mM NAD^+ . The reaction was started by addition of isocitrate to a final concentration of 2 mM (maximum activity). The blank was measured without isocitrate. The reaction was stopped after 40 min with 20 μL of 0.5 M NaOH.

3.6.3.4 Fumarase (FUM: EC 4.2.1.2)

Activity was assayed in the malate-forming direction according to Gibon et al. (2004). Extracts, as well as malate standards prepared in the EB and ranging from 0 to 100 μM , were incubated in a medium containing 100 mM Tricine/KOH, pH 8, 5 mM MgCl_2 , 5 mM K_2HPO_4 , 0.15 mM NAD^+ , 0.2 mM acetyl-CoA, 100 U/mL MDH, and 1 U/mL CS. The reaction was started by addition of fumarate to a final concentration of 10 mM (maximum

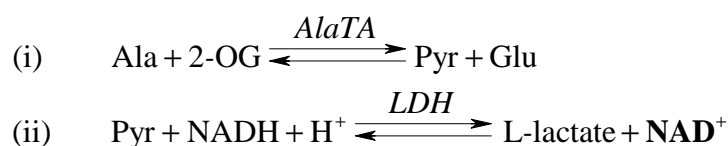
activity). The blank was measured without fumarate. The reaction was stopped after 20 min with 20 μ L of 0.5 M NaOH.

3.6.3.5 Glutamate dehydrogenase (GLDH: EC 1.4.1.2)



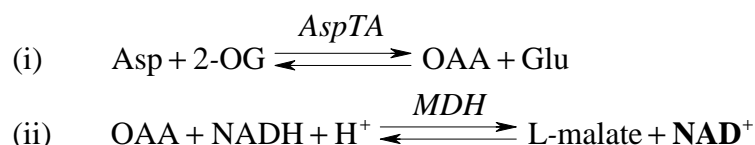
Activity was assayed in the direction of reductive amination of 2-OG in conditions adapted from Cho et al. (1995). Extracts, as well as NAD^+ standards prepared in the EB and ranging from 0 to 200 μ M, were incubated in a medium containing 100 mM Tricine/KOH, pH 8, 1 mM CaCl_2 , 640 mM ammonium acetate, 0.1 mM NADH, and 1 mM ADP. Before adding NADH, contaminating NAD^+ was removed from the NADH stock solution (20 mM in 100 mM NaOH) by heating for 10 min at 95 °C. The reaction was started by addition of 2-OG to a final concentration of 15 mM (maximum activity). The blank was measured without 2-OG. The reaction was stopped after 20 min with 20 μ L of 0.5 M HCl in 100 mM Tricine/KOH, pH 9.

3.6.3.6 Alanine transaminase (AlaTA: EC 2.6.1.2)



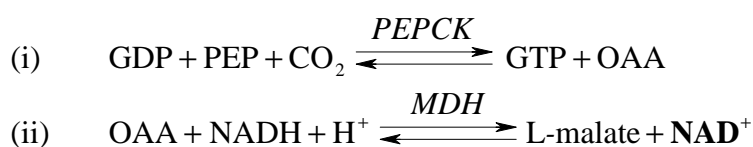
Activity was assayed in conditions adapted from Moss et al. (1987). Extracts, as well as Pyr standards prepared in the EB and ranging from 0 to 200 μ M, were incubated in a medium containing 100 mM Tricine/KOH, pH 8, 60 mM Ala, 0.1 mM NADH, and 0.3 U/mL LDH. Before adding NADH, contaminating NAD^+ was removed from the NADH stock solution (20 mM in 100 mM NaOH) by heating for 10 min at 95 °C. The reaction was started by addition of 2-OG to a final concentration of 5 mM (maximum activity). The blank was measured without 2-OG. The reaction was stopped after 20 min with 20 μ L of 0.5 M HCl in 100 mM Tricine/KOH, pH 9.

3.6.3.7 Aspartate transaminase (AspTA: EC 2.6.1.1)



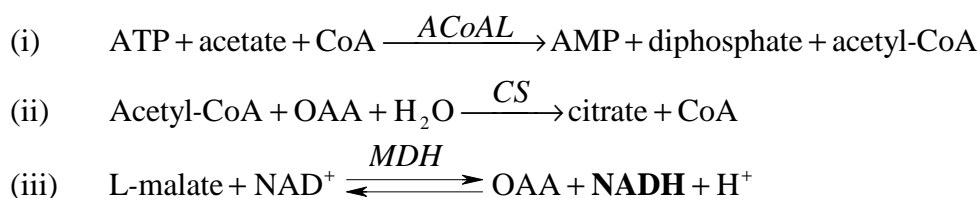
Activity was assayed in conditions adapted from Imperial et al. (1989). Extracts, as well as OAA standards prepared in the EB and ranging from 0 to 100 μM , were incubated in a medium containing 100 mM Tricine/KOH, pH 8, 35 mM Asp, 0.1 mM NADH, and 0.25 U/mL MDH. Before adding NADH, contaminating NAD^+ was removed from the NADH stock solution (20 mM in 100 mM NaOH) by heating for 10 min at 95 $^{\circ}\text{C}$. The reaction was started by addition of 2-OG to a final concentration of 2.5 mM (maximum activity). The blank was measured without 2-OG. The reaction was stopped after 20 min with 20 μL of 0.5 M HCl in 100 mM Tricine/KOH, pH 9.

3.6.3.8 Phosphoenolpyruvate carboxykinase (PEPCK: EC 4.1.1.32)



Activity was assayed in the direction of carboxylation of PEP in conditions adapted from Gallwitz et al. (1988). Extracts, as well as OAA standards prepared in the EB and ranging from 0 to 200 μM , were incubated in a medium containing 50 mM Hepes/KOH, pH 7.5, 45 mM NaHCO_3 , 1 mM MgCl_2 , 1 mM MnCl_2 , 1 mM GDP, 0.15 mM NADH, and 6 U/mL MDH. Before adding NADH, contaminating NAD^+ was removed from the NADH stock solution (20 mM in 100 mM NaOH) by heating for 10 min at 95 $^{\circ}\text{C}$. The reaction was started by addition of PEP to a final concentration of 2 mM (maximum activity). The blank was measured without PEP. The reaction was stopped after 20 min with 20 μL of 0.5 M HCl in 100 mM Tricine/KOH, pH 9.

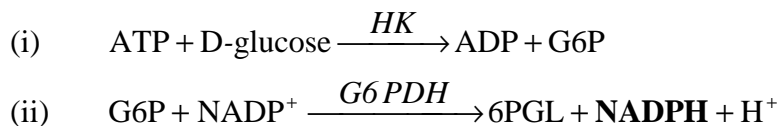
3.6.3.9 Acetate-CoA ligase (ACoAL: EC 6.2.1.1)



Activity was assayed in conditions adapted from Ishikawa et al. (1995). Extracts, as well as NADH standards prepared in the EB and ranging from 0 to 200 μM , were incubated in a medium containing 100 mM Tricine/KOH, pH 8.5, 10 mM MgCl_2 , 50 mM KCl, 10 mM acetate, 1 mM CoA, 0.3 mM malate, 0.25 mM NAD^+ , 1 U/mL CS, and 5 U/mL MDH. The reaction was started by addition of ATP to a final concentration of 6 mM (maximum

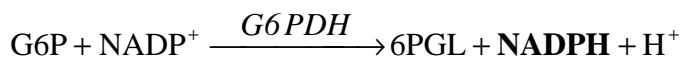
activity). The blank was measured without ATP. The reaction was stopped after 20 min with 20 μ L of 0.5 M NaOH.

3.6.3.10 Hexokinase (HK: EC 2.7.1.1)



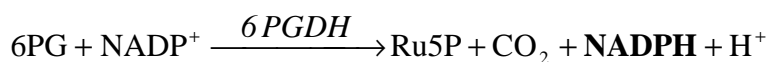
Activity was assayed in conditions adapted from Scheer et al. (1978). Extracts, as well as G6P standards prepared in the EB and ranging from 0 to 100 μ M, were incubated in a medium containing 100 mM Tricine/KOH, pH 8, 5 mM MgCl₂, 2 mM Gluc, 0.5 mM NADP⁺, and 1 U/mL G6P dehydrogenase grade II (lower purity of the enzyme preparation). The reaction was started by addition of ATP to a final concentration of 1 mM (maximum activity). The blank was measured without ATP. The reaction was stopped after 20 min with 20 μ L of 0.5 M NaOH.

3.6.3.11 Glucose-6-phosphate dehydrogenase (G6PDH: EC 1.1.1.49)



Activity was assayed according to conditions adapted from Postma et al. (1989). Extracts, as well as NADPH standards prepared in the EB and ranging from 0 to 100 μ M, were incubated in a medium containing 100 mM Tricine/KOH, pH 8, 10 mM MgCl₂, and 0.5 mM NADP⁺. The reaction was started by addition of G6P to a final concentration of 5 mM (maximum activity). The blank was measured without G6P. The reaction was stopped after 20 min with 20 μ L of 0.5 M NaOH.

3.6.3.12 6-Phosphogluconate dehydrogenase (6PGDH: EC 1.1.1.44)



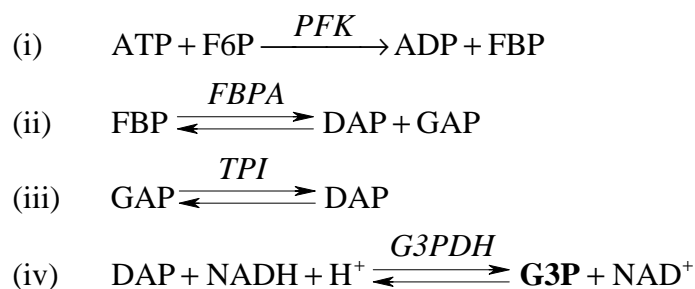
Activity was assayed basically by the method of Bailey-Serres & Nguyen (1992). Extracts, as well as NADPH standards prepared in the EB and ranging from 0 to 100 μ M, were incubated in a medium containing 100 mM Tricine/KOH, pH 8, 10 mM MgCl₂, 1 mM EDTA, and 0.5 mM NADP⁺. The reaction was started by addition of 6PG to a final concentration of 2 mM (maximum activity). The blank was measured without 6PG. The reaction was stopped after 20 min with 20 μ L of 0.5 M NaOH.

3.6.3.13 NADP⁺-dependent isocitrate dehydrogenase (NADP-ICDH: EC 1.1.1.42)

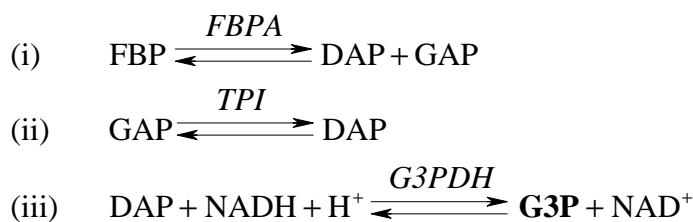
Activity was assayed in conditions adapted from Sugden & Newsholme (1975). Extracts, as well as NADPH standards prepared in the EB and ranging from 0 to 200 μM , were incubated in a medium containing 100 mM Tricine/KOH, pH 8.5, 8 mM MgCl_2 , and 5 mM NADP^+ . The reaction was started by addition of isocitrate to a final concentration of 2 mM (maximum activity). The blank was measured without isocitrate. The reaction was stopped after 20 min with 20 μL of 0.5 M NaOH.

3.6.3.14 Malic enzyme (ME: EC 1.1.1.40)

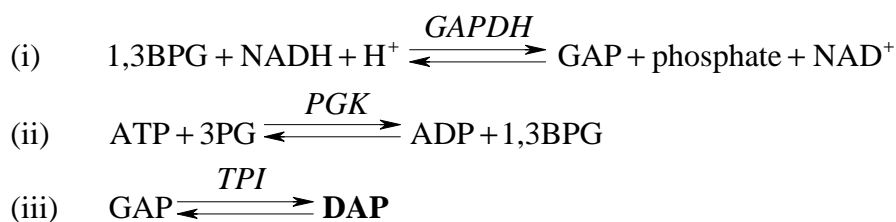
Activity was assayed in conditions adapted from Pongratz et al. (2007). Extracts, as well as NADPH standards prepared in the EB and ranging from 0 to 100 μM , were incubated in a medium containing 100 mM Tricine/KOH, pH 8, 1 mM MnCl_2 , and 0.5 mM NADP^+ . The reaction was started by addition of malate to a final concentration of 10 mM (maximum activity). The blank was measured without malate. The reaction was stopped after 20 min with 20 μL of 0.5 M NaOH.

3.6.3.15 Phosphofructokinase (PFK: EC 2.7.1.11)

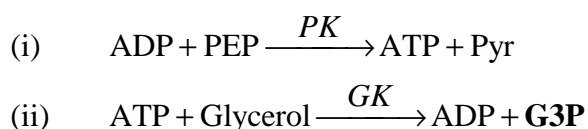
Activity was assayed in conditions adapted from Rais et al. (2000). Extracts, as well as FBPA standards prepared in the EB and ranging from 0 to 200 μM , were incubated in a medium containing 100 mM Tricine/KOH, pH 8, 5 mM MgCl_2 , 5 mM F6P, 0.25 mM NADH, 1 U/mL FBPA, 1 U/mL TPI, and 2 U/mL glycerol-3-phosphate dehydrogenase (G3PDH). The reaction was started by addition of ATP to a final concentration of 1 mM (maximum activity). The blank was measured without ATP. The reaction was stopped after 20 min with 20 μL of 0.5 M HCl in 100 mM Tricine/KOH, pH 9.

3.6.3.16 Fructose-1,6-bisphosphate aldolase (FBPA: EC 4.1.2.13)

Activity was assayed in conditions adapted from Holden & Storey (1994). Extracts, as well as DAP standards prepared in the EB and ranging from 0 to 200 μM , were incubated in a medium containing 100 mM Tricine/KOH, pH 8.5, 5 mM MgCl_2 , 1 mM EDTA, 0.3 mM NADH, 1 U/mL TPI, and 2 U/mL G3PDH. The reaction was started by addition of FBP to a final concentration of 5 mM (maximum activity). The blank was measured without FBP. The reaction was stopped after 20 min with 20 μL of 0.5 M HCl in 100 mM Tricine/KOH, pH 9.

3.6.3.17 Glyceraldehyde-3-phosphate dehydrogenase (GAPDH: EC 1.2.1.12)

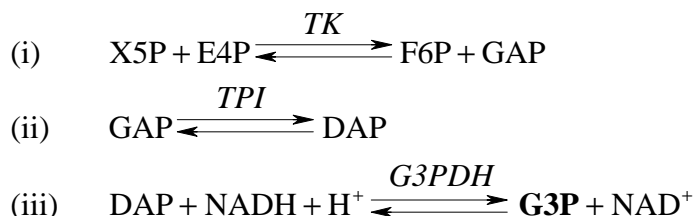
Activity was assayed according to conditions adapted from Lambeir et al. (1991). Extracts, as well as DAP standards prepared in the EB and ranging from 0 to 200 μM , were incubated in a medium containing 100 mM Tricine/KOH, pH 8, 30 mM MgCl_2 , 20 mM KCl, 2 mM EDTA, 0.5 mM DTT, 5 mM ATP, 0.5 mM NADH, 10 U/mL PGK, and 1 U/mL TPI. The reaction was started by addition of 3PG to a final concentration of 4 mM (maximum activity). The blank was measured without 3PG. The reaction was stopped after 20 min with 20 μL of 0.5 M HCl in 100 mM Tricine/KOH, pH 9.

3.6.3.18 Pyruvate kinase (PK: EC 2.7.1.40)

Activity was assayed by measuring the PEP-dependent production of ATP from ADP. The concentrations used for PEP, ADP, and KCl were chosen according to Faustova & Järvi (2001). Extracts, as well as ATP standards prepared in the EB and ranging from 0 to 200 μM , were incubated in a medium containing 50 mM HEPES/KOH, pH 7.5, 10 mM MgCl_2 ,

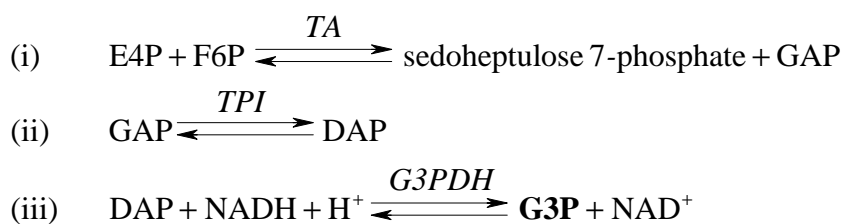
100 mM KCl, 0.4 mM EDTA, 120 mM glycerol, 1 mM ADP, 1 mM AMP, and 2 U/mL GK. The reaction was started by addition of PEP to a final concentration of 5 mM (maximum activity). The blank was measured without PEP. The reaction was stopped after 20 min with 20 μ L of 0.5 M HCl in 100 mM Tricine/KOH, pH 9.

3.6.3.19 Transketolase (TK: EC 2.2.1.1)

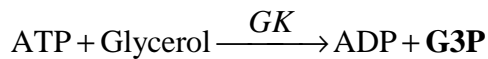


Activity was assayed according to conditions adapted from Sprenger et al. (1995). Extracts, as well as DAP standards prepared in the EB and ranging from 0 to 100 μ M, were incubated in a medium containing 50 mM Hepes/KOH, pH 7.5, 5 mM MgCl₂, 0.5 mM thiamine pyrophosphate, 0.6 mM NADH, 1 U/mL TPI, and 2 U/mL G3PDH. The reaction was started by addition of erythrose 4-phosphate (E4P) and xylulose 5-phosphate (X5P) to final concentrations of 1.5 mM and 5 mM, respectively. The blank was measured without E4P and X5P. The reaction was stopped after 20 min with 20 μ L of 0.5 M HCl in 100 mM Tricine/KOH, pH 9.

3.6.3.20 Transaldolase (TA: EC 2.2.1.2)



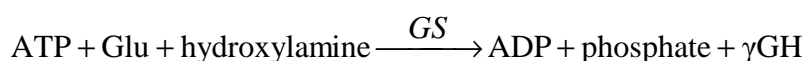
Activity was assayed in conditions adapted from Heinrich et al. (1976). Extracts, as well as DAP standards prepared in the EB and ranging from 0 to 100 μ M, were incubated in a medium containing 50 mM Hepes/KOH, pH 7.5, 2 mM EDTA, 0.6 mM NADH, 10 mM F6P, 1 U/mL TPI, and 2 U/mL G3PDH. The reaction was started by addition of E4P to a final concentration of 1 mM (maximum activity). The blank was measured without E4P. The reaction was stopped after 20 min with 20 μ L of 0.5 M HCl in 100 mM Tricine/KOH pH, 9.

3.6.3.21 Glycerokinase (GK: EC 2.7.1.30)

The assay was used for the activity measurement of the recombinant His₆-tagged GK (see chapter 4.2). Activity was assayed in conditions adapted from Guan et al. (2002). Extracts, as well as G3P standards prepared in the EB and ranging from 0 to 200 μM, were incubated in a medium containing 100 mM Tricine/KOH, pH 7.5, 50 mM MgCl₂, 100 mM KCl, 0.4 mM EDTA, and 120 mM glycerol. The reaction was started by addition of ATP to final concentrations of 5 (maximum activity). The blank was measured without ATP. The reaction was stopped after 20 min with 20 μL of 0.5 M HCl in 100 mM Tricine/KOH, pH 9.

3.6.3.22 Glutaminase (GLNase: EC 3.5.1.2)

Activity was assayed in conditions adapted from Curthoys & Weiss (1974). Extracts, as well as Glu standards prepared in the EB and ranging from 0 to 200 μM, were incubated in a medium containing 100 mM Tricine/KOH, pH 8.5, 0.2 mM EDTA, and 150 mM K₂HPO₄. The reaction was started by addition of Gln to a final concentration of 40 mM (maximum activity). The blank was measured without Gln. The reaction was stopped after 20 min with 20 μL of 0.5 M HCl in 100 mM Tricine/KOH, pH 9.

3.6.3.23 Glutamine synthetase (GS: EC 6.3.1.2)

Activity was measured in a “synthetic” reaction by which the ammonia was replaced by hydroxylamine as essentially described by Meister (1985). Extracts (5 μL), as well as γ-glutamyl hydroxamate (γGH) standards prepared in the EB and ranging from 0 to 5 mM were dispensed in flat bottom 96-well microplates kept at 0 to 4 °C. Then, the microplate was transferred to 37 °C and 45 μL of assay mix with (V_{max}) or without (V_{blank}) substrate were added to start the reaction followed by gentle shaking (37 °C, 60 min, sealed with adhesive aluminum foil). The assay medium contained, in final concentrations, 50 mM imidazole/HCl, pH 7.5, 20 mM MgCl₂, 10 mM ATP, 100 mM hydroxylamine-HCl, adjusted to pH 7.5, 10 mM creatine phosphate, and 2 U/mL creatine kinase (CK). The reaction was started by addition of Glu to a final concentration of 50 mM (maximum activity). The blank was

measured without Glu. The reaction was terminated by addition of 50 μL of stop solution containing 200 mM $\text{FeCl}_3 \cdot 6\text{H}_2\text{O}$, 120 mM trichloroacetic acid, and 250 mM HCl. The amount of γGH was measured from the absorbance at 505 nm (PowerWave XS, BioTek) by comparison with a standard curve of γGH . The microplate reader ELx808 (faster readout) could not be used for the GS assay due to the absence of the respective wavelength filter.

3.6.3.24 Lactate dehydrogenase (LDH: EC 1.1.1.27)



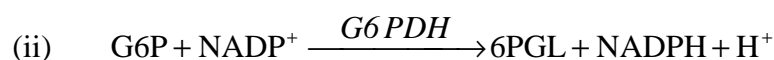
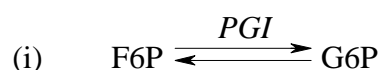
Activity was assayed in conditions adapted from Javed et al. (1997). Extracts prepared in the EB were incubated in a medium containing 100 mM Tricine/KOH, pH 8, 0.1 mM EDTA, and 1.2 mM NADH. The reaction was started by addition of Pyr to a final concentration of 2.25 mM (maximum activity). The blank was measured without Pyr.

3.6.3.25 Malate dehydrogenase (MDH: EC 1.1.1.37)

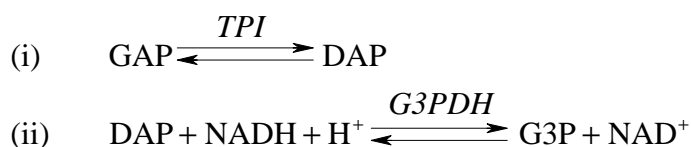


Activity was assayed in conditions adapted from Crow et al. (1982). Extracts prepared in the EB were incubated in a medium containing 100 mM Tricine/KOH, pH 8, 0.1 mM EDTA, and 1.2 mM NADH. The reaction was started by addition of OAA to a final concentration of 1.1 mM (maximum activity). The blank was measured without OAA.

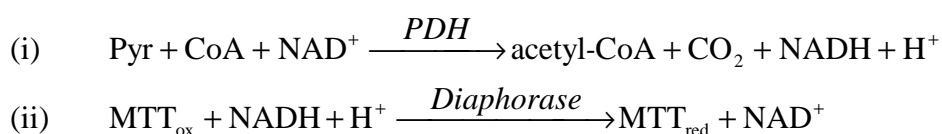
3.6.3.26 Phosphoglucose isomerase (PGI: EC 5.3.1.9)



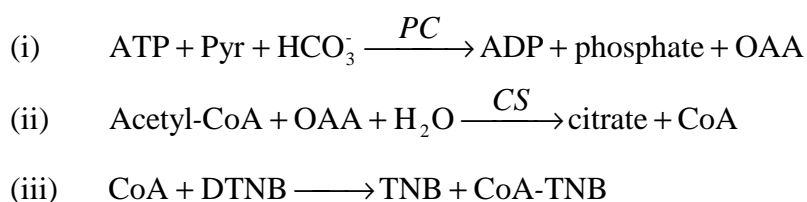
Activity was assayed in conditions adapted from Tsuboi et al. (1971). Extracts prepared in the EB were incubated in a medium containing 100 mM Tricine/KOH, pH 8, 100 mM MgCl_2 , 2 mM EDTA, 1.2 mM NADP^+ , and 1 U/mL G6PDH grade II. The reaction was started by addition of F6P to a final concentration of 2.25 mM (maximum activity). The blank was measured without F6P.

3.6.3.27 Triose-phosphate isomerase (TPI: EC 5.3.1.1)

Activity was assayed in conditions adapted from Merkle & Pretsch (1989). Extracts prepared in the EB were incubated in a medium containing 100 mM Hepes/KOH, pH 7.5, 5 mM EDTA, 0.6 mM NADH, and 1 U/mL G3PDH. The reaction was started by addition of GAP to a final concentration of 2.25 mM (maximum activity). The blank was measured without GAP.

3.6.3.28 Pyruvate dehydrogenase (PDH: EC 1.2.4.1)

Activity was assayed according to conditions adapted from Schwab et al. (2005), except that MTT was used as electron acceptor. Extracts prepared in the EB without DTT were incubated in a medium containing 50 mM Hepes/KOH, pH 7.5, 1 mM MgCl₂, 20 μM CaCl₂, 5 mM L-carnitine, 25 mM oxamate, 0.2 mM thiamine pyrophosphate, 0.1 mM CoA, 2.5 mM NAD⁺, 1 mM MTT, and 1 U/mL diaphorase. The reaction was started by addition of Pyr to a final concentration of 5 mM (maximum activity). The blank was measured without Pyr.

3.6.3.29 Pyruvate carboxylase (PC: EC 6.4.1.1)

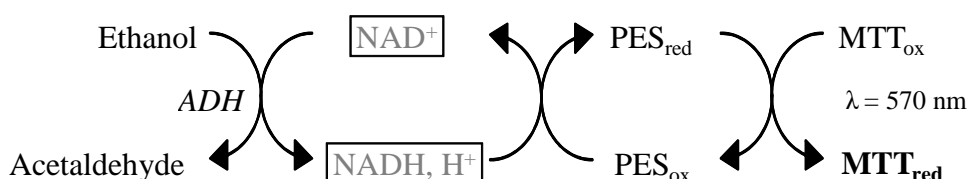
Activity was assayed by coupling the production of OAA to the reduction of 5,5'-dithiobis(2-nitrobenzoic acid) (DTNB), using CS, as described by Scrutton & White (1974). Extracts prepared in the EB without DTT were incubated in a medium containing 100 mM Tricine/KOH, pH 8, 10 mM MgCl₂, 50 mM KHCO₃, 2.5 mM ATP, 0.5 mM acetyl-CoA, 0.25 mM DTNB, 5 mM creatine phosphate, 5 U/mL CK, and 5 U/mL CS. The reaction was started by addition of Pyr to a final concentration of 5 mM (maximum activity). The blank was measured without Pyr.

3.6.4 Cycling assay reagents

The second step of the indirect assays with enzymatic cycling involves the quantification of the product by sensitive cycling assays as described in the following.

3.6.4.1 NAD⁺ cycling assay

The NAD⁺ cycling assays consisted of the enzymatic reaction as a first step, then the degradation of NAD⁺ or NADH and its subsequent analysis. The enzymatic cycling is based on the following reaction.

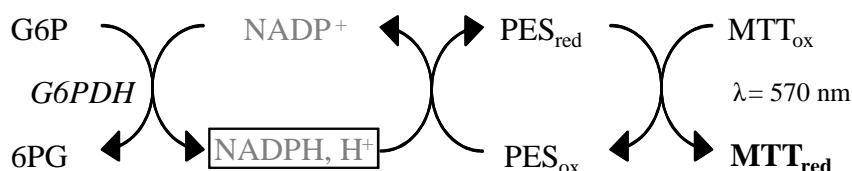


For the degradation of NAD⁺ or NADH the plates were sealed with an adhesive aluminum foil, gently mixed and heated at 70 °C for 20 min. After cooling, plates were centrifuged (2 min at 2,000 g) and 20 μ L of 0.5 M HCl in 100 mM Tricine/KOH, pH 9, or 0.5 M NaOH were added to adjust the pH to 9.

NADH or NAD⁺ was then measured indirectly via the reduction of thiazolyl blue tetrazolium bromide (MTT) according to Bernofsky & Swan (1973), in the presence of 100 mM Tricine/KOH, pH 9, 8 mM EDTA, 1 % (v/v) ethanol, 1 mM MTT, 0.2 mM PES, and 300 U/mL ADH. The absorbance of MTT was read at 570 nm until the rates were stabilized. The rates of reactions were calculated as the increase of the absorbance in mOD/min.

3.6.4.2 NADP⁺ cycling assay

The NADP⁺ cycling assays and the destruction of NADP⁺ were performed according to the previous chapter (3.6.4.1). The enzymatic cycling is based on the following reaction.

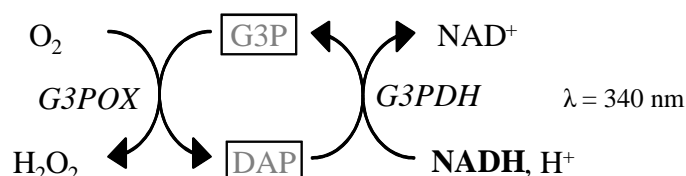


The amount of NADPH was determined indirectly by measuring reduced MTT (MTT_{red}) according to the methods of Vilee (1962) and Nisselbaum & Green (1969), in the presence of 100 mM Tricine/KOH, pH 9, 8 mM EDTA, 5 mM G6P, 1 mM MTT, 0.2 mM PES, and

2.5 U/mL G6PDH grade I (higher purity of the enzyme preparation was needed for the cycling assay). Determination of rates was performed according to the previous chapter.

3.6.4.3 G3P cycling assay

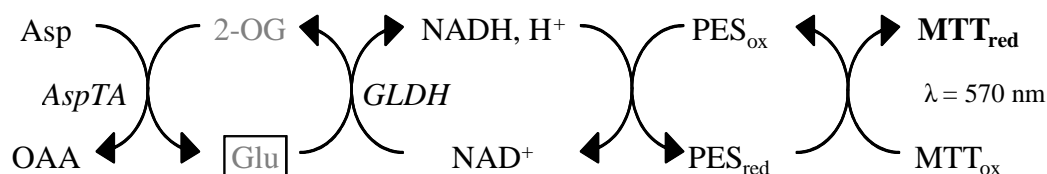
The G3P cycling assays consisted of the enzymatic reaction as a first step and the analysis of G3P. The enzymatic cycling is based on the following reaction.



G3P or DAP was measured via NADH absorbance decrease after neutralizing with 20 μL of 0.5 M NaOH according to Misaki (1987) and Gibon et al. (2002), in the presence of 100 mM Tricine/KOH, pH 8, 2 mM MgCl_2 , 0.6 mM NADH, 1 U/mL G3PDH, and 2.5 U/mL glycerol-3-phosphate oxidase (G3POX). For determination of FBPA or GAPDH, 0.5 U/mL TPI were added. The absorbance of NADH was read at 340 nm until the rates were stabilized. The rates of reactions were calculated as the decrease of the absorbance in mOD/min.

3.6.4.4 Glu cycling assay

Glu was measured indirectly by photometric measurement of MTT_{red} according to conditions adapted from Mayer et al. (1999) after neutralization with 20 μL of 0.5 M NaOH, in the presence of 100 mM Tricine/KOH, pH 8, 1 mM EDTA, 1.5 mM NAD^+ , 0.5 mM ADP, 100 mM Asp, 1 mM MTT, 0.2 mM PES, 5 U/mL AspTA, and 10 U/mL GLDH. Determination of rates was performed according to chapter 3.6.4.1. The enzymatic cycling is based on the following reaction.



3.6.5 Expression of results

All maximum enzyme activities are expressed as nmol of substrate consumed or product formed per min per 10^6 cells at 37 °C. All data given in Table 4.5 and Table 4.10 were compared by Student's *t*-test (Microsoft® Excel) with $p \leq 0.05$ being considered significant. To evaluate the significance of changes in maximum enzyme activities a minimum cut-off criterion taking into account errors imposed by biological (*in vivo* or *in vitro*) and technical (procedure noise) variation is required (McCarthy and Smyth, 2009; Molloy et al., 2003). Here, enzyme activities were calculated from measurement of absorbance (product per time) divided by the concentration of viable cells used in the assay. The error, which was introduced by the determination of the cell density (automatic cell counter Vi-CELL®) was estimated to be maximum 10 % (relative SD of the validated method of 9 %). The average error of all enzyme activity measurements (relative SD of four to six biological replicates) did also not exceed 10 %, whereas the highest value of 16 % was observed for PC (relative SD of six replicates) in GMEM-Pyr^{stat} (see Table 4.10, chapter 4.3.2). Therefore, and to comprise day-to-day and user-to-user variability, enzyme activities with fold changes higher than 1.3 or lower than -1.3 (overall maximum error about 26 %, ~1.3) between the different cultivation conditions (GMEM-Gln and GMEM-Pyr) were considered significantly different.

3.7 Cloning, expression, purification, and characterization of *Pichia farinosa* glycerokinase

This chapter summarizes the basic materials and methods requirements to produce the recombinant GK for the application as a coupling enzyme in sensitive G3P cycling assays as given by Janke et al. (2010a). Additional information can be found in the appendix section.

3.7.1 Strains, plasmids, enzymes and reagents

The *E. coli* TOP10F' strain (Invitrogen, Carlsbad, CA, USA) was used for propagation of plasmid DNA. *E. coli* cells with plasmids were cultured aerobically at 37 °C in LB medium (10 g/L trypton, 5 g/L yeast extract, 10 g/L NaCl) supplemented with 25 µg/mL kanamycin or 100 µg/mL ampicillin. The methylotrophic *P. pastoris* yeast strain GS115 (*his4*; Mut⁺) was purchased from Invitrogen, and was used for the expression of His₆-tagged GK. Minimal dextrose (MD) medium, minimal methanol (MM) medium, buffered minimal glycerol (BMG) medium, buffered minimal methanol (BMM) medium and fermentation basal salts

medium (BSM) supplemented with *P. pastoris* trace metals 1 (PTM₁) were prepared according to the manufacturer's instructions (Invitrogen, 2002a; Invitrogen, 2002b).

The bacterial expression vector pETM-11-GK, in which the coding region of the *P. farinosa* *GUT1* gene (obtained by Prof. Cândida Lucas, University of Minho, Braga, Portugal) was cloned between the *NcoI* and *EcoRI* sites of expression plasmid pETM-11, was kindly provided by Dr. John Lunn (MPI for Molecular Plant Physiology, Golm/Potsdam, Germany) (Gibon et al., 2009). The *GUT1* gene (GenBank Accession No. AY391774) from *P. farinosa* (CBS 7064) was first cloned and sequenced by Neves et al. (2004). The pETM-11 plasmid was originally derived from a pET (Novagen, Madison, WI, USA) backbone, which includes an N-terminal His₆-tag and a TEV (tobacco etch virus) protease cleavage site before the inserted gene (Dümmler et al., 2005). The integrative yeast expression vector pPIC3.5 (Invitrogen) containing the promoter and terminator of the alcohol oxidase gene (*AOX1*) was used as the expression cassette and the *HIS4* selectable marker.

Restriction enzymes were purchased from New England Biolabs (Ipswich, MA, USA). Enzymes for analysis were purchased from Roche, except alcohol oxidase and GK from *E. coli* (Sigma). Chemicals were purchased from Sigma, except NADH (Roche).

3.7.2 Construction of the expression vector

The DNA fragment containing the *GUT1* gene was obtained from the pETM-11-GK plasmid (containing a His₆-tag) after digestion with *XbaI* and *NotI* restriction enzymes, and was used as template for the polymerase chain reaction (PCR). The digestion product (~2,000 bp) was isolated from an agarose gel band using a Wizard[®] SV Gel and a PCR Clean-Up System kit (Promega, Madison, WI, USA). The following two primers were designed to amplify the entire coding sequence, and to introduce an *AvrII* site at the 5' end and a *NotI* site at the 3' end (underlined): forward primer GKforAvrII, 5'-GCTACCTAGGATGAAACATCACC ATCACCA-3', and reverse primer GKrevNotI, 5'-GTCAGCGGCCGCTCGAATTCTTAGT CATTGTTCTGA-3' (letters in bold indicate the His₆-tag and *GUT1* coding sequence, respectively). PCR was performed using Phusion[®] DNA Polymerase (Finnzymes, Espoo, Finland) for 30 cycles consisting of an annealing temperature of 64 °C for 30 s and an elongation time of 70 s at 72 °C. After purification (PCR Clean-Up System kit), the *AvrII*–*NotI* fragment of the PCR product (containing a His₆-tag and the coding region of GK) was ligated into pPIC3.5 *AvrII*–*NotI* sites. The resulting plasmid was named pPIC3.5-GK (Figure 3.2), and the expected structure was verified by restriction digestion and sequencing

from both ends of the inserted segment (GATC Biotech, Konstanz, Germany). The resulting DNA sequence was analyzed with sequence database searches using BLAST sequence comparison algorithms at NCBI (<http://blast.ncbi.nlm.nih.gov/Blast.cgi>). Competent *E. coli* TOP10F' cells were transformed with the vectors pETM-11-GK or pPIC3.5-GK, and grown on LB agar plates supplemented with kanamycin or ampicillin, respectively.

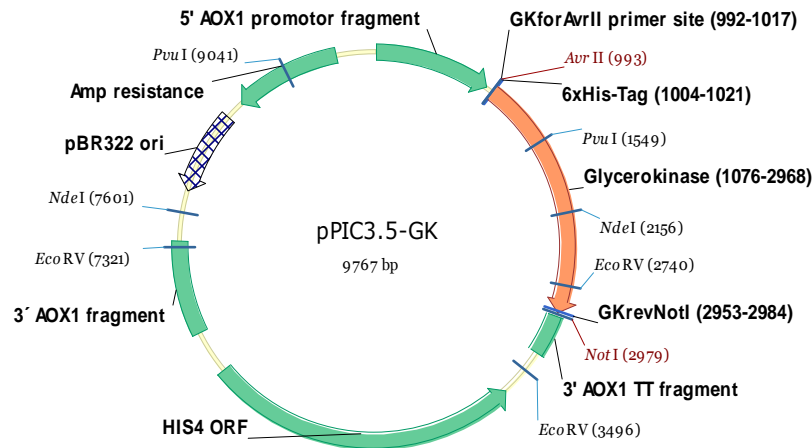


Figure 3.2: Construction of pPIC3.5-GK expression vector.

The *AvrII*–*NotI* fragment of the PCR product (containing a His₆-tag and the *GUT1* coding region) was inserted into the *AvrII* and *NotI* sites of the pPIC3.5 vector.

3.7.3 Transformation of *Pichia pastoris*

The construct pPIC3.5-GK was isolated from *E. coli* cells using a NucleoSpin[®] Plasmid Kit (Macherey-Nagel, Düren, Germany), and was linearized by digestion with *StuI* in order to favor integration at the *P. pastoris his4* locus. Approximately 11 µg of linearized plasmid DNA was used to electroporate *P. pastoris* GS115 cells using an Easyject Prima (Equibio, Ashford, UK) at 1.8 kV, 15 µF, and 335 Ω. As a reference, yeast cells were also transformed with the empty vector (pPIC3.5) using the same method. Selection of His⁺ transformants was done on minimal selective MD or MM agar plates. *P. pastoris* transformants were randomly selected and analyzed for integration of the *GUT1* gene into the genome by PCR.

For selection of high yield strains, colonies of positive *P. pastoris* clones were inoculated into 2 mL of BMG medium and incubated in round-bottom 14 mL polypropylene tubes (Greiner Bio-One, Kremsmünster, Austria) for approximately 16 h (27 °C, shaking at 150 rpm). When the culture reached an OD₆₀₀ of 2 to 5, the cells were collected by centrifugation and resuspended to an OD₆₀₀ of 1 in 2 mL BMM medium. To promote methanol-inducible expression of GK, cultures were incubated (27 °C, shaking at 150 rpm), and supplemented with methanol to a final concentration of 1 % (v/v) every 24 h. Aliquots of fresh culture were

collected after 45 h, the cells were lysed with glass beads according to the protocol of Invitrogen (Invitrogen, 2002a), and then screened for GK activity. The clone showing highest expression level (maximum GK activity) was chosen for recombinant protein production.

3.7.4 Production of *Pichia farinosa* glycerokinase by *Pichia pastoris*

A colony containing pPIC3.5-GK from a MD plate was inoculated into 300 mL BMG and split in three 1-L shaking flasks. Cells were grown for approximately 22 h at 30 °C and 250 rpm. Cultures were then combined, centrifuged (5 min at 16,000 g) and resuspended in 30 mL BMG. The cultivation procedure was done according to the guideline of Invitrogen (Invitrogen, 2002b), which is based on fermentation of Mut⁺ *Pichia* strains in a 15-L glass fermenter. The fed-batch cultivation was performed in a 5-L stirred-tank bioreactor (Sartorius BBI Systems, Melsungen, Germany) with a water cooler, gas mix station, and with feeding pumps. Process control and data acquisition was carried out by a Simatic PCS7 automation system (Siemens, Munich, Germany). For feeding control, flow rates (mass flow) were adjusted using peristaltic pumps and balances. Samples were taken for determination of OD₆₀₀, dry cell weight (DCW), GK activity, glycerol, methanol, and protein concentration.

In brief, 3 L BSM supplemented with PTM₁ trace salts were inoculated with 30 mL preculture. Temperature was kept at 30 °C, and pH was maintained at 5 with 28 % ammonium hydroxide. Aeration (oxygen and air) and agitation were adjusted to keep dissolved oxygen levels above 30 % during the fermentation process. After glycerol exhaustion (19 h), a methanol pulse was added to the fermenter (final concentration approximately 55 mM) to adapt the culture to growth on methanol. The 1.5 L methanol (100 % containing 18 mL PTM₁) feed adjusted to a growth-limiting rate ($\mu_{\text{set}} = 0.04 \text{ h}^{-1}$) was initiated after 21 h. The fed-batch control strategy used was based on the calculation of a time-dependent feeding rate following an exponential function. The methanol utilization phase (induced expression) was maintained for 54 h. Afterwards, cells were removed from the culture medium by centrifugation at 3,660 g for 30 min at 4 °C, and the cell pellets were stored at -80 °C until needed.

Exponential feeding was performed using equation 3.5 (Korz et al., 1995; Zeiger and Grammel, 2010). Parameters for the exponential feed equation are given in Table 3.2.

$$M_S(t) = F(t) \cdot S_F = \rho_S \cdot \left(\frac{\mu_{set}}{Y_{X/S}} + m_S \right) \cdot \frac{V_0 \cdot X_0}{S_F} \cdot e^{\mu_{set}(t-t_0)} \quad \text{(Equation 3.5)}$$

$M_S(t)$	mass feeding rate	(g h ⁻¹)
$F(t)$	feeding rate	(L h ⁻¹)
ρ_S	density of the feed solution	(g L ⁻¹)
μ_{set}	desired specific growth rate	(h ⁻¹)
$Y_{X/S}$	yield coefficient of biomass/substrate	(g g ⁻¹)
m_S	specific maintenance coefficient	(g g ⁻¹ h ⁻¹)
V_0	culture volume at the start of feeding	(L)
X_0	biomass concentration at the start of feeding	(g L ⁻¹)
S_F	substrate concentration in the feeding solution	(g L ⁻¹)
$t-t_0$	time span since starting of the feed	(h)

Table 3.2: Control parameters for the exponential fed-batch process according to equation 3.5.

ρ_S	790 (g L ⁻¹)
μ_{set}	0.04 (h ⁻¹)
$Y_{X/S}$	0.347 (g g ⁻¹)
m_S	0.013 ^a (g g ⁻¹ h ⁻¹)
V_0	3 (L)
X_0	30 (g L ⁻¹)
S_F	780 (g L ⁻¹)

^a from Jahic et al. (2002)

3.7.5 Purification of His₆-tagged recombinant glycerokinase

P. pastoris cell pellets (7.5 g of frozen cells) were thawed and resuspended in 500 mL lysis buffer (50 mM NaH₂PO₄, 5 % (v/v) glycerol, 1 % (v/v) Triton X-100, 1 mM PMSF, 1 mM benzamidine, 1 mM ε-aminocaproic acid, 20 μM leupeptin, 0.5 mM DTT, pH 7.4) and kept at 0 to 4 °C. Cells were disrupted by an EmulsiFlex-C5 high pressure homogenizer (Avestin, Ottawa, ON, Canada) at 172 MPa. Clarification of the crude extract was done by centrifugation at 10,000 g and 4 °C for 20 min, and a subsequent filtration through a bottle-top 0.2-μm-pore-size cellulose acetate filter (Nalgene, Rochester, NY, USA).

The recombinant GK was purified by a two-step procedure consisting of nickel affinity chromatography followed by anion exchange chromatography at room temperature. The clarified supernatant (about 450 mL) was applied directly onto a Ni²⁺-Sepharose column (5 mL bed volumes, BV) using an ÄKTA Purifier system (GE Healthcare Europe, Munich, Germany). The column (XK 16/20, GE Healthcare) was packed with IMAC Sepharose 6 Fast

Flow (GE Healthcare), charged with Ni²⁺ ions, and then pre-equilibrated with buffer A (50 mM NaH₂PO₄, 0.5 M NaCl, 20 mM imidazole, pH 7.4). After loading, the column was washed with the equilibration buffer until absorbance (280 nm) reached the baseline level (~20 BV). Bound enzyme was eluted subsequently with buffer B (buffer A containing 0.5 M imidazole). Aliquots of collected fractions were analyzed by SDS-PAGE and MS, and assayed for GK activity and protein concentration, respectively. Fractions (1.5 mL) containing GK activity were pooled and then concentrated by Amicon Ultra-15 filter units (10 kDa cut-off) (Millipore, Billerica, MA, USA) at 4 °C and 5,000 g for 25 min.

Concentrated protein (about 8 mL, ~15 mg) was subsequently transferred to 100 mL of buffer C (15 mM NaH₂PO₄, pH 6.8) and applied onto a pre-equilibrated (buffer C) HiTrap Q HP column (1 mL BV; GE Healthcare). After washing the column (buffer C; ~10 BV), the enzyme was eluted with buffer D (buffer C containing 1 M NaCl). Aliquots of collected fractions were analyzed as described above, and active fractions were pooled and concentrated by ultracentrifugation (Amicon Ultra-15). Aliquots of the concentrated enzyme were stored in 10 mM NaH₂PO₄, pH 7.4, containing 50 % (v/v) glycerol at -80 °C until use in the respective enzyme assays.

3.7.6 Protein analysis

Total protein concentration was determined by the BCA assay (standard test tube protocol, see chapter 3.4.4). Enzyme purity was assessed by SDS-PAGE according to conditions developed by Laemmli (1970) using a 10 % separating gel and with Coomassie Brilliant Blue R-250 staining. For non-reducing conditions, β-mercaptoethanol was omitted. Protein bands were digested tryptically and identified by using a nanoHPLC-nanoESI-MS/MS (QStar XL, Applied Biosystems/MDS SCIEX, Darmstadt, Germany). Mass spectrometric detection, data processing and interpretation of online acquired ESI-MS/MS peptide spectra were carried out by Dr. Erdmann Rapp (MPI for Dynamics of Complex Technical Systems) as described by Schwarzer et al. (2008).

3.7.7 Determination of glycerol and methanol

Changes in glycerol and methanol concentrations were analyzed during the production of the recombinant GK. Glycerol was determined by an enzyme assay kit (Roche) according to the manufacturer's protocol. Methanol concentration was determined according to the procedure described by Anthon & Barrett (2004) using alcohol oxidase and the reagent Purpald[®]

(4-amino-3-hydrazino-5-mercapto-1,2,4-triazole). In brief, 50 μL of culture supernatant, as well as methanol standards ranging from 0 to 1 M were incubated (30 $^{\circ}\text{C}$) in a medium (150 μL) containing 67 mM Tris/HCl, pH 7.5, and 6.7 U/mL alcohol oxidase. After 10 min, 200 μL of Purpald[®] (5 g/L in 0.5 M NaOH) were added and the reaction mixture was incubated (30 $^{\circ}\text{C}$) again. After 30 min, the mixture was diluted with 600 μL of H_2O and the concentration of methanol was measured from the absorbance at 550 nm (PowerWave XS, Biotek) by comparison with a standard curve of methanol.

3.7.8 Enzymatic characterization of recombinant His₆-tagged GK

His₆-tagged GK activity was assayed in 96-well plates as described in chapter 3.6.3.21. The effect of pH on purified GK activity was studied at 37 $^{\circ}\text{C}$ with different buffer media at 100 mM final concentrations: sodium phosphate (pH 4.5, 5, 5.5, 6, 6.5, and 7), tricine (pH 7.5, 8, and 8.5), and sodium borate buffer (pH 9, 9.5, and 10). The optimum temperature for GK activity was investigated at 4 to 70 $^{\circ}\text{C}$ and pH 7. The kinetic parameters were determined at 37 $^{\circ}\text{C}$ and pH 7 with 120 mM glycerol and a range of concentrations of ATP, UTP, ITP, CTP, and GTP. Lineweaver-Burk plots were used to calculate the K_m and V_{\max} values of each substrate. One unit (U) of activity was defined as the amount of enzyme that produced 1 μmol of G3P per minute at the respective temperature and pH.

4 Results

The Results section is divided into four main parts: (i) chapter 4.1 deals with the development of an assay platform to measure enzyme activities of central metabolism in mammalian cells, (ii) chapter 4.2 then describes the production, purification and the biochemical characterization of a GK from *P. farinosa* as well as its application as a coupling enzyme in G3P cycling assays, (iii) chapter 4.3 is related to the effect of Gln substitution by Pyr on maximum activities of key metabolic enzymes in MDCK cells grown in GMEM by using the established assay platform, and (iv) chapter 4.4 deals with the influence of influenza A virus infection on the metabolism of MDCK cells regarding key enzyme activities.

The major results have previously been published in the *Biotechnology and Bioengineering* journal (Janke et al., 2011a; Janke et al., 2010b), in the *Journal of Biotechnology* (Janke et al., 2010a), and in the *BioMed Central Proceedings* journal (Janke et al., 2011b) and are included in this thesis (with permission from the publishers). Moreover, selected results from supervised theses (Rühmkorf, 2009; Schäfer, 2009; Seidemann, 2010; Händel, 2010; Wetzel, 2011) that were part of this study (see first page of the Reference section) are also incorporated in this thesis.

4.1 Development of an enzymatic assay platform for mammalian cells

As a starting point for the development of the enzyme platform for mammalian cells, 17 enzyme assays from a high-throughput platform established for plant cells (Gibon et al., 2004), which uses three cycling systems for enzyme activity measurements were adapted for intended use. Overall, 28 enzymes from the central carbon metabolism (glycolysis, pentose phosphate pathway, TCA cycle, glutaminolysis) of mammalian cells were selected to be investigated in adherent MDCK cells in more detail. The first step was to optimize the extraction and reaction conditions, which was checked for all enzymes under investigation. However, the following optimization process is exemplarily shown only for selected enzymes from different metabolic pathways.

4.1.1 Optimization of extraction and reaction conditions for enzymes from mammalian cells

One major modification of the enzyme assay platform from plant cells to mammalian cells was necessary for the preparation of crude cell extracts. The extraction of intracellular compounds from plant cells is difficult due to the rigid cell wall, and most enzymes can only be extracted by vigorous vortexing at low temperatures (Gibon et al., 2004). As mammalian cells possess only a cell membrane, intracellular enzymes could easily be extracted by a combination of chemical and mechanical (ultrasonic treatment) cell disruption in this study. However, concentrations of various EB components, especially the detergent and protease inhibitors were adapted to ensure the release of membrane-bound enzymes and to prevent enzymes of interest from degradation. The concentrations of the EB components for plant cells in comparison to the adapted EB for mammalian cells are shown in Table 4.1.

Table 4.1: Composition of the enzyme extraction buffer (EB) for plant and mammalian cells.

Compound	Concentration	
	Plant cells ^a	Mammalian cells
Hepes/KOH, pH 7.5 (mM)	50	50
Glycerol (% v/v)	10	17
Triton X-100 (% v/v)	0.1	1
MgCl ₂ (mM)	10	10
EDTA (mM)	1	1
EGTA (mM)	1	1
Benzamidine (mM)	1	1
ε-aminocaproic acid (mM)	1	1
Leupeptin (μM)	10	20
DTT (mM) ^b	1	0.5
PMSF (mM)	1	1
BSA (% w/v)	0.25	-

^a As described by Gibon et al. (2004).

^b DTT was omitted in the EB for plant cells when using MTT-based indicator reactions and in the EB for mammalian cells when assaying the activity of PC or PDH.

As a first modification, the BSA (bovine serum albumin) in the EB for mammalian cells was omitted to ensure proper determination of intracellular protein concentrations in MDCK cell extracts and to allow for a calculation of enzyme activities on a basis of protein content. However, BSA was used in the EB for plant cells to prevent the enzymes in question from degradation as it serves as a substrate for several proteases also present in crude cell extracts. It was then decided to increase the concentrations of glycerol (1.7-fold) and leupeptin (2-fold). Glycerol is known to stabilize the catalytic activity of different purified enzymes in

solution and leupeptin is a reversible inhibitor for cysteine and serine proteases (Umezawa, 1976). With these modifications, no significant influence of protease degradation on enzyme activities was found for MDH and LDH (see Figure 4.1 below). The third step in the adaptation of the EB for mammalian cells was to increase the Triton X-100 concentration by a factor of 10 to favor the extraction yield. Triton X-100 is a detergent commonly used in lysis buffers to permeabilize cell membranes of eukaryotes without denaturing proteins/enzymes. However, extraction of enzymes from plant cells based on increasing the Triton X-100 concentration alone would be very unlikely (rigid cell wall). In the contrary, aliquots of plant rosettes were extracted by vigorous vortexing with EB at -180 °C (Gibon et al., 2004). At last, the concentration of DTT, which is used to stabilize enzyme preparations by preventing the formation of disulfides from sulfhydryl groups, was decreased by 50 %. Due to its reducing power on MTT, this chemical was completely omitted from the EB in the assay platform for plant cells when MTT (thiazolyl blue tetrazolium bromide)-based indicator reactions were used. However, by decreasing the concentration in the formulation to 0.5 mM, DTT could still be present in the EB without significantly increasing the reduction rate of MTT (data not shown).

The adapted EB for mammalian cells was finally tested on confluent MDCK cells in six-well plates and the lysis ability was compared to the original EB for plant cells (Figure 4.1). These scouting experiments were performed using direct assays for the measurement of LDH and MDH activities. One reason for choosing MDH was due to the intracellular localization of the enzyme, which can be found in the cytosol as well as in mitochondria (representing different compartments of the cell), whereas LDH is a cytosolic enzyme. Furthermore, as the catalytic activities of LDH and MDH are very high in many mammalian cell lines (Neermann and Wagner, 1996), cell extracts could be highly diluted to minimize interferences from crude extract (e.g., other enzymes). Finally, the assay procedures for these enzymes are comparatively fast and easy to apply (see chapters 3.6.3.24 and 3.6.3.25).

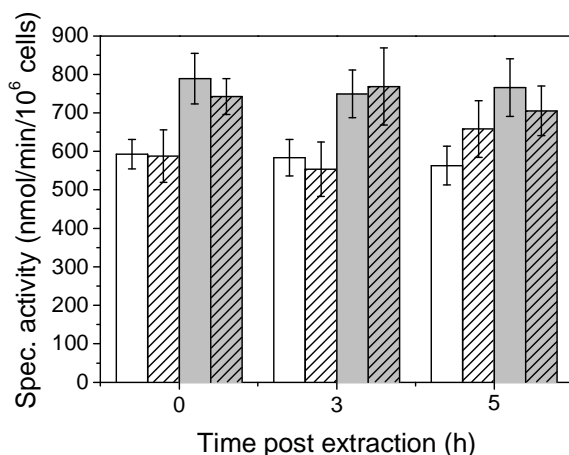


Figure 4.1: Influence of extraction buffer (EB) composition on the specific activities of MDH (white bar) and LDH (grey) in crude cell extracts.

MDCK cells were grown in GMEM-Gln and extracted with EB for mammalian cells or plant cells (hatched) at 0 to 4 °C without additional sonification (Table 4.1). Each determination was performed in three biological replicates; results are given as mean \pm SD.

No significant differences were found for the specific activities of MDH and LDH, and hence, for the extraction efficiency between the two buffers. The EB for plant cells seems to be also applicable to mammalian cells. However, as mentioned above, it does not allow for the quantification of the protein content in cell extracts due to the added BSA. Furthermore, no significant change in specific activities was found after 3 or 5 h post extraction (stored at 0 to 4 °C), which showed that MDH and LDH could be stabilized in the EB for a prolonged time period.

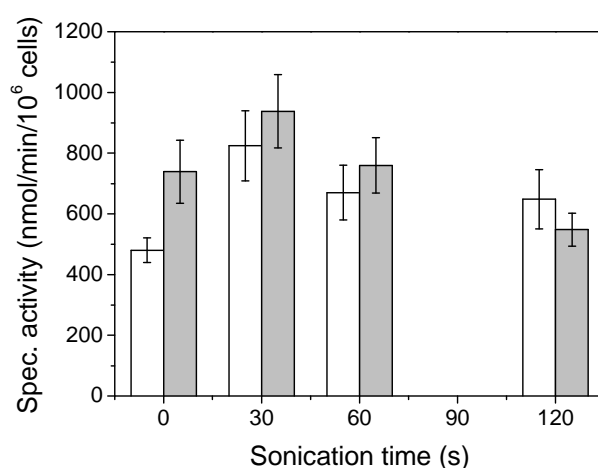


Figure 4.2: Effect of sonication time on the specific activities of MDH (white bar) and LDH (grey) in crude cell extracts.

MDCK cells grown in GMEM-Gln were extracted with EB at 0 to 4 °C. Each determination was performed in three biological replicates; results are given as mean \pm SD.

The effect of sonication treatment on the additional release of the selected enzymes MDH and LDH from adherent MDCK cells in EB was further investigated (Figure 4.2). The additional sonication procedure of MDCK cell extracts had an obvious effect on the release of enzymes. The specific enzyme activities of MDH (cytosolic and mitochondrial) and LDH (only cytosolic) were both maximum when applying 30 s of sonication at maximum power to MDCK cell extracts (1.7-fold and 1.3-fold increase, respectively). Longer ultrasonic treatment did not result in a further increase of specific MDH and LDH activities. Although the release of LDH or the maximum cell-specific LDH activity did not change significantly between the different time points, the specific activity of MDH increased significantly during ultrasonic treatment. Therefore, to maximize the extraction efficiency, a combination of chemical (Triton X-100) and mechanical (30 s of sonication) cell disruption was used for all enzymes under investigation in this study.

The pH optima and substrate affinities of most enzymes differ for plants and mammalian cells. Therefore, the substrate and coupling enzyme concentrations, as well as the pH of the assay buffers had to be adapted. Different databases (<http://www.brenda-enzymes.org/> and <http://enzyme.expasy.org/>) were used to identify relevant publications for the enzymes under investigation. The appropriate substrate concentrations including cofactors and activators (if any), and pH values for the different enzymes were taken from the literature to ensure the determination of maximum catalytic activities (see the Materials and Methods section for optimal assay conditions). Additionally, scouting experiments with different pH values of the assay solutions ranging from 7.5 to 8.5 were conducted to identify optimal conditions. Higher or lower pH values were not considered due to time requirements, and because a significant increase in the catalytic rates of central metabolic enzymes was not expected for this extended range. The overall intracellular pH of MDCK cells grown under different cultivation conditions (e.g., isosmotic or hyperosmotic-acidic) was determined to be approximately 7.4 (Feifel et al., 1997). However, this does not necessarily represent the pH optimum for all intracellular enzymes in MDCK cells. The optimum pH values for three different metabolic enzymes from MDCK cells under the assay conditions used in this study are exemplarily shown in Figure 4.3.

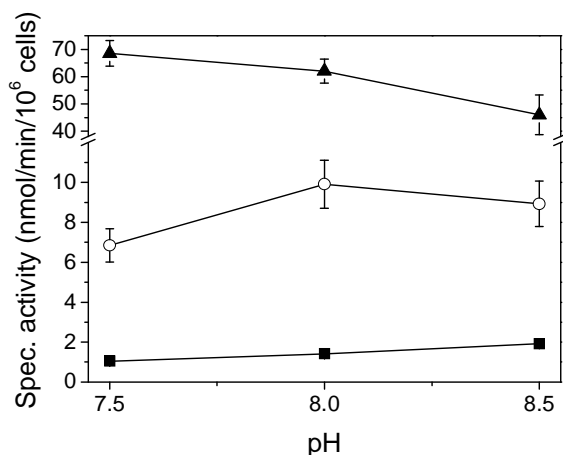


Figure 4.3: Influence of pH on the specific activities of PEPCK (▲), ME (○), and ACoAL (■) from confluent MDCK cells in GMEM-Gln.

Enzymes were incubated at 37 °C for 20 min in 100 mM of Hepes (pH 7.5) or Tricine (pH 8 and 8.5). Each determination was performed in three biological replicates; results are given as mean ± SD (some error bars are smaller than symbols).

PEPCK, which catalyzes the carboxylation of PEP to OAA with the generation of GTP, exerted the highest activity at pH 7.5 (68.5 ± 4.7 nmol/min/ 10^6 cells). At a pH of 8 and 8.5, the specific PEPCK activity decreased by 1.10 and 1.49-fold, respectively. The optimum pH for the oxidative decarboxylation of malate to Pyr via ME was found to be at pH 8 in adherent MDCK cells (9.9 ± 1.2 nmol/min/ 10^6 cells). At a pH of 7.5 and 8.5, the activities decreased by 1.45 and 1.11-fold, respectively. For ACoAL, the optimum was found at pH 8.5 (1.9 ± 0.1 nmol/min/ 10^6 cells), whereas the specific activity at pH of 8.0 and 7.5 decreased by 1.36- and 1.84-fold. As mentioned above, the effect of the buffer pH on the specific enzyme activities was studied in the limited range from pH 7.5 to 8.5 (in 0.5 pH unit intervals). However, if pH 7.5 or 8.5 was the pH optimum for, e.g., PEPCK and ACoAL, respectively, could not be clarified and still has to be investigated in future studies by extending the pH range to higher and lower levels (e.g., pH 6 to 10) and by decreasing the pH interval (e.g., from 0.5 pH units to 0.2 pH units).

Similar to the existing enzyme assays for plant cells (17), 11 new assays were set up for mammalian cells. One important key enzyme of Gln metabolism in mammalian cells is the GLNase, which could not be analyzed with the available cycling systems. Therefore, a new assay based on substrate cycling between GLDH and AspTA was established. The cycling assay generates an accumulating product (MTT), which absorbs light at a wavelength of 570 nm. Details of the method development are described in the following and the validation results of all other assays will be provided in chapter 4.1.3.

4.1.2 Establishment of a new glutaminase assay

This chapter describes the approach for the establishment of a new assay to determine GLNase activity in crude MDCK cell extracts, the first enzyme of glutaminolysis in mammalian cells. The study by Gibon et al. (2004) focused on the investigation of transcripts and the enzyme activities involved in central carbon and nitrogen metabolism of *Arabidopsis thaliana* during diurnal changes, however, without considering GLNase. The protein encoded by the *A. thaliana* gene *PDX2* was shown to have GLNase activity and to be involved in *de novo* vitamin B₆ (pyridoxal 5'-phosphate) biosynthesis (Denslow et al., 2007; Tambasco-Studart et al., 2007). For the establishment of the GLNase assay in this study, all reaction conditions had to be determined, calibration curves, extraction, recovery and validation had to be optimized and performed. This is shown here in detail for the new assay. For all other enzyme assays, the same verification procedures were performed. Due to the high amount of data, details are not given. Final conditions can be found in the Materials and Methods section, and validation results are provided in chapter 4.1.3.

GLNase catalyzes the deamination of Gln to Glu. This enzyme is strongly activated by phosphate (Haser et al., 1985) and, therefore, a concentration of 150 mM was used in the specific assay mix. After incubation for a fixed time period (20 min), the assay was stopped with an excess of HCl, the extract neutralized with NaOH, and the amount of produced Glu determined using the newly developed AspTA/GLDH/(PES + MTT) cycling system (Figure 4.4).

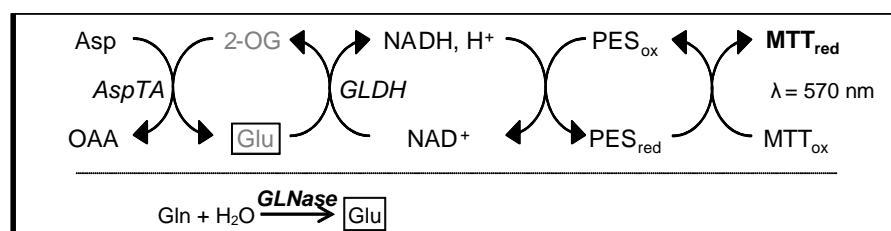


Figure 4.4: Assay principle for GLNase activity. The determination is based on the Glu cycling assay.

The reaction below the cycling system represents the assay for GLNase (highlighted in bold italics). Products that are not measured have been omitted. Metabolites (in grey) are detected indirectly via the reduction of MTT (in bold).

In the first step of the Glu cycling assay, GLDH catalyzes the deamination of Glu to 2-OG, simultaneously NAD⁺ is reduced to NADH + H⁺. In the second step, AspTA catalyzes the reaction in the opposite direction by converting 2-OG with Asp back to Glu. A third step is added to drive the reaction into the direction of 2-OG formation and to increase the

sensitivity of this assay ($\epsilon_{340\text{ nm}} = 6.22\text{ mM}^{-1}\text{ cm}^{-1}$ [NADH]; $\epsilon_{570\text{ nm}} = 17\text{ mM}^{-1}\text{ cm}^{-1}$ [MTT_{red}], Kistler and Lin, 1972). Electrons from NADH are transferred to the electron acceptor dye MTT via the electron transmitter compound PES, and the pyridine nucleotide is subsequently oxidized again. The net reaction ($\text{Asp} + \text{H}_2\text{O} + \text{oxidized MTT (MTT}_{\text{ox}}) = \text{OAA} + \text{NH}_4^+ + \text{reduced MTT (MTT}_{\text{red}})$) is a reaction of pseudo zero-order with a rate ($d[\text{MTT}_{\text{red}}]/dt = -d[\text{Asp}]/dt$) that depends on the sum of Glu and 2-OG in the assay. Amplification is obtained because each molecule of Glu or 2-OG is cycled many times, leading to the accumulation of OAA, NH_4^+ and MTT_{red}. The increase of MTT_{red} concentration can be directly monitored at 570 nm. During the establishment of this cycling assay for the determination of GLNase activity (and of all other cycling assays, see chapter 4.1.3), three major points were considered: (i) the effect of enzyme and substrate concentrations on cycling rates was investigated (chapter 4.1.2.1), (ii) the linear range of amplification with standard curves from dilutions of Glu was checked (chapter 4.1.2.2), and (iii) the influence of cell extracts on the response of the cycling system was examined (chapter 4.1.2.3).

4.1.2.1 Optimization of cycling reagent concentrations

The substrate concentrations Asp and NAD^+ had to be high enough to be saturating or remain constant during the complete reaction time. AspTA was found to be fully saturated with Asp at concentrations higher than 20 mM (data not shown) and, therefore, the assay concentrations were set to 100 mM. The concentration of the substrate NAD^+ for GLDH remained constant due to the recycling at approximately 1.5 mM. The K_{eq} for GLDH ($[\text{2-OG}] [\text{NADH}] [\text{NH}_4^+] / [\text{Glu}] [\text{NAD}^+] = 3.87 \times 10^{-3}\text{ mM}$; Williamson et al., 1967) strongly favors reductive amination of 2-OG with NADH and the K_{m} of 4.5 mM for Glu (Prisco and Garofano, 1975) indicates a low affinity for its substrate relative to AspTA ($K_{\text{m},\text{2-OG}} = 0.15\text{ mM}$ and $K_{\text{m},\text{Asp}} = 2.0\text{ mM}$; Martinez-Carrion et al., 1967). GLDH was therefore included in excess of AspTA to obtain sufficient cycling rates. A linear increase in the rate of NADH-coupled MTT_{red} production was reached at 10 U/mL GLDH and 5 U/mL AspTA (Figure 4.5).

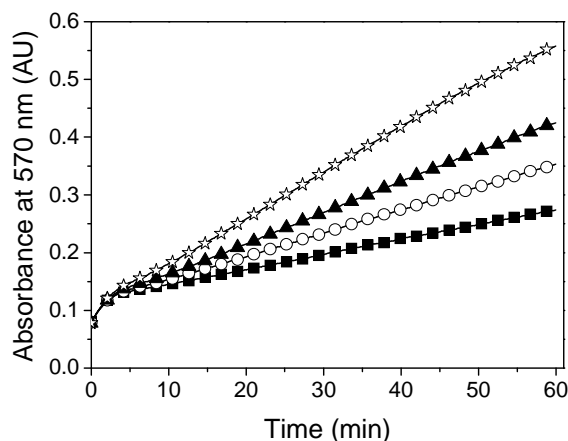


Figure 4.5: Reaction rates of the Glu cycling assay with 10 U/mL GLDH and 5 U/mL AspTA at Glu concentrations of 0 (■), 0.0625 (○), 0.125 (▲), and 0.25 (★) nmol/well.

After a short lag-phase of approximately 5 min, the reaction rate was constant over a period of at least 40 min. The rate of cycling was optimized at pH 8 (data not shown) with 1 mM EDTA included to trap inhibiting Mg^{2+} ions present in cell extracts (Kuo et al., 1994). ADP (0.5 mM) was used as an allosteric activator of GLDH (Hornby et al., 1984). During cycling the concentrations of Glu and 2-OG had to be clearly lower than their Michaelis constants ($K_{m,Glu}$ and $K_{m,2-OG}$ toward GLDH and AspTA, respectively), so that the reaction rates remained proportional to the corresponding concentrations. Under these conditions and with relatively high activities of AspTA and GLDH, a small amount of 2-OG or Glu could produce large quantities of the product NADH, and accordingly MTT_{red} . Thus, the system acted as a chemical amplifier in the quantitative determination of low levels of 2-OG and Glu when MTT_{red} was measured.

4.1.2.2 Calibration curve with standard liquid samples

The linearity of the cycling system was checked with reference liquids containing the analyte at a known concentration. Figure 4.6 shows sensitivity and linearity for the measurement at low levels of Glu. Due to the cycling of Glu/2-OG, similar data could be obtained for 2-OG.

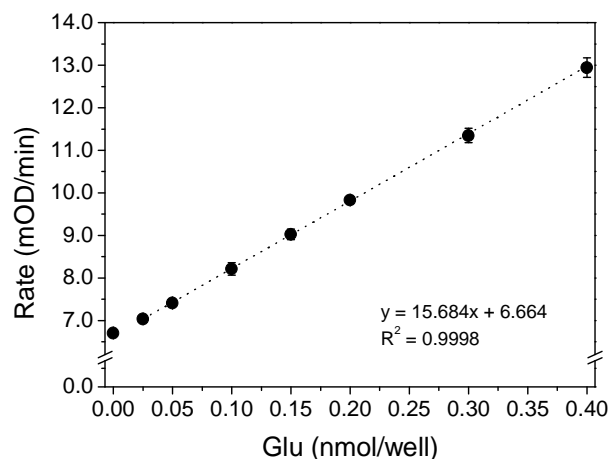


Figure 4.6: Calibration curve of the Glu cycling assay for Glu.

The cycling reaction was run for 30 min, including different amounts of Glu (0, 0.025, 0.05, 0.1, 0.15, 0.2, 0.3, and 0.4 nmol) per reaction. The specific assay mix (including Gln) and the EB (in which the Glu was added) are described in the Materials and Methods section. Each determination was performed in four replicates, results are given as mean \pm SD (some error bars are smaller than symbols). Dotted line obtained from linear regression analysis.

The assay validation was performed with a defined dilution series of Glu over a range of 0 to 0.4 nmol/well (higher concentrations were not considered). Eight replicate measurements at the lower (25 pmol) and upper (0.4 nmol) working range were performed to investigate homogeneity of variances (F-Test; 99 %). The Glu cycling assay showed homogeneous variances and, therefore, an unweighted regression analysis was carried out. Linearity was checked by quantification of four replicates of each dilution (Mandel's fitting test was performed at the 99 % confidence level). The LOD, with a signal to noise ratio of 3.3, was found to be 6.3 pmol/well. The LOQ was 19.0 pmol/well, and the absolute and relative SD of the method was 1.9 pmol/well and 1.24 %, respectively. The high offset in the absence of added Glu (\sim 6.7 mOD/min) was due to Gln in the assay mix preparation (V_{\max} conditions).

4.1.2.3 Confirmation with cell extract

After developing and validating this new cycling assay for measuring low amounts of Glu (or 2-OG), determination of GLNase activity in MDCK cells (grown to confluency in GMEM-Gln) was evaluated. Samples of MDCK cell extracts were incubated under " V_{\max} " conditions with an excess of Gln (40 mM) and phosphate (150 mM) for a fixed time period (20 min) before stopping the reaction with HCl (step 1, Figure 3.1). The control (V_{blank}) was performed without Gln. The amount of produced Glu under each condition was then measured in the second step of the GLNase assay. The enzyme activity was determined by subtracting the V_{blank} from the V_{\max} rates.

At first, the influence of MDCK cells on the enzyme activity had to be characterized. Therefore, different amounts of extracted MDCK cells were included in the new GLNase assay to ensure proportionality between product formation and cell amount or time, respectively (Figure 4.7).

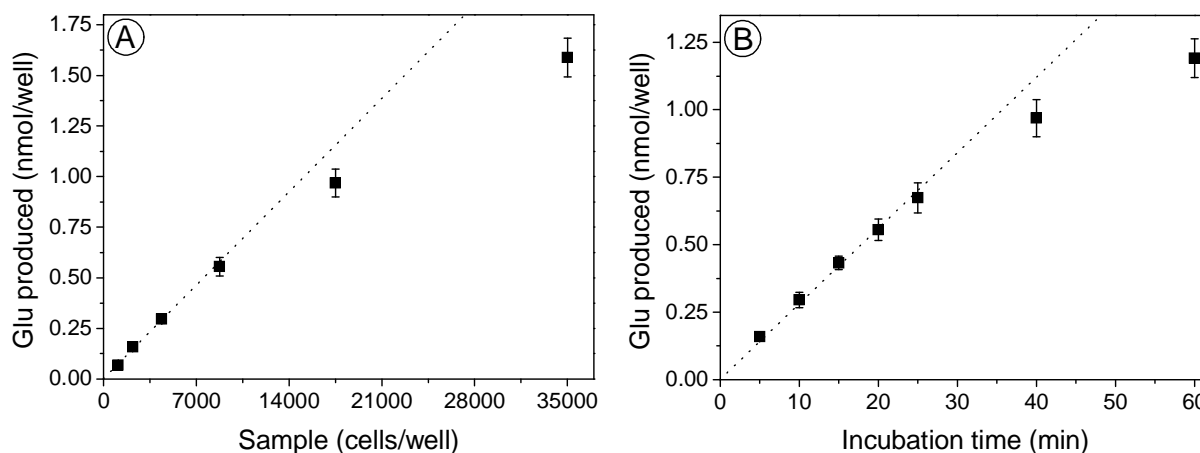


Figure 4.7: Glu production against (A) the cell concentration and (B) the incubation time for GLNase activity determination in extracts of MDCK cells grown in six-well plates with GMEM-Gln.

For panel (A), the GLNase reaction was stopped after 20 min and for panel (B), 8,750 cells per well were used. Results are given as mean \pm SD of three independent determinations (some error bars are smaller than symbols).

The amount of Glu formed was linear with the cell concentration in the range of 1,100 to ~9,000 cells/well when the reaction was stopped after 20 min (Figure 4.7 A). Linearity with time was checked by stopping the reaction after various time periods (Figure 4.7 B) with a concentration of 8,750 cells/well. The progress of the enzymatic reaction was linear with time at least up to 25 min. In general, the reaction was linear until about 0.6 nmol product per assay was formed. The rate of cycling reaction was not linearly proportional to the concentration of Glu if more than 1.2 nmol Gln were reduced in the assay system (suggesting the conversion of Gln by GLNase into equimolar quantities of Glu and NH_3).

Secondly, the recovery of the product of the GLNase was checked by spiking the assay mixture with different amounts of Glu before starting the reaction with extract addition (V_{extract}) and comparing this with the response when Glu was added in the absence of extract (V_{buffer}). Product recoveries of 98 and 107 % were obtained in V_{blank} (Figure 4.8 B) and V_{max} (Figure 4.8 A) conditions, respectively.

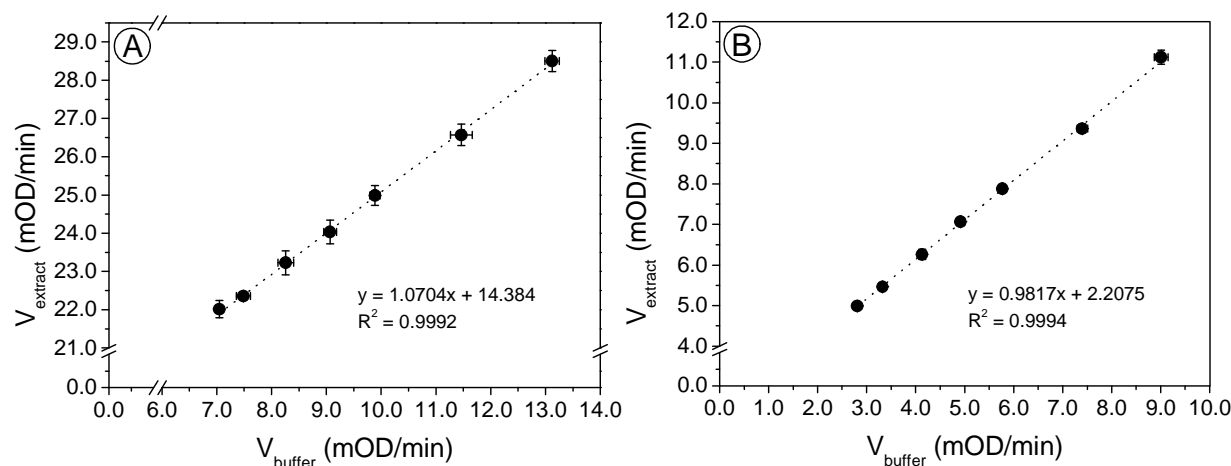


Figure 4.8: Recovery of Glu standards in extracts of MDCK cells grown in six-well plates with GMEM-Gln during the assay of GLNase.

Before starting the GLNase assay, 0.025, 0.05, 0.1, 0.15, 0.2, 0.3, and 0.4 nmol of Glu were added to the assay mix before starting the reaction by adding extract (V_{extract}) or, as a reference, EB (V_{buffer}). This test was carried out with assay mix containing (A) Gln (V_{max}), or (B) from which Gln was omitted (V_{blank}). The slope of the line gives the fraction of Glu recovered. The GLNase reaction was stopped after 20 min and a cell concentration of 4,400 cells per well was used. Data are given as mOD/min \pm SD ($n=3$, some error bars are smaller than symbols).

GLNase activity was not inhibited by the Glu that accumulated during the assay because the amount was orders below the inhibition concentration of the enzyme (Shapiro et al., 1982). Compounds in the extract did not seem to inhibit the cycling reaction significantly. The extract was highly diluted prior to addition to the cycling assay. Figure 4.6 and Figure 4.8 show that the sensitivity limit for routine measurement in MDCK cell extracts was ~ 0.025 nmol product per assay, which accounts for less than 10 % of the GLNase activity at a cell amount of 8,750 cells and an assay duration of 20 min (Figure 4.7).

The coefficient of variation (CV) was calculated from five paired determinations of GLNase activity in which three to four technical replicates were measured. V_{blank} and V_{max} conditions gave a mean CV of 3.4 and 2.2 %, respectively.

4.1.3 Validation of the remaining enzyme assays

The remaining enzyme assays were validated according to the above mentioned GLNase assay. Aliquots of extracts were incubated with the respective substrates for a fixed time period before stopping the reaction. Afterwards the product concentration was determined in the respective cycling assay. An assay validation with standards in EB was performed to evaluate the quality of the established microassays. Eight replicate measurements at the lower (25 pmol) and upper (0.3 or 0.4 nmol) working range were performed to investigate

homogeneity of variances (F-Test; 99 %). All investigated cycling assays showed homogeneous variances, and unweighted regression analysis was carried out with a defined dilution series of the respective standard over a range of 0 to 0.4 nmol. Linearity was checked by quantification of four replicates of each dilution and was found for all assays over the respective range (Mandel's fitting test was performed at the 99 % confidence level). If necessary, the concentration range was constricted (0 to 0.3 nmol per well) to avoid quadratic regression. For all assays, the coefficient of determination (R^2) was above 0.99. For most cycling assays, the LOD (3.3 x SD of the method) was in the lower pmol range (<10 pmol) and the LOQ (10 x SD of the method) below the lower working range (<25 pmol).

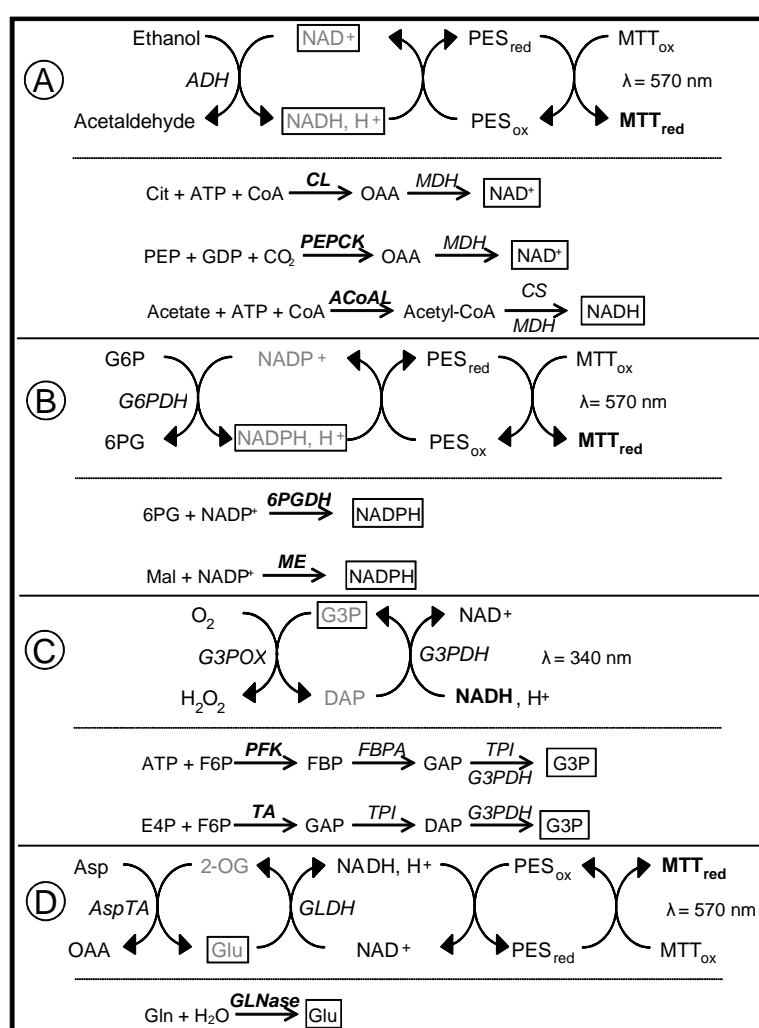


Figure 4.9: Principles of indirect assays with enzymatic cycling. Determinations are based on **(A)** the NAD⁺ cycling assay, **(B)** the NADP⁺ cycling assay, **(C)** the G3P cycling assay, and **(D)** the Glu cycling assay.

The reactions below the respective cycling assays represent the 8 enzyme assays additionally established. All other enzyme reactions are described in the Materials and Methods section. Enzymes analyzed are highlighted in bold italics, detectable molecules in grey. Products as well as co-substrates that are not measured have been omitted.

An overview of the principles of the newly developed assays with enzymatic cycling is provided in Figure 4.9 and the results of the enzyme assay validation are reported in the following three tables: Table 4.2 summarizes the validation results obtained from calibration curves of the remaining cycling assays and the GS assay with the respective standards, Table 4.3 shows the linear range (proportionality between product formation and cell amount or time) for the different enzyme assays, and Table 4.4 summarizes the results found for the recoveries of spiked standards when using the cycling assays and the GS assay.

Table 4.2: Summary of assay validation from calibration curves of the different cycling assays with the respective standards.

No.	Enzyme	Method	Standard	Amount ^a (nmol)	Linear regression ^b	R ²	LOD (pmol)	LOQ (pmol)	Relative SD of the method (%)
1	CS (EC 2.3.3.1)	NAD ⁺ cycle via ADH/(PES + MTT)	NADH	0, 0.025, 0.05, 0.1, 0.15, 0.2, 0.3 and 0.4	y = 151.032x + 4.311	0.9998	6.7	20.4	1.34
2	CL (EC 2.3.3.8)	as 1	OAA	0, 0.025, 0.05, 0.1, 0.15, 0.2, 0.3 and 0.4	y = 126.905x + 9.528	0.9999	6.1	18.5	1.21
3	NAD-ICDH (EC 1.1.1.41)	as 1	NADH	0, 0.025, 0.05, 0.1, 0.15, 0.2, 0.3 and 0.4	y = 159.749x + 3.711	0.9998	7.9	23.9	1.56
4	FUM (EC 4.2.1.2)	as 1	Malate	0, 0.025, 0.05, 0.1, 0.15, 0.2, and 0.3	y = 73.855x + 5.567	0.9998	5.3	16.1	1.37
5	GLDH (EC 1.4.1.2)	as 1	NAD ⁺	0, 0.025, 0.05, 0.1, 0.15, 0.2, 0.3 and 0.4	y = 173.070x + 3.967	0.9997	8.2	24.7	1.62
6	AlaTA (EC 2.6.1.2)	as 1	Pyr	0, 0.025, 0.05, 0.1, 0.15, 0.2, 0.3 and 0.4	y = 176.809x + 7.300	0.9999	4.4	13.4	0.88
7	AspTA (EC 2.6.1.1)	as 1	OAA	0, 0.025, 0.05, 0.1, 0.15, 0.2, and 0.3	y = 140.456x + 4.685	0.9997	7.0	21.2	1.80
8	PEPCK (EC 4.1.1.32)	as 1	OAA	0, 0.025, 0.05, 0.1, 0.15, 0.2, 0.3 and 0.4	y = 135.318x + 24.594	0.9999	4.8	14.5	0.95
9	ACoAL (EC 6.2.1.1)	as 1	NADH	0, 0.025, 0.05, 0.1, 0.15, 0.2, 0.3 and 0.4	y = 132.411x + 16.539	0.9997	8.0	24.1	1.58
10	HK (EC 2.7.1.1)	NADP ⁺ cycle via G6PDH/(PES + MTT)	G6P	0, 0.025, 0.05, 0.1, 0.15, 0.2, and 0.3	y = 174.909x + 3.130	0.9998	5.9	17.7	1.51
11	G6PDH (EC 1.1.1.49)	as 10	NADPH	0, 0.025, 0.05, 0.1, 0.15, 0.2, and 0.3	y = 230.548x + 0.823	0.9996	7.5	22.7	1.93
12	6PGDH (EC 1.1.1.43)	as 10	NADPH	0, 0.025, 0.05, 0.1, 0.15, 0.2, and 0.3	y = 217.790x + 0.935	0.9996	7.4	22.6	1.91
13	NADP-ICDH (EC 1.1.1.42)	as 10	NADPH	0, 0.025, 0.05, 0.1, 0.15, 0.2, 0.3 and 0.4	y = 225.488x + 0.900	0.9998	6.4	19.3	1.26
14	ME (EC 1.1.1.40)	as 10	NADPH	0, 0.025, 0.05, 0.1, 0.15, 0.2, and 0.3	y = 299.432x + 0.610	0.9997	7.1	21.5	1.82

Table 4.2: (Continued from previous page.)

No.	Enzyme	Method	Standard	Amount ^a (nmol)	Linear regression ^b	R ²	LOD (pmol)	LOQ (pmol)	Relative SD of the method (%)
15	PFK (EC 2.7.1.11)	G3P cycle via G3POX/G3PDH	FBP	0, 0.025, 0.05, 0.1, 0.15, 0.2, 0.3 and 0.4	y = -40.870x - 1.084	0.9999	3.7	11.3	0.74
16	FBPA (EC 4.1.2.13)	as 15	DAP	0, 0.025, 0.05, 0.1, 0.15, 0.2, 0.3 and 0.4	y = -16.642x - 3.567	0.9998	6.6	20.1	1.31
17	GAPDH (EC 1.2.1.12)	as 15	DAP	0, 0.025, 0.05, 0.1, 0.15, 0.2, 0.3 and 0.4	y = -14.850x - 1.010	0.9998	7.4	22.4	1.46
18	PK (EC 2.7.1.40)	as 15	ATP	0, 0.025, 0.05, 0.1, 0.15, 0.2, 0.3 and 0.4	y = -13.694x - 7.367	0.9998	7.4	22.5	1.47
19	TK (EC 2.2.1.1)	as 15	DAP	0, 0.025, 0.05, 0.1, 0.15, 0.2, 0.3 and 0.4	y = -12.815x - 14.373	0.9991	15.3	46.5	3.04
20	TA (EC 2.2.1.2)	as 15	DAP	0, 0.025, 0.05, 0.1, 0.15, 0.2, 0.3 and 0.4	y = -11.431x - 13.292	0.9998	7.7	23.2	1.52
21	GLNase (EC 3.5.1.2)	Glu cycle via AspTA/ GLDH/(PES + MTT)	Glu	0, 0.025, 0.05, 0.1, 0.15, 0.2, 0.3 and 0.4	y = 15.684x + 6.664	0.9998	6.3	19.0	1.24
22	GS (EC 6.3.1.2)	indirect via NH ₂ OH·HCl + FeCS	γGH	0, 1.5625, 3.125, 6.25, 12.5, 25 and 50	y = 0.002x + 0.048	0.9998	985	2,986	2.12

Note. Details for the specific enzyme mixes (V_{max} conditions) and the EB (in which the respective standard was added) can be found in the Materials and Methods section. Eight replicate measurements at the lower (25 pmol) and upper (0.3 or 0.4 nmol) working range were performed to investigate homogeneity of variances (F-Test; 99 %).

^a The cycling reactions were run for ~30 min, including different amounts of standards per reaction.

^b Assay validation with unweighted regression analysis was performed with a defined dilution series of the respective standard over a range of 0 to 0.3 or 0.4 nmol. Four replicates of each dilution were quantified by the respective cycling system to check the linearity (Mandel's fitting test; 99 %). Equations from the linear regressions are given.

Table 4.3: Linear ranges of enzyme activity for the different assay conditions in extracts of MDCK cells grown in six-well plates in GMEM-Gln.

No.	Enzyme	Method	Linear range ^a (cells)	Time ^b (min)	Sample size ^c (cells)	Av tech error ^d (%)
1	CS	NAD ⁺ cycle via ADH/(PES + MTT)	10-115	40	115	5.8
2	CL	as 1	715-1,820	40	1,580	4.5
3	NAD-ICDH	as 1	910-8,450	60	8,450	7.9
4	FUM	as 1	5-115	40	60	10.1
5	GLDH	as 1	455-2,690	40	1,690	5.1
6	AlaTA	as 1	455-9,100	60	1,210	7.4
7	AspTA	as 1	10-225	40	115	6.9
8	PEPCK	as 1	15-125	25	125	6.1
9	ACoAL	as 1	530-16,900	60	2,115	4.7
10	HK	NADP ⁺ cycle via G6PDH/(PES + MTT)	30-910	60	230	9.0
11	G6PDH	as 10	115-910	60	455	12.8
12	6PGDH	as 10	25-810	25	810	12.6
13	NADP-ICDH	as 10	115-910	40	455	9.4
14	ME	as 10	220-3,500	60	880	9.8
15	PFK	G3P cycle via G3POX/G3PDH	30-450	60	230	3.3
16	FBPA	as 15	15-910	60	115	4.4
17	GAPDH	as 15	10-180	60	45	4.5
18	PK	as 15	5-90	60	25	3.5
19	TK	as 15	115-820	60	455	3.3
20	TA	as 15	100-1620	60	810	5.0
21	GLNase	Glu cycle via AspTA/ GLDH/(PES + MTT)	1,095-9,000	25	8,750	5.6
22	GS	indirect via NH ₂ OH·HCl + FeCS	42,240-168,960	120	168,960	3.4
23	LDH	direct	5-150	n/a	n/a	7.7
24	MDH	direct	5-150	n/a	n/a	7.8
25	PGI	direct via G6PDH	130-8,110	n/a	n/a	2.5
26	TPI	direct via G3PDH	5-150	n/a	n/a	2.3
27	PDH	direct via DP + MTT	21,120-168,960	n/a	n/a	8.7
28	PC	direct via CS + DTNB	2,500-80,000	n/a	n/a	5.2

Note. Different amounts of extracted MDCK cells (grown to confluency in GMEM-Gln) were included in the assay to check proportionality between product formation and cell amount or time, respectively.

^a Reaction rates were linear in the given range of MDCK cells in 2 or 5 μ L EB for cycling and standard assays, respectively. Cycling assays were run for 20 min, except for CS and NAD-ICDH (40 min). The assay of GS was run for 60 min.

^b The assays were checked for linearity with time at the respective sample size (^c). The upper limit is given.

^c Sample sizes refer to cells in 2 (cycling assays) or 5 (GS) μ L EB.

^d Average technical error expressed as CV from 5 to 6 independent determinations of enzyme activity in which three to four technical replicates were measured ($V_{\text{blank}} + V_{\text{max}}$ conditions).

Table 4.4: Recovery of standards in extracts of MDCK cells grown in six-well plates in GMEM-Gln for the enzyme assay validation.

No.	Enzyme	Standard	Amount ^a (nmol)	Sample size ^b	V _{blank} conditions ^c		V _{max} conditions ^d	
					Linear regression	R ²	Linear regression	R ²
1	CS (EC 2.3.3.1)	NADH	0.025, 0.05, 0.1, 0.15, 0.2, and 0.3	80	y = 1.0142x - 0.6019	0.9992	y = 1.0116x + 5.6794	0.9996
2	CL (EC 2.3.3.8)	OAA	0.025, 0.05, 0.1, 0.15, 0.2, and 0.3	1,170	y = 1.096x + 0.8081	0.9995	y = 1.128x + 11.655	0.9999
3	NAD-ICDH (EC 1.1.1.41)	NADH	0.025, 0.05, 0.1, 0.15, 0.2, and 0.3	4,090	y = 0.845x + 4.431	0.9997	y = 0.9028x + 6.5872	0.9991
4	FUM (EC 4.2.1.2)	Malate	0.025, 0.05, 0.1, 0.15, 0.2, and 0.3	30	y = 0.9913x + 0.7573	0.9998	y = 0.9577x + 4.6982	0.9992
5	GLDH (EC 1.4.1.2)	NAD ⁺	0.025, 0.05, 0.1, 0.15, 0.2, and 0.3	820	y = 0.9759x + 4.5614	0.9994	y = 0.9782x + 9.3754	0.9997
6	AlaTA (EC 2.6.1.2)	Pyr	0.025, 0.05, 0.1, 0.15, 0.2, and 0.3	1,640	y = 1.009x + 0.7555	0.9997	y = 1.015x + 14.288	0.9999
7	AspTA (EC 2.6.1.1)	OAA	0.025, 0.05, 0.1, 0.15, 0.2, and 0.3	30	y = 1.0489x - 0.3095	0.9997	y = 0.9811x + 9.974	0.9994
8	PEPCK (EC 4.1.1.32)	OAA	0.025, 0.05, 0.1, 0.15, 0.2, and 0.3	80	y = 1.0965x - 3.4111	0.9997	y = 1.0338x + 32.505	0.9992
9	ACoAL (EC 6.2.1.1)	NADH	0.025, 0.05, 0.1, 0.15, 0.2, and 0.3	1,640	y = 0.9994x - 0.2884	0.9997	y = 1.0747x + 3.2807	0.9994
10	HK (EC 2.7.1.1)	G6P	0.025, 0.05, 0.1, 0.15, 0.2, and 0.3	205	y = 1.1519x + 0.083	0.9991	y = 1.1453x + 12.92	0.9996
11	G6PDH (EC 1.1.1.49)	NADPH	0.025, 0.05, 0.1, 0.15, 0.2, and 0.3	80	y = 1.0037x + 0.032	0.9993	y = 0.9862x + 14.637	0.9996
12	6PGDH (EC 1.1.1.43)	NADPH	0.025, 0.05, 0.1, 0.15, 0.2, and 0.3	80	y = 1.0073x - 0.1642	0.9995	y = 1.013x + 9.6467	0.9997
13	NADP-ICDH (EC 1.1.1.42)	NADPH	0.05, 0.1, 0.15, 0.2, 0.3 and 0.4	120	y = 1.0021x - 0.0596	0.9998	y = 1.0122x + 13.386	0.9999
14	ME (EC 1.1.1.40)	NADPH	0.05, 0.1, 0.15, 0.2, 0.3 and 0.4	270	y = 1.0136x + 0.469	0.9996	y = 1.0086x + 13.125	0.9999

Table 4.4: (Continued from previous page.)

No.	Enzyme	Standard	Amount ^a (nmol)	Sample size ^b (cells)	V _{blank} conditions ^c		V _{max} conditions ^d	
					Linear regression	R ²	Linear regression	R ²
15	PFK (EC 2.7.1.11)	FBP	0.05, 0.1, 0.15, 0.2, 0.3 and 0.4	410	y = 0.9862x – 0.1324	0.9999	y = 0.9933x – 6.4561	0.9998
16	FBPA (EC 4.1.2.13)	DAP	0.05, 0.1, 0.15, 0.2, 0.3 and 0.4	205	y = 0.9865x – 0.0665	0.9994	y = 0.9838x – 3.9869	0.9993
17	GAPDH (EC 1.2.1.12)	DAP	0.05, 0.1, 0.15, 0.2, 0.3 and 0.4	30	y = 0.9887x + 0.0745	0.9997	y = 0.9929x – 4.772	0.9993
18	PK (EC 2.7.1.40)	ATP	0.05, 0.1, 0.15, 0.2, 0.3 and 0.4	20	y = 0.9998x – 0.369	0.9993	y = 1.0065x – 9.0716	0.9995
19	TK (EC 2.2.1.1)	DAP	0.05, 0.1, 0.15, 0.2, 0.3 and 0.4	545	y = 0.9776x + 0.0256	0.9998	y = 1.0102x – 1.2411	0.9992
20	TA (EC 2.2.1.2)	DAP	0.05, 0.1, 0.15, 0.2, 0.3 and 0.4	410	y = 1.009x - 0.1639	0.9997	y = 0.9862x – 2.494	0.9991
21	GLNase (EC 3.5.1.2)	Glu	0.025, 0.05, 0.1, 0.15, 0.2, 0.3 and 0.4	4,400	y = 0.9817x + 2.2075	0.9994	y = 1.0704x + 14.384	0.9992
22	GS (EC 6.3.1.2)	γGH	1.5625, 3.125, 6.25, 12.5, 25 and 50	42,240	y = 0.9951x + 0.0662	0.9992	y = 0.9929x + 0.0657	0.9996

Note. The cycling reactions were run for ~30 min, including different amounts of standards per reaction. Details for the specific enzyme mixes can be found in the Materials and Methods section.

^a Before starting the respective assay, different amounts of standard were added to the assay mix before starting the reaction by adding extract (V_{extract}) or, as a reference, EB (V_{buffer}).

^b Sample sizes refer to cells in 2 (cycling assays) or 5 (GS) μL EB.

^c This test was carried out with assay mix from which the respective substrate was omitted (V_{blank}). The slope of the function gives the fraction of standard recovered.

^d This test was carried out with assay mix containing the respective substrate (V_{max}).

4.1.4 Application of the established enzyme platform on MDCK cells

As a first application of the established method, key enzymes of the central metabolic pathways in adherent MDCK cells grown in GMEM-Gln^{stat} and Episerf^{stat} medium were investigated (Figure 4.10). To determine the maximum enzyme activities during maintenance metabolism (in the stationary phase) in MDCK cells, cultures were grown to confluency (~5 d of growth). Both cell culture media contained similar initial concentrations of the main carbon and energy sources Gluc (30 mM) and Gln (2 mM). GMEM-Gln was a serum-containing (10 % (v/v) FCS) medium, which is typically used in the growth phase of cell cultures. Episerf was chosen as a serum-free alternative in this study because adherent MDCK cells showed similar growth characteristics and maximum cell densities ($\sim 4.0 \times 10^6$ viable cells/well) in six-well plates in this medium (data not shown). Furthermore, a serum-free environment is beneficial for the production phase of, e.g., influenza viruses in adherent MDCK and Vero cells as well as for the subsequent purification step (Genzel et al., 2010). Washing steps and medium exchange to remove the serum are therefore not required for Episerf compared to GMEM-Gln (Genzel et al., 2006a).

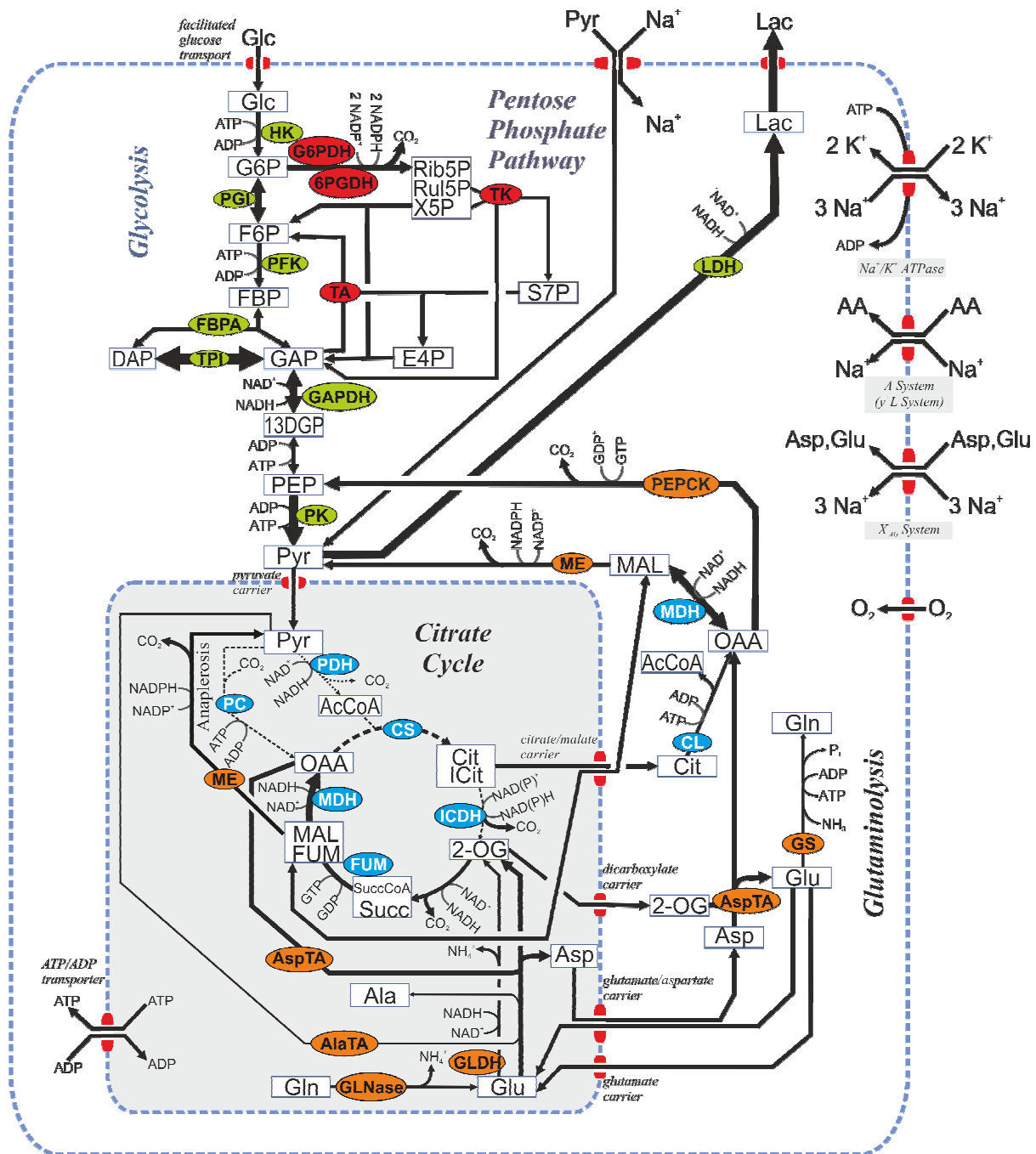


Figure 4.10: Reaction network of the central carbon metabolism of adherent MDCK cells (modified from Wahl et al., 2008).

Enzymes (oval symbols) measured in this study are highlighted in green for glycolysis, in red for pentose phosphate pathway, in blue for citrate cycle and in orange for glutaminolysis. Transporters are shown in red. Blue broken lines separate the cytosol and mitochondrion (grey). Metabolites/lumped metabolites are depicted as white squares. Thickness of arrows indicates the relative magnitude of enzyme activity in GMEM-Gln^{stat} (Table 4.5).

A total of 28 enzymes from four metabolic pathways (glycolysis, pentose phosphate pathway, TCA cycle, and glutaminolysis) were determined and each enzyme was measured in five to six biological replicates (Table 4.5).

Table 4.5: Measured activities of 28 metabolic enzymes from confluent MDCK cells in GMEM-Gln and Episerf.

Enzyme	EC No.	Specific activity (nmol/min/10 ⁶ cells) ^a	
		GMEM-Gln ^{stat}	Episerf ^{stat}
<i>Glycolysis</i>			
HK	2.7.1.1	19.20 ± 2.00 (5)	17.77 ± 1.23 (5)
PGI	5.3.1.9	271.88 ± 15.73 (6)	407.53 ± 16.51 (6)
PFK	2.7.1.11	16.78 ± 2.92 (5)	46.15 ± 2.37 (6)
FBPA	4.1.2.13	23.60 ± 3.53 (6)	42.34 ± 4.79 (6)
TPI	5.3.1.1	6771.68 ± 133.73 (6)	7803.62 ± 350.87 (6)
GAPDH	1.2.1.12	360.57 ± 13.90 (6)	306.50 ± 22.53 (6)
PK	2.7.1.40	1233.77 ± 75.40 (6)	1366.18 ± 95.76 (6)
LDH	1.1.1.27	948.48 ± 45.37 (6)	1844.58 ± 62.24 (6)
<i>Pentose phosphate pathway</i>			
G6PDH	1.1.1.49	58.12 ± 3.92 (6)	96.11 ± 7.99 (5)
6PGDH	1.1.1.44	44.82 ± 3.03 (6)	65.90 ± 5.51 (6)
TK	2.2.1.1	11.23 ± 1.23 (5)	23.17 ± 0.62 (6)
TA	2.2.1.2	15.57 ± 0.75 (6)	24.92 ± 2.79 (6)
<i>Tricarboxylic acid cycle</i>			
PDH	1.2.4.1	0.25 ± 0.02 (5)	0.05 ± 0.01 (6)
PC	6.4.1.1	0.62 ± 0.07 (6)	0.88 ± 0.07 (6)
CS	2.3.3.1	12.88 ± 0.67 (5)	28.05 ± 1.80 (6)
CL	2.3.3.8	5.87 ± 0.27 (6)	9.28 ± 0.28 (6)
NAD-ICDH	1.1.1.41	0.43 ± 0.03 (6)	0.63 ± 0.06 (6)
NADP-ICDH	1.1.1.42	36.48 ± 2.44 (5)	53.19 ± 4.83 (5)
FUM	4.2.1.2	125.93 ± 21.20 (5)	71.23 ± 5.52 (5)
MDH	1.1.1.37	795.05 ± 52.07 (6)	1247.58 ± 47.66 (6)
<i>Glutaminolysis</i>			
GLNase	3.5.1.2	3.58 ± 0.29 (6)	7.03 ± 0.54 (6)
GS	6.3.1.2	0.60 ± 0.08 (5)	Not detected (6)
GLDH	1.4.1.2	4.63 ± 0.48 (6)	6.89 ± 0.63 (6)
AlaTA	2.6.1.2	1.97 ± 0.14 (6)	2.18 ± 0.12 (6)
AspTA	2.6.1.1	124.75 ± 18.18 (5)	96.90 ± 1.84 (6)
ME	1.1.1.40	10.41 ± 0.57 (6)	11.13 ± 0.48 (6)
PEPCK	4.1.1.32	72.50 ± 7.01 (5)	193.42 ± 19.34 (6)
<i>Miscellaneous</i>			
ACoAL	6.2.1.1	1.84 ± 0.18 (6)	2.87 ± 0.22 (6)

^a Mean values and 95 % confidence intervals for the number of biological replicates shown in parentheses.

Activities of different enzymes (even from the same pathway) are spanning several orders of magnitude in MDCK cells grown in GMEM-Gln^{stat} and Episerf^{stat}. The overall range of stationary-phase cells comprises values from 0.25±0.02 nmol/min/10⁶ cells (PDH) to 6771.68±133.73 nmol/min/10⁶ cells (TPI) in GMEM-Gln^{stat} and from 0.05±0.01 nmol/min/10⁶ cells (PDH) to 7803.62±350.87 nmol/min/10⁶ cells (TPI) in Episerf^{stat}. In both media, very high activities (>700 nmol/min/10⁶ cells) were found for the

glycolytic enzymes TPI, PK and LDH, and MDH, while the other activities were in the range of 1 to 500 nmol/min/10⁶ cells. The lowest enzyme activities in both media were found for PDH, PC, and NAD-ICDH (<1 nmol/min/10⁶ cells). A very low activity was also detected for GS in GMEM-Gln^{stat} (0.60±0.08 nmol/min/10⁶ cells), whereas no activity was detected for GS under serum-free conditions (GS activity was below the detection level of the assay in Episerf^{stat}).

Existing assays for enzyme activity measurements often use continuous procedures based on direct assays, which are not as sensitive and relatively laborious when using cuvettes instead of 96-well microplates. The established enzyme platform using four sensitive cycling assays (0.025 to 0.4 nmol product per assay) allowed precise determination of enzyme activities in very small sample volumes or samples with low enzyme levels. This makes cycling assays extremely valuable for studies on metabolic control and capacity of different continuous cell lines typically used for manufacturing of biopharmaceuticals. Compared to the platform for plant cells, sample preparation steps were less laborious for mammalian cell lines as disruption of cell walls was not required. The analysis of key enzyme activities showed typical characteristics of glycolysis (high PK and LDH activities), citrate cycle (low PDH, PC and NAD-ICDH activities) and glutaminolysis in both media supporting the hypothesis of a truncated TCA cycle in confluent MDCK cell cultures (see the Discussion section). Changes in specific enzyme activities of adherent MDCK cells could be recorded during their growth under different cultivation conditions because enzyme activities are determined in cell extracts under maximum substrate supply, so that any change in enzyme activity measured can be referred to a direct change in enzyme protein content. Moreover, these tools can easily be adapted to the detection of key enzyme activities in other cell lines.

4.2 Production of *Pichia farinosa* glycerokinase for the application in sensitive cycling assays

This chapter describes the production of a new coupling enzyme, namely GK from *P. farinosa*, with the *P. pastoris* expression system to measure the activity of PK in MDCK cell extracts, and to provide the flexibility to analyze, e.g., UTP-generating enzymes in future studies on cell metabolism. The assay to measure the activity of PK, which produces Pyr and ATP from PEP and ADP, is based on coupling of ATP via GK. GK catalyzes the phosphorylation of glycerol to yield G3P, which can then be analyzed using the G3P cycling system of the enzyme platform (Figure 4.9 C and Figure 4.11).

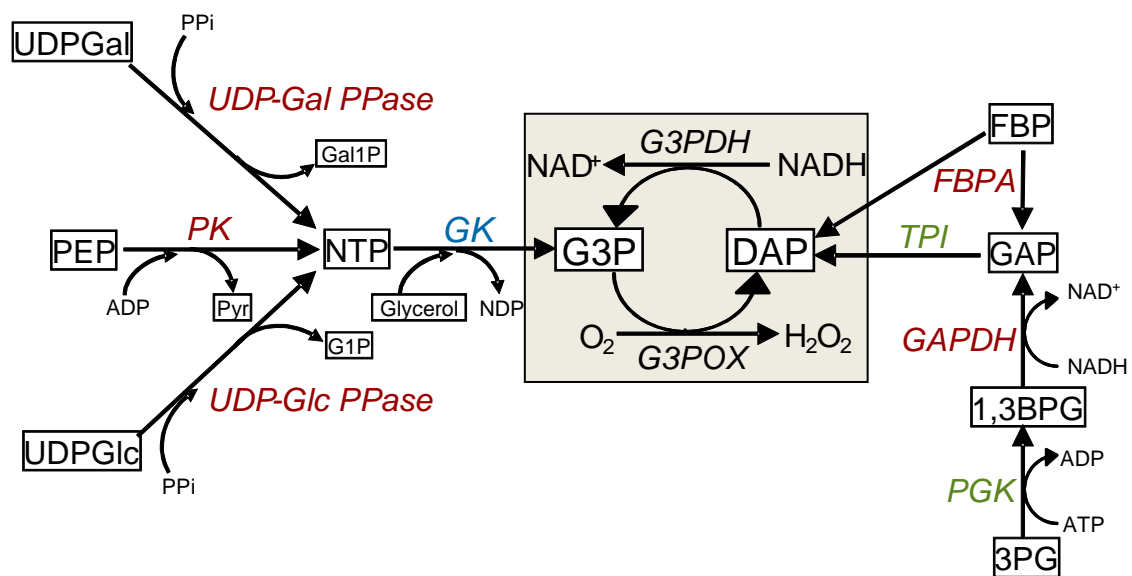


Figure 4.11: Principles of GK-coupled assays and other selected assays based on the G3P cycling.

GAPDH and FBPA (highlighted in red) activities can be determined via the coupling enzyme TPI (in green), which converts GAP to DAP. The coupling enzyme PGK is needed to deliver 1,3BPG (not commercially available) from 3PG in the assay for GAPDH. GK from *P. farinosa* (in blue) is useful to couple the reactions catalyzed by UDP-Gal PPase, UDP-Glc PPase or PK, as it converts any NTP to G3P. G3P and DAP can be quantified by the G3P cycling assay (in grey) via the G3POX/G3PDH-driven depletion of NADH. Metabolites are depicted as white squares and all enzymes in italic type.

In contrast to other GKs (e.g., from *E. coli*; Hayashi and Lin, 1967), GK from *P. farinosa* can also utilize different nucleoside triphosphates (NTPs) for phosphorylation of glycerol, which makes this enzyme very valuable for the application as a coupling enzyme in G3P cycling assays (Figure 4.11). In the following, the construction of the expression vector, the production in *P. pastoris* and the purification will be described in detail.

4.2.1 Construction of expression vector for His₆-tagged glycerokinase

For the production of active His₆-tagged *P. farinosa* GK, the yeast *P. pastoris* and the vector pPIC3.5 were selected as the host and the expression vector, respectively. Parallel investigations concerning the expression of this enzyme with the vector pPIC9 (Invitrogen) for extracellular production was not successful (data not shown), probably due to adverse cultivation conditions (e.g., medium, pH and temperature influences). The DNA fragment encoding for a His₆-tagged GK (~2,000 bp) was amplified from plasmid DNA (pETM-11-GK) using PCR with specific primers containing restriction sites at the 5' ends and cloned into the *AvrII* and *NotI* sites of pPIC3.5. The resulting vector pPIC3.5-GK (Figure 3.2) was purified from TOP10F' *E. coli* cells, and its digestion with *NdeI* or *PvuI* indicated two nucleotide fragments at the expected sizes of 4.3 and 5.5 kb or 2.3 and 7.5 kb, respectively (Figure 4.12, lanes 3 and 4). The digestion of the plasmid by the restriction endonuclease *EcoRV* resulted in three fragments of the expected sizes of 0.8, 3.8 and 5.2 kb (Figure 4.12, lane 5). Finally, the integrity of the construct was confirmed by DNA sequencing (see appendix).

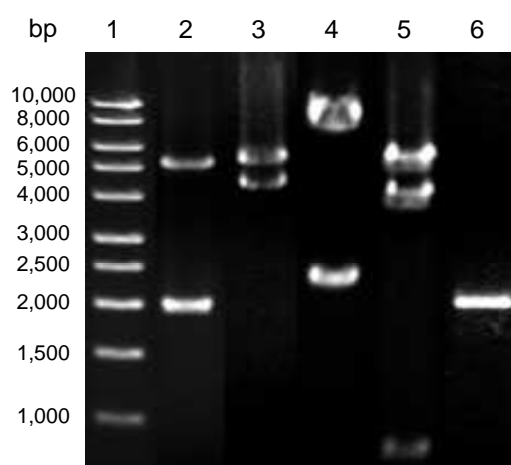


Figure 4.12: PCR and restriction enzyme analysis of the constructed pPIC3.5-GK vector on 1 % (w/v) agarose gel.

Lane 1: size marker 1 kb (Sigma); lane 2: pETM-11-GK double digested with *XbaI* and *NotI*, showing the ~2,000 bp *GUT1* gene; lanes 3 to 5: pPIC3.5-GK digested with *NdeI*, *PvuI* or *EcoRV*, respectively; lane 6: PCR amplification of *GUT1* gene on recombinant *P. pastoris* cells using specific primers.

The *P. pastoris* GS115 strain was transformed using pPIC3.5-GK plasmid DNA linearized by digestion with *StuI* to generate His⁺ strains (Invitrogen, 2002a). Chromosomal integration of *GUT1* gene in *P. pastoris* was evidenced by PCR and gene-specific primers (Figure 4.12, lane 6). Transformants carrying the His₆-tagged GK were grown on BMM medium and the

clone showing highest GK activity (~ 2.5 U/mg protein) was selected for production of recombinant GK (clone 32, Figure 4.13).

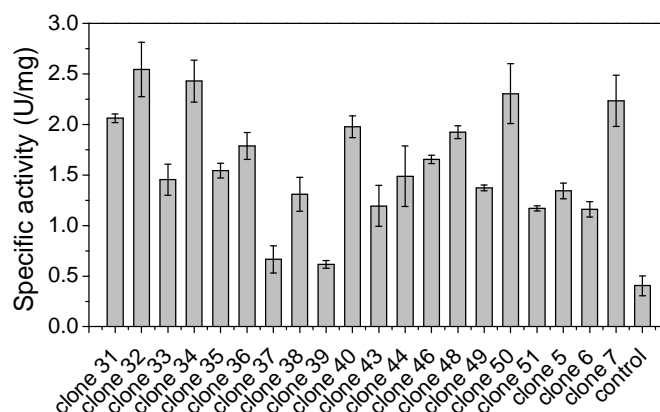


Figure 4.13: Intracellular GK activity of selected pPIC3.5-GK-carrying transformants (clones 5 to 51) and of the control clone (carrying the empty vector pPIC3.5) after 45 h of cultivation.

The cells were grown in BMM medium (27 °C, shaking at 150 rpm), and supplemented with methanol to a final concentration of 1 % (v/v) every 24 h. Each determination was performed in two replicates (results are given as mean \pm SD).

4.2.2 Glycerokinase production by exponential feeding of methanol

A fed-batch culture (Figure 4.14) using an exponential feeding strategy was carried out to achieve high cell density cultivation of *P. pastoris* GS115 harboring pPIC3.5-GK (clone 32, Figure 4.13).

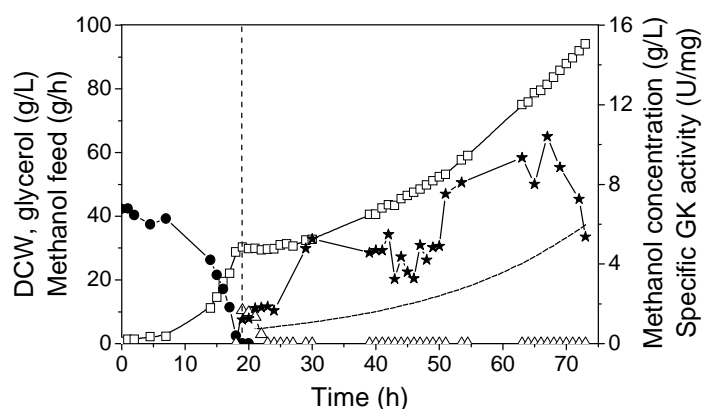


Figure 4.14: High cell density cultivation of recombinant *P. pastoris* expressing His₆-tagged GK from *P. farinose* (clone 32) in BSM supplemented with PTM₁ trace salts in a 5-L bioreactor at 30 °C and pH 5. Dissolved oxygen was kept above 30 % during the fermentation process.

After unlimited growth in the batch phase ($\mu_{\max} = 0.23$ h⁻¹) with glycerol as substrate (0 to 19 h), protein expression was induced with 1.8 g/L of methanol (dashed vertical line). After adaptation to methanol, the fed-batch mode with methanol as only carbon source was started at 21 h with a specific growth rate of $\mu_{\text{set}} = 0.04$ h⁻¹. Time course of DCW (□), concentrations of glycerol (●) and methanol (Δ), mass flow of methanol into the bioreactor (-), and specific GK activity (★).

Production of GK was induced after 19 h of culture in glycerol-containing medium with a final methanol concentration of 1.8 g/L. The methanol fed-batch process was initiated after 21 h at 29.8 g/L DCW. According to Trinh et al. (2003), the methanol flow rate was increased exponentially, and the specific culture growth rate was kept at 0.04 h^{-1} to prevent accumulation of methanol to a toxic level. The maximum specific growth rate in BSM on methanol for clone 32 was determined as $\mu_{\max} = 0.07 \text{ h}^{-1}$, which was half as much (0.14 h^{-1}) as the *P. pastoris* wild-type strain (Brierley et al., 1990). The specific GK activity increased for 48.5 h after induction to a maximum value of 10.4 U/mg cellular protein at 81.4 g/L DCW. The cultivation was stopped after decrease in specific GK activity was observed. Total biomass was harvested after 73 h of cultivation with 94.1 g/L CDW and a specific GK activity of 5.4 U/mg cellular protein.

4.2.3 Purification of recombinant glycerokinase

Recombinant His₆-tagged GK was purified by a combination of an affinity and anion exchange chromatography. First, the crude protein from *P. pastoris* lysate (cell free extract obtained from homogenization of 7.5 g of frozen cells in 500 mL lysis buffer and the subsequent clarification process) was directly applied to Ni²⁺-Sephacrose 6 FF, a typical column for His-tagged proteins (Figure 4.15). The GK was then eluted from the column at an imidazole concentration of ~25 to 150 mM in buffer B. At this stage, the sample (pooled fractions) was purified 46.8-fold with a specific activity of 154.5 U/mg protein and 56 % recovery (see Table 4.6 at the end of this chapter).

After affinity chromatography, enzyme fractions (561 to 628 mL) were combined and loaded onto a Q-Sepharose HP column (Figure 4.16).

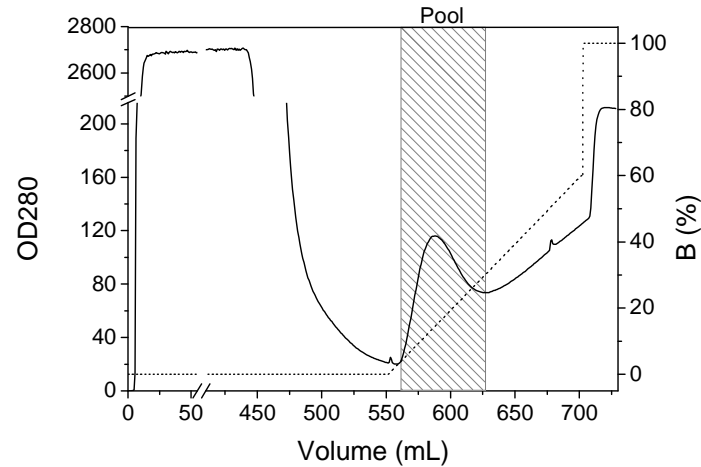


Figure 4.15: First purification step of recombinant His₆-tagged GK isolated from *P. pastoris* (clone 32) cell lysate using Ni²⁺-Sepharose 6 FF chromatography.

450 mL of a cell-free extract (~1.2 g) was loaded onto a Ni²⁺-Sepharose column (5 mL BV). The column was equilibrated with 50 mM sodium phosphate buffer, pH 7.4, containing 0.5 M NaCl and 20 mM imidazole at a flow rate of 5 mL/min. After loading, the column was washed with the same buffer and the proteins containing GK activity were then eluted from the column with a gradient of buffer B (containing 500 mM imidazole). The active fractions (561 to 628 mL, indicated by the hatched area) were pooled and concentrated. The solid lines indicate the absorbance at 280 nm (total protein concentration) and the dotted lines the buffer concentration.

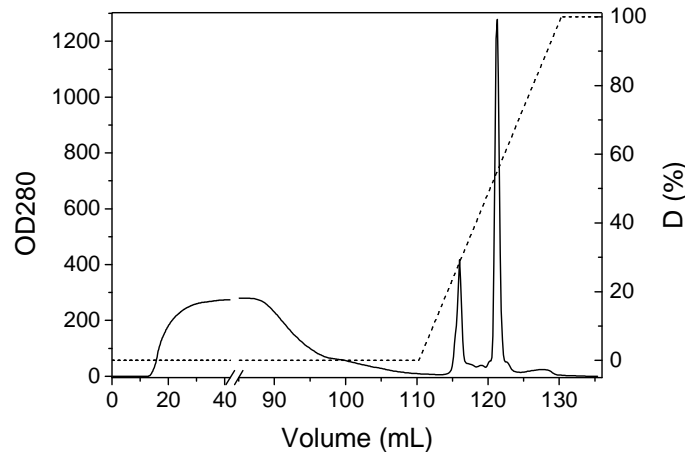


Figure 4.16: Second purification step of recombinant His₆-tagged GK from the collected fractions of step 1 (Figure 4.15) using Q-Sepharose HP.

100 mL of buffer C containing active fractions (~15 mg) from the Ni²⁺-Sepharose 6 FF column were applied to a HiTrap Q HP column (1 mL BV). The column was pre-equilibrated with 15 mM sodium phosphate buffer, pH 6.8, at a flow rate of 1 mL/min. After loading, the column was washed with the same buffer and the GK enzyme was then eluted from the column with a gradient of buffer D (containing 1 M NaCl). The active fractions (119 to 124 mL, second peak) were separated from contaminating proteins (first peak) and were pooled, concentrated, and stored at -80 °C. The solid lines indicate the absorbance at 280 nm (total protein concentration) and the dotted lines the buffer concentration.

Two peaks appeared during this final purification step. The target enzyme was eluted from the column at a NaCl concentration of ~430 to 680 mM in buffer D. Contaminating proteins from the first peak were identified by MS-analysis mainly as being *P. pastoris* mitochondrial alcohol dehydrogenase (ADH) with a molecular weight of 37 kDa (Figure 4.17, lane 4). The enzymatically active fractions (checked by assay of GK activity) corresponding to the second peak (119 to 124 mL, Figure 4.16) were combined and used for further experiments (chapters 4.2.4 and 4.2.5).

SDS-PAGE analysis revealed that the two-step purification resulted in a nearly homogeneous preparation of His₆-tagged GK (Figure 4.17, lane 5).

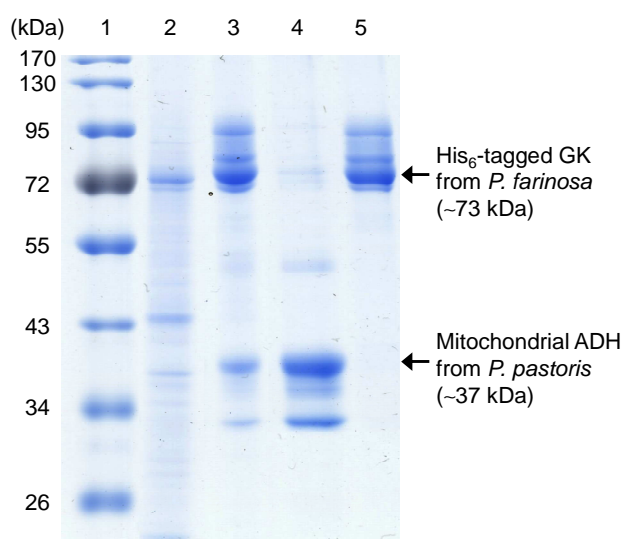


Figure 4.17: SDS-PAGE analysis under non-reducing conditions of His₆-tagged GK from *P. farinosa* at various stages of purification.

Lane 1: molecular mass marker (Fermentas, Vilnius, Lithuania); lane 2: cell-free extract; lane 3: sample of pooled active fractions from Ni²⁺-Sepharose 6 FF chromatography (Figure 4.15); lanes 4 and 5: samples from Q-Sepharose HP (Figure 4.16) chromatography showing the impurity (first peak) and the purified recombinant GK (second peak), respectively.

A major band corresponding to a molecular weight of approximately 73 kDa (Figure 4.17, lanes 3 and 5) agreed with the predicted molecular weight of *P. farinosa* GK (70 kDa) combined with a His₆-tag (3 kDa). The overall yield from an initial 1229.3 mg of total protein supernatant was 0.3 % (Table 4.6). The purification of GK was 61.1-fold with a specific activity of 201.6 U/mg protein and the recovery (or yield) of total enzyme activity was 21 %. During storage, GK activity decreased fast without a stabilizing agent such as (NH₄)₂SO₄ or glycerol. The addition of glycerol (50 %, v/v) to the buffer solution retained GK activity for several months at -80 °C and withstood several freeze-thawing cycles (data not shown).

Table 4.6: Summary on purification of His₆-tagged GK expressed in *P. pastoris*.

Purification steps	Volume (mL)	Total protein (mg)	Total activity (U)	Specific activity (U/mg protein)	Yield (%)	Purification (fold)
Cell-free extract	450	1229.3	4056.7	3.3	100	1.0
Ni ²⁺ -Sephacrose 6 FF	8	14.7	2271.2	154.5	56	46.8
Q-Sephacrose HP	2	4.2	846.7	201.6	21	61.1

4.2.4 Biochemical characterization of glycerokinase

Recombinant His₆-tagged GK from *P. farinosa* showed an optimum pH around 7 (100 %) (Figure 4.18 A), and more than 70 % activity was found within a broad pH range from 6 to 8.5. The optimum temperature for the enzymatic activity was determined as 45 °C (100 %, Figure 4.18 B).

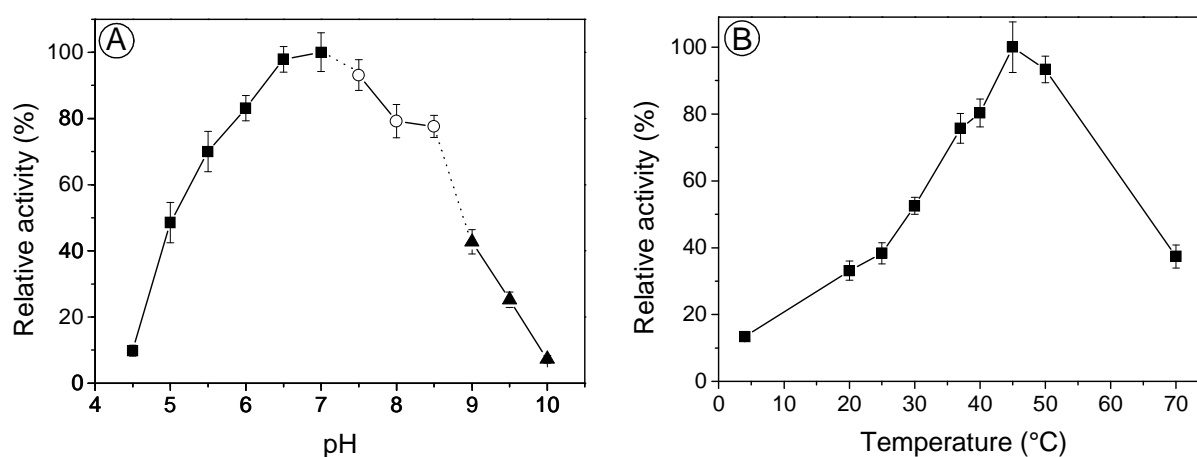


Figure 4.18: Effect of pH and temperature on the activity of purified GK from *P. farinosa*. (A) Effect of pH: purified enzyme was incubated at 37 °C for 20 min in 100 mM of sodium phosphate (■), tricine (○) or sodium borate (▲) buffer. (B) Effect of temperature: reactions were carried out for 20 min at pH 7.0. The conditions that gave maximum GK activity were set to 100 %. Error bars: mean \pm SD of three enzymatic reactions.

Initial velocity studies of *P. farinosa* GK in the forward direction (glycerol + ATP \rightarrow G3P + ADP) at 37 °C and pH 7 were performed with different NTPs (ATP, UTP, ITP, CTP, and GTP). Michaelis-Menten and Lineweaver-Burk plots were generated to calculate the kinetic parameters. The Michaelis constants and the maximum enzyme activities are given at the end of this chapter in Table 4.7.

As expected, ATP saturation curves were hyperbolic, yielding linear double reciprocal plots (Figure 4.19). The K_m value of *P. farinosa* GK for ATP was determined as 428 μ M.

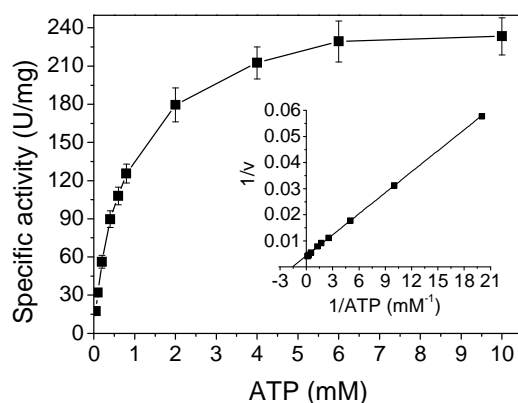


Figure 4.19: Effect of substrate concentration (ATP) on the activity of purified GK from *P. farinosa*.

Michaelis-Menten and Lineweaver-Burk plot (inset) of the initial rate data for His₆-tagged GK were determined over a 20 min incubation period at various concentrations of ATP. Error bars: mean \pm SD of three enzymatic reactions.

Most remarkable was the ability of the GK from *P. farinosa* to utilize different NTPs for the phosphorylation of glycerol to yield G3P. ATP was shown to be the most efficient phosphoryl group donor of the tested NTPs. At concentrations of 10 mM ITP, GTP, UTP, and CTP resulted only in 87, 76, 66, and 29 % of the activity observed with ATP (Table 4.7). Interestingly, the relation between reaction velocity and GTP, UTP or CTP concentration at saturating glycerol was unusual in this study. When the activity was measured over a wide range of NTP concentrations (0 to 10 mM), the normal Michaelis-Menten kinetics could not be observed. As shown in Figure 4.20, the double reciprocal plots were biphasic, which suggested that the enzyme from *P. farinosa* exhibited negative cooperativity with respect to GTP, UTP and CTP.

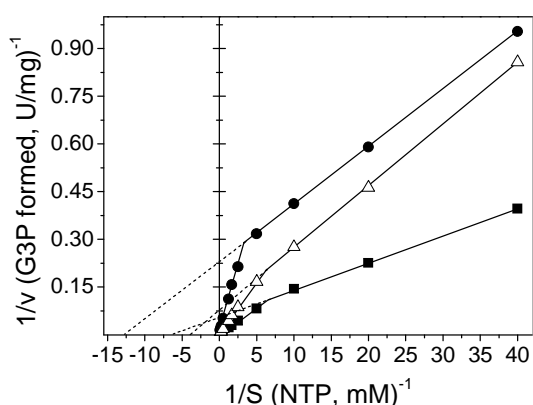


Figure 4.20: Relation between reaction velocity and NTP concentration of purified GK from *P. farinosa*.

The activity of GK at varying concentrations of GTP (■), CTP (●), and UTP (Δ) was measured over a 20 min incubation period at 37 °C and pH 7.

The biphasic behavior did not change when different GK concentrations were used or by aging (prolonged storage and several freeze-thaw cycles) of the enzyme (data not shown). The K_m values of 4.1, 9.6 and 11.4 mM were estimated by extrapolating the linear portion of the curve corresponding to the GTP, UTP and CTP concentrations above 0.2 mM, respectively (Table 4.7).

Table 4.7: K_m and V_{max} values of purified GK from *P. farinosa* for various NTPs.

NTP	$K_{m,1}$ (mM)	$K_{m,2}$ (mM)	V_{max} (U/mg protein)	Specific activity ^a (U/mg protein)
ATP ^b	0.428	n/a	249.9	235.8 ± 30.7
ITP ^b	0.845	n/a	228.0	205.2 ± 19.0
GTP ^c	4.134	0.142	262.2	180.0 ± 17.0
UTP ^c	9.640	0.267	292.3	156.5 ± 12.1
CTP ^c	11.430	0.079	135.0	68.5 ± 6.3

Phosphorylation of glycerol was measured at 37 °C and pH 7. Kinetic data were obtained from three replicate analyses. The values shown are mean ± SD. Values for SD are omitted for clarity but did not exceed 15 %.

^a NTP was present at a concentration of 10 mM.

^b Kinetic constants ($K_{m,1}$ and V_{max}) were determined with NTP concentrations ranging from 25 μM to 10 mM.

^c $K_{m,2}$ or $K_{m,1}$ and V_{max} values were determined with NTP concentrations ranging from 25 to 200 μM or 0.2 to 10 mM, respectively.

4.2.5 Use of the recombinant glycerokinase as a coupling enzyme

Finally, the purified GK from *P. farinosa* was used as a coupling enzyme to determine the specific PK activity in extracts of stationary-phase MDCK cells grown in GMEM-Pyr or serum-free Episerf medium. The specific activity of PK in MDCK cells grown with Episerf medium was approximately 1,362 nmol/min/10⁶ cells and, therefore, considerably higher than in cells grown in GMEM-Pyr (~1,087 nmol/min/10⁶ cells). As a control, bacterial GK from *E. coli* was also used for determination of PK activity (Table 4.8). No significant differences in the specific PK activity were found with either source of GK, which demonstrated good performance as a coupling enzyme for the PK assay (chapter 3.6.3.18).

Table 4.8: Measured activities of PK from confluent grown MDCK cells in six-well plates.

Culture medium	Coupling enzyme	Specific PK activity ^a (nmol/min/10 ⁶ cells)	Av biol. error ^b (%)
GMEM-Pyr	GK from <i>P. farinosa</i>	1086.7 ± 68.3	2.5
	GK from <i>E. coli</i>	1105.0 ± 125.0	4.6
Episerf	GK from <i>P. farinosa</i>	1361.7 ± 91.7	2.7
	GK from <i>E. coli</i>	1355.0 ± 148.3	4.4

^a Mean value and 95 % confidence interval of three replicates.

^b Average biological error expressed as coefficient of variation from three enzymatic reactions.

4.3 Central metabolic enzymes in MDCK cells under different cultivation conditions

This chapter describes the effect of Gln substitution by Pyr on the metabolic enzyme activities of the central carbon metabolism in MDCK cells. Different assumptions concerning the activity of critical enzymes in metabolic pathways made in former studies (Sidorenko et al., 2008; Wahl et al., 2008) are checked by using the established high-throughput platform for enzyme activity measurements of mammalian cells.

Genzel et al. (2005) found out that Gln can be substituted by Pyr without reduction in specific growth rate of different adherent cell lines (MDCK, BHK21, CHO-K1) in serum-containing and serum-free media. In Gln-free medium with Pyr as carbon source, MDCK cells grew to high cell densities without the need of a long adaptation process. Gluc consumption and Lac production was reduced significantly while cells released no ammonia during growth. To assess the influence of Pyr substitution for Gln on enzyme activity levels during exponential and stationary growth, adherent MDCK cells were either cultivated in Pyr or in Gln-containing GMEM medium in six-well plates (chapter 4.3.2).

4.3.1 Cell growth in six-well plates in glutamine and pyruvate-containing medium

In addition to the measurement of maximum enzyme activities of central carbon and Gln metabolism, the cell growth in six-well plates was evaluated. MDCK cells were cultivated in the same media as in previous studies (Gln- and Pyr-containing GMEM), where roller bottles and stirred-tank bioreactors were used (Genzel et al., 2005; Sidorenko et al., 2008). For all experiments, viable cell numbers (adherent) and extracellular metabolites (Gluc, Lac, Gln, Glu and Amm) were determined. The concentration of Pyr was only measured in GMEM-Pyr. To compensate for batch-to-batch variations and to improve data quality, all measurements were performed at least in triplicates using six-well plates.

4.3.1.1 Cell densities

A representative example for the cultivation of adherent MDCK cells in six-well plates in Gln-containing GMEM medium (GMEM-Gln) and Pyr-containing GMEM medium (GMEM-Pyr) is shown in Figure 4.21.

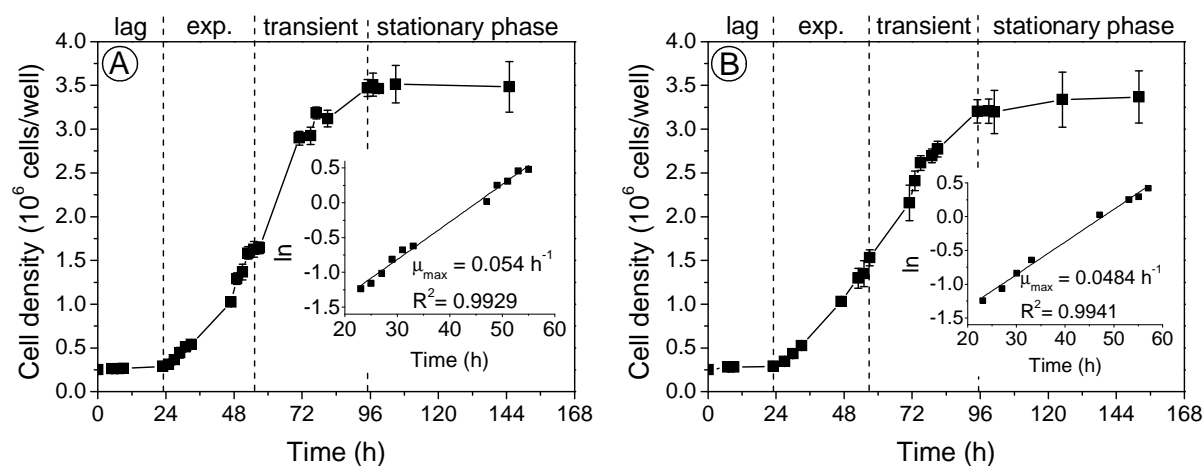


Figure 4.21: Viable cell density and maximum specific growth rate μ_{max} (inset) of adherent MDCK cells during the cultivation in six-well plates in (A) GMEM-Gln and (B) GMEM-Pyr. After cell attachment and adaptation (0 to 23 h), cells grew exponentially to a density of $\sim 1.6 \times 10^6$ cells/well followed by a reduced cell growth due to contact inhibition (~ 56 to 95 h). From this time point, the cell monolayer became confluent and no significant further growth could be observed after 95 h (3.2 to 3.5×10^6 cells/well). Error bars: mean \pm SD of six biological replicates. Some error bars are smaller than symbols and did not exceed 10 %.

The growth behavior of adherent MDCK cells in GMEM-Gln was comparable to that achieved with GMEM-Pyr. The increase in viable cell density of MDCK cells in stationary culture can be described by four characteristic phases (Wahl et al., 2008). During the lag phase (0 to 23 h), in which the cells attached to the surface of the six-well plate and adapted to fresh medium, no significant changes in the cell density were measured. During the exponential phase (23 to ~ 56 h), MDCK cells in GMEM-Gln grew at maximum specific rate with a doubling time of 12.8 h to $\sim 1.6 \times 10^6$ cells/well (Figure 4.21 A), whereas MDCK cells in GMEM-Pyr reached a cell density of $\sim 1.5 \times 10^6$ cells/well with a doubling time of 14.3 h (Figure 4.21 B). Increasing cell density resulted in reduced cell growth due to contact inhibition (transient phase). During this phase (~ 56 to 95 h), the cells reached a maximum density of $\sim 3.2 \times 10^6$ (GMEM-Pyr) and $\sim 3.5 \times 10^6$ cells/well (GMEM-Gln). In the stationary growth phase, when the cells were confluent and no space was left on the surface, cell growth ceased. A cell viability of >95 % was maintained throughout the cultivation (data not shown).

4.3.1.2 Extracellular metabolites

The progress of extracellular metabolites in GMEM-Gln medium for MDCK cells grown in six-well plates according to the previous chapter is shown in Figure 4.22.

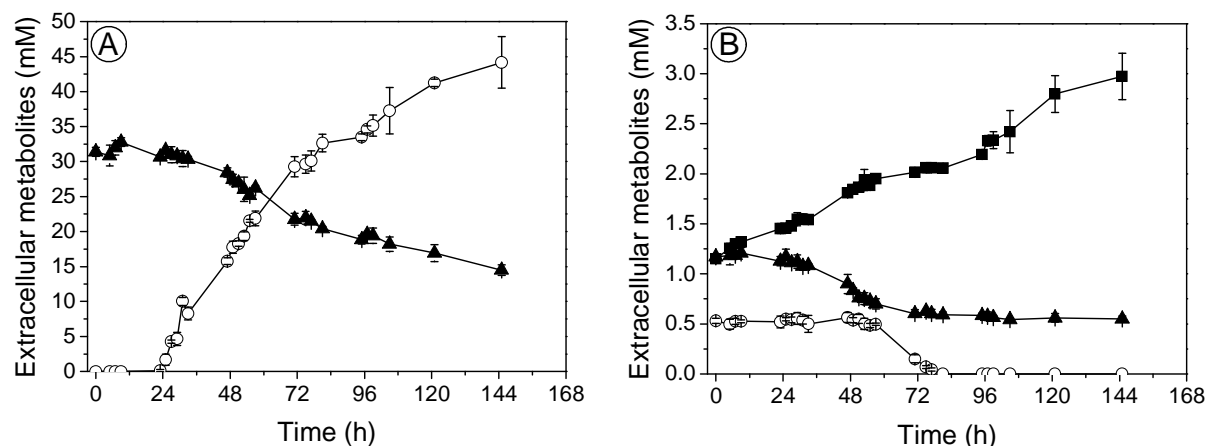


Figure 4.22: Extracellular metabolites of adherent MDCK cells during the cultivation in six-well plates in GMEM-Gln.

(A) After the lag phase (0 to 23 h), Gluc (▲) was continuously taken up by the cells until the end of the cultivation (145 h). At the same time, Lac (○) was produced and accumulated in the medium to concentrations of ~44 mM. (B) Gln (▲) was taken up by the cells and Amm (■) was continuously produced until the end of the cultivation period (~3 mM after 145 h). Glu (○) concentrations remained constant until 51 h and then decreased below the detection limit after ~80 h. Error bars: mean \pm SD of three biological replicates. Some error bars are smaller than symbols and did not exceed 15 %.

During the lag phase (0 to 23 h), in which the cells adapted to the fresh medium and attached to the surface of the six-well plate, Gluc concentrations remained nearly constant (31.40 mM at the beginning) and then decreased to 14.49 mM after 145 h (Figure 4.22 A). Simultaneously, Lac was released by the cells into the culture medium and accumulated to concentrations of 44.18 mM. The total yield coefficient Lac to Gluc ($Y_{\text{Lac/Gluc}}$) during cell growth was determined as approximately 2.61. In theory, one mole of Gluc can be converted to a maximum of two moles of Pyr (and hence Lac) in glycolysis. Therefore, additional Lac is most likely derived from degradation/consumption of other substrates (e.g., amino acids) in GMEM-Gln. The elevated $Y_{\text{Lac/Gluc}}$ value can be further explained by the evaporation of the culture medium. The loss of volume for GMEM-Gln during the cultivation of MDCK cells in six-well plates (2.75 $\mu\text{L/h/well}$) was previously determined by Ritter (2010). Therefore, the measured concentration differences were apparently too low for Gluc and too high for Lac. Considering of volume loss (~399 μL after 145 h) caused by evaporation, the corrected $Y_{\text{Lac/Gluc}}$ would be ~2.17.

The profiles of Gln, Amm and Glu concentrations are shown in Figure 4.22 B. Gln was continuously taken up by the cells from 1.17 mM at the beginning of the cultivation to 0.55 mM at the end. However, after about 95 h, the rate of Gln consumption significantly decreased (stationary growth phase). During growth of MDCK cells in GMEM-Gln, Amm was excreted by the cells and accumulated into the medium (1.15 mM at t_0 to 2.97 mM after 145 h). The $Y_{\text{Amm}/\text{Gln}}$ was determined as about 2.94. Theoretically, two moles of Amm can be produced per mole of Gln consumed (via GLNase and GLDH reactions) (Glacken et al., 1986). The remaining amount of Amm in GMEM-Gln was therefore most likely produced from the consumption of Glu (via GLDH). The concentration of Glu in the culture medium remained constant until 51 h (~ 0.55 mM) and then decreased below the detection limit after approximately 80 h. Furthermore, the loss of volume during the cultivation in six-well plates could also have led to the increased $Y_{\text{Amm}/\text{Gln}}$. By taking the evaporation of culture medium and the formation of Amm from Glu consumption into account, the total yield coefficient of Amm from Gln and Glu ($Y_{\text{Amm}/(2 \times \text{Gln} + \text{Glu})}$) would be ~ 0.81 .

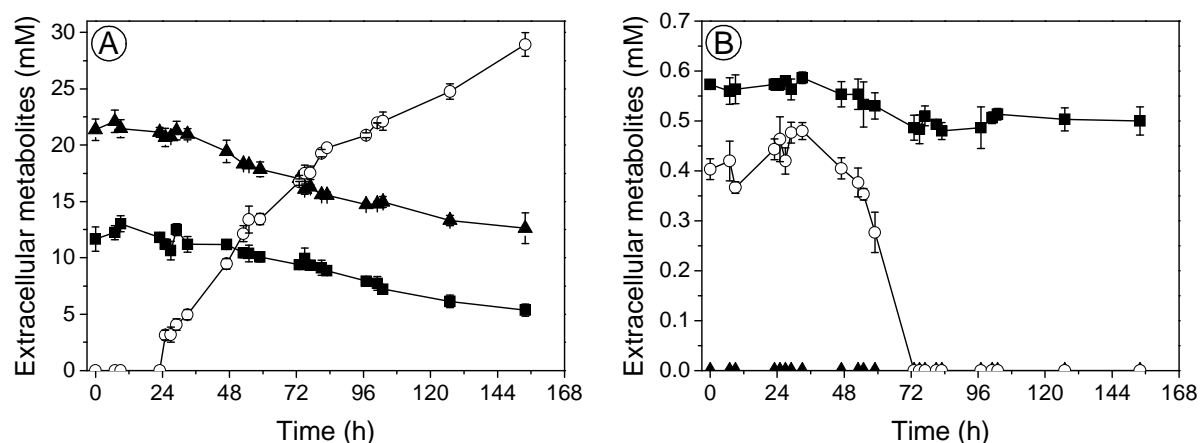


Figure 4.23: Extracellular metabolites of adherent MDCK cells during the cultivation in six-well plates in GMEM-Pyr.

(A) After the lag phase (0 to 23 h), Gluc (▲) and Pyr (■) were continuously taken up by the cells until the end of the cultivation (154 h). At the same time, Lac (○) was produced and accumulated in the medium to concentrations of ~ 29 mM. (B) Gln (▲) concentrations were below the detection limit during the whole cultivation period. Amm (■) did not accumulate in the medium and remained almost constant (~ 0.5 mM). However, a slight decrease was observed from 0.57 at the beginning to 0.48 after 83 h. Glu (○) concentrations remained constant until 47 h and then decreased below the detection limit after ~ 72 h. Error bars: mean \pm SD of three biological replicates. Some error bars are smaller than symbols and did not exceed 15 %.

When MDCK cells were grown in GMEM-Pyr (Figure 4.23), a significant uptake of Pyr could be observed during the whole cultivation period (Figure 4.23 A). Pyr was continuously taken up by the cells from 11.67 mM at t_0 to 5.36 mM after 154 h. Gluc profiles showed

basically the same trend. During the first 23 h, Gluc concentrations remained nearly constant (21.37 mM at the beginning) and then decreased to 12.62 mM after 154 h. Compared to GMEM-Gln, significantly less Gluc was consumed by the cells during growth in Pyr-containing medium (8.75 mM for GMEM-Pyr compared to 16.91 mM for GMEM-Gln). Consequently, MDCK cells also produced less Lac that accumulated in the medium to concentrations of 28.94 mM at the end of the cultivation. By taking the loss of volume as a result of evaporation into account ($\sim 424 \mu\text{L}$), the corrected $Y_{\text{Lac/Gluc}}$ was determined as approximately 2.56, which was slightly higher than for GMEM-Gln (2.17) probably due to additional Lac production from Pyr in GMEM-Pyr.

During growth of MDCK cells in GMEM-Pyr, Gln could not be observed and concentrations remained below the detection limit over the whole time period (Figure 4.23 B). As a consequence, no ammonia accumulation was detected. Rather, a slight decrease of Amm could be observed from 0.57 mM at the beginning of the cultivation to 0.50 mM at the end. Similar to GMEM-Gln (Figure 4.22 B), the concentrations of Glu in GMEM-Pyr remained constant until 47 h ($\sim 0.43 \text{ mM}$) and then decreased below the detection limit after about 72 h.

A short summary of the growth properties of MDCK cells on six-well plates in GMEM-Gln and GMEM-Pyr medium is given in Table 4.9.

Table 4.9: Impact of Gln substitution by Pyr on MDCK cell growth and “basic” metabolism (extracellular metabolites).

	GMEM-Gln	GMEM-Pyr
Maximum cell density (cells/well)	3.5×10^6	3.2×10^6
μ_{max} (h^{-1})	0.0540	0.0484
t_d (h)	12.8	14.3
$Y_{\text{Lac/Gluc}}^a$	2.17	2.56
$Y_{\text{Amm}/(2x\text{Gln}+\text{Glu})}^b$	0.81	n/a
Glucose uptake (mM) ^c	16.91	8.75
Lactate release (mM) ^d	44.18	28.94
Glutamine uptake (mM) ^c	0.62	n/a
Glutamate uptake (mM) ^c	0.55	0.43
Pyruvate uptake (mM) ^c	n/a	6.31
Ammonium release (mM) ^d	1.82	n/a

Note. Adherent MDCK cells were grown in six-well plates in either Gln (2 mM) or Pyr (10 mM)-containing GMEM medium for ~ 6 d.

^a The values were corrected for the loss of volume ($2.75 \mu\text{L/h/well}$) during the cultivation as a result of the evaporation of culture medium (Ritter, 2010).

^b The value was corrected for the loss of volume (evaporation), and the formation of Amm from Glu was taken into account.

^c Overall consumed Gluc, Gln, Glu and Pyr

^d Overall produced Lac and Amm

4.3.1.3 Cellular protein concentration

To evaluate the change in the cell-specific protein concentration of adherent MDCK cells during the cultivation in six-well plates, an additional experiment was performed separately, where the cells were grown in GMEM-Gln medium (Figure 4.24). For each sampling point, adherent cell numbers, extracellular metabolites (data not shown) and intracellular protein concentrations (enhanced test tube protocol, see chapter 3.4.4) were determined.

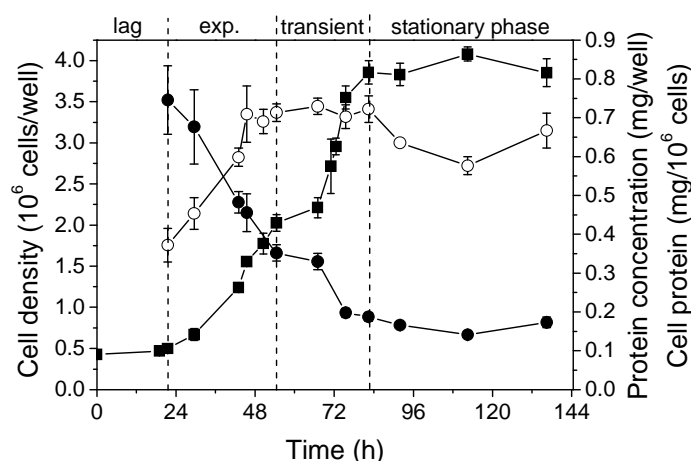


Figure 4.24: Progress of the intracellular protein concentration of MDCK cells during growth in six-well plates in GMEM-Gln.

After cell attachment and adaptation (0 to 21.5 h), cells grew exponentially to a density of $\sim 2.0 \times 10^6$ cells/well followed by a reduced cell growth due to contact inhibition (54.5 to 82.5 h). From this time point, the cell monolayer became confluent and no significant further growth could be observed after 82.5 h (3.9 to 4.1×10^6 cells/well). Time profiles of viable cell number (\blacksquare), protein concentration (\circ), and cell protein (\bullet). Error bars: mean \pm SD of three biological replicates. Some error bars are smaller than symbols and did not exceed 15 %.

In this experiment with GMEM-Gln as culture medium, similar growth characteristics were observed as shown before in chapter 4.3.1.1. However, the maximum cell density ($\sim 4.0 \times 10^6$ cells/well) was already reached after 82.5 h compared to the previous cultivation with GMEM-Gln (95 h; Figure 4.21 A), probably due to differences in medium and/or serum. Gln and Gluc in the medium were both reduced to about 50 % of their initial concentrations and a cell viability of >95 % was maintained throughout the cultivation (data not shown). The intracellular protein content varied from a maximum of 0.75 mg per 10^6 cells at the beginning of the exponential growth phase to a minimum of 0.14 mg per 10^6 cells in the stationary growth phase. This behavior (decrease in intracellular protein concentration during cell growth) could also be observed for a murine B-lymphocyte hybridoma cultivated in RPMI

(Roswell Park Memorial Institute) 1640 medium supplemented with 10 % (v/v) horse serum in 250 mL spinner flasks (Fitzpatrick et al., 1993).

4.3.2 Maximum enzyme activities in glutamine- and pyruvate-containing medium

At two time points of growth (~2 and ~5 d), representing the exponential and the stationary phase in both media (GMEM-Gln and GMEM-Pyr), a total number of 28 key metabolic enzyme activities were measured in MDCK cell extracts using the developed assay platform for mammalian cells (Table 4.10).

Table 4.10: Maximum enzyme activities of glycolysis, pentose phosphate pathway, TCA cycle, and glutaminolysis in MDCK cells grown to exponential phases with GMEM-Gln and GMEM-Pyr, and to stationary phases with GMEM-Gln and GMEM-Pyr.

		Enzyme activities in adherent MDCK cells (nmol/min/10 ⁶ cells) ^a							
Enzyme	EC No.	exponential growth phase (2 days of growth)				stationary growth phase (5 days of growth)			
		GMEM-Gln		GMEM-Pyr		GMEM-Gln ^b		GMEM-Pyr	
<i>Glycolysis</i>									
HK	2.7.1.1	18.43 ± 1.47 (6)	26.61 ± 1.76 (6)	#	19.20 ± 2.00 (5)	12.51 ± 0.94 (6)	#,‡		
PGI	5.3.1.9	200.61 ± 7.59 (6)	324.73 ± 19.97 (6)	#	271.88 ± 15.73 (6)	†	369.91 ± 31.40 (6)	#	
PFK	2.7.1.11	16.06 ± 0.47 (6)	15.52 ± 2.03 (4)		16.78 ± 2.92 (5)		14.72 ± 1.60 (6)		
FBPA	4.1.2.13	31.99 ± 4.54 (6)	43.96 ± 1.24 (6)	#	23.60 ± 3.53 (6)	†	19.51 ± 1.14 (6)	‡	
TPI	5.3.1.1	5740.24 ± 534.20 (6)	8317.32 ± 882.85 (6)	#	6771.68 ± 133.73 (6)		9746.64 ± 579.07 (6)	#	
GAPDH	1.2.1.12	406.24 ± 48.15 (6)	557.78 ± 56.37 (6)	#	360.57 ± 13.90 (6)		413.24 ± 25.75 (6)	‡	
PK	2.7.1.40	765.57 ± 19.49 (6)	1031.90 ± 55.42 (6)	#	1233.77 ± 75.40 (6)	†	1078.96 ± 49.72 (6)		
LDH	1.1.1.27	791.24 ± 26.63 (5)	964.57 ± 97.16 (6)		948.48 ± 45.37 (6)		947.24 ± 40.95 (6)		
<i>Pentose phosphate pathway</i>									
G6PDH	1.1.1.49	74.27 ± 4.00 (6)	122.34 ± 5.18 (6)	#	58.12 ± 3.92 (6)		48.86 ± 1.55 (6)	‡	
6PGDH	1.1.1.44	40.41 ± 3.22 (6)	86.00 ± 6.39 (6)	#	44.82 ± 3.03 (6)		29.95 ± 1.19 (6)	#,‡	
TK	2.2.1.1	7.72 ± 0.78 (5)	18.19 ± 1.76 (6)	#	11.23 ± 1.23 (5)	†	11.64 ± 0.67 (6)	‡	
TA	2.2.1.2	16.91 ± 1.08 (6)	23.60 ± 1.96 (5)	#	15.57 ± 0.75 (6)		19.31 ± 0.57 (6)		
<i>Tricarboxylic acid cycle</i>									
PDH	1.2.4.1	0.31 ± 0.03 (6)	1.28 ± 0.10 (6)	#	0.25 ± 0.02 (5)		0.51 ± 0.06 (6)	#,‡	
PC	6.4.1.1	0.87 ± 0.05 (6)	1.66 ± 0.08 (6)	#	0.62 ± 0.07 (6)	†	0.51 ± 0.09 (6)	‡	
CS	2.3.3.1	39.80 ± 1.36 (6)	34.21 ± 2.44 (6)		12.88 ± 0.67 (5)	†	10.82 ± 0.84 (6)	‡	
CL	2.3.3.8	5.42 ± 0.24 (6)	6.91 ± 0.38 (6)		5.87 ± 0.27 (6)		2.47 ± 0.07 (6)	#,‡	
NAD-ICDH	1.1.1.41	0.11 ± 0.00 (6)	0.29 ± 0.03 (6)	#	0.43 ± 0.03 (6)	†	0.43 ± 0.01 (6)	‡	
NADP-ICDH	1.1.1.42	33.53 ± 2.34 (6)	42.99 ± 2.47 (6)		36.48 ± 2.44 (5)		30.16 ± 1.74 (6)	‡	
FUM	4.2.1.2	92.29 ± 9.09 (6)	130.65 ± 6.13 (6)	#	125.93 ± 21.20 (5)	†	105.68 ± 11.03 (5)		
MDH	1.1.1.37	938.18 ± 52.06 (6)	762.42 ± 32.90 (6)		795.05 ± 52.07 (6)		856.13 ± 46.70 (6)		

Table 4.10: (Continued from previous page.)

		Enzyme activities in adherent MDCK cells (nmol/min/10 ⁶ cells) ^a									
Enzyme	EC No.	exponential growth phase (2 days of growth)					stationary growth phase (5 days of growth)				
		GMEM-Gln		GMEM-Pyr			GMEM-Gln ^b		GMEM-Pyr		
<i>Glutaminolysis</i>											
GLNase	3.5.1.2	7.39 ± 0.54 (6)	6.80 ± 0.56 (6)			3.58 ± 0.29 (6)	†	1.46 ± 0.16 (4)	#, ‡		
GS	6.3.1.2	2.20 ± 0.27 (6)	6.51 ± 0.55(6)	#		0.60 ± 0.08 (5)	†	2.59 ± 0.32 (5)	#, ‡		
GLDH	1.4.1.2	4.92 ± 0.38 (5)	6.63 ± 0.62 (5)	#		4.63 ± 0.48 (6)		4.84 ± 0.41 (6)	‡		
AlaTA	2.6.1.2	6.18 ± 0.53 (6)	2.54 ± 0.16 (6)	#		1.97 ± 0.14 (6)	†	1.20 ± 0.05 (6)	#, ‡		
AspTA	2.6.1.1	150.39 ± 9.89 (6)	99.28 ± 11.25 (5)	#		124.75 ± 18.18 (5)		99.00 ± 7.23 (6)			
ME	1.1.1.40	9.70 ± 0.74 (6)	6.44 ± 0.37 (6)	#		10.41 ± 0.57 (6)		8.29 ± 0.77 (6)			
PEPCK	4.1.1.32	42.19 ± 3.69 (6)	28.87 ± 3.81 (4)	#		72.50 ± 7.01 (5)	†	57.63 ± 4.55 (6)	‡		
<i>Miscellaneous</i>											
ACoAL	6.2.1.1	1.14 ± 0.03 (5)	2.77 ± 0.20 (6)	#		1.84 ± 0.18 (6)	†	2.24 ± 0.12 (6)			

Note. Potential “bottlenecks” in metabolic pathways of adherent MDCK cells are highlighted in grey.

^a Mean values and 95 % confidence intervals for the number of biological replicates shown in parentheses.

^b For values in GMEM-Gln^{stat}, see also Table 4.5.

Significantly different from GMEM-Gln during the respective growth phase as determined by Student's *t*-test ($p \leq 0.05$; ≥ 1.3 -fold or ≤ -1.3 -fold change)

†, ‡ Significantly different during exponential growth phase of GMEM-Gln and GMEM-Pyr, respectively ($p \leq 0.05$; ≥ 1.3 -fold or ≤ -1.3 -fold change)

The overall range in GMEM-Pyr^{stat}, for instance, comprises values from 0.43±0.01 (NAD-ICDH) to 9746.64±579.07 nmol/min/10⁶ cells (TPI). For all media, very high activities (>700 nmol/min/10⁶ cells) were found for TPI, PK, LDH, and MDH, while the other activities were in the range of 1 to 600 nmol/min/10⁶ cells. The lowest enzyme activities were found for PDH, PC, and NAD-ICDH (<1 nmol/min/10⁶ cells), indicating possible rate-limiting steps in the metabolic pathway.

4.3.2.1 Glycolysis

For a better data evaluation, the fold changes in glycolytic enzyme activities for growth under different cultivation conditions were calculated (Figure 4.25). The first two values represent the changes between GMEM-Pyr and GMEM-Gln in the exponential and stationary growth phase, and the last two values represent the changes in maximum enzyme activity between the different growth phases with GMEM-Gln and GMEM-Pyr. For simplification in the following chapters (4.3.2.1 to 4.3.2.4), the conditions during exponential and stationary growth phase of Gln- and Pyr-containing GMEM are referred to as GExp and GStat or PExp and PStat, respectively.

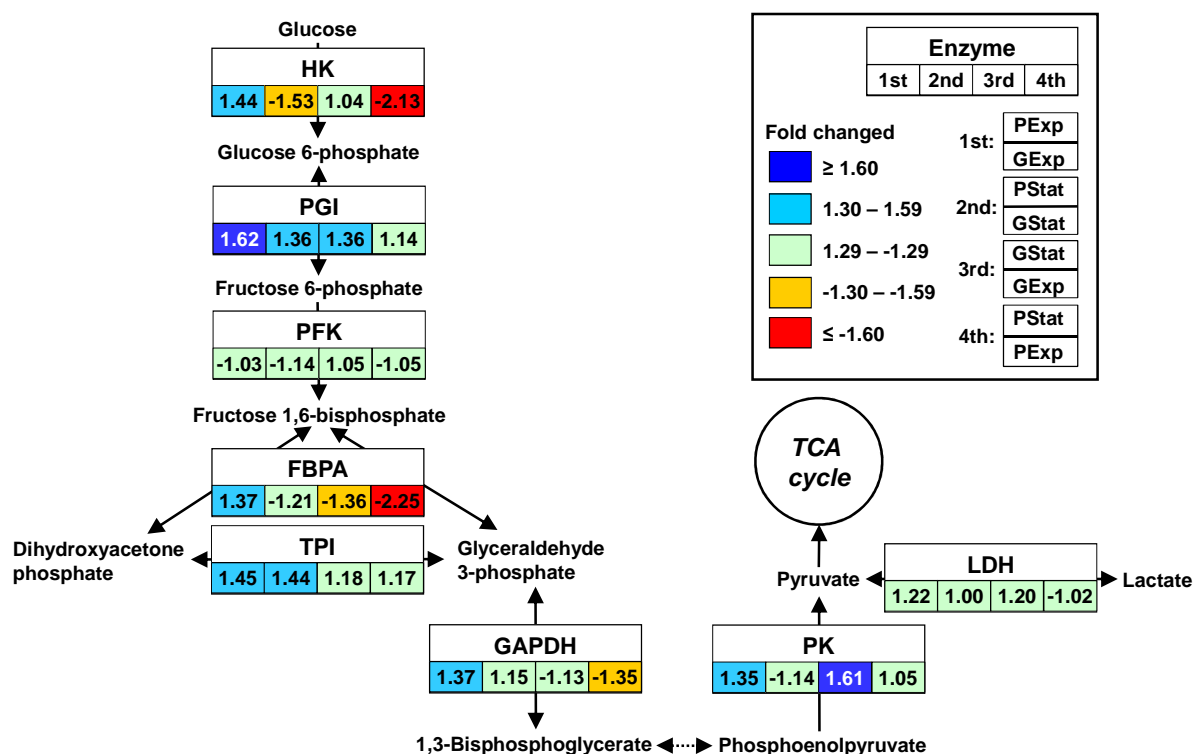


Figure 4.25: Simplified reaction scheme of glycolysis with fold changes of enzyme activities for MDCK cell growth in different media.

The fold changes presented below the name of the enzymes in the squares are for 1) PExp compared with GExp, 2) PStat compared with GStat, 3) GStat compared with GExp, and 4) PStat compared with PExp. Values ≥ 1.30 or ≤ -1.30 indicate significant differences (see Table 4.10).

During exponential growth in PExp, a significant increase in maximum *in vitro* activities was observed for most of the enzymes in glycolysis compared to GExp. Maximum activities of several key enzymes, for example, HK, FBPA, GAPDH, and PK were increased by 1.35 to 1.62-fold. However, one of the important enzymes of glycolysis, PFK, remained unchanged. When the MDCK cells were grown to stationary phases in PStat, there was a significant decrease in HK activity (-1.53-fold change) compared to GStat.

Furthermore, there existed significant differences in enzyme activities between the stationary-phase and the exponential-phase cells in GMEM-Pyr: A significant decrease in the HK and GAPDH activities was observed when the cells switched from exponential to stationary growth phase (-2.13-fold and -1.35-fold change, respectively). For both media (GStat and PStat compared to GExp and PExp, respectively), there was also a decrease in the activity of FBPA.

4.3.2.2 Pentose phosphate pathway

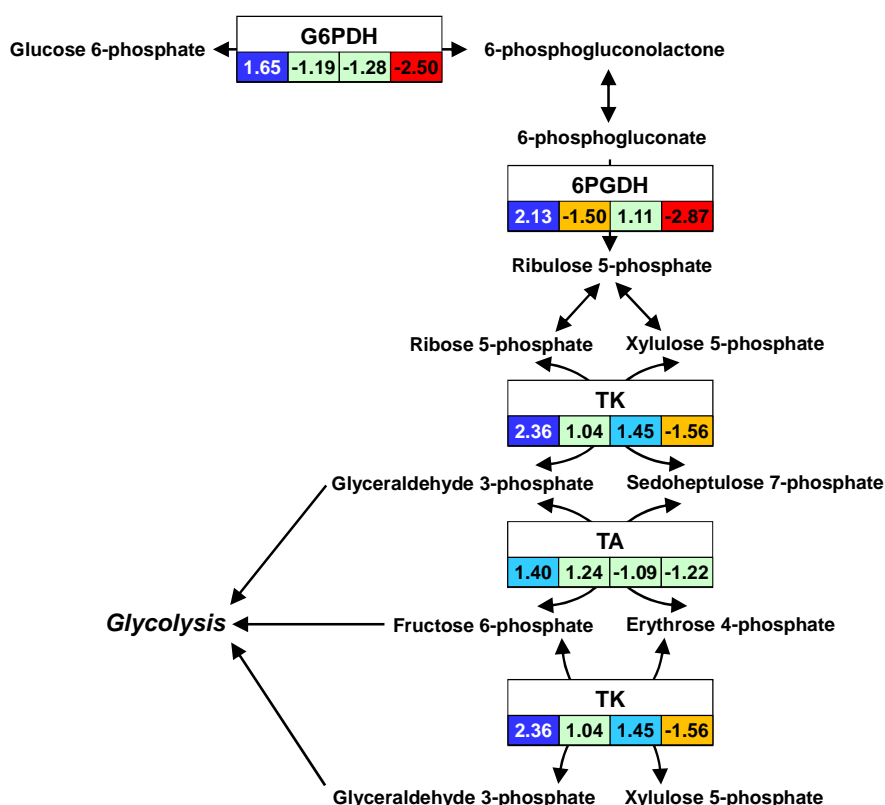


Figure 4.26: Simplified reaction scheme of pentose phosphate pathway with fold changes of enzyme activities for MDCK cell growth in different media.

The fold changes presented below the name of the enzymes in the squares are for 1) PExp compared with GExp, 2) PStat compared with GStat, 3) GStat compared with GExp, and 4) PStat compared with PExp. Values ≥ 1.30 or ≤ -1.30 indicate significant differences (see Table 4.10).

The enzyme activities of exponential-phase cells grown in PExp consistently increased by 1.40 to 2.36-fold compared to GExp, indicating that more Gluc-derived carbon units could potentially be metabolized via this pathway (Figure 4.26). In the stationary phase with Pyr (PStat compared to GStat), only one major change of the oxidative part occurred. In contrast to the exponential phase, there was a decrease in 6PGDH activity by 1.50-fold.

For stationary-phase cells grown with Gln (GStat), an increase by 1.45-fold was found for TK activity from the non-oxidative part compared to cells from the exponential growth phase (GExp). On the other hand, for stationary-phase cells grown with Pyr (PStat compared to PExp), a significant decrease in the enzyme activities of G6PDH, 6PGDH, and TK was observed (-1.56 to -2.87-fold change). In general, lower maximum cell-specific activities were found for the enzymes of the non-oxidative branch compared to the oxidative branch of the pentose phosphate pathway (Table 4.10).

4.3.2.3 Tricarboxylic acid cycle

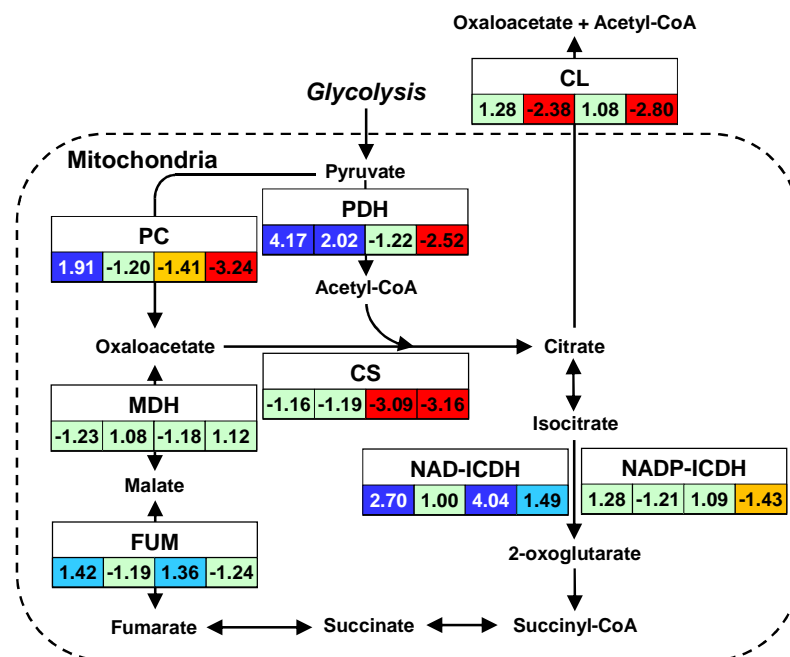


Figure 4.27: Simplified reaction scheme of TCA cycle with fold changes of enzyme activities for MDCK cell growth in different media.

The fold changes presented below the name of the enzymes in the squares are for 1) PExp compared with GExp, 2) PStat compared with GStat, 3) GStat compared with GExp, and 4) PStat compared with PExp. Values ≥ 1.30 or ≤ -1.30 indicate significant differences (see Table 4.10). The broken line separates the mitochondrion from the cytosol.

The activity of PDH that catalyzes the first step of the TCA cycle was significantly increased (4.17-fold change) during exponential growth in GMEM-Pyr compared to GMEM-Gln, indicating that more Pyr could potentially be converted to acetyl-CoA (Figure 4.27). In

contrast, LDH activity was not significantly increased (Figure 4.25). However, the enzyme activity of NAD-ICDH was significantly increased in PExp (2.70-fold change). Additionally, the anaplerotic enzyme PC, which “refills” the TCA cycle with OAA from Pyr, showed also an increased activity in PExp (1.91-fold change), and also the activity of FUM was increased by 1.42-fold in PExp compared to GExp. No significant changes in maximum enzyme activities were found for CS, NADP-ICDH, MDH, and CL in PExp compared to GExp. When comparing the stationary-phase cells (PStat compared with GStat), the activity of PDH was still significantly increased (2.02-fold change), whereas the activity of CL, which is responsible for the synthesis of cytosolic acetyl-CoA, decreased in Pyr-containing medium (-2.38-fold change).

A different behavior was found when comparing the stationary growth phases with the exponential growth phases of MDCK cells (GStat and PStat compared to GExp and PExp, respectively). For both culture media, a significant decrease of CS activity was observed for cells from the stationary growth phase (<-3-fold change). In addition, when the cells were grown with Pyr, the activity levels of PDH (-2.52-fold change), PC (-3.24-fold change), CL (-2.80-fold change), and NADP-ICDH (-1.43-fold change), decreased in the stationary growth phase (PStat compared to PExp). However, the activity of NAD-ICDH in GStat and PStat increased by 4.04-fold and 1.49-fold, respectively.

4.3.2.4 Glutaminolysis

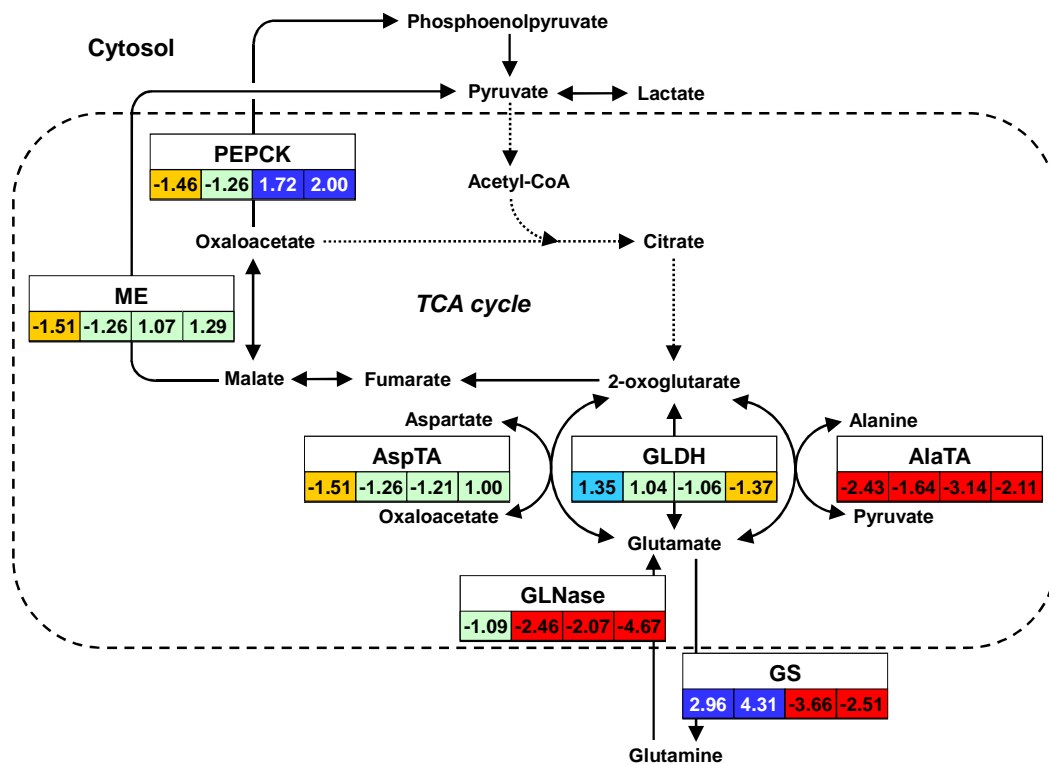


Figure 4.28: Simplified reaction scheme of glutaminolysis with fold changes of enzyme activities for MDCK cell growth in different media.

The fold changes presented below the name of the enzymes in the squares are for 1) PExp compared with GExp, 2) PStat compared with GStat, 3) GStat compared with GExp, and 4) PStat compared with PExp. Values ≥ 1.30 or ≤ -1.30 indicate significant differences (see Table 4.10). The broken line separates the mitochondrion from the cytosol.

During growth of MDCK cells in GMEM-Pyr, a major change in GS activity of both growth phases was observed compared to GMEM-Gln (Figure 4.28): GS activity increased by 2.96-fold in the exponential phase and 4.31-fold in the stationary phase, which emphasizes the importance of the amino acid Gln as a precursor for several biosynthetic reactions in the cell (e.g., nucleotide synthesis). In contrast, other enzymes of Gln metabolism were down-regulated. A significant decrease (< -1.30 -fold change) in enzyme activities of AspTA, ME, and PEPCK was seen in exponential-phase cells grown in PExp compared to GExp. An even more pronounced decrease was found for AlaTA activity that decreased by 2.43-fold in PExp. In the stationary phase (PStat), however, the activity of GLNase was decreased by 2.46-fold, compared to GStat, and the change in AlaTA activity was less distinct (-1.64-fold change).

In both media (GStat and PStat compared to GExp and PExp, respectively), there was a significant decrease in GS, GLNase and AlaTA activities, when the cells reached confluency.

In contrast, PEPCK activities increased by 1.72-fold and 2.00-fold in GStat and PStat, respectively.

Overall, a major shift of maximum enzyme activities between the two growth phases (exponential and stationary) and also between Gln- and Pyr-containing GMEM medium could be observed. Most cell-specific enzyme activities of central carbon and Gln metabolism were higher during the exponential growth phase compared to the stationary phase in GMEM-Gln and GMEM-Pyr. However, the cell-specific protein concentration of MDCK cells decreased from 0.75 (exponential phase) to 0.14 (stationary) mg/10⁶ cells during growth in GMEM-Gln (see Figure 4.24). Therefore, when the maximum enzyme activities measured would be related to the biomass (cellular protein concentration) and not to the viable cell number (as in this study), likely higher differences between the two growth phases could be expected with overall higher protein-specific enzyme activities in MDCK cells during the stationary phase compared to the exponential growth phase in GMEM-Gln and GMEM-Pyr (see chapter 5.3). Major changes in enzyme activity were observed when the cells were grown in GMEM-Pyr compared to GMEM-Gln. In particular, the activities of the “bottleneck” enzymes PDH and PC were significantly increased in Pyr-containing medium, which suggested that more Pyr was shunted into the TCA cycle for growth and precursor supply. Furthermore, the maximum activity of GS and the activities of the pentose phosphate pathway significantly increased under Gln-free conditions, probably due to the need of Gln as a precursor for, e.g., protein synthesis and of NADPH for reductive biosynthesis reactions (e.g., fatty acid synthesis), respectively. However, an increase or decrease in maximum enzyme activity was not restricted to only one or two enzymes of a particular metabolic pathway but activities seemed to overall change during growth under different cultivation conditions, which indicated that changes in pathway fluxes could only be attained by parallel changes in activity of many or all of the enzymes in the pathway.

4.4 Influence of influenza virus infection on key metabolic enzyme activities in MDCK cells

MDCK cells are considered a suitable substrate for cell culture-based influenza vaccine manufacturing (Genzel and Reichl, 2009; Halperin and Doroshenko, 2009). Like all viruses, influenza viruses take advantage of the host cell metabolism to replicate their genetic material and to synthesize viral proteins. However, only few studies have characterized the influence of an influenza infection on the central carbon metabolism of host cells (Ritter et al., 2010).

Therefore, adherent MDCK cells grown in GMEM-Gln (~5 days) were infected with an H1N1 influenza strain and the maximum catalytic activities of 28 enzymes from central carbon metabolism were measured. Again, most measurements (except for HA titers) were performed in triplicates using six-well plates to compensate for batch-to-batch variations and to improve data quality. Before infection, the GMEM was replaced by serum-free VMM containing trypsin to cleave the HA protein into the two subunits (HA1 and HA2). Post-translational cleavage of HA is essential for the infectivity of the virus particle and entry of the virus into the host cell's cytoplasm (Klenk et al., 1975). To compensate the effect of medium exchange (high substrate concentrations, trypsin activity, no FCS) on metabolic changes, a mock-infection (same conditions but without virus) was performed in parallel to infection on separate six-well plates. For comparison with previous data on intracellular metabolite concentrations in infected MDCK cells (Ritter et al., 2010) and to ensure simultaneous infection of almost all cells in a well, a high MOI of 20 was used for the enzyme activity experiments in this work. At these conditions, virus and mock-infected MDCK cells showed comparable cell densities until about 8 to 12 hpi, which was also the time point of virus release in infected cells (Ritter et al., 2010). It was therefore decided to analyze key enzyme activities 9 hpi in infected MDCK cells (chapter 4.4.2).

4.4.1 Cell numbers and virus replication

The viable cell densities of mock- and influenza infected cells as well as virus titers of infected cultures from an infection experiment conducted at a MOI of 5 are shown in Figure 4.29. For a thorough investigation of virus infection under the same conditions (MDCK cells, six-well plates, same virus strain) but at a MOI of 20, the reader is referred to the study by Ritter et al. (2010).

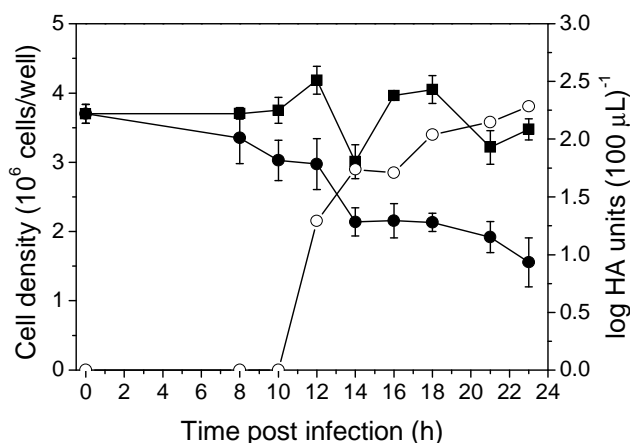


Figure 4.29: Viable cell density of adherent MDCK cells after mock-infection (■) or infection with influenza A (●), and virus titer (○).

Cells were cultured in GMEM-Gln until confluency was reached (~5 days of growth). For virus replication, the medium was replaced by serum-free VMM containing trypsin. MDCK cells were either mock-infected or infected with influenza virus A/Puerto Rico/8/34 (H1N1) at a MOI of 5. Cell density: mean \pm SD of three biological replicates. Titer: error bars are not shown for clarity reasons (relative SD of the validated assay 9.3 %).

The initial cell number at time of infection was about 3.7×10^6 cells/well. Under both conditions, the cell numbers were constant for at least 8 hpi. In influenza infected MDCK cells, the viable cell numbers then decreased slowly until 12 hpi and dropped to $\sim 1.6 \times 10^6$ cells/well after 23 hpi. The overall cell density of mock-infected cultures remained nearly constant at $\sim 3.5 \times 10^6$ cells/well over the cultivation period. The high variability of cell numbers (for instance, between 10 and 16 hpi in mock-infection experiments) most likely resulted from erroneous cell counts due to trypsin activity in VMM (irregularities in cell detachment). Virus titers started to increase after 10 hpi parallel to the beginning of cell detachment in infected cells. The final HA titer was determined as approximately 2.3 log HA units per 100 μ L, which is typical when a high MOI is used (Ritter et al., 2010; Vester et al., 2010).

4.4.2 Maximum enzyme activities in influenza infected cells

The maximum catalytic activities of the glycolytic enzymes in mock-infected MDCK cells and influenza A (H1N1) infected cells 9 hpi are shown in Figure 4.30 (the infection in this experiment was performed at a MOI of 20). For the calculation of the cell-specific enzyme activities under both conditions (mock- and influenza infected cells), the viable cell density at time of infection was used ($4.1 \pm 0.2 \times 10^6$ cells/well, mean \pm SD of nine biological replicates;

data not shown). The numerical values for all measured enzyme activities are given by Janke et al. (2011b).

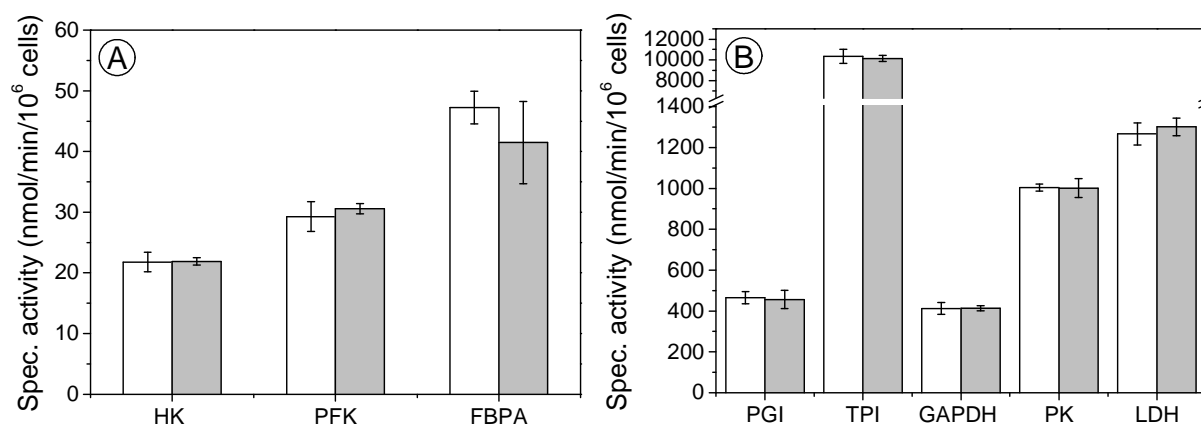


Figure 4.30: Specific activities of glycolytic enzymes in influenza A infected MDCK cells 9 hpi.

Cells were cultivated in six-well plates with GMEM-Gln to stationary phases and then either mock-infected (white) or infected (grey) with human influenza A (H1N1) in VMM at a MOI of 20. Error bars: mean ± SD of three biological replicates.

No significant changes in specific activities were found for enzymes of the glycolytic pathway in influenza infected MDCK cells compared to mock infection 9 hpi. However, an increase of several TCA cycle enzymes was observed in infected cells compared to mock (Figure 4.31).

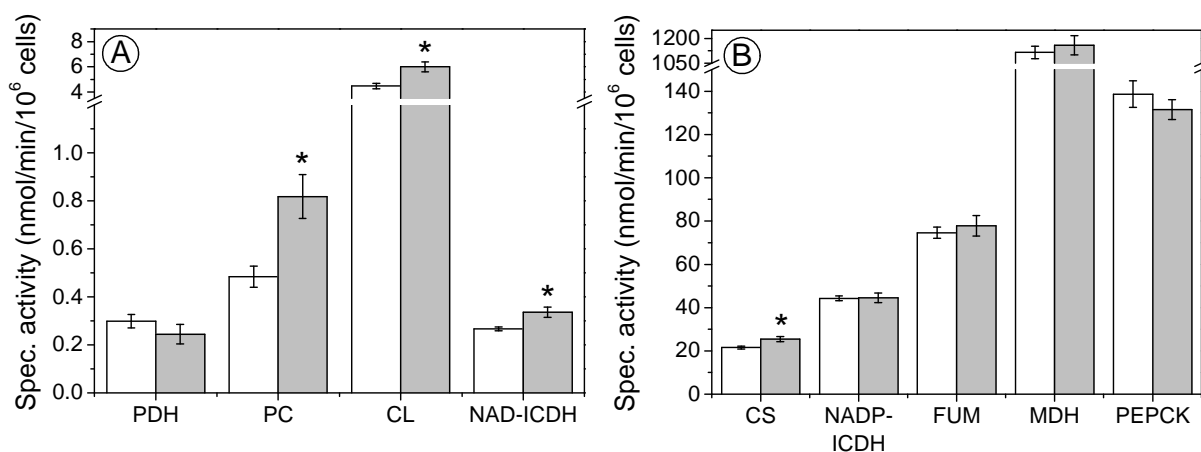


Figure 4.31: Specific activities of TCA cycle enzymes in influenza A infected MDCK cells 9 hpi.

Cells were cultivated in six-well plates with GMEM-Gln to stationary phases and then either mock-infected (white) or infected (grey) with human influenza A (H1N1) in VMM at a MOI of 20. Error bars: mean ± SD of three biological replicates. The star symbol indicates a significant difference from control as determined by Student's t-test (p ≤ 0.05).

During infection of MDCK cells, a major change in the activity of PC was observed: PC activity increased by 1.69-fold in infected cells compared to mock. Furthermore, a significant increase in the activity of CL (1.34-fold), which catalyzes the production of cytosolic acetyl-CoA from citrate, was seen in infected cells. Acetyl-CoA is an important precursor of many cellular “building blocks” including cholesterol and fatty acids (Wakil et al., 1964). Finally, the activities of NAD-ICDH and CS were increased in infected cells by 1.26-fold and 1.18-fold, respectively.

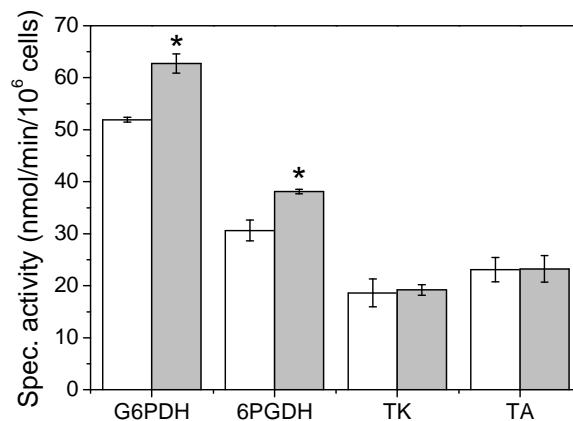


Figure 4.32: Specific activities of pentose phosphate pathway enzymes in influenza A infected MDCK cells 9 hpi.

Cells were cultivated in six-well plates with GMEM-Gln to stationary phases and then either mock-infected (white) or infected (grey) with human influenza A (H1N1) in VMM at a MOI of 20. Error bars: mean \pm SD of three biological replicates. The star symbol indicates a significant difference from control as determined by Student's t-test ($p \leq 0.05$).

The activities of G6PDH and 6PGDH, the first and the third enzyme of the oxidative branch of the pentose phosphate pathway were also increased in infected cells by 1.21-fold and 1.25-fold, respectively (Figure 4.32). Both enzymes provide NADPH for reductive biosynthetic reactions (e.g., amino acid, cholesterol, and fatty acid synthesis) (Salati and Amir-Ahmady, 2001). No significant changes were found in the maximum activities of TK and TA that participate in reactions of the non-oxidative branch.

The specific enzyme activities of glutaminolysis as well as the specific activity of acetate-CoA ligase (ACoAL) for influenza A and mock-infected MDCK cells are shown in Figure 4.33.

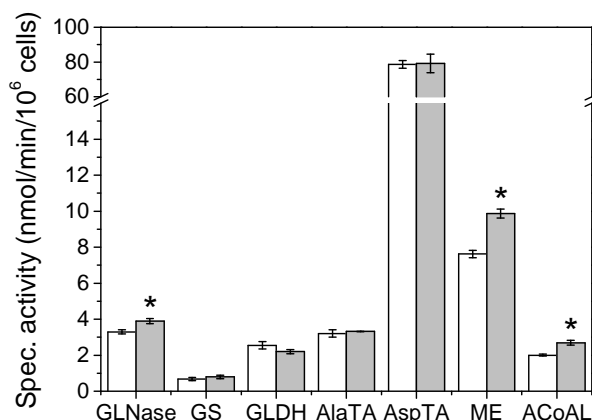


Figure 4.33: Specific activities of glutaminolytic enzymes and ACoAL in influenza A infected MDCK cells 9 hpi.

Cells were cultivated in six-well plates with GMEM-Gln to stationary phases and then either mock-infected (white) or infected (grey) with human influenza A (H1N1) in VMM at a MOI of 20. Error bars: mean \pm SD of three biological replicates. The star symbol indicates a significant difference from control as determined by Student's t-test ($p \leq 0.05$).

Within the glutaminolytic pathway, the GLNase (1.18-fold change) and the ME (1.30-fold change), which catalyzes the oxidative decarboxylation of malate to Pyr and the production of NADPH, exerted significantly higher catalytic activities in influenza infected cells compared to mock infection of MDCK cells. In addition, the activity of ACoAL, which physiological role is to activate acetate to acetyl-CoA, was increased by 1.34-fold in infected cells.

The fact that maximum enzyme activities in influenza A infected MDCK cells were always higher than in mock-infected cells suggests an up-regulation of metabolic activities during early virus replication (Figure 4.34). As mentioned at the beginning of this chapter, the viable cell density at time of infection was used for both conditions (mock- and influenza infection) to avoid incorrect calculation of the cell-specific enzyme activities due to varying cell counts post infection (see Figure 4.29). However, even if the cell densities slightly decreased 9 hpi in this experiment (MOI of 20) and the calculation of enzyme activities was performed by using lower cell numbers for the virus condition (compared to mock), the same tendency could be expected with increased enzyme activities in infected MDCK cells compared to mock-control cells.

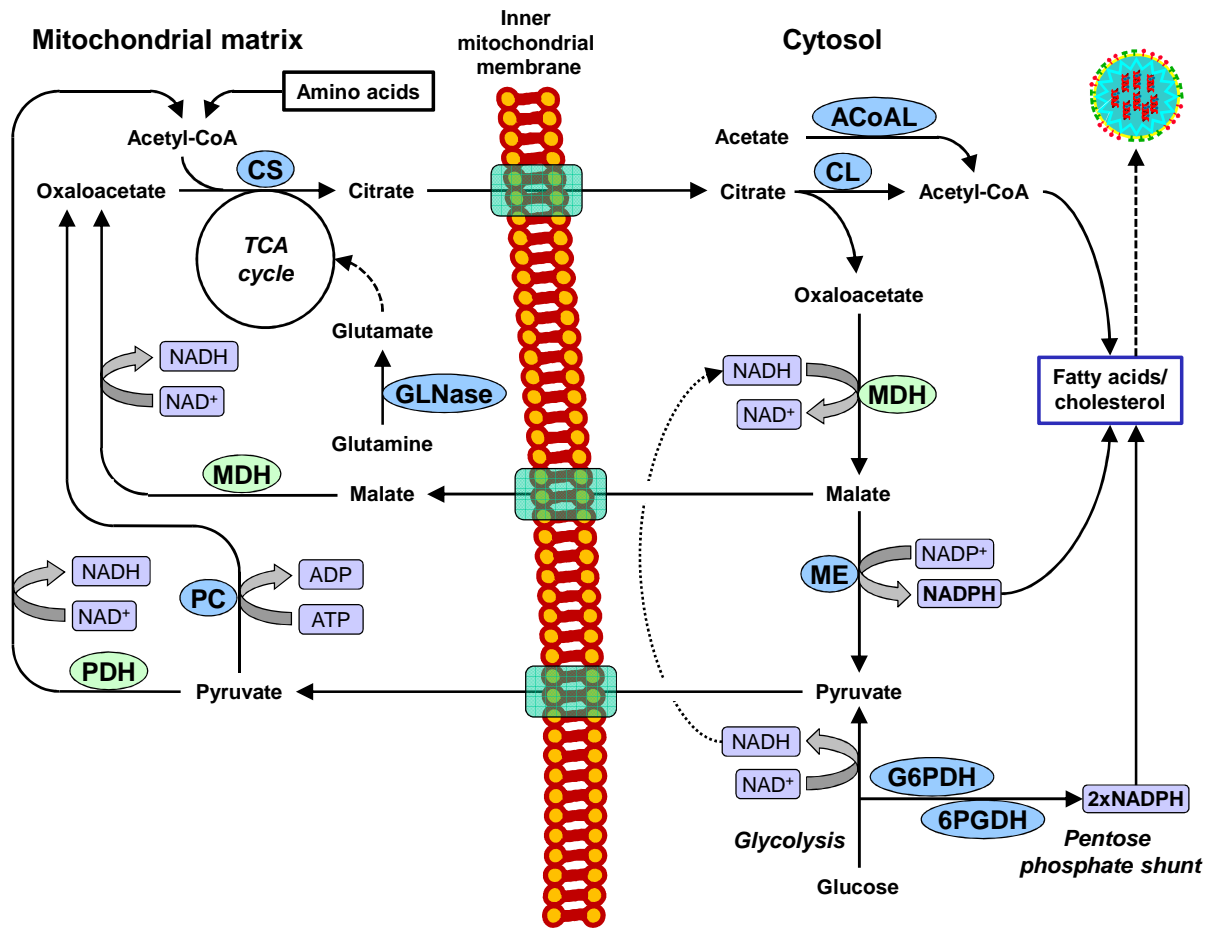


Figure 4.34: Simplified scheme for a reaction network of the central carbon metabolism of adherent MDCK cells.

Enzymes up-regulated in influenza A (H1N1) infected cells are highlighted in blue. Enzymes shown in green (MDH and PDH) were not affected by virus infection but were included for clarity reasons.

5 Discussion

Systems biology aims to tightly link mathematical modeling with experimental approaches for analysis, design and optimization of biological systems (e.g., cells, tissues, and organs). Therefore, systems biology depends on high-computation performance and sophisticated software and, among others, on high-throughput technologies for generation of high-quality quantitative data. By following a systems biology approach and to better understand the mammalian cell metabolism, different analytical procedures, such as the determination of intracellular metabolite levels (Ritter, 2010; Ritter et al., 2007), uptake and release of amino acids (Genzel et al., 2004b) or enzyme activity measurements (Neermann and Wagner, 1996) could be combined to provide further information about the physiological status of a cell and to create a full picture of a system's behavior relevant for cell line and media optimization. The basic strategy in the present work towards a better understanding of Gln and central carbon metabolism of mammalian cells was to use a set of sensitive cycling assays for measuring key metabolic enzyme activities in MDCK cells under different cultivation conditions. Previous studies focused, for example, on the measurement of extra- and intracellular metabolites or on metabolic flux models (Genzel et al., 2004b; Ritter et al., 2008; Ritter et al., 2010; Sidorenko et al., 2008; Wahl et al., 2008), and made significant progress in better understanding the central metabolism of adherent MDCK cells. Comprehensive data on maximum enzyme activities in these cells grown under different conditions are, however, shown for the first time in this study.

The following discussion is divided into four main parts. The first chapter (5.1) covers the development of the assay platform for mammalian cells, followed by a discussion of the findings for the recombinant GK from *P. farinosa* (chapter 5.2). The third section examines effects of different cultivation conditions on the maximum activity of central metabolic enzymes in MDCK cells (chapter 5.3), and the fourth part focuses on the influence of an influenza A virus infection on key metabolic enzyme activities in MDCK cells (chapter 5.4).

5.1 Development of an enzymatic assay platform for mammalian cells

A high-throughput platform established for plant cells (Gibon et al., 2004), which uses three cycling systems for enzyme activity measurements (G3P, NAD⁺, and NADP⁺ cycle), served as a basis for the development of an enzymatic assay platform for mammalian cells. The main

physiological difference between plant and mammalian cells is that plant cells have chloroplasts and a cell wall while mammalian cells only have a cell membrane. Modifications of the enzymatic assay platform taking this difference into account were therefore required in sample preparation, i.e., cell culture samples were prepared by quenching the cells immediately after harvesting in liquid nitrogen and extracting under ultrasonic treatment. Concentrations of various EB components, especially protease inhibitors and detergents were adapted to prevent enzymes of interest from degradation and to ensure the release of membrane-bound enzymes. As a starting point for investigation of enzyme activities of central carbon metabolism of MDCK cells, 17 enzyme assays for plant cells were adapted. Most enzymes from plants differ substantially in their substrate affinity and pH optimum compared to mammalian cell cultures. Therefore, care had to be taken when adapting the enzyme assays regarding the substrate and coupling enzyme concentrations, as well as the pH of the assay buffer. Additionally, the temperature optimum for enzyme activity measurements in mammalian cells is higher (37 °C) than for plant cells (room temperature). Analogous to the existing cycling assays, 11 new assays were established and optimized for enzyme reactions relevant in mammalian cell culture. A small number of enzymes (e.g., PDH, PC) could not be transferred to enzymatic cycling due to the high activity of LDH in mammalian cell cultures (Neermann and Wagner, 1996). These enzymes were analyzed using direct assays. One important key enzyme from the Gln metabolism in mammalian cells is GLNase, which produces Glu and ammonia from Gln. The activity of GLNase could not be analyzed with the existing cycling systems. Several methods to determine the reaction product Glu are based on the enzymatic recycling of the substrate (Glu), for example spectrophotometric methods (Valero and Garcia-Carmona, 1998) or fluorometric methods (Chapman and Zhou, 1999). To avoid fluorometric analysis and to use a similar approach as for the other 27 enzymes described here, a new GLNase assay was developed, which is based on substrate cycling between GLDH and AspTA. It generates an accumulating product (MTT_{red}), which absorbs light at 570 nm.

Although most of the enzyme assays presented in this study can easily be adapted to other cell lines, care has to be taken when preparing cellular extracts for enzyme analysis because optimal dilution varies from enzyme to enzyme as activities can differ in magnitude (Table 4.3 and Table 4.5). Furthermore, it has to be pointed out that linearity of assay (step 1, see Figure 3.1) with time and cell/protein concentration (first order conditions) needs to be

established for each cell line or tissue independently (confirmation with cell extract; see chapter 4.1.2.3 and Table 4.3).

5.1.1 Development of 28 enzyme assays

All enzyme assays were validated according to the GLNase assay. Aliquots of extracts were incubated with the respective substrates for a fixed time period before stopping the reaction. Afterwards the product concentration was determined in the respective cycling assay. Tables 4.2 to 4.4 list enzymes for which assays were developed based on the NAD^+ cycle, NADP^+ cycle, G3P cycle and Glu cycle, and summarize information about the validation results. The NAD^+ and NADP^+ cycling systems were used for the amplified quantitative determination of low levels of $\text{NAD}^+(\text{H})$ or $\text{NADP}^+(\text{H})$, respectively (Figure 4.9 A+B). The third substrate cycle was beneficial for the determination of low amounts of G3P or DAP (Figure 4.9 C) (Gibon et al., 2002). In this reaction scheme, G3P is continuously interconverted into DAP by means of G3POX and G3PDH working in opposite directions. Scouting experiments indicated that the concentrations of substrates, potential activators, coupling enzymes, ionic conditions and pH values of the buffers used resulted in maximum enzyme activities. For example, ACoAL, an enzyme participating in Pyr metabolism, was assayed using the sensitive NAD^+ cycle (Figure 4.9 A). The enzyme catalyzes the formation of acetyl-CoA from acetate, ATP and CoA. To feed acetyl-CoA into the cycling assay, CS and MDH were included in the assay mix as coupling enzymes to produce citrate and simultaneously reduce NAD^+ to NADH. In principle, one molecule of NADH generated by ACoAL can catalyze the production of many molecules of formazan dye because in each turn of the cycle, one molecule of the tetrazolium salt MTT is reduced to the blue-colored compound (formazan). As the enzyme has an absolute requirement for certain univalent cations and bivalent metal ions, KCl and MgCl_2 were added, respectively (Londesborough and Webster, 1974). The enzyme activity was determined by subtracting the signal “without substrate” (V_{blank}) from the signal “with the complete assay mix” (V_{max}) using a standard curve obtained with pure NADH. It was important to treat all standards, blanks and samples in a uniform manner throughout the assay, so that the cycling rate would be the same even when some components (e.g., substrates, coupling enzymes) of the previous steps might have affected the rate.

A small number of enzymes could not be adapted to the cycling systems and were therefore analyzed using direct assays (Table 4.3). The anaplerotic enzyme PC catalyzes the reaction of Pyr, ATP and CO_2 to form OAA, ADP and phosphate. Unfortunately, OAA production could

not be determined in the presence of NADH and MDH by following the oxidation of NADH because of the highly active LDH present in MDCK homogenates (Table 4.5). Therefore, the formation of OAA was measured in the presence of CS by its reaction with acetyl-CoA, which is also an allosteric activator of the enzyme (Jitrapakdee and Wallace, 1999), to form citrate and CoA. The CoA then reacted with DTNB to form a compound, which absorbs light at 405 nm. Kinetic studies have shown that certain monovalent cations were effective activators (Barden and Scrutton, 1974) and Mg^{2+} was an essential cofactor of the reaction (Bais and Keech, 1972). Therefore, the potassium-form of the substrate HCO_3^- , and $MgCl_2$ were added to the assay mix. To reduce the effect of substrate inhibition creatine phosphate and CK were added to rapidly recycle consumed ATP (McClure and Lardy, 1971). Unlike the PC from rat liver (McClure et al., 1971), chicken liver PC (Irias et al., 1969; Scrutton and Utter, 1965) has been reported to be unstable at low temperatures (0 to 15 °C). Reactivation of enzyme activity and protection from cold inactivation has been achieved by simply re-warming the enzyme mixture and by the addition of enzyme substrates to the sample buffer, respectively (Irias et al., 1969). This effect was verified with crude extracts from MDCK cells by extracting the cells at room temperature directly after cultivation compared to the standard extraction at 4 °C after thawing the samples. The PC activity measurements showed no significant difference with either extraction procedure (data not shown).

The multienzyme complex PDH, consisting of three catalytic enzymes (E1, pyruvate decarboxylase, EC 1.2.4.1; E2, dihydrolipoyl transacetylase EC 2.3.1.12; E3, dihydrolipoyl dehydrogenase, EC 1.8.1.4) and two regulatory enzymes (PDH kinase, EC 2.7.1.99; PDH phosphatase, EC 3.1.3.43), catalyzes the oxidative decarboxylation of Pyr with concomitant formation of acetyl-CoA (Butterworth, 1989). To measure PDH activity, the NADH production of the enzyme complex was coupled to the reduction of MTT via diaphorase as electron transfer mediator (Antiochia et al., 1997). The enzyme assay had an absolute requirement for the cofactors NAD^+ , CoA and thiamine pyrophosphate, and $MgCl_2$ and Pyr (data not shown). Because PDH is regulated by acetyl-CoA feedback inhibition, L-carnitine was added to the assay mix (Behal et al., 1993). Oxamate has been shown to act as a potent competitive inhibitor of LDH and was included in order to obtain linear reaction rates of the PDH (Chretien et al., 1995). The PDH was not inhibited by oxamate at the concentrations present in the assay. The PDH phosphatase was stimulated by Ca^{2+} and Mg^{2+} ions to activate the E1 component of the PDH multienzyme complex (Severson et al., 1974).

GS catalyzes the ATP-dependent amidation of Glu to Gln in the presence of divalent cations. The first attempts to measure this “biosynthetic reaction” in crude cell extracts by coupling the GS-induced production of ADP to G6P via an ADP-dependent HK from *Pyrococcus furiosus* (Asahi Kasei, Tokyo, Japan) were not successful (data not shown). Typically, G6P formation can easily be coupled via G6PDH to NADPH, which can then be analyzed using the sensitive NADP⁺ cycling assay (Figure 4.9 B). However, the activities of other ATP-utilizing enzymes, such as HK (see Table 4.5) or ATPases, in the crude extracts were comparatively high and interfered with the measurement of ADP from the GS reaction. Therefore, GS was assayed by a procedure commonly used for determining its activity. The “synthetic reaction” involved the replacement of NH₃ by hydroxylamine, and the γ GH formed in this reaction gave a characteristic color reaction on addition of ferric chloride (Wellner and Meister, 1966). Since GS was inhibited by ADP, creatine phosphate and CK were added to the assay mixture (Berl, 1966). Maximum activity was attained, when the ratio of Mg²⁺ to ATP was about 2 (Rowe, 1985).

The activities of MDH, LDH, PGI and TPI were high enough to measure the products directly by oxidation or reduction of pyridine nucleotides. All standard assays contained optimized concentrations of substrates, activators (if any) and coupling enzymes, ionic conditions and pH values of the buffers. Activities were calculated from the rate of change of absorbance within a linear range and appropriate corrections were made by subtracting blank rates (V_{blank}) from maximum rates (V_{max}).

5.1.2 Advantages and disadvantages of enzymatic cycling assays

The four sensitive enzymatic cycling systems of the established enzyme platform that were applied to determine most enzyme activities of central carbon metabolism in MDCK cell extracts had a sensitivity limit between 0.025 and 0.4 nmol product per well (Table 4.2). This limit was in the same range as described for routine measurements in plant leaf extracts (Gibon et al., 2004). Cell extracts could therefore be highly diluted, which (i) minimized interferences from other components (enzymes, specific or non-specific activators or inhibitors) in the extract, (ii) minimized over- and underestimations of actual enzyme activities as substrate concentration could be maintained at a near constant level (which, in addition, minimized product inhibition), and (iii) allowed to detect low enzyme levels. Mid-throughput was achieved by adapting the enzyme assays to a 96-well microplate format and by using electronic 8-channel pipettes allowing one operator to measure three to four

different enzyme activities in 20 samples per working day including extraction, assay, and calculation. Throughput can still be further increased by using 96-channel pipetting robots (Gibon et al., 2004).

However, there are also potential disadvantages of stop-time assays: (i) they are generally more time-consuming (more pipetting steps) compared to direct assays, (ii) volume inaccuracies may be introduced, and (iii) progress curves (enzymatic reactions) are not monitored directly. Hence, it is important to check that the estimated rates are truly proportional to enzyme concentration and time. Furthermore, contaminating components (e.g., pyridine nucleotides) in the cycling (step 2, see Figure 3.1) and pre-cycling reagents (specific assay mix; step 1) can have a significant influence on the cycling blank of, e.g., the NAD(P)⁺ cycle system, and thus, on the sensitivity limit of the method (Lowry, 1980). It is therefore essential to treat all samples, standards and blanks in a uniform manner throughout the assay, so that the cycling rate will be the same even if several factors (e.g., temperature, pH levels, substrates, and coupling enzymes) of the previous steps affect the rate.

5.1.3 Enzyme activities in confluent MDCK cells

As a first application of the established enzyme platform for mammalian cells, maximum activities (V_{\max}) of 28 central metabolic enzymes of confluent MDCK cells in GMEM-Gln and Episerf were investigated (Table 4.5 and Figure 4.10). V_{\max} values set theoretical upper limits to flux, and V_{\max} values obtained *in vitro* can be expressed in the same units as flux rates *in vivo*. Therefore, determination of maximum enzyme activities (V_{\max}) under optimal conditions *in vitro* (equal to $[E_0] \times k_{\text{cat}}$, where $[E_0]$ and k_{cat} are enzyme concentration and turnover number, respectively) serve as a valid estimate of maximum flux capacities through metabolic pathways (Newsholme and Crabtree, 1986; Suarez et al., 1997). In combination with other data (e.g., intracellular metabolite concentrations) and physiological flux, these rates provide insights into enzyme function, and can be used to determine how capacities correlate to physiological loads (Staples and Suarez, 1997; Suarez et al., 1997).

Among the glycolytic enzymes, the measured activities of HK, PFK and FBPA were comparatively low in GMEM-Gln^{stat} (around 20 nmol/min/10⁶ cells). Biochemical textbooks describe the first enzyme in glycolysis (HK) to regulate the entry of Gluc into the glycolytic pathway. The PFK is known to catalyze a rate-limiting step in glycolysis and is regulated by substrate inhibition at high ATP concentrations. To overcome this inhibitory effect, PFK can

be allosterically activated by high levels of AMP and fructose 2,6-bisphosphate (Muniyappa et al., 1983; Sola et al., 1993). However, in MDCK cells the measured activities of PFK did not seem to be a bottleneck in the glycolytic pathway with a ratio of HK to PFK of about 1 and 0.4 in GMEM-Gln^{stat} and Episerf^{stat}, respectively. For brain tumor cells this ratio is described to be 0.1 to 0.9 (Lowry et al., 1983). Gstraunthaler et al. (1999) showed a ratio between 0.5 and 5 for renal epithelial cells, while the HK/PFK ratio for mammalian lymphocytes ranged between 0.5 and 1 (Ardawi and Newsholme, 1982; Newsholme et al., 1986). The highest activities of glycolytic enzymes in MDCK cells were found for PK and LDH, which might be correlated with the high Lac excretion during growth of continuous cell lines (Häggström, 2000; Häggström et al., 1996).

Although previous MFA studies have assumed that the flux through the oxidative branch of the pentose phosphate pathway can be neglected (Sidorenko et al., 2008; Wahl et al., 2008), the measured maximum activities of G6PDH and 6PGDH, the first and the third enzyme of the oxidative shunt suggest that this route might be important in the Gluc metabolism in MDCK cells. Both enzymes supply NADPH for lipid and nucleotide synthesis and were more active than TK and TA (see Figure 4.10), which catalyze the non-oxidative reactions of the pentose phosphate pathway.

The PC is described to be a major anaplerotic enzyme involved in the maintenance of the TCA metabolite pool and is known to be post-translational regulated (Crabtree et al., 1972; Jitrapakdee and Wallace, 1999; McClure and Lardy, 1971). The entry of carbon from Pyr is also regulated by the PDH complex. Both enzyme activities measured in MDCK cells were relatively low (<1 nmol/min/ 10^6 cells).

The specific enzyme activity of NAD-ICDH was found to be significantly lower than the activity of FUM in MDCK cells. Taking into account that PDH and PC activities were low this might suggest that the metabolic activity of the right part of the TCA cycle was decreased in MDCK cells and that most of the 2-OG supplied to the TCA cycle originated from Glu rather than from Pyr entering the TCA cycle as acetyl-CoA or OAA, respectively (truncated TCA cycle, Figure 4.10). Flux studies in MDCK cells with Gln- and Pyr-containing medium clearly suggested that Gluc was mainly metabolized via glycolysis and the Pyr produced excreted via Lac formation (Sidorenko et al., 2008; Wahl et al., 2008). Only 2 % of the Gluc uptake entered the TCA cycle, while Gln was taken up by the cells at a rate of about 10 % of the Gluc uptake rate. Therefore, as for other mammalian cells (Reitzer et al., 1979; Zielke et al., 1984), the enzyme activity measurements confirm that Gln is the major carbon source

refilling the TCA cycle of MDCK cells cultivated in GMEM medium (Wahl et al., 2008; Zielke et al., 1984).

The measured GLNase activity, the entrance enzyme of glutaminolysis, was comparatively low in MDCK cells grown in GMEM-Gln. This suggests that GLNase rather than GLDH and AspTA regulated the glutaminolytic flux. However, as the activity of GLDH, as well as AlaTA, was comparatively low, 2-OG might be supplied through the transamination of Asp via AspTA. Although, the transaminase pathway is described to yield only 9 moles of ATP per mole Gln, compared to 27 ATP for the GLDH pathway (Glacken, 1988; Häggström, 2000), the relatively high AspTA activity measured confirms the central role of this enzyme in the malate-aspartate shuttle, which transfers high-energy electrons produced during glycolysis to the electron transport chain.

Theoretically, malate and citrate could leave the TCA cycle by the citrate/malate carrier to be converted to Pyr and OAA via the ME or the CL, respectively (see Figure 4.10). The MDH activity, which is not restricted to the mitochondria, was found to be very high in MDCK cells. Finally, the low specific activity of GS measured could reflect the fact that the extracellular Gln concentration during growth in GMEM-Gln was always above critical levels.

Many of the measured maximum enzyme activities in MDCK cells during stationary growth were higher under serum-free compared to serum-containing conditions (Table 4.5). However, it remains unclear if the different composition of the different media (Episerf/GMEM-Gln), the absence of certain FSC components, or cell stress from adaptation (at least two passages) were responsible for the increased enzyme activities under serum-free conditions. Nevertheless, these findings give valuable clues concerning the flexibility of cellular metabolism in response to substrate availability and metabolic state. Together with the higher activities observed during exponential growth compared to the stationary phase in batch culture (Table 4.10), these results clearly indicate that the specific enzyme activities of MDCK cells depend on culture conditions and change with the physiological state. This flexibility of cells to adapt their metabolism to particular growth conditions was, for instance, also described for a murine B-lymphocyte hybridoma (Fitzpatrick et al., 1993), and different mammalian cell lines, insect and primary liver cells grown in batch culture (Neermann and Wagner, 1996).

5.2 Production of *Pichia farinosa* glycerokinase: “missing enzyme” for PK analysis in G3P cycling assay

When methods are used that rely on, e.g., spectrophotometric or fluorometric determination of enzyme activity, most enzymes cannot be monitored directly. Often, one or more coupled reactions are necessary to convert a reaction product of the enzyme under investigation into a detectable metabolite. Therefore, a variety of coupling enzymes were used in the assay platform for mammalian cells to exploit all the benefits of the different cycling systems (e.g., NAD⁺ and G3P cycle). For example, MDH is an important coupling enzyme in the application of the NAD⁺ cycle, as it can be used for the measurement of, for instance, CL and CS activities by coupling the formation of OAA or malate to the production of NAD⁺ or NADH, respectively. The motivation for the production of GK from *P. farinosa* in recombinant yeast was threefold: (i) GK from *P. farinosa* has the potential to use any NTP as phosphate donor for the formation of G3P that can then be analyzed using the sensitive G3P cycle, (ii) this enzyme (or a GK with similar properties) is not commercially available, and (iii) it can be applied to measure the activity of, e.g., PK in MDCK cell extracts.

The nucleotide sequence of the *GUT1* gene coding for GK from *P. farinosa* was successfully cloned into a vector (pPIC3.5) for intracellular production in *P. pastoris*. The integrity of the construct was confirmed by restriction analysis and by DNA sequencing. This expression vector contains a ~0.9 kb fragment from *AOX1* composed of the 5' promotor sequence and a second *AOX1*-derived fragment with sequences required for transcription termination (Cereghino and Cregg, 2000; Invitrogen, 2002a). The *GUT1* gene for GK from *P. farinosa* was inserted into the MCS of pPIC3.5 between the promotor and terminator sequences. Highest expression levels can be reached when the distance between the start codon (ATG) of the heterologous coding sequence and the position of the *AOX1* ATG is small, which corresponds to the first restriction site (*Bam*HI) in pPIC3.5 (Cereghino and Cregg, 2000). In this study, however, the coding sequence for GK from *P. farinosa* was ligated downstream of the *Bam*HI site into *Avr*II–*Not*I restriction sites. Furthermore, the expression level could also be increased by multiple integration of the expression vector containing the *GUT1* gene sequence into the genome of *P. pastoris* (Clare et al., 1991).

The production of the recombinant GK was performed at 30 °C and pH 5 (dissolved oxygen levels above 30 % of saturation) in a 5-L bioreactor in fed-batch mode. An exponential feeding strategy was used in fed-batch culture, which allowed cells to grow at a constant

growth rate (0.04 h^{-1}). The recombinant *Pichia* cells were harvested after 73 h with a specific activity of the His₆-tagged GK of about 5 U/mg cellular protein. When the cells were grown under the same conditions but at higher growth rates ($\mu_{\text{set}} = 0.06 \text{ h}^{-1}$), no significant increase in the specific GK activity could be achieved (data not shown). Furthermore, a glycerin fed-batch prior to the induction phase with methanol was shown to be beneficial for the yield of different heterologous proteins (Bahrami et al., 2008; Chiruvolu et al., 1997), but did also not result in an increased production of His₆-tagged GK in *P. pastoris* (data not shown). However, the specific GK activity under the cultivation conditions used in this study could be doubled ($\sim 10 \text{ U/mg}$ cellular protein) by simply harvesting the cells at an earlier time point of approximately 65 h (see Figure 4.14). Finally, the use of different pH values and/or temperatures during the cultivation process could have a positive effect on the production yield of recombinant His₆-tagged GK. For example, Li et al. (1999) showed that the yield of biologically active herring antifreeze protein expressed at 23 °C increased about 10 times in *P. pastoris* compared to the expression at 30 °C after 4 days of culture. The authors suggested that the increase in the expression level of this product resulted from better protein folding at a lower temperature and from a higher viability of *Pichia* cells during the cultivation at 23 °C (Li et al., 2001). The optimum pH for experimentation and for stability of recombinant proteins in *P. pastoris* is described to be in the range of 2.8 to 6.5 (Sreekrishna et al., 1997). However, the pH optimum for expression of recombinant hookworm (*Ancylostoma caninum*) anticoagulant peptide in *P. pastoris* was found at pH 7 and the lowest peptide production occurred between pH 4 and 5 (Inan et al., 1999). That the level of expressed protein is affected strongly by the pH of the culture medium was also shown by Zhu et al. (1995). During the entire methanol induction phase of recombinant *P. pastoris* in shake flasks, significantly higher activity levels of coffee bean α -galactosidase were observed at a pH of 5.5 and 6.5 compared to pH 7.5. However, the pH optimum for the stability of recombinant α -galactosidase activity in the bioreactor culture supernatant was found to be at 4.5 (Zhu et al., 1995).

The purification of the produced His₆-tagged GK in *P. pastoris* (final activity of $\sim 200 \text{ U/mg}$ protein) was performed in three steps: i) cell disruption (high pressure homogenizer) followed by clarification of the crude cell extract by centrifugation and filtration at 4 °C, ii) nickel affinity chromatography, and iii) anion exchange chromatography at room temperature (see chapter 4.2.3). The third purification step was needed to obtain an almost homogeneous preparation of His₆-tagged GK for the subsequent biochemical characterization of this

recombinant enzyme, as other proteins from the crude cell-free extract (mainly a mitochondrial ADH from *P. pastoris*) coeluted from the affinity column (see Figure 4.17). The extraction was optimized with respect to the extraction conditions (e.g., buffer composition, temperature) and the chromatographic processes were performed with different buffer concentrations, washing steps and elution profiles to find the optimal purification strategy for this enzyme (data not shown). However, a further improvement in yield could be expected by performing the chromatographic runs at a lower temperature (in a cold room), as the GK from *P. farinosa* was shown to lose its activity faster over time at room temperature than at, e.g., 4 °C in the respective purification buffer (data not shown).

5.2.1 Biochemical characterization of glycerokinase

The pH optimum of the purified His₆-tagged GK from *P. farinosa* of 7 was similar to the optimal values reported in studies on *Trypanosoma brucei* (Krakow and Wang, 1990), and *Debaryomyces hansenii* (Nilsson et al., 1989). However, an unusual behavior was found for GK from larvae of *Culex pipiens fatigans*, which showed pH optima at 7 and 10 (Ramabrahmam and Subrahmanyam, 1983). A relatively high pH optimum was also observed for GK from chicken liver (pH 10) (Rao and Kou, 1977). The optimum temperature for the enzymatic activity was about 45 °C. Previous studies indicated that the temperature optimum ranged from 25 to 80 °C for GK from different species (Hayashi and Lin, 1967; Koga et al., 1998; Pasteris and de Saad, 1998).

Michaelis-Menten and Lineweaver-Burk plots were generated from initial velocity studies of *P. farinosa* GK with ATP, UTP, ITP, CTP, and GTP in the forward direction (glycerol + ATP → G3P + ADP) to calculate the kinetic parameters. The K_m value of *P. farinosa* GK for ATP was generally higher than those of other GKs. While the K_{m,ATP} was estimated to be 428 μM, the enzymes from *Pyrococcus kodakaraensis*, *T. brucei*, and *Pediococcus pentosaceus* had values ranging from 15 to 370 μM for ATP (Koga et al., 1998; Krakow and Wang, 1990; Pasteris and de Saad, 1998). Besides, the GK from *E. coli* (Novotny et al., 1985), *Haemophilus influenzae* (Pawlyk and Pettigrew, 2001) and *Salmonella typhimurium* (Novotny et al., 1985) exhibited negative cooperativity. The respective K_m values were reported to be 60 μM, 45 μM and 250 μM at low concentrations of ATP, and 0.9 mM, 2.5 mM and 0.9 mM at high ATP concentrations. As expected, GK from *P. farinosa* could also utilize other NTPs for glycerol phosphorylation, which was checked by the formation of G3P. ATP was shown to be the most efficient phosphoryl group donor of the

tested NTPs (Table 4.7). Other species that showed catalytic GK activity with different phosphate donors include *Candida mycoderma* (Janson and Cleland, 1974), *P. kodakaraensis* (Koga et al., 1998), cucumber radicle tissue (Sadava and Moore, 1987), *C. pipiens fatigans* (Ramabrahmam and Subrahmanyam, 1983), and chicken liver (Rao and Kou, 1977), whereas the enzyme from *E. coli* was shown to be specific for ATP only (Hayashi and Lin, 1967). Furthermore, a remarkable behavior of the GK from *P. farinosa* was found in the relation between the reaction velocity and GTP, UTP or CTP concentration at saturating glycerol. When the activity was measured over a wide range of NTP concentrations (0 to 10 mM), the double reciprocal plots were biphasic (Figure 4.20), which suggested that the enzyme from *P. farinosa* exhibited negative cooperativity with respect to GTP, UTP and CTP.

5.2.2 Use of the recombinant glycerokinase as a coupling enzyme

After the production, purification and characterization processes, the recombinant His₆-tagged GK from *P. farinosa* was successfully applied as a coupling enzyme to determine the specific activity of PK in extracts of MDCK cells. No significant differences in the determination of the specific activities of PK were found when the recombinant GK was compared to a bacterial GK from *E. coli*, which demonstrated good performance as a coupling enzyme for the PK assay. In principle, any NTP could be coupled to G3P formation by GK from *P. farinosa*, as this enzyme was not specific for ATP. For example, Gibon et al. (2004) described an assay for ADP-glucose pyrophosphorylase (AGPase, EC 2.7.7.27) activity in the reverse direction by measuring the PP_i-dependent production of ATP from ADP-glucose. Therefore, the UTP-producing enzymes glucose-1-phosphate uridylyltransferase (UDP-Glc PPase) (EC 2.7.7.9) and galactose-1-phosphate uridylyltransferase (UDP-Gal PPase) (EC 2.7.7.10) could be assayed by determining the amount of UTP formed from UDP-glucose and UDP-galactose, respectively. In previous studies, determination of UDP-Glc PPase and UDP-Gal PPase activities were carried out with an excess of phosphoglucomutase (EC 5.4.2.2) and G6PDH (EC 1.1.1.49) (Turnquist et al., 1974) or PGK (EC 2.7.2.3) and GAPDH (EC 1.2.1.12) (Chacko et al., 1972) as auxiliary enzymes. Hence, the use of GK as the only coupling enzyme could simplify the assays for UDP-Glc PPase and UDP-Gal PPase, and in combination with the G3P cycling assay (Gibon et al., 2002) sensitivity could be increased significantly.

5.3 Effect of different cultivation conditions on central metabolic enzymes in MDCK cells

The motivation for analyzing maximum enzyme activities of adherent MDCK cells under different cultivation conditions was to improve the understanding of Gluc and Gln metabolism as well as substrate requirements during growth in batch culture. In a previously published report (Genzel et al., 2005), it was shown that different mammalian cell lines (MDCK, BHK21, CHO-K1) can be cultivated in Gln-free media when Pyr was added to the culture medium. During growth of adherent MDCK cells in GMEM-Pyr, an apparent shift to a more efficient metabolism was observed, i.e., no ammonia was released and Gluc consumption and Lac production were reduced significantly. Sidorenko et al. (2008) applied MFA to adherent MDCK cells in microcarrier culture during different growth phases (exponential and stationary) to further investigate the influence of Pyr substitution on metabolism. It was suggested from flux distributions that metabolism of MDCK cells during exponential growth did not change dramatically when Pyr was substituted for Gln. However, it seemed that the consumption of ATP in futile cycles (e.g., glucose-fatty acid cycle) was significantly reduced and more Pyr entered the TCA cycle, whereas most of the Gluc consumed was excreted as Lac leading to a reduction of the Gluc uptake necessary for cellular metabolism in Gln-free but Pyr-containing GMEM medium. Based on the assumption that a significant fraction of the consumed Pyr enters the TCA cycle, the activities of PDH and PC (key enzymes connecting the glycolysis with the TCA cycle), and GS (catalyzing the synthesis of Gln from Glu) should be up-regulated in GMEM-Pyr. Therefore, the influence of Gln substitution by Pyr on central metabolic enzymes will be discussed in more detail in the following two chapters (5.3.1 and 5.3.2).

In this study, the specific enzyme activities of MDCK cells were related to the viable cell number per well at time of harvest, which increased from 1.0-1.5 x 10⁶ cells/well after ~2 days of growth (exponential phase) to 3.5-4.0 x 10⁶ cells/well after ~5 days (stationary) in six-well plates in GMEM-Gln and GMEM-Pyr (see Figure 4.21 and Figure 4.24). However, the biomass/cellular protein concentration per well decreased from ~0.7 (2 days) to about 0.6 mg/well (~5 days) in GMEM-Gln (Figure 4.24). It could also be shown that the cellular volume of adherent MDCK cells changed during growth in six-well plates in GMEM-Gln (Ritter, 2010). Cellular volumes were highest during exponential growth (average cell diameter of about 20 µm) and lowest values were obtained in the stationary phase (~16 µm).

Different results could therefore be expected when the enzyme activities were related to the biomass and not to the viable cell number (as in this study). Higher protein-specific enzyme activities of central metabolism would likely be obtained in adherent MDCK cells of the stationary growth phase compared to exponential-phase cells. This should be considered in future studies on enzyme activity measurements in mammalian cell cultures at different growth stages.

5.3.1 Glucose metabolism

Gluc is used by almost all mammalian cell lines for cell functioning and cell proliferation since it provides a source of ATP and NADPH as well as phospholipid and nucleic acid precursors (Newsholme et al., 2003). The first step of the glycolytic pathway is the conversion of Gluc to G6P, catalyzed by HK. It has been previously suggested that HK plays an important role for adjusting the glycolytic rate in most continuous cell lines (Neermann and Wagner, 1996). When examining the metabolism of transformed mammalian cells, continuous insect cells and primary liver cells, Neermann & Wagner (1996) found relatively high PK/HK ratios (49 to 106) in mammalian cell lines. The PK/HK ratios measured in this study were in a similar range as for other mammalian cell lines (39 to 87, depending on the cultivation condition/physiological state of the cell). Fitzpatrick et al. (1993) also found a high PK/HK ratio between 26 and 560 for a murine hybridoma cell line. On the other hand, insect and primary cells with PK/HK ratios of 4 to 10 exhibited a more balanced glycolytic activity, which indicates better regulatory capabilities (Neermann and Wagner, 1996). When adherent MDCK cells were grown in GMEM-Pyr, the cells consumed less Gluc and released less Lac into the culture supernatant with similar growth behaviors (see Genzel et al., 2005; compare also Figure 4.21 to Figure 4.23). It was suggested that the inhibition of Gluc consumption upon Pyr supplementation may eventually reflect a feedback controlling effect on the activity of glycolytic enzymes (Genzel et al., 2005; Hassell and Butler, 1990). Sidorenko et al. (2008) then proposed from experimental data and calculated flux distributions that the fluxes through the glycolytic pathway were decreased with Pyr. However, this did not correspond to the decrease in HK activity in exponential-phase cells (2 d of growth) grown with Pyr. The HK activity was higher in GMEM-Pyr^{exp} compared to GMEM-Gln^{exp}. Although the activity of HK then decreased in stationary-phase cells (5 d of growth) and was lower in GMEM-Pyr^{stat} compared to GMEM-Gln^{stat}, the reduced uptake rate of Gluc by the cells grown with Pyr might not be explained solely by a change in activity of HK. A similar effect was observed in a recent study by Carinhas et al. (2010) where insect

cells were infected with baculovirus. When the cultures were supplemented with 12 mM Pyr at the time of infection, the overall activity of the glycolytic pathway was peaking during the initial phase of infection (until 48 to 72 h post infection) when compared to control cultures (without Pyr). During the second phase (from 48 to 72 hpi), the estimated glycolytic fluxes were smaller. This effect, however, disappeared with increasing Pyr concentrations (24 mM) and the glycolytic fluxes were then generally smaller compared to the control. Therefore, the initial amount of Pyr present in the medium was likely to be responsible for the change in glycolytic fluxes during different states of insect cells. According to the enzyme activity data in this study, this may eventually be an indication that the glycolytic pathway is more likely regulated via the key regulatory enzyme of glycolysis, PFK, and not HK in adherent MDCK cells. In particular, as the maximum catalytic activity of PFK did not change during growth in either medium and was generally lower than the activity of HK in exponentially growing MDCK cells (Table 4.10).

G6P from Gluc and ATP can serve as a substrate for G6PDH (pentose phosphate pathway). Alternatively, it can be further metabolized to Pyr for entry into the TCA cycle or for release into the medium as Lac. G6PDH and 6PGDH, which catalyze the first and third reaction of the pentose phosphate pathway, are important enzymes regulating the biosynthesis of nucleic acid precursors (R5P) and the supply of reducing equivalents in form of NADPH (Stryer, 1995). Previous work has shown that the pentose phosphate shunt and G6PDH in particular were activated by addition of growth factors (Stanton and Seifter, 1988; Stanton et al., 1991). When comparing the maximum pentose phosphate pathway activities of exponentially growing MDCK cells in response to Pyr, it seems that more G6P was channeled into the oxidative branch of the pathway suggesting that more NADPH is required. In dividing glioblastoma cells, the NADPH production needed for fatty acid synthesis was shown to be supported by Gln metabolism via the ME (DeBerardinis et al., 2007). However, the ME activity was decreased in MDCK cells grown in medium without Gln indicating a decreased potential for regeneration of NADPH. It can be assumed from the enzyme activity results that the G6PDH reaction possibly compensated for the NADPH requirements of fatty acid synthesis in proliferating MDCK cells grown with GMEM-Pyr in which extracellular Gln was not available. These findings, however, are in contrast to the zero flux assumption through the oxidative branch of the pentose phosphate pathway in the study by Sidorenko et al. (2008). Additionally, the flux through the non-oxidative branch of this pathway was described to be low with a similar value in both media. Isotopomer labeling experiments

could be used in the laboratory of the Bioprocess Engineering group to further investigate these findings.

An option to decrease the yield coefficient of Lac produced per Gluc ($Y_{\text{lac/gluc}}$) is by stimulation of the PDH and/or PC reaction. Irani et al. (1999) demonstrated that BHK cells harboring a cytosolic yeast PC required less Gluc and Gln than untransfected cells. Thus, an increase in the PC activity resulted in a more efficient Gluc metabolism and reduced Lac production as Pyr was shunted directly into the TCA cycle. Neermann & Wagner (1996) could not detect any PDH or PC activity in their examined mammalian cell lines, whereas activity was found in continuous insect cells as well as primary liver cells, which possibly could explain the higher flux of Gluc metabolites into the TCA cycle in these cells. For MDCK cells, Sidorenko et al. (2008) assumed that the flux through the anaplerotic enzyme PC was zero for both cultivation conditions (Gln-containing as well as Pyr-containing medium). The flux through the PDH pathway was set to zero in Gln-containing medium only, whereas a significant increase was assumed for this flux with Pyr. The anaplerotic role was suggested to be fulfilled by a mitochondrial ME operated in the direction of malate. In this study, both enzymes PDH and PC were detected, although with very low activities. Furthermore, both enzymes seemed to be up-regulated in GMEM-Pyr, which was indicated by an increase in maximum activities compared to Gln-containing conditions.

For adherent MDCK cells grown with Pyr-containing media, no decrease in $Y_{\text{lac/gluc}}$ could be observed although less Gluc was taken up (Genzel et al., 2005). MFA studies suggested that even when Gln was substituted by Pyr, only a small portion of Gluc-derived carbon was oxidized in the TCA cycle (Sidorenko et al., 2008; Wahl et al., 2008). More than 98 % of Gluc seemed to be secreted as Lac in the culture medium. In fact, it was assumed that only extracellular Pyr was taken up by the cell and was directly shunted into the TCA cycle. As mentioned above, the respective enzymes involved are most likely PDH and PC. A significant fraction of carbon units in TCA cycle intermediates could then be used to synthesize Gln as shown by a significant increase in NAD-ICDH and GS activity under Pyr-containing conditions. However, if there was an increase in the flux through the right part of the TCA cycle, and if the increase in enzyme activities was most likely required to compensate for the energy demand and to replenish the Gln pool during growth of the MDCK cells remains to be investigated. In the end, these hypotheses can only be validated by further research using ^{13}C -labeled substrates, such as L-[3- ^{13}C]Gln and D-[1,6- $^{13}\text{C}_2$]Gluc, and analyzing the isotopomer distribution data (DeBerardinis et al., 2007). However, studies with

labeled substrates and the analysis of isotopomer distributions of the central metabolic metabolites are generally much more complex and time-consuming compared to enzyme activity measurements.

5.3.2 Glutamine metabolism

Gln is an important precursor for the synthesis of peptides and proteins, amino sugars as well as nucleic acids and nucleotides. Furthermore, Gln is known to be the major energy source refilling the TCA cycle of mammalian cells cultivated in Gln-containing media (DeBerardinis et al., 2008; Newsholme et al., 2003; Reitzer et al., 1979; Wahl et al., 2008; Zielke et al., 1984). The immediate product of glutaminolysis is Glu, which is catalyzed by GLNase, an enzyme associated with the mitochondria (Kvamme et al., 2000). The observed maximum enzyme activity of GLNase of exponential-phase MDCK cells was similar in GMEM-Gln and GMEM-Pyr medium. In stationary-phase cells, however, the activities were clearly decreased by 2.07-fold and 4.67-fold in both media. Sevdalian et al. (1980) found similar results for cultured human diploid fibroblasts. The GLNase activity reached its maximum after two days of growth independently of the Gln concentration (0.2 to 2.0 mM) and decreased once the cells reached confluency. The Glu produced can either enter the TCA cycle as 2-OG or serve as a substrate for anabolic pathways (e.g., amino acid biosynthesis). Generated ammonia, which is known to be a primary growth inhibitor in adherent cells, is released into the culture medium (Glacken et al., 1986). However, no ammonia release was observed for MDCK cells grown under Pyr-containing conditions (Genzel et al., 2005). This is most likely due to the absence of Gln in the culture medium.

In cultures grown in media devoid of Gln, Gln is produced from Glu and NH_4^+ by the action of GS, a key enzyme in nitrogen metabolism supplying the cells with Gln needed for protein synthesis (McDermott and Butler, 1993; Sanders and Wilson, 1984). This finding was also demonstrated by label incorporation of ^{15}N from $^{15}\text{NH}_4\text{Cl}$ into the amide position of Gln in CHO cells expressing high levels of GS (Street et al., 1993). Data of enzyme activity measurements showed that the Gln limitation in MDCK cells under Pyr-containing conditions was overcome with an increase in the activity of GS (compared to GMEM-Gln). Similar findings were reported for CHO and BHK cells when the Gln concentration in the medium was decreased or the medium was supplemented with Glu instead of Gln, respectively (Christie and Butler, 1999; Sanfeliu and Stephanopoulos, 1999).

As mentioned above, the right part of the citric acid cycle seemed to be up-regulated under Pyr-containing conditions. Especially, there was a significant increase in cell-specific activity of PC, PDH, NAD-ICDH, GLDH, and GS in proliferating MDCK cells cultivated with Pyr. Furthermore, the activities of AspTA, AlaTA, ME and PEPCK decreased in MDCK cells from the exponential growth phase. Ardawi & Newsholme (1982) have suggested that the conversion of OAA to PEP via PEPCK is part of the pathway for Gln oxidation. By using an inhibitor of PEPCK (3-mercaptopycolinate), the authors could confirm the participation of this enzyme in the oxidation of Gln in lymphocytes (Ardawi and Newsholme, 1983). Together with the decreased GLNase activity in stationary-phase MDCK cells, this is a strong indicator of a decreased Gln metabolism in the presence of Pyr. Previous studies using flux analysis (DeBerardinis et al., 2007; Street et al., 1993) and enzyme activity measurements (Neermann and Wagner, 1996; Vriezen and van Dijken, 1998a) suggested that the transaminase pathway is the main pathway in mammalian cell lines for Gln utilization, although only 9 moles of ATP are produced compared to the GLDH pathway yielding 27 ATP (Glacken, 1988; Häggström, 2000). As previously suggested, AspTA seems to be the major enzyme in MDCK cell metabolism with AlaTA at a clearly lower level (Table 4.5). Genzel et al. (2005) observed for extracellular Ala concentrations a slight (not significant) decrease (10 %) during growth of the cells in Pyr-containing medium. Moreover, the authors found even a slight decrease in Amm concentration during cell growth in Pyr-containing medium, which was also observed during growth in six-well plates (Figure 4.23 B). In this study, a decrease in the activity of AlaTA was seen in GMEM-Pyr. The decrease in AlaTA activity in the presence of Pyr and during cell growth suggested that the AlaTA route may be an important pathway in glutaminolysis of MDCK cells. Finally, the activity of GLDH slightly increased in exponentially growing cells. This enzyme can catalyze the reverse reaction *in vivo* ($2\text{-OG} + \text{NADH} + \text{NH}_4^+ \rightarrow \text{Glu} + \text{NAD}^+ + \text{H}_2\text{O}$), which has been observed, for example, in hybridoma cells stressed with high concentrations of extracellular ammonia (Bonarius et al., 1998). This could therefore be a strong indication that the GLDH route was used for Gln synthesis in MDCK cells grown with Pyr.

It is evident from several studies on metabolism of animal cells that changes in enzyme activities highlight metabolic changes (Fitzpatrick et al., 1993; Leveille and Hanson, 1966; Neermann and Wagner, 1996; Segner and Verreth, 1995; Vriezen and van Dijken, 1998a; Yallop et al., 2003). It is, however, worth mentioning that although change in enzyme activity is mostly represented by change in the total amount of an enzyme, catalytic activity can also

be altered by allosteric effectors that, for instance, change the substrate affinity (K_m) of the enzyme. Interestingly, this study shows that most enzymes in the affected pathways are coordinately up- or down-regulated. These correlated changes are in agreement with the proposed “multisite-modulation” mechanism of Fell & Thomas (1995), which states that large changes in metabolic flux can only be attained by parallel changes in activity of many or all of the enzymes in a pathway. To which extent flux changes in this cell system can be predicted by using enzyme activity information alone (without any knowledge on enzyme kinetics and intracellular metabolite concentrations) remains to be explored in future studies. However, a recent study by Rossell et al. (2011) describes a method for the construction of mathematical functions in which flux changes could be predicted solely on the basis of changes in total amounts of enzymes/enzyme concentrations. The approach was based on “Metabolic Control Analysis”, which defines a flux control coefficient to provide a quantitative estimation of control of the flux through a pathway exerted by an enzyme (Fell, 1998). The validity of the methodology was checked *in silico* by using a multi-branched kinetic model and *in vivo* by using enzyme activity and flux measurements of the glycolytic and fermentative pathways of *Lactococcus lactis*.

In vitro maximum enzyme activities can only be used as a flux indicator by investigating the relative activity changes under specific conditions and serve as a valid measure of maximum flux capacities through metabolic pathways (Newsholme and Crabtree, 1986; Suarez et al., 1997). But the actual *in vivo* flux and the direction of flux through a pathway cannot be inferred. As mentioned above, for example, the flux through GLDH was reversed in ammonia-stressed hybridoma cells (Bonarius et al., 1998). Therefore, additional future flux analysis studies using ^{15}N and ^{13}C labeled nutrients would be useful to clarify some of the open questions (DeBerardinis et al., 2007; Martinelle et al., 1998; Metallo et al., 2009; Street et al., 1993). For cells grown with Pyr-containing medium it would be interesting, for instance, to investigate the metabolic fluxes through the glycolysis and the TCA cycle with labeled Gluc and Pyr, respectively. Together with the enzyme activity data and extra- and intracellular metabolite concentrations (Genzel et al., 2004b; Ritter et al., 2008), this approach may lead to a more comprehensive view of metabolism and show how the extracellular Pyr is distributed, and clarify whether the substrate indeed passes the GLDH pathway for Gln synthesis in MDCK cells. Finally, a combination of the methods will provide a sound basis for establishing detailed dynamic mathematical models to analyze key

parts of cellular metabolism and, therefore, contribute significantly towards a systems biology understanding of mammalian cells cultivated for production of biologicals.

5.4 Influence of influenza virus infection on key metabolic enzyme activities in MDCK cells

The motivation to measure the activity of 28 enzymes that are involved in central carbon and Gln metabolism in influenza A infected MDCK cells comes from recent studies that showed changes in metabolic activity (e.g., altered fatty acid biosynthesis and cholesterol metabolism) during viral replication in different cells (Heaton et al., 2010; Lin et al., 2010; Munger et al., 2008). Up to now, only few studies have described the effects of virus infection on the central carbon metabolism (e.g., intracellular metabolite concentrations) of host cells (Hollenbaugh et al., 2011; Munger et al., 2006; Ritter et al., 2010). Like all viruses, influenza relies on the host's metabolic network to provide energy and macromolecular precursors for viral replication. Influenza viruses bud from the apical host plasma membrane with an envelope containing lipid rafts, which are enriched in cholesterol and glycosphingolipids (Gerl et al., 2012; Nayak et al., 2009; Rossman and Lamb, 2011; Scheiffele et al., 1999; Zhang et al., 2000). A very recent study by Gerl et al. (2012) who quantitatively analyzed the lipidomes of the influenza virus envelope and the MDCK cell apical membrane, confirmed these results. The authors found the apical membrane to be enriched in sphingolipids and cholesterol, and the virus membrane exhibited a further enrichment of sphingolipids and cholesterol compared to the host cell membrane.

When analyzing the effect of influenza A virus infection at a MOI of 20 on enzyme activities of the central carbon metabolism of MDCK cells, 9 of 28 enzymes were found to be up-regulated compared to the control group 9 hpi (Figure 4.30 to Figure 4.33). The high MOI was used to ensure simultaneous infection of cells and for comparison with previous data on intracellular metabolite concentrations in the study by Ritter et al. (2010). At the time post-infection (9 hpi) when the cells were harvested, key metabolic enzyme activities were analyzed in virus and mock-infected MDCK cells. No enzyme of the glycolytic pathway was increased during early virus infection in adherent MDCK cells compared to mock-infected cells (see Figure 4.30). This is in agreement with the findings by Ritter et al. (2010) who also could not find an effect of influenza A infection on intracellular metabolite concentrations of infected MDCK cells during the first 10 to 12 hpi at the same culture conditions. However,

after 12 hpi intracellular metabolite concentrations of the upper part of glycolysis were significantly increased.

Other studies also found an increase of glycolysis during virus infection. It has to be pointed out that the kinetics of viral replication may differ significantly between different viruses and host cells. For example, viral DNA replication in HCMV infected fibroblasts begins between 24 and 48 hpi, and highest virus yields are expected after 72 to 96 hpi (Furukawa et al., 1973). However, large changes in metabolite concentrations in MRC-5 fibroblasts infected with HCMV at a MOI of 3 appeared after 48 hpi (Munger et al., 2006). HCMV is a medically relevant herpesvirus, which also contains a host-derived lipid envelope. Furthermore, transcript levels for PFK and PDH were found to be increased in HCMV infected cells at 24, 48 and 72 hpi. In a subsequent study, metabolic flux profiling using [¹³C]Gluc of uninfected and virally infected cells then revealed that the glycolytic flux increased approximately 2-fold in HCMV infected MRC-5 fibroblasts after 48 hpi (Munger et al., 2008). For BHK21 cell cultures infected with rubella virus at a high MOI of 10 to 20, the first increase in total virus titer was found at 12 hpi and maximal titers were reached between 36 to 48 hpi, after which the cells began to detach from the surface (Vaheri and Cristofalo, 1967). The first evidence of an increased aerobic glycolytic rate occurred between 24 and 36 hpi in rubella infected BHK21 cells. Enveloped viruses therefore seem to stimulate aspects of the glycolytic pathway. However, virus induced alteration of glycolysis in these cells occurred only during late virus infection.

One hypothesis for the increased metabolic load during late stages of infection might be related to the onset of apoptosis in influenza infected cells (Lowy, 2003). As a result of programmed cell death, mitochondria undergo permeabilization processes that cause the release of metabolites and the stop of cellular respiration. The cells therefore seem to respond with an increase in glycolytic rate to compensate for the energy requirements. Furthermore, it could be shown that the energy charge ($([ATP] + 1/2 [ADP]) / ([ATP] + [ADP] + [AMP])$) dropped below physiological levels (<0.9) in influenza infected MDCK cells as well as in reovirus infected Vero cells, indicating the breakdown of metabolism after virus infection (Burgener et al., 2006; Ritter et al., 2008; Ritter et al., 2010).

In contrast to glycolysis, the specific enzyme activities of PC, CS, CL, and NAD-ICDH, which are related to the TCA cycle were increased in influenza infected MDCK cells during early virus infection (Figure 4.31). Among these enzymes, the PC showed the highest change in maximum specific activity (1.69-fold change). The PC catalyzes the ATP-dependent

carboxylation of Pyr to OAA, which is an important anaplerotic reaction within the central carbon metabolism of mammalian cells, replenishing the pools of metabolic intermediates in the TCA cycle. Munger et al. (2008) also found an up-regulation of the flux for the anaplerotic pathway for formation of four-carbon units by ~4-fold from Pyr to OAA in HCMV infected cells after 48 hpi. Moreover, the CL also showed a significantly increased activity in influenza infected MDCK cells (1.34-fold change). Subsequent to the transport of mitochondrial citrate into the cytosol (via the citrate/malate shuttle), citrate is cleaved by ATP-dependent CL to yield acetyl-CoA and OAA. OAA can then be transported back into the mitochondria as malate (via MDH and the shuttle system). Malate can also be decarboxylated to form Pyr and NADPH (via ME), while cytosolic acetyl-CoA can be used to feed *de novo* biosynthesis of fatty acids and cholesterol. As mentioned above, assembly and budding of influenza particles is organized in lipid raft domains in the cellular membrane of the host. In addition to the increased activity of CL, an up-regulation was observed for ACoAL (Figure 4.33), which also produces acetyl-CoA (ATP-dependent reaction) that can be used for energy production (mitochondrial) or lipid and cholesterol synthesis (cytosolic) (Luong et al., 2000; Starai and Escalante-Semerena, 2004). For example, studies with L929 cells showed that [¹⁴C]acetate was incorporated into cell lipids when the cultures were grown in serum-containing medium devoid of exogenous lipids (Howard et al., 1974). A dramatic increase in intracellular acetyl-CoA concentrations was observed when fibroblasts were infected with HCMV and flux studies using ¹³C-labeled Gluc and Gln showed that the efflux of two-carbon units to fatty acid biosynthesis (from citrate to malonyl-CoA, which is an intermediate in fatty acid synthesis) was up-regulated (Munger et al., 2006; Munger et al., 2008). The requirement of fatty acid biosynthesis for virus replication was also identified in [¹⁴C]acetate-pulsed human embryonic lung cells infected with dengue virus (Heaton et al., 2010). Unfortunately, no data of intracellular acetyl-CoA concentrations are available for influenza infected MDCK cells (Ritter et al., 2010). However, the increased citrate concentrations after 10 hpi in virally infected cells together with the measured increase in CL and ACoAL activities may be a strong indication for a virus-induced activation/up-regulation of the fatty acid biosynthetic pathway. This hypothesis is supported by a recent study, which employed GC/MS for analysis of the dynamic courses for influenza A virus infection in different cell lines (Lin et al., 2010). The authors found that endogenous metabolites of cholesterol and fatty acids differed in influenza infected A549 and AGS cells, which indicated an altered cholesterol metabolism and fatty acid biosynthesis upon virus infection in these cell lines.

Fatty acid and cholesterol biosynthesis not only require sufficient concentrations of acetyl-CoA but also NADPH as reducing equivalent. The reducing power can be supplied from the reactions of the first and the third enzyme of the pentose phosphate pathway, G6PDH and 6PGDH. These enzymes were both up-regulated to a similar degree during early influenza infection of MDCK cells in this study (Figure 4.32). Besides, G6PDH and 6PGDH indirectly participate in the production of R5P and X5P. R5P is an important intermediate metabolite of nucleotide synthesis and can be produced from GAP and sedoheptulose 7-phosphate (S7P) catalyzed by TK or from Ru5P via the R5P isomerase (EC 5.3.1.6). Munger et al. (2008) could show that the incorporation of R5P into nucleotides was increased in HCMV infected fibroblast cultures. Increase in intracellular R5P levels was also observed for MDCK cells infected with influenza virus from 10 hpi until the end of the period (Ritter et al., 2010). In contrast, measured ATP concentrations in influenza infected cells showed a clear decrease. However, virus-induced up-regulation of nucleotide biosynthesis and thus also RNA synthesis might be essential for viral replication (Tanaka et al., 1975). Another important metabolite regulating lipid synthesis in mammalian cells is X5P, which can be produced from Ru5P by Ru5P epimerase (EC 5.1.3.1) or from GAP and F6P (or S7P) via TK (see Figure 4.26). It was shown that X5P can activate protein phosphatase 2A (EC 3.1.3.16), an enzyme with broad substrate specificity, which plays a major role in the long-term control of the enzymes required for fatty acid synthesis (Kabashima et al., 2003; Veech, 2003). Another explanation for the increased G6PDH activity in infected MDCK cells could be the oxidative stress as a result of the propagation of influenza viruses in infected cells (Buffinton et al., 1992; Lowy, 2003). Prévaille and coworkers (1999) found that small stress proteins protect against oxidative stress in L929 cells through their ability to increase the activity of G6PDH.

NADPH can also be produced by the conversion of malate to Pyr via the ME. This reaction was found to be the predominant route for NADPH supply in HeLa cells during growth on Gln (Reitzer et al., 1980). Here, the activity of ME significantly increased (1.30-fold change), which suggests the need of NADPH for fatty acid synthesis in infected MDCK cells (Figure 4.33). This is in agreement with the findings by Munger et al. (2006) who measured increased transcript levels of ME in HCMV infected cells. Furthermore, Ritter et al. (2010) found increased levels of intracellular Pyr in influenza infected MDCK cells after 10 hpi. As mentioned above, the activity of PC in infected cells was significantly increased compared to mock-infected cells (~1.7-fold). Part of the increase in specific PC activity therefore may directly contribute to the NADPH production via ME (Wise and Ball, 1964). Another enzyme

of glutaminolysis that showed increased activity in infected MDCK cells was the GLNase (Figure 4.33). However, the concentration profile of extracellular Gln between infected and mock-infected cells was basically the same and no significant differences could be detected (Ritter et al., 2010). If the rise of GLNase activity in infected cells was necessary to maintain the increased demand in carbon atoms for citrate formation (and hence acetyl-CoA for lipid synthesis) remains to be investigated in future studies by investigating the metabolic fluxes through the TCA cycle using labeled Gln.

Taken together, these results may indicate that fatty acid biosynthesis is necessary for influenza replication in MDCK cells. It can be further suggested that transcription of enzymes involved in cholesterol and fatty acid biosynthesis was coordinately controlled as the G6PDH, 6PGDH and the ME, producers for NADPH, were increased by influenza virus infection. Furthermore, the activities of CL and ACoAL, which are also required for fatty acid synthesis by providing acetyl-CoA, were increased in infected MDCK cells. However, to validate these findings, experiments at different time points post infection (e.g., late virus infection) as well as with different influenza virus strains should be taken into account. Furthermore, measurements of other enzymes participating in lipid synthesis should be considered. For example, the V_{\max} of the fatty acid synthase complex (EC 2.3.1.85) is a major rate controlling step in the process of fatty acid synthesis (Guynn et al., 1972). Moreover, labeling experiments with ^{13}C -labeled substrates could be used to elucidate the fluxes of the central carbon metabolism in cultured cells and clarify which fraction of labeled citrate comes from Gluc and Gln in virally infected cells (Munger et al., 2008). In addition, cell lysates from infected and mock-infected cells could be incubated with [^{14}C]malonyl-CoA as a direct measure of fatty acid synthesis (Heaton et al., 2010). Finally, experiments with pharmacological inhibitors of enzymes participating in lipid and/or cholesterol biosynthesis (e.g., 5-(tetradecyloxy)-2-furoic acid specifically inhibits acetyl-CoA carboxylase, EC 6.4.1.2) could be used to determine whether influenza-induced up-regulation of fatty acid/cholesterol synthesis is required for viral replication in MDCK cells (Munger et al., 2008).

6 Conclusions

The presented project aimed at a better understanding of central metabolism of MDCK cells typically used for manufacturing of influenza vaccines. Therefore, central metabolic key enzyme activities under different growth conditions as well as during virus replication were investigated. As a first step, 17 enzyme assays based on a high-throughput platform developed for plant cells (Gibon et al., 2004) were adapted to use for monitoring enzyme activities in mammalian cell cultures. The use of enzymatic cycling methods combined with the application of 96-well microplates allowed a more sensitive and faster determination of enzyme activities than most of the existing continuous assays. Compared to the platform for plant cells, sample preparation steps were less laborious for mammalian cells as disruption of cell walls was not required. Furthermore, continuous cell lines can be easily grown under controlled conditions and studies were not as time-consuming as experiments using parts of plants.

On the basis of a reaction network for adherent MDCK cells (Wahl et al., 2008), 11 new assays were established for selected enzymes relevant in central carbon and Gln metabolism to set up a platform with 28 assays for monitoring enzyme activities in mammalian cells. For the assay procedures and for sample preparation and handling, including sample extraction, a new set of SOPs was generated to minimize variability and to promote a standard for future enzyme studies. All cycling assays were validated according to the standards of the Bioprocess Engineering group. The linear range of the different cycling assays was checked with calibration curves from serial dilutions of the respective standards. For all enzyme assays, proportionality between product formation and cell amount or time was evaluated. Finally, spiking experiments with standards were carried out to examine the influence of cell extracts on the response of the cycling assays. This new enzyme platform allowed measurement of enzyme activities at maximum velocity (V_{\max}), as all assays were optimized to proceed under substrate-saturating (optimal) conditions. Analysis of key enzyme activities in extracts of MDCK cells grown in serum-containing GMEM-Gln (stationary phase) showed typical characteristics of glycolysis (high PK and LDH activities), citrate cycle (low PDH, PC and NAD-ICDH activities) and glutaminolysis supporting the hypothesis of a truncated TCA cycle in confluent MDCK cell cultures.

The comparison with stationary-phase cells grown in serum-free Episerf medium clearly indicated that the specific enzyme activities of MDCK cells depend on culture conditions and

change with the physiological state. Although these enzyme assays do not differentiate between isoforms (e.g., cytosolic or mitochondrial MDH, PEPCK, AspTA, AlaTA), the sensitivity of the cycling assays (0.025 to 0.4 nmol product per assay) allowed precise determination of enzyme activities in very small sample volumes or samples with low enzyme levels.

To provide the flexibility for future studies on cell metabolism, the developed enzyme platform for mammalian cells was extended with a new coupling enzyme, namely GK from *P. farinosa*. The His₆-tagged *GUT1* gene (Gibon et al., 2009; Neves et al., 2004) was cloned into pPIC3.5 vector for intracellular expression. The resulting recombinant plasmid (pPIC3.5-GK) was then transformed and expressed in *P. pastoris* GS115 cells. The following fed-batch cultivation in a 5-L stirred-tank bioreactor resulted in production of recombinant GK with a specific activity of 5.4 U/mg cellular protein at the time of harvest. A subsequent two-step purification procedure (nickel affinity chromatography followed by anion exchange chromatography) resulted in a high purity enzyme product (~200 U/mg protein).

The biochemical characterization revealed that the pH and temperature optimum was at 7 and 45 °C, respectively. Furthermore, it was shown that the GK from *P. farinosa* not only phosphorylates glycerol with ATP but also with ITP, UTP, CTP or GTP, which makes this coupling enzyme extremely valuable for studies on NTP-producing enzymes. Finally, this enzyme was applied for the measurement of specific PK activities in MDCK cell extracts by coupling the PK-induced ATP formation to G3P. The reproducibility was compared with a commercially available preparation of GK from *E. coli*, which can only use ATP as substrate.

In this study, all enzyme activities were determined in cell extracts under maximum substrate supply, so that any change in enzyme activity measured could be referred to a direct change in enzyme amount. The maximum capacity for metabolic flux is a function of the total amount of enzyme and the catalytic efficiency. Thus, studies on maximum enzyme activities *in vitro* can provide a quantitative indication of the maximum flux through metabolic pathways *in vivo*, as V_{\max} values set theoretical upper limits to flux in metabolic pathways. The next step was to determine changes in specific enzyme activities of MDCK cells during their growth under different cultivation conditions. It is known that Pyr can be used as a carbon source and is expected to be shunted directly into the TCA cycle (Genzel et al., 2005; Sidorenko et al., 2008). To analyze the flexibility of central carbon metabolism in cultured adherent MDCK cells in response to changes of substrate and cultivation conditions, cells were grown in either Gln- or Pyr-containing GMEM medium and two growth phases

(exponential and stationary) were selected for enzyme activity measurements. Metabolic adaptation to Pyr- and Gln-containing medium in MDCK cells was correlated with up- and down-regulation of enzyme activity levels. In particular, the overall activity of the pentose phosphate pathway was up-regulated during exponential cell growth in Pyr-containing medium, which suggests that more G6P was channeled into the oxidative branch and, therefore, more NADPH was required via this route. The anaplerotic enzymes PC and PDH showed higher cell-specific activities in Pyr-containing medium. Furthermore, higher enzyme activities were also found for NAD-ICDH, GLDH and GS indicating an up-regulation of the right part of the TCA cycle in MDCK cells grown on Pyr. The increase in enzyme activities was most likely required to compensate for the energy demand and to replenish the Gln pool. A down-regulation was observed for the glutaminolytic enzymes AspTA, AlaTA, ME and PEPCCK in cells grown in Pyr-containing medium, which seems to be related to a decrease in Gln metabolism. However, further studies (e.g., ¹³C-labeling experiments) will have to be performed to better understand the switch from Gln-containing to Gln-free (Pyr) medium.

The last part focused on the effect of an influenza virus infection on host cell metabolism. So far, only few studies identified changes in central carbon metabolism of cells upon viral infection, e.g., up-regulation of intracellular metabolite concentrations in HCMV or influenza infected cells (Munger et al., 2006; Ritter et al., 2010). Here, an up-regulation of key metabolic enzyme activities in influenza A infected MDCK cells during early virus infection was observed. This shift in metabolism was most likely required to compensate for the metabolic imbalance caused by viral replication. Interestingly, activities of some key enzymes producing the reducing equivalent NADPH (G6PDH, 6PGDH, and ME) and acetyl-CoA (CL and ACoAL), a precursor needed for lipid and cholesterol biosynthesis, were increased by at least 1.20-fold in infected cells. It seems that fatty acid and cholesterol synthesis play a crucial role for the replication of influenza viruses in adherent MDCK cells as they acquire lipid envelopes from their host cells during budding, and their glycoproteins (HA and NA) are associated with sphingolipid-cholesterol membrane domains (lipid rafts). However, these results will have to be verified in prospective studies using, for example, inhibitors of lipid metabolism.

Taken together, an efficient high-throughput platform for the measurement of 28 metabolic enzyme activities in mammalian cells was established and successfully applied to six different cultivation conditions (two growth phases, three different media, and influenza virus infection) of MDCK cells. The enzyme platform was adapted to a 96-well microplate format,

which allowed the reduction of assay volumes to 20 μL (the first step of stop-time assays). The cost of assays could therefore be reduced significantly, especially when comparatively expensive reagents (e.g., acetyl-CoA, X5P, and G3POX) were used. Furthermore, by using electronic 8-channel pipettes, one operator could measure three to four different enzyme activities in 20 samples per working day including extraction, assay, and calculation. Throughput can still be further increased by using automated multi-channel pipetting robots (Gibon et al., 2004), which allow the measurement of enzyme activities in 100 to 1,000 samples per day (depending on the platform). Enzyme activity measurements, together with the ability to measure more than 20 extracellular as well as intracellular metabolites, clearly allow to produce unique datasets for characterization of cell culture processes and will serve as a major contribution to the understanding of cell metabolism during growth and product formation (also without performing ^{13}C -labeling experiments). This allows further characterization of metabolic states of typical production cell lines or other interesting animal cells. This platform can certainly be used to improve the understanding of metabolic pathways relevant for cell line and media optimization. Furthermore, it will support the validation of mathematical models of cellular metabolism in systems biology approaches.

7 Outlook

The developed enzyme platform, which consists of four sensitive cycling assays allowed the measurement of 28 enzyme activities involved in central carbon and Gln metabolism of mammalian cells. This assay platform was optimized for adherent MDCK cells. However, these tools can easily be adapted to the detection of key enzyme activities in other cell lines, such as adherent Vero cells or human suspension AGE1.HN cells (ProBioGen, Germany, Berlin), which is currently done in the Bioprocess Engineering group (MPI in Magdeburg) by A. Rath (studies on AGE1.HN cell metabolism).

Here, the extraction conditions were set up and optimized to release all enzymes from intracellular organelles of mammalian cells at once. However, it would be interesting to discriminate between different cell compartments, for example, to determine the cytosolic and the mitochondrial activities of NADP-ICDH, MDH, ME, AspTA, and AlaTA. This could be done by selective permeabilization of cellular membranes using different concentrations of digitonin and Triton[®] X-100 (Niklas et al., 2011). Furthermore, enzyme activities were measured under optimized conditions to obtain maximum catalytic rates (V_{\max}), which means that each enzyme assay was performed in different buffers at different pH values and in different ionic strength conditions. However, for mathematical models of cellular pathways, which strongly depend on reliable data from different aspects of metabolism, it is often desired to obtain realistic *in vivo* parameters. Therefore, it might be of interest to use separate *in vivo*-like assay media for mammalian cells that reflect approximately the intracellular condition/environment of various cell compartments (e.g., mitochondrion, cytosol) in which the enzymes function. With such standard assay media for the measurement of enzyme activities, data could be obtained that are representative for the *in vivo* situation as proposed by van Eunen et al. (2010) for *S. cerevisiae*. Whether this can be achieved in higher eukaryotes (such as mammalian cells) taking all the different enzyme and metabolite concentrations as well as pH levels into account, remains to be investigated in future studies.

Moreover, the established enzyme platform for mammalian cells could be further extended to measure the activities of enzymes from other metabolic pathways or cell compartments. For example, assays for the quantification of enzyme activities from fatty acid biosynthesis or endoplasmic reticulum and the Golgi apparatus could be useful to better understand the metabolic response of host cells upon viral infection and post-translational modifications (e.g., glycosylation), respectively. Finally, the high sensitivity makes cycling assays not only suitable for the measurement of maximum rates (V_{\max}) but also for the determination of

Michaelis constants (K_m). This was shown, for instance, with the sensitive G3P cycling assay by assaying ribulose-bisphosphate carboxylase (EC 4.1.1.39) or AGPase in *A. thaliana* at different substrate levels (Hädrich et al., 2011; Sulpice et al., 2007).

Enzyme measurements can be used as a qualitative tool in order to verify the presence of cellular enzymes in metabolic pathways and quantitatively because V_{max} values serve as a valid measure of maximum flux capacities through metabolic pathways (Suarez et al., 1997). Therefore, based on the established enzyme platform, the metabolic states of mammalian cell lines used for production of biologicals could be further characterized. One intention of this work was to better characterize the switch from Gln to Pyr-containing conditions by investigating the general effect of Gln substitution by Pyr on key metabolic enzyme activities in adherent MDCK cells. To compensate for batch-to-batch variations and to improve data quality, replicate measurements in six-well plates were performed. In contrast, the cultivations reported in the studies by Genzel et al. (2005) and Sidorenko et al. (2008) were performed in roller bottles and 5-L bioreactors. However, the set-up of the experiments in six-well plates was based for analyzing the exponential and stationary growth phases but not the complete cultivation period. In a next step, bioreactor experiments should be conducted in which all assays (e.g., intracellular and extracellular metabolites, enzyme activity measurements) could be applied to obtain a more comprehensive view on MDCK cell metabolism. Furthermore, high resolution dynamics for selected enzymes could help to identify regulatory principles for metabolic adjustment in response to change in cultivation conditions.

Additionally, the assumptions about the intracellular distribution of extracellular Pyr made in former studies on the effect of Gln substitution (Genzel et al., 2005; Sidorenko et al., 2008) could be reviewed. For instance, it might be interesting to elucidate the fluxes of the central carbon and Gln metabolism in cultured MDCK cells during growth on Gln or Pyr. Furthermore, investigation of the fate of Gluc and Gln in influenza infected cells may clarify which substrate fractions are hijacked during viral replication. Therefore, future studies should focus on the quantification of intracellular fluxes in central carbon metabolism using MFA based on ^{13}C labeling experiments (DeBerardinis et al., 2007; Munger et al., 2008). In the end, the information obtained could then be used to validate mathematical models of cellular metabolism and to improve the understanding of intracellular metabolic interactions relevant for product formation, growth to high cell densities, and process optimization.

List of Figures and Tables

Figures

Figure 2.1: Schematic overview of glucose metabolism (modified from Häggström, 2000).	7
Figure 2.2: Schematic overview of Gln metabolism (modified from Häggström, 2000).	11
Figure 2.3: Schematic representation of an influenza A virus. Reprinted from Subbarao and Joseph (2007), with permission.	17
Figure 2.4: Schematic overview of Gln metabolism involving the lipid cycle (modified from Häggström, 2000).	18
Figure 2.5: High-throughput “omics” research tools and technologies. Reprinted from Lee et al. (2005), with permission.	19
Figure 2.6: Free energy diagram according to the transition state theory for a simple unimolecular exothermic reaction ($S \rightarrow P$, indices) (modified from Rogers and Gibon, 2009).	23
Figure 2.7: Relationship between the reaction rate (v) and substrate concentration ($[S]$) for an enzymatic reaction based on equation 2.6. The Michaelis constant (K_m) is equal to $[S]$ corresponding to one-half V_{max} .	26
Figure 2.8: (A) Lineweaver-Burk plot (double-reciprocal plot of $1/v$ against $1/[S]$) and (B) the Hanes plot ($[S]/v$ against $[S]$) of the Michaelis-Menten equation (Hanes, 1932; Lineweaver and Burk, 1934).	27
Figure 2.9: Choice of assay for determination of enzyme activity.	34
Figure 3.1: Flow chart of the procedure for the indirect assays with enzymatic cycling.	45
Figure 3.2: Construction of pPIC3.5-GK expression vector.	61
Figure 4.1: Influence of extraction buffer (EB) composition on the specific activities of MDH (white bar) and LDH (grey) in crude cell extracts.	69
Figure 4.2: Effect of sonication time on the specific activities of MDH (white bar) and LDH (grey) in crude cell extracts.	69
Figure 4.3: Influence of pH on the specific activities of PEPCCK (\blacktriangle), ME (\circ), and ACoAL (\blacksquare) from confluent MDCK cells in GMEM-Gln.	71
Figure 4.4: Assay principle for GLNase activity. The determination is based on the Glu cycling assay.	72
Figure 4.5: Reaction rates of the Glu cycling assay with 10 U/mL GLDH and 5 U/mL AspTA at Glu concentrations of 0 (\blacksquare), 0.0625 (\circ), 0.125 (\blacktriangle), and 0.25 (\star) nmol/well.	74
Figure 4.6: Calibration curve of the Glu cycling assay for Glu.	75
Figure 4.7: Glu production against (A) the cell concentration and (B) the incubation time for GLNase activity determination in extracts of MDCK cells grown in six-well plates with GMEM-Gln.	76
Figure 4.8: Recovery of Glu standards in extracts of MDCK cells grown in six-well plates with GMEM-Gln during the assay of GLNase.	77
Figure 4.9: Principles of indirect assays with enzymatic cycling. Determinations are based on (A) the NAD^+ cycling assay, (B) the $NADP^+$ cycling assay, (C) the G3P cycling assay, and (D) the Glu cycling assay.	78
Figure 4.10: Reaction network of the central carbon metabolism of adherent MDCK cells (modified from Wahl et al., 2008).	86
Figure 4.11: Principles of GK-coupled assays and other selected assays based on the G3P cycling.	89

Figure 4.12: PCR and restriction enzyme analysis of the constructed pPIC3.5-GK vector on 1 % (w/v) agarose gel.	90
Figure 4.13: Intracellular GK activity of selected pPIC3.5-GK-carrying transformants (clones 5 to 51) and of the control clone (carrying the empty vector pPIC3.5) after 45 h of cultivation.	91
Figure 4.14: High cell density cultivation of recombinant <i>P. pastoris</i> expressing His ₆ -tagged GK from <i>P. farinosa</i> (clone 32) in BSM supplemented with PTM ₁ trace salts in a 5-L bioreactor at 30 °C and pH 5. Dissolved oxygen was kept above 30 % during the fermentation process.	91
Figure 4.15: First purification step of recombinant His ₆ -tagged GK isolated from <i>P. pastoris</i> (clone 32) cell lysate using Ni ²⁺ -Sephacel chromatography.....	93
Figure 4.16: Second purification step of recombinant His ₆ -tagged GK from the collected fractions of step 1 (Figure 4.15) using Q-Sepharose HP.....	93
Figure 4.17: SDS-PAGE analysis under non-reducing conditions of His ₆ -tagged GK from <i>P. farinosa</i> at various stages of purification.	94
Figure 4.18: Effect of pH and temperature on the activity of purified GK from <i>P. farinosa</i>	95
Figure 4.19: Effect of substrate concentration (ATP) on the activity of purified GK from <i>P. farinosa</i>	96
Figure 4.20: Relation between reaction velocity and NTP concentration of purified GK from <i>P. farinosa</i>	96
Figure 4.21: Viable cell density and maximum specific growth rate μ_{\max} (inset) of adherent MDCK cells during the cultivation in six-well plates in (A) GMEM-Gln and (B) GMEM-Pyr.....	99
Figure 4.22: Extracellular metabolites of adherent MDCK cells during the cultivation in six-well plates in GMEM-Gln.	100
Figure 4.23: Extracellular metabolites of adherent MDCK cells during the cultivation in six-well plates in GMEM-Pyr.....	101
Figure 4.24: Progress of the intracellular protein concentration of MDCK cells during growth in six-well plates in GMEM-Gln.	103
Figure 4.25: Simplified reaction scheme of glycolysis with fold changes of enzyme activities for MDCK cell growth in different media.....	107
Figure 4.26: Simplified reaction scheme of pentose phosphate pathway with fold changes of enzyme activities for MDCK cell growth in different media.....	108
Figure 4.27: Simplified reaction scheme of TCA cycle with fold changes of enzyme activities for MDCK cell growth in different media.....	109
Figure 4.28: Simplified reaction scheme of glutaminolysis with fold changes of enzyme activities for MDCK cell growth in different media.....	111
Figure 4.29: Viable cell density of adherent MDCK cells after mock-infection (■) or infection with influenza A (●), and virus titer (○).....	114
Figure 4.30: Specific activities of glycolytic enzymes in influenza A infected MDCK cells 9 hpi. ..	115
Figure 4.31: Specific activities of TCA cycle enzymes in influenza A infected MDCK cells 9 hpi. ..	115
Figure 4.32: Specific activities of pentose phosphate pathway enzymes in influenza A infected MDCK cells 9 hpi.....	116
Figure 4.33: Specific activities of glutaminolytic enzymes and ACoAL in influenza A infected MDCK cells 9 hpi.....	117
Figure 4.34: Simplified scheme for a reaction network of the central carbon metabolism of adherent MDCK cells.	118

Tables

Table 2.1: Influence of different ammonium concentrations on cell growth and productivity (Wagner, 1997).	14
Table 2.2: Effect of different medium concentrations of lactate on cell growth and productivity at constant pH (Wagner, 1997).	14
Table 3.1: The validated range, LOD, LOQ, and the relative and absolute SD of the method for Gluc, Lac, Gln, Glu, and Amm measured with a Bioprofile 100 Plus.	41
Table 3.2: Control parameters for the exponential fed-batch process according to equation 3.5.	63
Table 4.1: Composition of the enzyme extraction buffer (EB) for plant and mammalian cells.	67
Table 4.2: Summary of assay validation from calibration curves of the different cycling assays with the respective standards.	80
Table 4.3: Linear ranges of enzyme activity for the different assay conditions in extracts of MDCK cells grown in six-well plates in GMEM-Gln.	82
Table 4.4: Recovery of standards in extracts of MDCK cells grown in six-well plates in GMEM-Gln for the enzyme assay validation.	83
Table 4.5: Measured activities of 28 metabolic enzymes from confluent grown MDCK cells in GMEM-Gln and Episerf.	87
Table 4.6: Summary on purification of His ₆ -tagged GK expressed in <i>P. pastoris</i>	95
Table 4.7: K _m and V _{max} values of purified GK from <i>P. farinosa</i> for various NTPs.	97
Table 4.8: Measured activities of PK from confluent grown MDCK cells in six-well plates.	97
Table 4.9: Impact of Gln substitution by Pyr on MDCK cell growth and “basic” metabolism (extracellular metabolites).	102
Table 4.10: Maximum enzyme activities of glycolysis, pentose phosphate pathway, TCA cycle, and glutaminolysis in MDCK cells grown to exponential phases with GMEM-Gln and GMEM-Pyr, and to stationary phases with GMEM-Gln and GMEM-Pyr.	105

References

Results from the following papers and supervised theses were included in this study:

Publications related to this thesis

Janke R, Genzel Y, Wahl A, Reichl U. 2010. Measurement of key metabolic enzyme activities in mammalian cells using rapid and sensitive microplate-based assays. *Biotechnol Bioeng* 107(3):566-581.

Janke R, Genzel Y, Freund S, Wolff MW, Grammel H, Rühmkorf C, Seidemann J, Wahl A, Reichl U. 2010. Expression, purification, and characterization of a His₆-tagged glycerokinase from *Pichia farinosa* for enzymatic cycling assays in mammalian cells. *J Biotechnol* 150(3):396-403.

Janke R, Genzel Y, Händel N, Wahl A, Reichl U. 2011. Metabolic adaptation of MDCK cells to different growth conditions: Effects on catalytic activities of central metabolic enzymes. *Biotechnol Bioeng* 108(11):2691-2704.

Janke R, Genzel Y, Wetzel M, Reichl U. 2011. Effect of influenza virus infection on key metabolic enzyme activities in MDCK cells. *BMC Proceedings* 5(Suppl 8):P129.

Supervised theses

Rühmkorf C. 2009. Klonierung und Produktion einer hochaffinen Glycerokinase in *Pichia pastoris*. Diploma thesis. Fachhochschule Oldenburg/Ostfriesland/Wilhelmshaven.

Schäfer P. 2009. Optimierung der intrazellulären Expression rekombinanter Glycerokinase in *Pichia pastoris*. Bachelor thesis. Hochschule Esslingen.

Seidemann J. 2010. Aufreinigung und Charakterisierung des rekombinant hergestellten Enzyms Glycerokinase aus *Pichia farinosa*. Diploma thesis. Fachhochschule Jena.

Händel N. 2010. Untersuchungen zu Enzymaktivitäten des Zentralstoffwechsels verschiedener Zelllinien. Master thesis. Hochschule Anhalt (FH).

Wetzel M. 2011. Einfluss der Infektion mit Influenzaviren auf die Aktivität von Schlüsselenzymen des Zentralstoffwechsels adhärenter MDCK Zellen. Bachelor thesis. Otto-von-Guericke-Universität Magdeburg.

Posters and talks

Janke R, Wahl A, Reichl U. 2008. Determination of key enzyme activities in the central carbon metabolism of MDCK cells. Poster at the FORSYS Meeting, Germany, Berlin (19-20 June).

Janke R, Wahl A, Reichl U. 2008. Enzyme Activities in Central Carbon Metabolism of MDCK Cells under Different Growth Conditions. Poster at the European BioPerspectives, Germany, Hannover (7-9 Oct).

Janke R, Genzel Y, Wahl A, Reichl U. 2009. A high-throughput platform to measure key enzyme activities in mammalian cells. Poster at the German Symposium on Systems Biology, Germany, Heidelberg (12-15 May).

Janke R, Genzel Y, Wahl A, Reichl U. 2009. Catalytic activity changes of key enzymes in MDCK cells under different growth conditions. Poster at the 21st ESACT Meeting, Ireland, Dublin (07-10 June).

Janke R, Genzel Y, Wahl A, Reichl U. 2009. Influence of cell culture medium on the catalytic activity of key enzymes in MDCK cells. Talk at the 27th DECHEMA's Biotechnology Annual Meeting, Germany, Mannheim (08-10 Sep).

Janke R, Genzel Y, Wahl A, Reichl U. 2010. Changes in specific enzyme activities of MDCK cells during growth under different cultivation conditions. Poster at the 8th European Symposium on Biochemical Engineering Science, Italy, Bologna (06-08 Sep).

Janke R, Genzel Y, Wahl A, Reichl U. 2011. Effects of different growth conditions on the catalytic activities of central metabolic enzymes in MDCK cells. Poster at the 22nd ESACT Meeting, Austria, Vienna (15-19 May).

Janke R, Genzel Y, Wahl A, Reichl U. 2011. Recombinant glycerokinase from *Pichia farinosa*: Intracellular expression, purification, characterization, and application. Talk at the 1st European Congress of Applied Biotechnology, Germany, Berlin (25-29 Sep).

Janke R, Genzel Y, Wahl A, Reichl U. 2012. A high-throughput assay to assess enzyme activity in central metabolism of production cell lines. Talk at the 13th Cell Culture Engineering, USA, Arizona, Scottsdale (22-27 April).

- Aggarwal K, Jing F, Maranga L, Liu J. 2011. Bioprocess optimization for cell culture based influenza vaccine production. *Vaccine* 29(17):3320-3328.
- Ahn WS, Antoniewicz MR. 2011. Metabolic flux analysis of CHO cells at growth and non-growth phases using isotopic tracers and mass spectrometry. *Metabolic Engineering* 13(5):598-609.
- Alexander MA, Jeffries TW. 1990. Respiratory Efficiency and Metabolite Partitioning as Regulatory Phenomena in Yeasts. *Enzyme and Microbial Technology* 12(1):2-19.
- Anthon GE, Barrett DM. 2004. Comparison of three colorimetric reagents in the determination of methanol with alcohol oxidase. Application to the assay of pectin methylesterase. *Journal of Agricultural and Food Chemistry* 52(12):3749-3753.
- Antiochia R, Cass AEG, Palleschi G. 1997. Purification and sensor applications of an oxygen insensitive, thermophilic diaphorase. *Analytica Chimica Acta* 345(1-3):17-28.
- Ardawi MSM, Newsholme EA. 1982. Maximum Activities of Some Enzymes of Glycolysis, the Tricarboxylic Acid Cycle and Ketone-Body and Glutamine Utilization Pathways in Lymphocytes of the Rat. *Biochemical Journal* 208(3):743-748.
- Ardawi MSM, Newsholme EA. 1983. Glutamine Metabolism in Lymphocytes of the Rat. *Biochemical Journal* 212(3):835-842.
- Ashizawa K, Willingham MC, Liang CM, Cheng SY. 1991. *In vivo* regulation of monomer-tetramer conversion of pyruvate kinase subtype M2 by glucose is mediated via fructose 1,6-bisphosphate. *J Biol Chem* 266(25):16842-16846.
- Ashour MBA, Gee SJ, Hammock BD. 1987. Use of a 96-Well Microplate Reader for Measuring Routine Enzyme Activities. *Analytical Biochemistry* 166(2):353-360.
- Aunins JG. 2000. Viral vaccine production in cell culture. In: Stier RE, editor. *Encyclopedia of Cell Technology*. New York: Wiley & Sons. p 1182-1217.
- Bahrami A, Shojaosadati SA, Khalilzadeh R, Farahani EV. 2008. Two-stage glycerol feeding for enhancement of recombinant hG-CSF production in a fed-batch culture of *Pichia pastoris*. *Biotechnol Lett* 30(6):1081-1085.
- Bailey-Serres J, Nguyen MT. 1992. Purification and characterization of cytosolic 6-phosphogluconate dehydrogenase isozymes from maize. *Plant Physiol* 100(3):1580-1583.
- Bais R, Keech B. 1972. The Magnesium Ion (Mg^{2+}) Activation of Sheep Kidney Pyruvate Carboxylase. *Journal of Biological Chemistry* 247(10):3255-3261.
- Baker KN, Rendall MH, Hills AE, Hoare M, Freedman RB, James DC. 2001. Metabolic control of recombinant protein N-glycan processing in NS0 and CHO cells. *Biotechnology and Bioengineering* 73(3):188-202.
- Barden RE, Scrutton MC. 1974. Pyruvate Carboxylase from Chicken Liver - Effects of Univalent and Divalent Cations on Catalytic Activity. *Journal of Biological Chemistry* 249(15):4829-4838.
- Barrett PN, Mundt W, Kistner O, Howard MK. 2009. Vero cell platform in vaccine production: moving towards cell culture-based viral vaccines. *Expert Review of Vaccines* 8(5):607-618.
- Behal RH, Buxton DB, Robertson JG, Olson MS. 1993. Regulation of the Pyruvate Dehydrogenase Multienzyme Complex. *Annual Review of Nutrition* 13:497-520.
- Bell SL, Bebbington C, Scott MF, Wardell JN, Spier RE, Bushell ME, Sanders PG. 1995. Genetic Engineering of Hybridoma Glutamine Metabolism. *Enzyme and Microbial Technology* 17(2):98-106.
- Bergmeyer HU, Bergmeyer Jr, Grassl M, Moss DW. 1983. Methods of enzymatic analysis. Volume III, Enzymes 1, Oxidoreductases, transferases. Weinheim: VCH. xxvi, 613 p. p.
- Bergmeyer HU, Bergmeyer Jr, Grassl M, Moss DW. 1984. Methods of enzymatic analysis. Volume IV, Enzymes 2, Esterases, glycosidases, lyases, ligases. Weinheim: Verlag Chemie. xxiii, 426 p. p.
- Bergmeyer HU, Scheibe P, Wahlefeld AW. 1978. Optimization of Methods for Aspartate Aminotransferase and Alanine Aminotransferase. *Clinical Chemistry* 24(1):58-73.
- Berl S. 1966. Glutamine Synthetase. Determination of Its Distribution in Brain during Development. *Biochemistry* 5(3):916-922.
- Bernofsky C, Swan M. 1973. An improved cycling assay for nicotinamide adenine dinucleotide. *Anal Biochem* 53(2):452-458.
- Bessho M, Miyauchi Y, Sano N, Nakamura T, Tajima T. 1988. Assay of rat plasma pyruvate kinase activity with luciferin-luciferase. *J Nutr Sci Vitaminol (Tokyo)* 34(6):607-14.
- Birch JR, Racher AJ. 2006. Antibody production. *Adv Drug Deliv Rev* 58(5-6):671-685.
- Blomstrand E, Challiss RAJ, Cooney GJ, Newsholme EA. 1983. Maximal Activities of Hexokinase, 6-Phosphofructokinase, Oxoglutarate Dehydrogenase, and Carnitine Palmitoyltransferase in Rat and Avian Muscles. *Bioscience Reports* 3(12):1149-1153.
- Board M, Humm S, Newsholme EA. 1990. Maximum activities of key enzymes of glycolysis, glutaminolysis, pentose phosphate pathway and tricarboxylic acid cycle in normal, neoplastic and suppressed cells. *Biochem J* 265(2):503-509.

- Bock A, Schulze-Horsel J, Schwarzer J, Rapp E, Genzel Y, Reichl U. 2010. High-density microcarrier cell cultures for influenza virus production. *Biotechnology Progress*.
- Bonarius HP, Hatzimanikatis V, Meesters KP, de Gooijer CD, Schmid G, Tramper J. 1996. Metabolic flux analysis of hybridoma cells in different culture media using mass balances. *Biotechnol Bioeng* 50(3):299-318.
- Bonarius HPJ, Houtman JHM, de Gooijer CD, Tramper J, Schmid G. 1998. Activity of glutamate dehydrogenase is increased in ammonia-stressed hybridoma cells. *Biotechnology and Bioengineering* 57(4):447-453.
- Bothner B, Chavez R, Wei J, Strupp C, Phung Q, Schneemann A, Siuzdak G. 2000. Monitoring enzyme catalysis with mass spectrometry. *J Biol Chem* 275(18):13455-13459.
- Brands R, Visser J, Medema J, Palache AM, van Scharrenburg GJ. 1999. Influvac: a safe Madin Darby Canine Kidney (MDCK) cell culture-based influenza vaccine. *Dev Biol Stand* 98:93-100; discussion 111.
- Brierley RA, Bussineau C, Kosson R, Melton A, Siegel RS. 1990. Fermentation development of recombinant *Pichia pastoris* expressing the heterologous gene: bovine lysozyme. *Ann N Y Acad Sci* 589:350-362.
- Briggs GE, Haldane JB. 1925. A Note on the Kinetics of Enzyme Action. *Biochem J* 19(2):338-339.
- Broschat KO, Gorka C, Kasten TP, Gulve EA, Kilpatrick B. 2002. A radiometric assay for glutamine:fructose-6-phosphate amidotransferase. *Anal Biochem* 305(1):10-15.
- Brown SW, Mehtali M. 2010. The Avian EB66(R) Cell Line, Application to Vaccines, and Therapeutic Protein Production. *PDA J Pharm Sci Technol* 64(5):419-425.
- Buckland BC. 2005. The process development challenge for a new vaccine. *Nature Medicine* 11(4 Suppl):S16-19.
- Buffinton GD, Christen S, Peterhans E, Stocker R. 1992. Oxidative stress in lungs of mice infected with influenza A virus. *Free Radic Res Commun* 16(2):99-110.
- Burgener A, Coombs K, Butler M. 2006. Intracellular ATP and total adenylate concentrations are critical predictors of reovirus productivity from Vero cells. *Biotechnol Bioeng* 94(4):667-679.
- Butler M, Christie A. 1994. Adaptation of mammalian cells to non-ammoniogenic media. *Cytotechnology* 15(1-3):87-94.
- Butler M, Spier RE. 1984. The effects of glutamine utilisation and ammonia production on the growth of BHK cells in microcarrier cultures *Journal of Biotechnology* 1(3-4):187-196.
- Butterworth RF. 1989. Enzymes of the pyruvate dehydrogenase complex of mammalian brain. In: Boulton AA, Baker GB, Butterworth RF, editors. *NeuroMethods*. New York: Humana. p 283-307.
- Carbonell J, Feliu JE, Marco R, Sols A. 1973. Pyruvate kinase. Classes of regulatory isoenzymes in mammalian tissues. *European Journal of Biochemistry* 37(1):148-156.
- Carinhas N, Bernal V, Monteiro F, Carrondo MJ, Oliveira R, Alves PM. 2010. Improving baculovirus production at high cell density through manipulation of energy metabolism. *Metabolic Engineering* 12(1):39-52.
- Castro MDL, Fernández-Romero JM. 1991. Photometric and Fluorimetric Determination of Creatine Kinase Activity by Using Co-Immobilized Auxiliary Enzymes and an Open/Closed Flow Injection Manifold. *Analytical Letters* 24(5):749-765.
- Cereghino JL, Cregg JM. 2000. Heterologous protein expression in the methylotrophic yeast *Pichia pastoris*. *FEMS Microbiol Rev* 24(1):45-66.
- Chacko CM, McCrone L, Nadler HL. 1972. Uridine diphosphoglucose pyrophosphorylase and uridine diphosphogalactose pyrophosphorylase in human skin fibroblasts derived from normal and galactosemic individuals. *Biochimica Et Biophysica Acta* 268(1):113-120.
- Chan RB, Tanner L, Wenk MR. 2010. Implications for lipids during replication of enveloped viruses. *Chem Phys Lipids* 163(6):449-459.
- Chapman J, Zhou M. 1999. Microplate-based fluorometric methods for the enzymatic determination of L-glutamate: application in measuring L-glutamate in food samples. *Analytica Chimica Acta* 402(1-2):47-52.
- Chen K, Liu Q, Xie L, Sharp PA, Wang DI. 2001. Engineering of a mammalian cell line for reduction of lactate formation and high monoclonal antibody production. *Biotechnol Bioeng* 72(1):55-61.
- Chi MMY, Manchester JK, Yang VC, Curato AD, Strickler RC, Lowry OH. 1988. Contrast in Levels of Metabolic Enzymes in Human and Mouse Ova. *Biology of Reproduction* 39(2):295-307.
- Ching TM. 1982. A sensitive and simple assay of starch synthase activity with pyruvate kinase and luciferase. *Anal Biochem* 122(1):139-43.
- Chiruvolu V, Cregg JM, Meagher MM. 1997. Recombinant protein production in an alcohol oxidase-defective strain of *Pichia pastoris* in fedbatch fermentations. *Enzyme and Microbial Technology* 21(4):277-283.
- Cho SW, Lee J, Choi SY. 1995. Two soluble forms of glutamate dehydrogenase isoproteins from bovine brain. *European Journal of Biochemistry* 233(1):340-346.

- Chotteau V, Wahlgren C, Pettersson H. 2007. Effect of peptones and study of feeding strategies in a CHO based fed-batch process for the production of a human monoclonal antibody. *Cell Technology for Cell Products*:371-374.
- Chretien D, Pourrier M, Bourgeron T, Séné M, Rötig A, Munnich A, Rustin P. 1995. An Improved Spectrophotometric Assay of Pyruvate Dehydrogenase in Lactate Dehydrogenase Contaminated Mitochondrial Preparations from Human Skeletal Muscle. *Clinica Chimica Acta* 240(2):129-136.
- Christie A, Butler M. 1999. The adaptation of BHK cells to a non-ammoniogenic glutamate-based culture medium. *Biotechnology and Bioengineering* 64(3):298-309.
- Clare JJ, Rayment FB, Ballantine SP, Sreekrishna K, Romanos MA. 1991. High-level expression of tetanus toxin fragment C in *Pichia pastoris* strains containing multiple tandem integrations of the gene. *Biotechnology (N Y)* 9(5):455-460.
- Cornish-Bowden A. 2004. *Fundamentals of enzyme kinetics*. London: Portland Press. XVI, 422 S. p.
- Cox NJ, Neumann G, Donis RO, Kawaoka Y. 2010. Orthomyxoviruses: Influenza. In: Mahy BWJ, Meulen V, editors. *Topley & Wilson's Microbiology and Microbial Infections*. 10 ed: John Wiley & Sons, Ltd. p 634-698.
- Crabtree B, Higgins SJ, Newsholme EA. 1972. The Activities of Pyruvate Carboxylase, Phosphoenolpyruvate Carboxylase and Fructose Diphosphatase in Muscles from Vertebrates and Invertebrates. *Biochemical Journal* 130(2):391-396.
- Cregg JM. 2007. *Pichia* protocols. Totowa, N.J.: Humana Press. xi, 268 p.
- Cregg JM, Cereghino JL, Shi J, Higgins DR. 2000. Recombinant protein expression in *Pichia pastoris*. *Mol Biotechnol* 16(1):23-52.
- Cregg JM, Madden KR, Barringer KJ, Thill GP, Stillman CA. 1989. Functional characterization of the two alcohol oxidase genes from the yeast *Pichia pastoris*. *Mol Cell Biol* 9(3):1316-1323.
- Cregg JM, Vedvick TS, Raschke WC. 1993. Recent advances in the expression of foreign genes in *Pichia pastoris*. *Biotechnology (N Y)* 11(8):905-910.
- Crow KE, Braggins TJ, Batt RD, Hardman MJ. 1982. Rat liver cytosolic malate dehydrogenase: purification, kinetic properties, role in control of free cytosolic NADH concentration. Analysis of control of ethanol metabolism using computer simulation. *J Biol Chem* 257(23):14217-14225.
- Cruz HJ, Freitas CM, Alves PM, Moreira JL, Carrondo MJ. 2000. Effects of ammonia and lactate on growth, metabolism, and productivity of BHK cells. *Enzyme Microb Technol* 27(1-2):43-52.
- Cuperlovic-Culf M, Barnett DA, Culf AS, Chute I. 2010. Cell culture metabolomics: applications and future directions. *Drug Discov Today* 15(15-16):610-621.
- Curthoys NP, Weiss RF. 1974. Regulation of renal ammoniogenesis - Subcellular localization of rat kidney glutaminase isoenzymes. *J Biol Chem* 249(10):3261-3266.
- Curtis RK, Oresic M, Vidal-Puig A. 2005. Pathways to the analysis of microarray data. *Trends Biotechnol* 23(8):429-435.
- Daly R, Hearn MT. 2005. Expression of heterologous proteins in *Pichia pastoris*: a useful experimental tool in protein engineering and production. *J Mol Recognit* 18(2):119-138.
- Davies SE, Brindle KM. 1992. Effects of overexpression of phosphofructokinase on glycolysis in the yeast *Saccharomyces cerevisiae*. *Biochemistry* 31(19):4729-4735.
- de Almeida AF, Curi R, Newsholme P, Newsholme EA. 1989. Maximal activities of key enzymes of glutaminolysis, glycolysis, Krebs cycle and pentose-phosphate pathway of several tissues in mature and aged rats. *International Journal of Biochemistry* 21(8):937-940.
- De RK, Das M, Mukhopadhyay S. 2008. Incorporation of enzyme concentrations into FBA and identification of optimal metabolic pathways. *Bmc Systems Biology* 2.
- DeBerardinis RJ, Mancuso A, Daikhin E, Nissim I, Yudkoff M, Wehrli S, Thompson CB. 2007. Beyond aerobic glycolysis: Transformed cells can engage in glutamine metabolism that exceeds the requirement for protein and nucleotide synthesis. *Proceedings of the National Academy of Sciences of the United States of America* 104(49):19345-19350.
- DeBerardinis RJ, Sayed N, Ditsworth D, Thompson CB. 2008. Brick by brick: metabolism and tumor cell growth. *Current Opinion in Genetics & Development* 18(1):54-61.
- Denslow SA, Rueschhoff EE, Daub ME. 2007. Regulation of the *Arabidopsis thaliana* vitamin B₆ biosynthesis genes by abiotic stress. *Plant Physiol Biochem* 45(2):152-161.
- Dettmer K, Aronov PA, Hammock BD. 2007. Mass spectrometry-based metabolomics. *Mass Spectrom Rev* 26(1):51-78.
- Dettmer K, Nurnberger N, Kaspar H, Gruber MA, Almstetter MF, Oefner PJ. 2011. Metabolite extraction from adherently growing mammalian cells for metabolomics studies: optimization of harvesting and extraction protocols. *Anal Bioanal Chem* 399(3):1127-1139.
- Dietmair S, Timmins NE, Gray PP, Nielsen LK, Kromer JO. 2010. Towards quantitative metabolomics of mammalian cells: development of a metabolite extraction protocol. *Anal Biochem* 404(2):155-164.

- Dinnis DM, Stansfield SH, Schlatter S, Smales CM, Alete D, Birch JR, Racher AJ, Marshall CT, Nielsen LK, James DC. 2006. Functional proteomic analysis of GS-NS0 murine myeloma cell lines with varying recombinant monoclonal antibody production rate. *Biotechnol Bioeng* 94(5):830-841.
- Dobson GP, Hitchins S, Teague WE, Jr. 2002. Thermodynamics of the pyruvate kinase reaction and the reversal of glycolysis in heart and skeletal muscle. *J Biol Chem* 277(30):27176-82.
- Donato MT, Jimenez N, Castell JV, Gomez-Lechon MJ. 2004. Fluorescence-based assays for screening nine cytochrome P450 (P450) activities in intact cells expressing individual human P450 enzymes. *Drug Metab Dispos* 32(7):699-706.
- Donnelly M, Scheffler IE. 1976. Energy metabolism in respiration-deficient and wild type Chinese hamster fibroblasts in culture. *Journal of Cellular Physiology* 89(1):39-51.
- Doroshenko A, Halperin SA. 2009. Trivalent MDCK cell culture-derived influenza vaccine Optaflu^(R) (Novartis Vaccines). *Expert Review of Vaccines* 8(6):679-688.
- Dümmler A, Lawrence A-M, de Marco A. 2005. Simplified screening for the detection of soluble fusion constructs expressed in *E. coli* using a modular set of vectors. *Microbial Cell Factories* 4:34.
- Dunaway GA. 1983. A review of animal phosphofructokinase isozymes with an emphasis on their physiological role. *Molecular and Cellular Biochemistry* 52(1):75-91.
- Eigenbrodt E, Reinacher M, Scheefers-Borchel U, Scheefers H, Friis R. 1992. Double role for pyruvate kinase type M2 in the expansion of phosphometabolite pools found in tumor cells. *Crit Rev Oncog* 3(1-2):91-115.
- Eisenberg D, Gill HS, Pfluegl GM, Rotstein SH. 2000. Structure-function relationships of glutamine synthetases. *Biochim Biophys Acta* 1477(1-2):122-145.
- Eisenthal R, Danson MJ. 2002. *Enzyme assays : a practical approach*. Oxford: Oxford University Press. xix, 282 p. p.
- Faustova I, Järv J. 2001. Kinetic analysis of cooperativity of phosphorylated L-type pyruvate kinase. *Proc Estonian Acad Sci Chem* 55(4):179-189.
- Feifel E, Krall M, Geibel JP, Pfaller W. 1997. Differential activities of H⁺ extrusion systems in MDCK cells due to extracellular osmolality and pH. *American Journal of Physiology-Renal Physiology* 273(4):F499-F506.
- Fell DA. 1992. Metabolic control analysis: a survey of its theoretical and experimental development. *Biochem J* 286 (Pt 2):313-30.
- Fell DA. 1998. Increasing the flux in metabolic pathways: A metabolic control analysis perspective. *Biotechnology and Bioengineering* 58(2-3):121-124.
- Fell DA, Thomas S. 1995. Physiological Control of Metabolic Flux: The Requirement for Multisite Modulation. *Biochemical Journal* 311:35-39.
- Fitzpatrick L, Jenkins HA, Butler M. 1993. Glucose and Glutamine Metabolism of a Murine B-Lymphocyte Hybridoma Grown in Batch Culture. *Applied Biochemistry and Biotechnology* 43(2):93-116.
- Furukawa T, Fioretti A, Plotkin S. 1973. Growth characteristics of cytomegalovirus in human fibroblasts with demonstration of protein synthesis early in viral replication. *J Virol* 11(6):991-997.
- Gaillet B, Gilbert R, Amziani R, Guilbault C, Gadoury C, Caron AW, Mullick A, Garnier A, Massie B. 2007. High-level recombinant protein production in CHO cells using an adenoviral vector and the cumate gene-switch. *Biotechnology Progress* 23(1):200-209.
- Gallwitz WE, Jacoby GH, Ray PD, Lambeth DO. 1988. Purification and characterization of the isozymes of phosphoenolpyruvate carboxykinase from rabbit liver. *Biochim Biophys Acta* 964(1):36-45.
- Garbis S, Lubec G, Fountoulakis M. 2005. Limitations of current proteomics technologies. *J Chromatogr A* 1077(1):1-18.
- Garrett R, Grisham CM. 2010. *Biochemistry*. Australia; United Kingdom: Brooks/Cole; Cengage Learning. 1059 p.
- Gellissen G, Kunze G, Gaillardin C, Cregg JM, Berardi E, Veenhuis M, van der Klei I. 2005. New yeast expression platforms based on methylotrophic *Hansenula polymorpha* and *Pichia pastoris* and on dimorphic *Arxula adenivorans* and *Yarrowia lipolytica* - a comparison. *FEMS Yeast Res* 5(11):1079-1096.
- Genzel Y, Behrendt I, König S, Sann H, Reichl U. 2004a. Metabolism of MDCK cells during cell growth and influenza virus production in large-scale microcarrier culture. *Vaccine* 22(17-18):2202-2208.
- Genzel Y, Dietzsch C, Rapp E, Schwarzer J, Reichl U. 2010. MDCK and Vero cells for influenza virus vaccine production: a one-to-one comparison up to lab-scale bioreactor cultivation. *Applied Microbiology and Biotechnology* 88(2):461-475.
- Genzel Y, Fischer M, Reichl U. 2006a. Serum-free influenza virus production avoiding washing steps and medium exchange in large-scale microcarrier culture. *Vaccine* 24(16):3261-3272.

- Genzel Y, König S, Reichl U. 2004b. Amino acid analysis in mammalian cell culture media containing serum and high glucose concentrations by anion exchange chromatography and integrated pulsed amperometric detection. *Analytical Biochemistry* 335(1):119-125.
- Genzel Y, Olmer RM, Schäfer B, Reichl U. 2006b. Wave microcarrier cultivation of MDCK cells for influenza virus production in serum containing and serum-free media. *Vaccine* 24(35-36):6074-6087.
- Genzel Y, Reichl U. 2009. Continuous cell lines as a production system for influenza vaccines. *Expert Review of Vaccines* 8(12):1681-1692.
- Genzel Y, Ritter JB, König S, Alt R, Reichl U. 2005. Substitution of glutamine by pyruvate to reduce ammonia formation and growth inhibition of mammalian cells. *Biotechnology Progress* 21(1):58-69.
- Gerl MJ, Sampaio JL, Urban S, Kalvodova L, Verbavatz JM, Binnington B, Lindemann D, Lingwood CA, Shevchenko A, Schroeder C and others. 2012. Quantitative analysis of the lipidomes of the influenza virus envelope and MDCK cell apical membrane. *J Cell Biol* 196(2):213-221.
- Gevaert K, Vandekerckhove J. 2000. Protein identification methods in proteomics. *Electrophoresis* 21(6):1145-1154.
- Gibon Y, Blaessing OE, Hannemann J, Carillo P, Höhne M, Hendriks JH, Palacios N, Cross J, Selbig J, Stitt M. 2004. A Robot-based platform to measure multiple enzyme activities in *Arabidopsis* using a set of cycling assays: comparison of changes of enzyme activities and transcript levels during diurnal cycles and in prolonged darkness. *Plant Cell* 16(12):3304-3325.
- Gibon Y, Pyl ET, Sulpice R, Lunn JE, Höhne M, Günther M, Stitt M. 2009. Adjustment of growth, starch turnover, protein content and central metabolism to a decrease of the carbon supply when *Arabidopsis* is grown in very short photoperiods. *Plant Cell Environ* 32(7):859-874.
- Gibon Y, Vigeolas H, Tiessen A, Geigenberger P, Stitt M. 2002. Sensitive and high throughput metabolite assays for inorganic pyrophosphate, ADPGlc, nucleotide phosphates, and glycolytic intermediates based on a novel enzymic cycling system. *Plant J* 30(2):221-235.
- Glacken MW. 1988. Catabolic Control of Mammalian Cell Culture. *Bio/Technology* 6(9):1041-1050.
- Glacken MW, Adema E, Sinskey AJ. 1988. Mathematical descriptions of hybridoma culture kinetics: I. Initial metabolic rates. *Biotechnol Bioeng* 32(4):491-506.
- Glacken MW, Fleischaker RJ, Sinskey AJ. 1986. Reduction of Waste Product Excretion Via Nutrient Control: Possible Strategies for Maximizing Product and Cell Yields on Serum in Cultures of Mammalian Cells. *Biotechnology and Bioengineering* 28(9):1376-1389.
- Gregersen JP, Schmitt HJ, Trusheim H, Broker M. 2011. Safety of MDCK cell culture-based influenza vaccines. *Future Microbiol* 6(2):143-152.
- Greis KD. 2007. Mass spectrometry for enzyme assays and inhibitor screening: an emerging application in pharmaceutical research. *Mass Spectrom Rev* 26(3):324-39.
- Griffin TJ, Seth G, Xie H, Bandhakavi S, Hu WS. 2007. Advancing mammalian cell culture engineering using genome-scale technologies. *Trends Biotechnol* 25(9):401-408.
- Groth N, Montomoli E, Gentile C, Manini I, Bugarini R, Podda A. 2009. Safety, tolerability and immunogenicity of a mammalian cell-culture-derived influenza vaccine: A sequential Phase I and Phase II clinical trial. *Vaccine* 27(5):786-791.
- Gstraunthaler G, Seppi T, Pfaller W. 1999. Impact of culture conditions, culture media volumes, and glucose content on metabolic properties of renal epithelial cell cultures. Are renal cells in tissue culture hypoxic? *Cell Physiol Biochem* 9(3):150-172.
- Guan HP, Li Y, Jensen MV, Newgard CB, Steppan CM, Lazar MA. 2002. A futile metabolic cycle activated in adipocytes by antidiabetic agents. *Nature Medicine* 8(10):1122-1128.
- Gupta V, Bamezai RNK. 2010. Human pyruvate kinase M2: a multifunctional protein. *Protein Science* 19(11):2031-2044.
- Guynn RW, Veloso D, Veech RL. 1972. The concentration of malonyl-coenzyme A and the control of fatty acid synthesis *in vivo*. *J Biol Chem* 247(22):7325-7331.
- Gyurcsanyi RE, Bereczki A, Nagy G, Neuman MR, Lindner E. 2002. Amperometric microcells for alkaline phosphatase assay. *Analyst* 127(2):235-240.
- Hädrich N, Gibon Y, Schudoma C, Altmann T, Lunn JE, Stitt M. 2011. Use of TILLING and robotised enzyme assays to generate an allelic series of *Arabidopsis thaliana* mutants with altered ADP-glucose pyrophosphorylase activity. *J Plant Physiol* 168(12):1395-1405.
- Häggström L. 2000. Cell metabolism, animal. In: Stier R, editor. *Encyclopedia of Cell Technology*. New York: Wiley & Sons. p 392-411.
- Häggström L, Ljunggren J, Öhman L. 1996. Metabolic engineering of animal cells. *Ann N Y Acad Sci* 782:40-52.
- Halperin SA, Doroshenko A. 2009. Trivalent MDCK cell culture-derived influenza vaccine Optaflu (R) (Novartis Vaccines). *Expert Review of Vaccines* 8(6):679-688.

- Hanes CS. 1932. Studies on plant amylases. I. The effect of starch concentration upon the velocity of hydrolysis by the amylase of germinated barley. *Biochemical Journal* 26:1406-1421.
- Hanocq-Quertier J, Baltus E, Schram E. 1988. Bioluminescent assay of ATPase activity in embryonic material using firefly luciferase. *J Biolumin Chemilumin* 2(1):17-24.
- Haser WG, Shapiro RA, Curthoys NP. 1985. Comparison of the Phosphate-Dependent Glutaminase Obtained from Rat Brain and Kidney. *Biochemical Journal* 229(2):399-408.
- Hassell T, Butler M. 1990. Adaptation to non-ammoniogenic medium and selective substrate feeding lead to enhanced yields in animal cell cultures. *Journal of Cell Science* 96 (Pt 3):501-508.
- Hassell T, Gleave S, Butler M. 1991. Growth inhibition in animal cell culture. The effect of lactate and ammonia. *Appl Biochem Biotechnol* 30(1):29-41.
- Hayashi S-I, Lin ECC. 1967. Purification and properties of glycerol kinase from *Escherichia coli*. *Journal of Biological Chemistry* 242(5):1030-1035.
- Hayflick L, Moorhead PS. 1961. The serial cultivation of human diploid cell strains. *Exp Cell Res* 25:585-621.
- Heaton NS, Perera R, Berger KL, Khadka S, Lacount DJ, Kuhn RJ, Randall G. 2010. Dengue virus nonstructural protein 3 redistributes fatty acid synthase to sites of viral replication and increases cellular fatty acid synthesis. *Proc Natl Acad Sci U S A* 107(40):17345-17350.
- Heinrich PC, Morris HP, Weber G. 1976. Behavior of transaldolase (EC 2.2.1.2) and transketolase (EC 2.2.1.1) activities in normal, neoplastic, differentiating, and regenerating liver. *Cancer Res* 36(9 pt.1):3189-3197.
- Heinrich R, Rapoport TA. 1974. A linear steady-state treatment of enzymatic chains. General properties, control and effector strength. *European Journal of Biochemistry* 42(1):89-95.
- Henry O, Durocher Y. 2011. Enhanced glycoprotein production in HEK-293 cells expressing pyruvate carboxylase. *Metab Eng* 13(5):499-507.
- Hickling J, D'Hondt E. 2006. A review of production technologies for influenza virus vaccines, and their suitability for deployment in developing countries for influenza pandemic preparedness. Geneva, Switzerland: World Health Organization Initiative for Vaccine Research. p 34.
- Higgins DR. 2001. Overview of protein expression in *Pichia pastoris*. *Curr Protoc Protein Sci* Chapter 5:Unit5 7.
- Holden CP, Storey KB. 1994. Purification and Characterization of Aldolase from the Cold Hardy Insect *Epiblema scudderiana*: Enzyme Role in Glycerol Biosynthesis. *Insect Biochemistry and Molecular Biology* 24(3):265-270.
- Hollenbaugh JA, Munger J, Kim B. 2011. Metabolite profiles of human immunodeficiency virus infected CD4+ T cells and macrophages using LC-MS/MS analysis. *Virology* 415(2):153-159.
- Horecker BL, Kornberg A. 1948. The extinction coefficients of the reduced band of pyridine nucleotides. *J Biol Chem* 175(1):385-390.
- Hornby DP, Aitchison MJ, Engel PC. 1984. The Kinetic Mechanism of Ox Liver Glutamate Dehydrogenase in the Presence of the Allosteric Effector ADP - The Oxidative Deamination of L-Glutamate. *Biochemical Journal* 223(1):161-168.
- Howard BV, Howard WJ, Bailey JM. 1974. Acetyl coenzyme A synthetase and the regulation of lipid synthesis from acetate in cultured cells. *J Biol Chem* 249(24):7912-7921.
- Imperial S, Busquets M, Cortes A, Bozal J. 1989. Purification and characterization of chicken brain cytosolic aspartate aminotransferase. *Neurochem Res* 14(6):517-521.
- Inan M, Chiruvolu V, Eskridge KM, Vlasuk GP, Dickerson K, Brown S, Meagher MM. 1999. Optimization of temperature-glycerol-pH conditions for a fed-batch fermentation process for recombinant hookworm (*Ancylostoma caninum*) anticoagulant peptide (AcAP-5) production by *Pichia pastoris*. *Enzyme and Microbial Technology* 24(7):438-445.
- Invitrogen. 2002a. *Pichia* Expression Kit - A Manual of Methods for Expression of Recombinant Proteins in *Pichia pastoris*. Catalog No. K1710-01.
- Invitrogen. 2002b. *Pichia* Fermentation Process Guidelines. Available from <http://www.invitrogen.com>.
- Irani N, Wirth M, van den Heuvel J, Wagner R. 1999. Improvement of the primary metabolism of cell cultures by introducing a new cytoplasmic pyruvate carboxylase reaction. *Biotechnology and Bioengineering* 66(4):238-246.
- Irias JJ, Olmsted MR, Utter MF. 1969. Pyruvate carboxylase. Reversible inactivation by cold. *Biochemistry* 8(12):5136-5148.
- Ishikawa M, Fujino T, Sakashita H, Morikawa K, Yamamoto T. 1995. Kinetic properties and structural characterization of highly purified acetyl-CoA synthetase from bovine heart and tissue distribution of the enzyme in rat tissues. *Tohoku J Exp Med* 175(1):55-67.
- Jahic M, Rotticci-Mulder JC, Martinelle M, Hult K, Enfors SO. 2002. Modeling of growth and energy metabolism of *Pichia pastoris* producing a fusion protein. *Bioprocess and Biosystems Engineering* 24(6):385-393.

- Janke R, Genzel Y, Freund S, Wolff MW, Grammel H, Rühmkorf C, Seidemann J, Wahl A, Reichl U. 2010a. Expression, purification, and characterization of a His₆-tagged glycerokinase from *Pichia farinosa* for enzymatic cycling assays in mammalian cells. *J Biotechnol* 150(3):396-403.
- Janke R, Genzel Y, Händel N, Wahl A, Reichl U. 2011a. Metabolic adaptation of MDCK cells to different growth conditions: Effects on catalytic activities of central metabolic enzymes. *Biotechnol Bioeng*.
- Janke R, Genzel Y, Wahl A, Reichl U. 2010b. Measurement of key metabolic enzyme activities in mammalian cells using rapid and sensitive microplate-based assays. *Biotechnol Bioeng* 107(3):566-581.
- Janke R, Genzel Y, Wetzel M, Reichl U. 2011b. Effect of influenza virus infection on key metabolic enzyme activities in MDCK cells. *BMC Proceedings* 5(Suppl 8):P129.
- Janson CA, Cleland WW. 1974. The Kinetic Mechanism of Glycerokinase. *Journal of Biological Chemistry* 249(8):2562-2566.
- Javed MH, Azimuddin SMI, Hussain AN, Ahmed A, Ishaq M. 1997. Purification and characterization of lactate dehydrogenase from *Varanus* liver. *Experimental and Molecular Medicine* 29(1):25-30.
- Jitrapakdee S, Wallace JC. 1999. Structure, function and regulation of pyruvate carboxylase. *Biochemical Journal* 340:1-16.
- Johnson CD, Russell RL. 1975. A rapid, simple radiometric assay for cholinesterase, suitable for multiple determinations. *Anal Biochem* 64(1):229-238.
- Johnson KA, Goody RS. 2011. The original Michaelis constant: translation of the 1913 Michaelis-Menten paper. *Biochemistry* 50(39):8264-8269.
- Kabashima T, Kawaguchi T, Wadzinski BE, Uyeda K. 2003. Xylulose 5-phosphate mediates glucose-induced lipogenesis by xylulose 5-phosphate-activated protein phosphatase in rat liver. *Proc Natl Acad Sci U S A* 100(9):5107-5112.
- Kacser H, Burns JA. 1973. The control of flux. *Symp Soc Exp Biol* 27:65-104.
- Kalbfuss B, Knöchlein A, Kröber T, Reichl U. 2008. Monitoring influenza virus content in vaccine production: precise assays for the quantitation of hemagglutination and neuraminidase activity. *Biologicals* 36(3):145-161.
- Khampha W, Meevootisom V, Wiyakrutta S. 2004. Spectrophotometric enzymatic cycling method using L-glutamate dehydrogenase and D-phenylglycine aminotransferase for determination of L-glutamate in foods. *Analytica Chimica Acta* 520(1-2):133-139.
- Kistler WS, Lin ECC. 1972. Purification and Properties of Flavine-Stimulated Anaerobic L-Alpha-Glycerophosphate Dehydrogenase of *Escherichia coli*. *Journal of Bacteriology* 112(1):539-547.
- Kistner O, Crowe BA, Wodal W, Kerschbaum A, Savidis-Dacho H, Sabarth N, Falkner FG, Mayerhofer I, Mundt W, Reiter M and others. 2010. A whole virus pandemic influenza H1N1 vaccine is highly immunogenic and protective in active immunization and passive protection mouse models. *PLoS One* 5(2):e9349.
- Kiyono T, Foster SA, Koop JI, McDougall JK, Galloway DA, Klingelutz AJ. 1998. Both Rb/p16INK4a inactivation and telomerase activity are required to immortalize human epithelial cells. *Nature* 396(6706):84-88.
- Klein JB, Thongboonkerd V. 2004. Overview of proteomics. *Contrib Nephrol* 141:1-10.
- Klenk HD, Rott R, Orlich M, Blödorn J. 1975. Activation of influenza A viruses by trypsin treatment. *Virology* 68(2):426-439.
- Klose J. 1975. Protein mapping by combined isoelectric focusing and electrophoresis of mouse tissues. A novel approach to testing for induced point mutations in mammals. *Humangenetik* 26(3):231-243.
- Koga Y, Morikawa M, Haruki M, Nakamura H, Imanaka T, Kanaya S. 1998. Thermostable glycerol kinase from a hyperthermophilic archaeon: gene cloning and characterization of the recombinant enzyme. *Protein Engineering* 11(12):1219-1227.
- Korz DJ, Rinas U, Hellmuth K, Sanders EA, Deckwer WD. 1995. Simple fed-batch technique for high cell density cultivation of *Escherichia coli*. *J Biotechnol* 39(1):59-65.
- Koshland DE. 1958. Application of a Theory of Enzyme Specificity to Protein Synthesis. *Proc Natl Acad Sci U S A* 44(2):98-104.
- Kotzé JP. 1967. Methods for the Determination of Intermediary Enzymes in Mixed Cultures Used for the Purification of Organic Polluted Waters. *Water Research* 1(5):351-365.
- Koutz P, Davis GR, Stillman C, Barringer K, Cregg J, Thill G. 1989. Structural comparison of the *Pichia pastoris* alcohol oxidase genes. *Yeast* 5(3):167-177.
- Krakow JL, Wang CC. 1990. Purification and characterization of glycerol kinase from *Trypanosoma brucei*. *Molecular and Biochemical Parasitology* 43(1):17-25.
- Krampe B, Swiderek H, Al-Rubeai M. 2008. Transcriptome and proteome analysis of antibody-producing mouse myeloma NS0 cells cultivated at different cell densities in perfusion culture. *Biotechnol Appl Biochem* 50(Pt 3):133-141.

- Kunert R, Steinfeldner W, Purtscher M, Assadian A, Katinger H. 2000. Stable recombinant expression of the anti HIV-1 monoclonal antibody 2F5 after IgG3/IgG1 subclass switch in CHO cells. *Biotechnology and Bioengineering* 67(1):97-103.
- Kuo N, Michalik M, Erecinska M. 1994. Inhibition of Glutamate Dehydrogenase in Brain Mitochondria and Synaptosomes by Mg^{2+} and Polyamines: A Possible Cause for Its Low In Vivo Activity. *Journal of Neurochemistry* 63(2):751-757.
- Kurata H, Zhao QY, Okuda R, Shimizu K. 2007. Integration of enzyme activities into metabolic flux distributions by elementary mode analysis. *Bmc Systems Biology* 1.
- Kvamme E, Roberg B, Torgner IA. 2000. Phosphate-activated glutaminase and mitochondrial glutamine transport in the brain. *Neurochemical Research* 25(9-10):1407-1419.
- Laemmli UK. 1970. Cleavage of Structural Proteins during Assembly of Head of Bacteriophage-T4. *Nature* 227(5259):680-685.
- Lambeir AM, Loiseau AM, Kuntz DA, Vellieux FM, Michels PAM, Opperdoes FR. 1991. The Cytosolic and Glycosomal Glyceraldehyde-3-Phosphate Dehydrogenase from *Trypanosoma brucei* - Kinetic Properties and Comparison with Homologous Enzymes. *European Journal of Biochemistry* 198(2):429-435.
- Le Ru A, Jacob D, Transfiguracion J, Ansoorge S, Henry O, Kamen AA. 2010. Scalable production of influenza virus in HEK-293 cells for efficient vaccine manufacturing. *Vaccine* 28(21):3661-3671.
- Lee SY, Lee DY, Kim TY. 2005. Systems biotechnology for strain improvement. *Trends Biotechnol* 23(7):349-358.
- Leveille GA, Hanson RW. 1966. Adaptive changes in enzyme activity and metabolic pathways in adipose tissue from meal-fed rats. *Journal of Lipid Research* 7(1):46-55.
- Li P, Anumanthan A, Gao XG, Ilangovan K, Suzara VV, Duzgunes N, Renugopalakrishnan V. 2007. Expression of recombinant proteins in *Pichia pastoris*. *Appl Biochem Biotechnol* 142(2):105-124.
- Li Z, Xiong F, Lin Q, d'Anjou M, Daugulis AJ, Yang DS, Hew CL. 2001. Low-temperature increases the yield of biologically active herring antifreeze protein in *Pichia pastoris*. *Protein Expr Purif* 21(3):438-445.
- Lin S, Liu N, Yang Z, Song W, Wang P, Chen H, Lucio M, Schmitt-Kopplin P, Chen G, Cai Z. 2010. GC/MS-based metabolomics reveals fatty acid biosynthesis and cholesterol metabolism in cell lines infected with influenza A virus. *Talanta* 83(1):262-268.
- Lin YY, Cheng WB, Wright CE. 1993. Glucose metabolism in mammalian cells as determined by mass isotopomer analysis. *Anal Biochem* 209(2):267-273.
- Lineweaver H, Burk D. 1934. The determination of enzyme dissociation constants. *Journal of the American Chemical Society* 56:658-666.
- Liu J, Shi X, Schwartz R, Kemble G. 2009. Use of MDCK cells for production of live attenuated influenza vaccine. *Vaccine* 27(46):6460-3.
- Ljunggren J, Häggström L. 1994. Catabolic Control of Hybridoma Cells by Glucose and Glutamine Limited Fed-Batch Cultures. *Biotechnology and Bioengineering* 44(7):808-818.
- Löffler G. 2005. Basiswissen Biochemie : mit Pathobiochemie ; mit 125 Tabellen ; [Bonusmaterial im Web]. Heidelberg: Springer Medizin. XVI, 818 S. p.
- Lohmann W, Lohmann C, Ibrahim M. 1988. Fluorescence spectra of NADH/NAD, kynurenine, tryptophan, and tyrosine. *Naturwissenschaften* 75(3):141-142.
- Lohr V, Rath A, Genzel Y, Jordan I, Sandig V, Reichl U. 2009. New avian suspension cell lines provide production of influenza virus and MVA in serum-free media: studies on growth, metabolism and virus propagation. *Vaccine* 27(36):4975-4982.
- Londesborough JC, Webster LT. 1974. Fatty acyl-CoA synthetases. In: Boyer PD, editor. *The Enzymes*. 3 ed. New York: Academic Press. p 469-488.
- Lowry CV, Kimmey JS, Felder S, Chi MMY, Kaiser KK, Passonneau PN, Kirk KA, Lowry OH. 1978. Enzyme Patterns in Single Human Muscle Fibers. *Journal of Biological Chemistry* 253(22):8269-8277.
- Lowry OH. 1980. Amplification by Enzymatic Cycling. *Molecular and Cellular Biochemistry* 32(3):135-146.
- Lowry OH, Berger SJ, Carter JG, Chi MMY, Manchester JK, Knor J, Pusateri ME. 1983. Diversity of Metabolic Patterns in Human Brain Tumors: Enzymes of Energy Metabolism and Related Metabolites and Cofactors. *Journal of Neurochemistry* 41(4):994-1010.
- Lowry RJ. 2003. Influenza virus induction of apoptosis by intrinsic and extrinsic mechanisms. *Int Rev Immunol* 22(5-6):425-449.
- Luong A, Hannah VC, Brown MS, Goldstein JL. 2000. Molecular characterization of human acetyl-CoA synthetase, an enzyme regulated by sterol regulatory element-binding proteins. *J Biol Chem* 275(34):26458-26466.
- Madej M, Lundh T, Lindberg JE. 1999. Activities of enzymes involved in glutamine metabolism in connection with energy production in the gastrointestinal tract epithelium of newborn, suckling and weaned piglets. *Biol Neonate* 75(4):250-258.

- Madin SH, Darby NB, Jr. 1958. Established kidney cell lines of normal adult bovine and ovine origin. *Proc Soc Exp Biol Med* 98(3):574-576.
- Mainou BA, Everly DN, Jr., Raab-Traub N. 2005. Epstein-Barr virus latent membrane protein 1 CTAR1 mediates rodent and human fibroblast transformation through activation of PI3K. *Oncogene* 24(46):6917-6924.
- Marin S, Lee WN, Bassilian S, Lim S, Boros LG, Centelles JJ, FernAndez-Novell JM, Guinovart JJ, Cascante M. 2004. Dynamic profiling of the glucose metabolic network in fasted rat hepatocytes using [1,2-¹³C₂]glucose. *Biochem J* 381(Pt 1):287-294.
- Martinelle K, Doverskog M, Jacobsson U, Chapman BE, Kuchel PW, Häggström L. 1998. Elevated glutamate dehydrogenase flux in glucose-deprived hybridoma and myeloma cells: Evidence from ¹H/¹⁵N NMR. *Biotechnol Bioeng* 60(4):508-517.
- Martinelle K, Häggström L. 1993. Mechanisms of ammonia and ammonium ion toxicity in animal cells: transport across cell membranes. *J Biotechnol* 30(3):339-350.
- Martinez-Carrion M, Turano C, Chiancone E, Bossa F, Giartosio A, Riva F, Fasella P. 1967. Isolation and characterization of multiple forms of glutamate-aspartate aminotransferase from pig heart. *J Biol Chem* 242(10):2397-2409.
- Marx MC, Wood M, Jarvis SC. 2001. A microplate fluorimetric assay for the study of enzyme diversity in soils. *Soil Biology & Biochemistry* 33(12-13):1633-1640.
- Mayer C, Frauer A, Schalkhammer T, Pittner F. 1999. Enzyme-based flow injection analysis system for glutamine and glutamate in mammalian cell culture media. *Anal Biochem* 268(1):110-116.
- Mazurek S. 2012. Pyruvate kinase M2: A key enzyme of the tumor metabolome and its medical relevance. *Biomedical Research* 23(SI):133-141.
- Mazurek S, Boschek CB, Hugo F, Eigenbrodt E. 2005. Pyruvate kinase type M2 and its role in tumor growth and spreading. *Semin Cancer Biol* 15(4):300-308.
- Mazurek S, Eigenbrodt E. 2003. The tumor metabolome. *Anticancer Res* 23(2A):1149-1154.
- Mazurek S, Zwerschke W, Jansen-Durr P, Eigenbrodt E. 2001. Effects of the human papilloma virus HPV-16 E7 oncoprotein on glycolysis and glutaminolysis: role of pyruvate kinase type M2 and the glycolytic-enzyme complex. *Biochem J* 356(Pt 1):247-256.
- McCarthy DJ, Smyth GK. 2009. Testing significance relative to a fold-change threshold is a TREAT. *Bioinformatics* 25(6):765-771.
- McClure WR. 1969. A Kinetic Analysis of Coupled Enzyme Assays. *Biochemistry* 8(7):2782-2786.
- McClure WR, Lardy HA. 1971. Rat Liver Pyruvate Carboxylase. IV. Factors Affecting Regulation *In vivo*. *Journal of Biological Chemistry* 246(11):3591-3596.
- McClure WR, Lardy HA, Kneifel HP. 1971. Rat liver pyruvate carboxylase. I. Preparation, properties, and cation specificity. *J Biol Chem* 246(11):3569-3578.
- McDermott RH, Butler M. 1993. Uptake of glutamate, not glutamine synthetase, regulates adaptation of mammalian cells to glutamine-free medium. *Journal of Cell Science* 104 (Pt 1):51-58.
- McKeehan WL. 1982. Glycolysis, glutaminolysis and cell proliferation. *Cell Biol Int Rep* 6(7):635-650.
- McQueen A, Bailey JE. 1990a. Effect of ammonium ion and extracellular pH on hybridoma cell metabolism and antibody production. *Biotechnol Bioeng* 35(11):1067-1077.
- McQueen A, Bailey JE. 1990b. Growth inhibition of hybridoma cells by ammonium ion: correlation with effects on intracellular pH. *Bioprocess and Biosystems Engineering* 6(1-2):49-61.
- McQueen A, Bailey JE. 1990c. Mathematical modeling of the effects of ammonium ion on the intracellular pH of hybridoma cells. *Biotechnol Bioeng* 35(9):897-906.
- Meister A. 1985. Glutamine synthetase from mammalian tissues. *Methods Enzymol* 113:185-199.
- Merkle S, Pretsch W. 1989. Characterization of triosephosphate isomerase mutants with reduced enzyme activity in *Mus musculus*. *Genetics* 123(4):837-844.
- Merten OW. 2002. Development of serum-free media for cell growth and production of viruses/viral vaccines--safety issues of animal products used in serum-free media. *Dev Biol (Basel)* 111:233-257.
- Merten OW, Hannoun C, Manuguerra JC, Ventre F, Petres S. 1996. Production of influenza virus in cell cultures for vaccine preparation. *Adv Exp Med Biol* 397:141-51.
- Merten OW, Kierulff JV, Castignolles N, Perrin P. 1994. Evaluation of the New Serum Free Medium (MDSS2) for the Production of Different Biologicals: Use of Various Cell Lines. *Cytotechnology* 14(1):47-59.
- Merten OW, Manuguerra JC, Hannoun C, van der Werf S. 1999. Production of influenza virus in serum-free mammalian cell cultures. *Dev Biol Stand* 98:23-37; discussion 73-4.
- Metallo CM, Walther JL, Stephanopoulos G. 2009. Evaluation of ¹³C isotopic tracers for metabolic flux analysis in mammalian cells. *Journal of Biotechnology* 144(3):167-174.
- Michaelis L, Menten ML. 1913. Die Kinetik der Invertinwirkung. *Biochem. Z.* 49:333-369.
- Miller WM, Wilke CR, Blanch HW. 1988. Transient responses of hybridoma cells to lactate and ammonia pulse and step changes in continuous culture. *Bioprocess Engineering* 3:113-122.

- Misaki H; Toyo Jozo Kabushiki Kaisha, assignee. 1987. Highly sensitive enzyme assay method. US Patent No. 4693971.
- Molloy MP, Brzezinski EE, Hang JQ, McDowell MT, VanBogelen RA. 2003. Overcoming technical variation and biological variation in quantitative proteomics. *Proteomics* 3(10):1912-1919.
- Moss DW, Bergmeyer HU, Bergmeyer J. 1987. *Enzymes 1 : Oxidoreductases, transferases*. Weinheim [u.a.]: VCH. XXVI, 613 S. p.
- Munger J, Bajad SU, Coller HA, Shenk T, Rabinowitz JD. 2006. Dynamics of the cellular metabolome during human cytomegalovirus infection. *PLoS Pathog* 2(12):e132.
- Munger J, Bennett BD, Parikh A, Feng XJ, McArdle J, Rabitz HA, Shenk T, Rabinowitz JD. 2008. Systems-level metabolic flux profiling identifies fatty acid synthesis as a target for antiviral therapy. *Nature Biotechnology* 26(10):1179-1186.
- Münger K, Werness BA, Dyson N, Phelps WC, Harlow E, Howley PM. 1989. Complex formation of human papillomavirus E7 proteins with the retinoblastoma tumor suppressor gene product. *Embo Journal* 8(13):4099-4105.
- Muniyappa K, Leibach FH, Mendicino J. 1983. Reciprocal Regulation of Fructose 1,6-Bisphosphatase and Phosphofructokinase by Fructose 2,6-Bisphosphate in Swine Kidney. *Life Sciences* 32(3):271-278.
- Munoz ME, Ponce E. 2003. Pyruvate kinase: current status of regulatory and functional properties. *Comp Biochem Physiol B Biochem Mol Biol* 135(2):197-218.
- Nadeau I, Sabatie J, Koehl M, Perrier M, Kamen A. 2000. Human 293 cell metabolism in low glutamine-supplied culture: interpretation of metabolic changes through metabolic flux analysis. *Metab Eng* 2(4):277-292.
- Nayak DP, Balogun RA, Yamada H, Zhou ZH, Barman S. 2009. Influenza virus morphogenesis and budding. *Virus Research* 143(2):147-161.
- Nayak DP, Hui EKW, Barman S. 2004. Assembly and budding of influenza virus. *Virus Research* 106(2):147-165.
- Neermann J, Wagner R. 1996. Comparative analysis of glucose and glutamine metabolism in transformed mammalian cell lines, insect and primary liver cells. *Journal of Cellular Physiology* 166(1):152-169.
- Negro A, Tavella A, Soranzo C, Petrelli L, Skaper SD. 1994. Establishment and Characterization of a CHO Cell Line Producing a Secreted Form of Human Ciliary Neurotrophic Factor: Neuroprotective Effects of the Recombinant Protein. *Molecular Brain Research* 21(1-2):124-132.
- Nelson DL, Cox MM, Lehninger AL. 2008. *Lehninger Biochemie*. Berlin [u.a.]: Springer. 1668 p.
- Neves L, Oliveira R, Lucas C. 2004. Yeast orthologues associated with glycerol transport and metabolism. *FEMS Yeast Res* 5(1):51-62.
- Newland M, Greenfield PF, Reid S. 1990. Hybridoma growth limitations: the roles of energy metabolism and ammonia production. *Cytotechnology* 3(3):215-229.
- Newsholme EA, Crabtree B. 1986. Maximum Catalytic Activity of Some Key Enzymes in Provision of Physiologically Useful Information About Metabolic Fluxes. *Journal of Experimental Zoology* 239(2):159-167.
- Newsholme EA, Crabtree B, Zammit VA. 1979. Use of enzyme activities as indices of maximum rates of fuel utilization. *Ciba Found Symp*(73):245-58.
- Newsholme P, Curi R, Gordon S, Newsholme EA. 1986. Metabolism of glucose, glutamine, long-chain fatty acids and ketone bodies by murine macrophages. *Biochem J* 239(1):121-125.
- Newsholme P, Lima MMR, Porcopio J, Pithon-Curi TC, Doi SQ, Bazotte RB, Curi R. 2003. Glutamine and glutamate as vital metabolites. *Brazilian Journal of Medical and Biological Research* 36(2):153-163.
- Niederberger P, Prasad R, Miozzari G, Kacser H. 1992. A strategy for increasing an *in vivo* flux by genetic manipulations. The tryptophan system of yeast. *Biochem J* 287 (Pt 2):473-479.
- Niklas J, Melnyk A, Yuan Y, Heinzle E. 2011. Selective permeabilization for the high-throughput measurement of compartmented enzyme activities in mammalian cells. *Anal Biochem* 416(2):218-227.
- Nilsson A, Thomson KS, Adler L. 1989. Purification and characterization of glycerol kinase in the salt-tolerant yeast *Debaryomyces hansenii*. *Biochimica Et Biophysica Acta* 991(2):296-302.
- Nisselbaum JS, Green S. 1969. A simple ultramicro method for determination of pyridine nucleotides in tissues. *Anal Biochem* 27(2):212-217.
- Novotny MJ, Frederickson WL, Waygood EB, Saier MH. 1985. Allosteric regulation of glycerol kinase by enzyme III^{glc} of the phosphotransferase system in *Escherichia coli* and *Salmonella typhimurium*. *Journal of Bacteriology* 162(2):810-816.
- Nowak T, Suelter C. 1981. Pyruvate kinase: activation by and catalytic role of the monovalent and divalent cations. *Molecular and Cellular Biochemistry* 35(2):65-75.
- O'Farrell PH. 1975. High resolution two-dimensional electrophoresis of proteins. *J Biol Chem* 250(10):4007-4021.

- Ozturk SS, Palsson BO. 1991. Effect of medium osmolarity on hybridoma growth, metabolism, and antibody production. *Biotechnol Bioeng* 37(10):989-993.
- Ozturk SS, Riley MR, Palsson BO. 1992. Effects of Ammonia and Lactate on Hybridoma Growth, Metabolism, and Antibody Production. *Biotechnology and Bioengineering* 39(4):418-431.
- Passonneau JV, Lowry OH. 1993. *Enzymatic analysis: a practical guide*. Totowa, NJ: Humana Press. X, 403 S p.
- Passos JF, Simillion C, Hallinan J, Wipat A, von Zglinicki T. 2009. Cellular senescence: unravelling complexity. *Age (Dordr)* 31(4):353-363.
- Pasteris SE, de Saad AMS. 1998. Characterization of glycerol kinase and NAD-independent glycerol-3-phosphate dehydrogenase from *Pediococcus pentosaceus* N5p. *Letters in Applied Microbiology* 27(2):93-97.
- Pau MG, Ophorst C, Koldijk MH, Schouten G, Mehtali M, Uytdehaag F. 2001. The human cell line PER.C6 provides a new manufacturing system for the production of influenza vaccines. *Vaccine* 19(17-19):2716-2721.
- Pawlyk AC, Pettigrew DW. 2001. Subcloning, expression, purification, and characterization of *Haemophilus influenzae* glycerol kinase. *Protein Expression and Purification* 22(1):52-59.
- Pérez O, Paolazzi CC. 1997. Production methods for rabies vaccine. *J Ind Microbiol Biotechnol* 18(5):340-347.
- Pongratz RL, Kibbey RG, Shulman GI, Cline GW. 2007. Cytosolic and mitochondrial malic enzyme isoforms differentially control insulin secretion. *J Biol Chem* 282(1):200-207.
- Post RL, Merritt CR, Kinsolving CR, Albright CD. 1960. Membrane adenosine triphosphatase as a participant in the active transport of sodium and potassium in the human erythrocyte. *J Biol Chem* 235:1796-1802.
- Postma E, Verduyn C, Scheffers WA, Van Dijken JP. 1989. Enzymic analysis of the crabtree effect in glucose-limited chemostat cultures of *Saccharomyces cerevisiae*. *Appl Environ Microbiol* 55(2):468-477.
- Prévaille X, Salvemini F, Giraud S, Chaufour S, Paul C, Stepien G, Ursini MV, Arrigo AP. 1999. Mammalian small stress proteins protect against oxidative stress through their ability to increase glucose-6-phosphate dehydrogenase activity and by maintaining optimal cellular detoxifying machinery. *Exp Cell Res* 247(1):61-78.
- Prisco G, Garofano F. 1975. Crystallization and Partial Characterization of Glutamate Dehydrogenase from Ox Liver Nuclei. *Biochemistry* 14(21):4673-4679.
- Quek LE, Dietmar S, Kromer JO, Nielsen LK. 2010. Metabolic flux analysis in mammalian cell culture. *Metab Eng* 12(2):161-171.
- Radzicka A, Wolfenden R. 1995. A proficient enzyme. *Science* 267(5194):90-93.
- Rais B, Ortega F, Puigjaner J, Comin B, Orosz F, Ovadi J, Cascante M. 2000. Quantitative characterization of homo- and heteroassociations of muscle phosphofructokinase with aldolase. *Biochim Biophys Acta* 1479(1-2):303-314.
- Ramabrahmam P, Subrahmanyam D. 1983. Mitochondrial glycerol kinase of *Culex pipiens fatigans*. *Insect Biochemistry* 13(5):523-528.
- Ramadoss CS, Uyeda K, Johnston JM. 1976. Studies on the fatty acid inactivation of phosphofructokinase. *J Biol Chem* 251(1):98-107.
- Ranganathan NS, Srere PA, Linn TC. 1980. Comparison of phospho- and dephospho-ATP citrate lyase. *Arch Biochem Biophys* 204(1):52-58.
- Rao DR, Kou AY. 1977. Partial purification and characterization of glycerokinase from chicken liver. *International Journal of Biochemistry* 8(4):295-298.
- Rathore R, Pribil P, Corr JJ, Seibel WL, Evdokimov A, Greis KD. 2010. Multiplex enzyme assays and inhibitor screening by mass spectrometry. *J Biomol Screen* 15(8):1001-7.
- Reddy GR, Ramaiah A. 1984. Purification of Rabbit Liver Phosphofructokinase and Its Properties under Simulating *in vivo* Conditions. *Journal of Biosciences* 6(5):643-653.
- Reitzer LJ, Wice BM, Kennell D. 1979. Evidence That Glutamine, Not Sugar, Is the Major Energy Source for Cultured Hela Cells. *Journal of Biological Chemistry* 254(8):2669-2676.
- Reitzer LJ, Wice BM, Kennell D. 1980. The pentose cycle. Control and essential function in HeLa cell nucleic acid synthesis. *J Biol Chem* 255(12):5616-5626.
- Reuveny S, Velez D, Macmillan JD, Miller L. 1986. Factors affecting cell growth and monoclonal antibody production in stirred reactors. *J Immunol Methods* 86(1):53-59.
- Ritter JB. 2010. Charakterisierung tierischer Zellkulturen anhand einer Quantifizierung intrazellulärer Metaboliten aus dem Zentralstoffwechsel. Gilles ED, editor. Magdeburg: Shaker. 250 p.
- Ritter JB, Genzel Y, Reichl U. 2007. Monitoring of extracellular TCA cycle intermediates in mammalian cell culture. *Cell Technology for Cell Products*:603-605.
- Ritter JB, Genzel Y, Reichl U. 2008. Simultaneous extraction of several metabolites of energy metabolism and related substances in mammalian cells: Optimization using experimental design. *Analytical Biochemistry* 373(2):349-369.

- Ritter JB, Wahl AS, Freund S, Genzel Y, Reichl U. 2010. Metabolic effects of influenza virus infection in cultured animal cells: Intra- and extracellular metabolite profiling. *Bmc Systems Biology* 4:-.
- Rogers A, Gibon Y. 2009. Enzyme kinetics: theory & practice. In: Schwender J, editor. *Plant Metabolic Networks*. Berlin Heidelberg New York: Springer. p 71-103.
- Romanos MA, Scorer CA, Clare JJ. 1992. Foreign gene expression in yeast: a review. *Yeast* 8(6):423-488.
- Rossell S, Solem C, Jensen PR, Heijnen JJ. 2011. Towards a quantitative prediction of the fluxome from the proteome. *Metab Eng*.
- Rossman JS, Lamb RA. 2011. Influenza virus assembly and budding. *Virology* 411(2):229-236.
- Rowe WB. 1985. Glutamine Synthetase from Muscle. *Methods in Enzymology* 113:199-212.
- Rüker F, Ebert V, Kohl J, Steindl F, Riegler H, Katinger H. 1991. Expression of a Human Monoclonal Anti-HIV-1 Antibody in CHO Cells. *Annals of the New York Academy of Sciences* 646:212-219.
- Sadava D, Moore K. 1987. Glycerol metabolism in higher plants: glycerol kinase. *Biochemical and Biophysical Research Communications* 143(3):977-983.
- Sagi A, Rishpon J, Shabat D. 2006. Amperometric assay for aldolase activity: antibody-catalyzed ferrocenylamine formation. *Anal Chem* 78(5):1459-1461.
- Salati LM, Amir-Ahmady B. 2001. Dietary regulation of expression of glucose-6-phosphate dehydrogenase. *Annual Review of Nutrition* 21:121-140.
- Sanders PG, Wilson RH. 1984. Amplification and Cloning of the Chinese Hamster Glutamine Synthetase Gene. *Embo Journal* 3(1):65-71.
- Sandig V, Jordan I; 2005. Immortalized avian cell lines for virus production. WO/2005/042728 A2.
- Sanfeliu A, Cairo JJ, Casas C, Sola C, Godia F. 1996. Analysis of nutritional factors and physical conditions affecting growth and monoclonal antibody production of the hybridoma KB-26.5 cell line. *Biotechnol Prog* 12(2):209-216.
- Sanfeliu A, Stephanopoulos G. 1999. Effect of glutamine limitation on the death of attached Chinese hamster ovary cells. *Biotechnology and Bioengineering* 64(1):46-53.
- Schaaff I, Heinisch J, Zimmermann FK. 1989. Overproduction of glycolytic enzymes in yeast. *Yeast* 5(4):285-290.
- Scheer WD, Lehmann HP, Beeler MF. 1978. An improved assay for hexokinase activity in human tissue homogenates. *Anal Biochem* 91(2):451-463.
- Scheffner M, Werness BA, Huibregtse JM, Levine AJ, Howley PM. 1990. The E6 oncoprotein encoded by human papillomavirus types 16 and 18 promotes the degradation of p53. *Cell* 63(6):1129-1136.
- Scheiffelle P, Rietveld A, Wilk T, Simons K. 1999. Influenza viruses select ordered lipid domains during budding from the plasma membrane. *J Biol Chem* 274(4):2038-2044.
- Schneider M, Marison IW, von Stockar U. 1996. The importance of ammonia in mammalian cell culture. *J Biotechnol* 46(3):161-185.
- Schoolwerth AC, Hoover WJ, Daniel CH, LaNoue KF. 1980. Effect of aminoxyacetate and alpha-ketoglutarate on glutamate deamination by rat kidney mitochondria. *International Journal of Biochemistry* 12(1-2):145-149.
- Schwab MA, Kölker S, van den Heuvel LP, Sauer S, Wolf NI, Rating D, Hoffmann GF, Smeitink JA, Okun JG. 2005. Optimized spectrophotometric assay for the completely activated pyruvate dehydrogenase complex in fibroblasts. *Clin Chem* 51(1):151-160.
- Schwarzer J, Rapp E, Reichl U. 2008. N-glycan analysis by CGE-LIF: Profiling influenza A virus hemagglutinin N-glycosylation during vaccine production. *Electrophoresis* 29(20):4203-4214.
- Scrutton MC, Utter MF. 1965. Pyruvate Carboxylase: III. Some Physical and Chemical Properties of the Highly Purified Enzyme. *J Biol Chem* 240:1-9.
- Scrutton MC, White MD. 1974. Purification and Properties of Human Liver Pyruvate Carboxylase. *Biochemical Medicine* 9(3):271-292.
- Segel LA. 1988. On the validity of the steady state assumption of enzyme kinetics. *Bull Math Biol* 50(6):579-593.
- Segner H, Verreth J. 1995. Metabolic Enzyme Activities in Larvae of the African Catfish, *Clarias gariepinus*: Changes in Relation to Age and Nutrition. *Fish Physiology and Biochemistry* 14(5):385-398.
- Sellick CA, Hansen R, Stephens GM, Goodacre R, Dickson AJ. 2011. Metabolite extraction from suspension-cultured mammalian cells for global metabolite profiling. *Nat Protoc* 6(8):1241-1249.
- Sevdalian DA, Ozand PT, Zielke HR. 1980. Increase in glutaminase activity during the growth cycle of cultured human diploid fibroblasts. *Enzyme* 25(2):142-144.
- Severson DL, Denton RM, Pask HT, Randle PJ. 1974. Calcium and Magnesium Ions as Effectors of Adipose-Tissue Pyruvate Dehydrogenase Phosphate Phosphatase. *Biochemical Journal* 140(2):225-237.
- Shapiro RA, Morehouse RF, Curthoys NP. 1982. Inhibition by Glutamate of Phosphate-Dependent Glutaminase of Rat Kidney. *Biochemical Journal* 207(3):561-566.

- Sharfstein ST, Tucker SN, Mancuso A, Blanch HW, Clark DS. 1994. Quantitative in vivo nuclear magnetic resonance studies of hybridoma metabolism. *Biotechnol Bioeng* 43(11):1059-1074.
- Shay JW, Pereira-Smith OM, Wright WE. 1991. A role for both RB and p53 in the regulation of human cellular senescence. *Exp Cell Res* 196(1):33-39.
- Shen CF, Lanthier S, Jacob D, Montes J, Beath A, Beresford A, Kamen A. 2012. Process optimization and scale-up for production of rabies vaccine live adenovirus vector (AdRG1.3). *Vaccine* 30(2):300-306.
- Shen S, Sulter G, Jeffries TW, Cregg JM. 1998. A strong nitrogen source-regulated promoter for controlled expression of foreign genes in the yeast *Pichia pastoris*. *Gene* 216(1):93-102.
- Shen Z, Go EP, Gamez A, Apon JV, Fokin V, Greig M, Ventura M, Crowell JE, Blixt O, Paulson JC and others. 2004. A mass spectrometry plate reader: monitoring enzyme activity and inhibition with a Desorption/Ionization on Silicon (DIOS) platform. *Chembiochem* 5(7):921-927.
- Shepherd D, Garland PB. 1969. The kinetic properties of citrate synthase from rat liver mitochondria. *Biochem J* 114(3):597-610.
- Sidorenko Y, Wahl A, Dauner M, Genzel Y, Reichl U. 2008. Comparison of metabolic flux distributions for MDCK cell growth in glutamine- and pyruvate-containing media. *Biotechnology Progress* 24(2):311-320.
- Smales CM, Dinnis DM, Stansfield SH, Alete D, Sage EA, Birch JR, Racher AJ, Marshall CT, James DC. 2004. Comparative proteomic analysis of GS-NS0 murine myeloma cell lines with varying recombinant monoclonal antibody production rate. *Biotechnol Bioeng* 88(4):474-488.
- Smits HP, Hauf J, Muller S, Hobley TJ, Zimmermann FK, Hahn-Hagerdal B, Nielsen J, Olsson L. 2000. Simultaneous overexpression of enzymes of the lower part of glycolysis can enhance the fermentative capacity of *Saccharomyces cerevisiae*. *Yeast* 16(14):1325-1334.
- Snodgrass PJ, Lund P. 1984. Allosteric properties of phosphate-activated glutaminase of human liver mitochondria. *Biochim Biophys Acta* 798(1):21-27.
- Sola MM, Salto R, Oliver FJ, Gutiérrez M, Vargas AM. 1993. Effects of AMP and Fructose 2,6-Bisphosphate on Fluxes between Glucose 6-Phosphate and Triose-Phosphate in Renal Cortical Extracts. *Journal of Biological Chemistry* 268(26):19352-19357.
- Spoden GA, Rostek U, Lechner S, Mitterberger M, Mazurek S, Zwerschke W. 2009. Pyruvate kinase isoenzyme M2 is a glycolytic sensor differentially regulating cell proliferation, cell size and apoptotic cell death dependent on glucose supply. *Experimental Cell Research* 315(16):2765-2774.
- Sprenger GA, Schörken U, Sprenger G, Sahm H. 1995. Transketolase A of *Escherichia coli* K12 - Purification and properties of the enzyme from recombinant strains. *European Journal of Biochemistry* 230(2):525-532.
- Sreekrishna K, Brankamp RG, Kropp KE, Blankenship DT, Tsay JT, Smith PL, Wierschke JD, Subramaniam A, Birkenberger LA. 1997. Strategies for optimal synthesis and secretion of heterologous proteins in the methylotrophic yeast *Pichia pastoris*. *Gene* 190(1):55-62.
- Stanton RC, Seifter JL. 1988. Epidermal Growth Factor Rapidly Activates the Hexose Monophosphate Shunt in Kidney Cells. *American Journal of Physiology* 254(2):C267-C271.
- Stanton RC, Seifter JL, Boxer DC, Zimmerman E, Cantley LC. 1991. Rapid Release of Bound Glucose-6-Phosphate Dehydrogenase by Growth Factors. Correlation with Increased Enzymatic Activity. *Journal of Biological Chemistry* 266(19):12442-12448.
- Staples JF, Suarez RK. 1997. Honeybee flight muscle phosphoglucose isomerase: Matching enzyme capacities to flux requirements at a near-equilibrium reaction. *Journal of Experimental Biology* 200(8):1247-1254.
- Starai VJ, Escalante-Semerena JC. 2004. Acetyl-coenzyme A synthetase (AMP forming). *Cellular and Molecular Life Sciences* 61(16):2020-30.
- Storer AC, Cornish-Bowden A. 1974. The kinetics of coupled enzyme reactions. Applications to the assay of glucokinase, with glucose 6-phosphate dehydrogenase as coupling enzyme. *Biochem J* 141(1):205-209.
- Street JC, Delort AM, Braddock PSH, Brindle KM. 1993. A $^1\text{H}/^{15}\text{N}$ n.m.r. study of nitrogen metabolism in cultured mammalian cells. *Biochemical Journal* 291:485-492.
- Stryer L. 1995. *Biochemistry*. New York: W.H. Freeman. xxxiv, 1064 p. p.
- Su AI, Pezacki JP, Wodicka L, Brideau AD, Supekova L, Thimme R, Wieland S, Bukh J, Purcell RH, Schultz PG and others. 2002. Genomic analysis of the host response to hepatitis C virus infection. *Proc Natl Acad Sci U S A* 99(24):15669-15674.
- Suarez RK, Darveau CA. 2005. Multi-level regulation and metabolic scaling. *Journal of Experimental Biology* 208(Pt 9):1627-1634.
- Suarez RK, Lighton JR, Joos B, Roberts SP, Harrison JF. 1996. Energy metabolism, enzymatic flux capacities, and metabolic flux rates in flying honeybees. *Proc Natl Acad Sci U S A* 93(22):12616-12620.

- Suarez RK, Staples JF, Lighton JRB, West TG. 1997. Relationships between enzymatic flux capacities and metabolic flux rates: Nonequilibrium reactions in muscle glycolysis. *Proceedings of the National Academy of Sciences of the United States of America* 94(13):7065-7069.
- Suarez RK, Welch KC, Jr., Hanna SK, Herrera ML. 2009. Flight muscle enzymes and metabolic flux rates during hovering flight of the nectar bat, *Glossophaga soricina*: further evidence of convergence with hummingbirds. *Comp Biochem Physiol A Mol Integr Physiol* 153(2):136-140.
- Subbarao K, Joseph T. 2007. Scientific barriers to developing vaccines against avian influenza viruses. *Nat Rev Immunol* 7(4):267-278.
- Sugden PH, Newsholme EA. 1975. Activities of citrate synthase, NAD⁺-linked and NADP⁺-linked isocitrate dehydrogenases, glutamate dehydrogenase, aspartate aminotransferase and alanine aminotransferase in nervous tissues from vertebrates and invertebrates. *Biochem J* 150(1):105-111.
- Sulpice R, Tschöp H, von Korff M, Büssis D, Usadel B, Höhne M, Witucka-Wall H, Altmann T, Stitt M, Gibon Y. 2007. Description and applications of a rapid and sensitive non-radioactive microplate-based assay for maximum and initial activity of D-ribulose-1,5-bisphosphate carboxylase/oxygenase. *Plant Cell Environ* 30(9):1163-1175.
- Swiderek H, Logan A, Al-Rubeai M. 2008. Cellular and transcriptomic analysis of NS0 cell response during exposure to hypoxia. *J Biotechnol* 134(1-2):103-111.
- Syed GH, Amako Y, Siddiqui A. 2010. Hepatitis C virus hijacks host lipid metabolism. *Trends Endocrinol Metab* 21(1):33-40.
- Tambasco-Studart M, Tews I, Amrhein N, Fitzpatrick TB. 2007. Functional analysis of PDX2 from *Arabidopsis*, a glutaminase involved in vitamin B₆ biosynthesis. *Plant Physiol* 144(2):915-925.
- Tanaka S, Furukawa T, Plotkin SA. 1975. Human cytomegalovirus stimulates host cell RNA synthesis. *Journal of Virology* 15(2):297-304.
- Tate SS, Meister A. 1971. Regulation of rat liver glutamine synthetase: activation by alpha-ketoglutarate and inhibition by glycine, alanine, and carbamyl phosphate. *Proc Natl Acad Sci U S A* 68(4):781-785.
- Tejwani GA. 1978. The role of phosphofructokinase in the Pasteur effect. *Trends in Biochemical Sciences* 3(1):30-33
- Thomas S, Mooney PJ, Burrell MM, Fell DA. 1997. Metabolic Control Analysis of glycolysis in tuber tissue of potato (*Solanum tuberosum*): explanation for the low control coefficient of phosphofructokinase over respiratory flux. *Biochem J* 322 (Pt 1):119-127.
- Thorner JW, Paulus H. 1971. Composition and subunit structure of glycerol kinase from *Escherichia coli*. *J Biol Chem* 246(12):3885-3894.
- Tian Q, Stepaniants SB, Mao M, Weng L, Feetham MC, Doyle MJ, Yi EC, Dai H, Thorsson V, Eng J and others. 2004. Integrated genomic and proteomic analyses of gene expression in mammalian cells. *Mol Cell Proteomics* 3(10):960-969.
- Tree JA, Richardson C, Fooks AR, Clegg JC, Looby D. 2001. Comparison of large-scale mammalian cell culture systems with egg culture for the production of influenza virus A vaccine strains. *Vaccine* 19(25-26):3444-3450.
- Trinh LB, Phue JN, Shiloach J. 2003. Effect of methanol feeding strategies on production and yield of recombinant mouse endostatin from *Pichia pastoris*. *Biotechnology and Bioengineering* 82(4):438-444.
- Tritsch GL, Moore GE. 1962. Spontaneous decomposition of glutamine in cell culture media. *Exp Cell Res* 28:360-364.
- Tschopp JF, Brust PF, Clegg JM, Stillman CA, Gingeras TR. 1987a. Expression of the *lacZ* gene from two methanol-regulated promoters in *Pichia pastoris*. *Nucleic Acids Res* 15(9):3859-3876.
- Tschopp JF, Sverlow G, Kosson R, Craig W, Grinna L. 1987b. High-Level Secretion of Glycosylated Invertase in the Methylophilic Yeast, *Pichia pastoris*. *Bio-Technology* 5(12):1305-1308.
- Tsuboi KK, Fukunaga K, Chervenka CH. 1971. Phosphoglucose isomerase from human erythrocyte - Preparation and properties. *J Biol Chem* 246(24):7586-7594.
- Turnquist RL, Gillett TA, Hansen RG. 1974. Uridine diphosphate glucose pyrophosphorylase - Crystallization and properties of the enzyme from rabbit liver and species comparisons. *Journal of Biological Chemistry* 249(23):7695-7700.
- Umezawa H. 1976. Structures and activities of protease inhibitors of microbial origin. *Methods Enzymol* 45:678-695.
- Vaheri A, Cristofalo VJ. 1967. Metabolism of rubella virus-infected BHK 21 cells. Enhanced glycolysis and late cellular inhibition. *Arch Gesamte Virusforsch* 21(3):425-436.
- Valero E, Garcia-Carmona F. 1998. A continuous spectrophotometric method based on enzymatic cycling for determining L-glutamate. *Analytical Biochemistry* 259(2):265-271.
- Valero E, García-Carmona F. 1996. Optimizing enzymatic cycling assays: Spectrophotometric determination of low levels of pyruvate and L-lactate. *Analytical Biochemistry* 239(1):47-52.

- Valero E, Varon R, Garcia-Carmona F. 2004. Kinetic analysis of a model for double substrate cycling: highly amplified ADP (and/or ATP) quantification. *Biophysical Journal* 86(6):3598-3606.
- Valero E, Varon R, Garcia-Carmona F. 1997. Mathematical model for the determination of enzyme activity based on enzymatic amplification by substrate cycling. *Analytica Chimica Acta* 346(2):215-221.
- Valero E, Varón R, Garcia-Carmona F. 1995. Kinetic Study of an Enzymic Cycling System Coupled to an Enzymic Step: Determination of Alkaline Phosphatase Activity. *Biochemical Journal* 309:181-185.
- van Diepen A, Brand HK, Sama I, Lambooy LH, van den Heuvel LP, van der Well L, Huynen M, Osterhaus AD, Andeweg AC, Hermans PW. 2010. Quantitative proteome profiling of respiratory virus-infected lung epithelial cells. *J Proteomics* 73(9):1680-1693.
- van Eunen K, Bouwman J, Daran-Lapujade P, Postmus J, Canelas AB, Mensonides FI, Orij R, Tuzun I, van den Brink J, Smits GJ and others. 2010. Measuring enzyme activities under standardized *in vivo*-like conditions for systems biology. *FEBS J* 277(3):749-760.
- Van Schaftingen E, Jett MF, Hue L, Hers HG. 1981. Control of liver 6-phosphofructokinase by fructose 2,6-bisphosphate and other effectors. *Proc Natl Acad Sci U S A* 78(6):3483-3486.
- van Urk H, Postma E, Scheffers WA, van Dijken JP. 1989. Glucose transport in Crabtree-positive and Crabtree-negative yeasts. *J Gen Microbiol* 135(9):2399-2406.
- Veech RL. 2003. A humble hexose monophosphate pathway metabolite regulates short- and long-term control of lipogenesis. *Proc Natl Acad Sci U S A* 100(10):5578-5580.
- Vester D, Lagoda A, Hoffmann D, Seitz C, Heldt S, Bettenbrock K, Genzel Y, Reichl U. 2010. Real-time RT-qPCR assay for the analysis of human influenza A virus transcription and replication dynamics. *Journal of Virological Methods* 168(1-2):63-71.
- Vester D, Rapp E, Gade D, Genzel Y, Reichl U. 2009. Quantitative analysis of cellular proteome alterations in human influenza A virus-infected mammalian cell lines. *Proteomics* 9(12):3316-3327.
- Villee CA. 1962. An enzymic method for the assay of pyridine nucleotides in extracts of animal tissues. *Biochem J* 83:191-194.
- Voet D, Voet JG, Pratt CW, Beck-Sickinger A. 2002. *Lehrbuch der Biochemie*. Weinheim: Wiley-VCH. XXII, 1062 S. p.
- Vriezen N, van Dijken JP. 1998a. Fluxes and enzyme activities in central metabolism of myeloma cells grown in chemostat culture. *Biotechnology and Bioengineering* 59(1):28-39.
- Vriezen N, van Dijken JP. 1998b. Subcellular localization of enzyme activities in chemostat-grown murine myeloma cells. *Journal of Biotechnology* 61(1):43-56.
- Wagner R. 1997. Metabolic Control of Animal Cell Culture Processes. In: Hauser H, Wagner R, editors. *Mammalian cell biotechnology in protein production*. Berlin [u.a.]: de Gruyter. p 191-232.
- Wagner R, Ryll T, Krafft H, Lehmann J. 1988. Variation of amino acid concentrations in the medium of HU β -IFN and HU IL-2 producing cell lines. *Cytotechnology* 1(2):145-150.
- Wahl A, Sidorenko Y, Dauner M, Genzel Y, Reichl U. 2008. Metabolic flux model for an anchorage-dependent MDCK cell line: characteristic growth phases and minimum substrate consumption flux distribution. *Biotechnology and Bioengineering* 101(1):135-152.
- Wakil SJ, Pugh EL, Sauer F. 1964. The Mechanism of Fatty Acid Synthesis. *Proc Natl Acad Sci U S A* 52:106-114.
- Wallace TC, Leh MB, Coughlin RW. 1977. Amperometric assay of coenzyme-dependent oxidoreductase enzymes in a flow-through cell. *Biotechnol Bioeng* 19(6):901-921.
- Warburg O. 1956. On the origin of cancer cells. *Science* 123(3191):309-314.
- Waterham HR, Digan ME, Koutz PJ, Lair SV, Cregg JM. 1997. Isolation of the *Pichia pastoris* glyceraldehyde-3-phosphate dehydrogenase gene and regulation and use of its promoter. *Gene* 186(1):37-44.
- Wazer DE, Liu XL, Chu Q, Gao Q, Band V. 1995. Immortalization of distinct human mammary epithelial cell types by human papilloma virus 16 E6 or E7. *Proc Natl Acad Sci U S A* 92(9):3687-3691.
- Wellner VP, Meister A. 1966. Binding of Adenosine Triphosphate and Adenosine Diphosphate by Glutamine Synthetase. *Biochemistry* 5(3):872-879.
- Williamson DH, Lund P, Krebs HA. 1967. The Redox State of Free Nicotinamide-Adenine Dinucleotide in Cytoplasm and Mitochondria of Rat Liver. *Biochemical Journal* 103(2):514-527.
- Willson VJC, Tipton KF. 1980. The Effect of pH on the Allosteric Behavior of Ox-Brain NAD⁺-Dependent Isocitrate Dehydrogenase. *European Journal of Biochemistry* 109(2):411-416.
- Wise EM, Jr., Ball EG. 1964. Malic Enzyme and Lipogenesis. *Proc Natl Acad Sci U S A* 52:1255-1263.
- Wittmann C. 2007. Fluxome analysis using GC-MS. *Microbial Cell Factories* 6.
- Wurm FM. 2004. Production of recombinant protein therapeutics in cultivated mammalian cells. *Nat Biotechnol* 22(11):1393-1398.
- Xu X, Nagarajan H, Lewis NE, Pan S, Cai Z, Liu X, Chen W, Xie M, Wang W, Hammond S and others. 2011. The genomic sequence of the Chinese hamster ovary (CHO)-K1 cell line. *Nat Biotechnol* 29(8):735-741.

- Yallop CA, Norby PL, Jensen R, Reinbach H, Svendsen I. 2003. Characterisation of G418-induced metabolic load in recombinant CHO and BHK cells: effect on the activity and expression of central metabolic enzymes. *Cytotechnology* 42(2):87-99.
- Yang W, Hood BL, Chadwick SL, Liu SF, Watkins SC, Luo GX, Conrads TP, Wang TY. 2008. Fatty Acid Synthase Is Up-Regulated During Hepatitis C Virus Infection and Regulates Hepatitis C Virus Entry and Production. *Hepatology* 48(5):1396-1403.
- Young RA. 2000. Biomedical discovery with DNA arrays. *Cell* 102(1):9-15.
- Yuan H, Veldman T, Rundell K, Schlegel R. 2002. Simian virus 40 small tumor antigen activates AKT and telomerase and induces anchorage-independent growth of human epithelial cells. *J Virol* 76(21):10685-10691.
- Zammit VA, Newsholme EA. 1976. The Maximum Activities of Hexokinase, Phosphorylase, Phosphofructokinase, Glycerol Phosphate Dehydrogenases, Lactate Dehydrogenase, Octopine Dehydrogenase, Phosphoenolpyruvate Carboxykinase, Nucleoside Diphosphatekinase, Glutamate-Oxaloacetate Transaminase and Arginine Kinase in Relation to Carbohydrate Utilization in Muscles from Marine Invertebrates. *Biochemical Journal* 160(3):447-462.
- Zeiger L, Grammel H. 2010. Model-based high cell density cultivation of *Rhodospirillum rubrum* under respiratory dark conditions. *Biotechnology and Bioengineering* 105(4):729-739.
- Zhang J, Pekosz A, Lamb RA. 2000. Influenza virus assembly and lipid raft microdomains: a role for the cytoplasmic tails of the spike glycoproteins. *Journal of Virology* 74(10):4634-4644.
- Zhou M, Crawford Y, Ng D, Tung J, Pynn AFJ, Meier A, Yuk IH, Vijayasankaran N, Leach K, Joly J, Snedecor B, Shen A. 2011. Decreasing lactate level and increasing antibody production in Chinese Hamster Ovary cells (CHO) by reducing the expression of lactate dehydrogenase and pyruvate dehydrogenase kinases. *Journal of Biotechnology* 153:27-34.
- Zhu A, Monahan C, Zhang Z, Hurst R, Leng L, Goldstein J. 1995. High-Level Expression and Purification of Coffee Bean α -Galactosidase Produced in the Yeast *Pichia pastoris*. *Archives of Biochemistry and Biophysics* 324(1):65-70.
- Zhu H, Bilgin M, Snyder M. 2003. Proteomics. *Annual Review of Biochemistry* 72:783-812.
- Zielke HR, Ozand PT, Tildon JT, Sevdalian DA, Cornblath M. 1978. Reciprocal regulation of glucose and glutamine utilization by cultured human diploid fibroblasts. *Journal of Cellular Physiology* 95(1):41-48.
- Zielke HR, Zielke CL, Ozand PT. 1984. Glutamine: A Major Energy Source for Cultured Mammalian Cells. *Federation Proceedings* 43(1):121-125.

Appendix

A. Chemicals, consumables and equipment

Table A1: List of Chemicals.

Name	Manufacturer	Cat. No.
Sodium acetate	Sigma, Taufkirchen, Germany	S8750
O-Acetyl-L-carnitine hydrochloride, min 99%	Sigma	A6706
Acetyl-CoA	Roche, Mannheim, Germany	11 585 371 001
Acetylphosphate lithium potassium salt	Sigma	01409
Acetylpyridine adenine dinucleotide, approx. 90%	Sigma	A5251
Acrylamide	Sigma	A8887
Adenosine-5'-diphosphate (ADP)	Roche	10 127 507 001
ADP disodium salt	Sigma	01897
ADP-Hexokinase (ADP-HKPII)	Asahi Kasei Pharma, Tokyo, Japan	0701A
AMP monohydrate from yeast	Sigma	A2252
Adenosine-5'-triphosphate (ATP)	Roche	10 127 523 001
ATP disodium salt, grade I, minimum 99%	Sigma	A2383
Agar, grade A	BD, Franklin Lakes, NJ, USA	212304
Agarose	Roth	2267
L-Alanine	Sigma	A7627
Alcohol dehydrogenase	Roche	10 127 558 001
Alcohol oxidase solution From <i>Pichia pastoris</i>	Sigma	A2404
Aldehyde dehydrogenase potassium-activated from baker's yeast	Sigma	A6338
Aldolase	Roche	10 102 652 001
Aldolase, from rabbit muscle	Sigma	A8811
6-Aminocaproic acid	Sigma	A2504
Ammonium acetate	Sigma	A1542
Ammonium chloride	Sigma	A9434
Ammonium hydroxide solution, 28.0-30.0%	Sigma	320145
Ammonium iron(III) sulfate dodecahydrate	Sigma	221260
Ammonium persulfate (APS)	AppliChem, Darmstadt, Germany	A1142
Ampicillin	Merck, Darmstadt, Germany	171257
Antifoam agent	Zschimmer & Schwarz, Lahnstein, Germany	Contraspum 210
L-Aspartic acid sodium salt monohydrate	Sigma	A6683
BCA Protein Assay Kit	Thermo Scientific, Waltham, MA, USA	23225
Benzamidine	Sigma	12072
Bromphenol blue	Roth, Karlsruhe, Germany	A512
Calcium chloride	Sigma	C5670

Caproic acid	Sigma	153745
L-Carnitine hydrochloride, approx. 98%	Sigma	C0283
L-Carnitine inner salt, approx. 98%	Sigma	C0158
Catalase preparation, from <i>Aspergillus niger</i>	Sigma	C3515
Cholesterol from lanolin	Sigma	26732
Sodium citrate tribasic dihydrate	Sigma	S4641
CASO Broth	Sigma	22098
Citrate synthase, from porcine heart	Sigma	C3260-
Coenzyme A trilithium salt	Sigma	C3019
Coenzyme Q ₁₀ ≥98% (HPLC)	Sigma	C9538
Coomassie Brilliant Blue R250	Roth	3862
Creatine kinase (CK)	Roche	10 127 566 001
Creatine phosphokinase, type I: from rabbit muscle	Sigma	C3755
Cytidine 5'-triphosphate disodium salt	Sigma	C1506
DL-Dithiothreitol	Sigma	43819
Diaphorase from <i>Chlostridium kluyveri</i>	Sigma	D5540
Dihydroxyacetone phosphate dilithium salt	Sigma	D7137
DNA ladder, 1 kb	Sigma	D0428
DNA ladder, 1 kb	Roth	Y014
DNA ladder, GeneRuler™ 1 kb	Fermentas, St. Leon-Rot, Germany	SM0311
EDTA	Sigma	EDS
EGTA	Sigma	E3889
Episerf medium	Gibco, Karlsruhe, Germany	10732-022
D-Erythrose 4-phosphate sodium salt	Sigma	E0377
Ethanol absolute	Merck	1070172511
Ethidium bromide	Roth	7870
Fetal calf derum (FCS)	Gibco	10270-106
Formaldehyde dehydrogenase, from <i>Pseudomonas putida</i>	Sigma	F1879
D-Fructose 6-phosphate dipotassium salt	Sigma	F1502
D-Fructose-1,6-diphosphate trisodium salt octahydrate	Sigma	47810
Fumarase, from porcine heart	Sigma	F1757
Sodium fumarate dibasic	Sigma	F1506
Glucose	Sigma	G8270
D-Glucose 6 phosphate sodium salt	Sigma	G7879
Glucose-6-Phosphate dehydrogenase, grade I	Roche	10 127 655 001
Glucose-6-Phosphate dehydrogenase, grade II	Roche	10 127 671 001
L-Glutamic acid, monosodium salt monohydrate	Sigma	49621
L-Glutamic acid γ-monohydroxamate	Sigma	G2253
L-Glutamic dehydrogenase solution from bovine liver	Sigma	G2626
Glutamic-oxalacetic transaminase, type I: from porcine heart	Sigma	G2751
L-Glutamine	Sigma	G3126
DL Glyceraldehyde 3-phosphate diethyl acetal barium salt	Sigma	G5376

Glyceraldehyde-3-phosphate dehydrogenase	Roche	10 105 686 001
D(+) Glyceric acid hemicalcium salt, 99.9% GC	Sigma	G8766
Glycerol	Sigma	G7757
Glycerol Testkit	Roche	10 148 270 035
sn-Glycerol 3-phosphate	Sigma	G7886
Glycerol-3-phosphate dehydrogenase	Roche	10 127 752 001
Glycerol 3-phosphate oxidase, from <i>Streptococcus thermophiles</i>	Sigma	G4388
Glycerokinase from <i>E. coli</i> , 300-600 units/mL	Sigma	G6278
Glycine	Merck	1041690250
Glyoxylic acid monohydrate	Sigma	50710
GMEM powder	Gibco	22100-093
GMEM Medium without glutamine	Sigma	G5154
Go Taq Polymerase	Promega, Madison, WI, USA	M300
Guanosine 5'-diphosphate sodium salt, type I, minimum 96% HPLC	Sigma	G7127
Guanosine 5'-triphosphate sodium salt hydrate	Sigma	G8877
HEPES	Roth	9105
Hexokinase	Roche	11 426 362 001
Hydrochloric acid, 37 %	Roth	4625
DL- β -Hydroxybutyl coenzyme A lithium salt	Sigma	H0261
Hydroxylamine hydrochloride	Sigma	159417
Imidazole	Sigma	I2399
Inosine 5'-triphosphate trisodium salt	Sigma	I0879
Iron(III) chloride hexahydrate	Sigma	31232
DL-Isocitric acid trisodium salt	Sigma	I1252
Isocitric dehydrogenase (NADP) solution, type IV: purified from porcine heart	Sigma	I2002
Isopropanol	Merck	1096342511
Kanamycin sulfate	Merck	420411
α -Ketoglutaric acid sodium salt (2-oxoglutarate)	Sigma	K1875
α -Ketoglutaric acid disodium salt dihydrate	Sigma	75892
L-Lactate dehydrogenase from rabbit muscle	Roche	10 127 876 001
Leupeptin hemisulfate	Roth	CN33
MagicMark™ XP Western Protein Standard	Invitrogen, Carlsbad, CA, USA	LC5602
Magnesium chloride hexahydrate	Roth	2189
Magnesium sulfate heptahydrate	Roth	P027
L-Malate dehydrogenase (L-MDH) from pig heart	Roche	10 127 248 001
L(-) Malic acid disodium salt	Sigma	M9138
Malonyl coenzyme A lithium salt	Sigma	M4263
Manganese(II) chloride	Sigma	328146
2-Mercaptoethanol	Roth	4227
Methanol, $\geq 99,5$ %	Roth	CP43
L-Methionine sulfoximine	Sigma	M5379
MOPS	Sigma	M1254
NAD, free acid, grade II, approx. 98%	Roche	10 127 990 001
NADH, disodium salt, grade II, approx. 98%	Roche	10 128 023 001

NADP, disodium salt approx. 98%	Roche	10 128 040 001
NADPH, tetrasodium salt, approx. 98%	Roche	10 107 824 001
Nickel(II) sulfate hexahydrate	Merck	1067270250
NucleoSpin® Plasmid Kit	Macherey-Nagel, Düren, Germany	740588
Oxaloacetate	Sigma	O4126
Oxamic acid sodium salt	Sigma	O2751
PageRuler™ Prestained Protein Ladder	Fermentas	SM0671
Peptone	Lab M, Lancs, UK	MC033
Peptone	BD	211677
Phenazine ethosulfate, approx. 95% (PES)	Sigma	P4544
Phenazine methosulfate	Sigma	P9625
Phenylmethanesulfonyl fluoride (PMSF)	Roth	6367
Phosphocreatine disodium salt hydrate	Sigma	P7936
Phospho(enol)pyruvate monopotassium salt	Sigma	860077
Phospho(enol)pyruvate monosodium Salt	Sigma	P0564
Phospho(enol)pyruvate carboxylase from corn	Sigma	P2023
6-Phosphogluconic acid trisodium salt, grade IV	Sigma	P7877
6-Phosphogluconic dehydrogenase, from yeast	Sigma	P4553
Phosphoglucose isomerase from baker's yeast	Sigma	P5381
D-(-)-3-Phosphoglyceric acid disodium salt	Sigma	P8877
3-Phosphoglyceric phosphokinase, from baker's yeast	Sigma	P7634
Phosphotransacetylase from <i>Bacillus stearothermophilus</i>	Sigma	P2783
Phusion Polymerase	Finnzymes (Thermo Scientific)	F-530S
Ponceau S	Roth	5938
Potassium chloride	Merck	1.04935.5000
Potassium dihydrogen phosphate	Merck	1048731000
Potassium hydroxide	Sigma	484016
Potassium phosphate dibasic trihydrate	Sigma	60349
Pyruvate decarboxylase, from baker's yeast	Sigma	P9474
Pyruvate dehydrogenase solution, from: porcine heart	Sigma	P7032
Pyruvate kinase (PK) from rabbit muscle	Roche	10 128 155 001
Pyruvate kinase preparation, type VII, from rabbit muscle	Sigma	P7768
Pyruvic acid 98%	Sigma	10736
Sodium pyruvate	Sigma	P8574
<i>Pichia</i> Expression Kit	Invitrogen	K1710-01
Purpald 99+%	Sigma	162892
Resazurin sodium salt	Sigma	199303
Restriction enzymes, different	New England Biolabs, Ipswich, MA, USA	
D-(-)-Ribose	Sigma	R7500
D-Ribose 5-phosphate disodium salt dihydrate	Sigma	83875
RNase A	Roth	7156
Saccharose	Sigma	84097

Sodium azide, purum p.a., ≥99.0%	Sigma	71290
Sodium bicarbonate	Merck	106329
Sodium chloride	Roth	P029
Sodium dodecyl sulfate (SDS)	Biomol, Hamburg, Germany	04051.1
Sodium hydroxide	Merck	1064950250
Sodium phosphate dibasic	Merck	1.06585.5000
D-Sorbitol	Sigma	85529
Succinic acid	Sigma	W502707
T4 DNA-Ligase	Promega, Madison, WI, USA	M1804
N,N,N',N'-Tetramethyl-ethylenediamine (TEMED)	Serva, Heidelberg, Germany	35925
Thiamine pyrophosphate	Sigma	C8754
Thiazolyl blue tetrazolium bromide (MTT)	Roth	4022
Trichloroacetic acid	Sigma	T6399
Tricine, ≥99%	Roth	6977
Triosephosphate isomerase	Roche	10 109 762 001
Triosephosphate isomerase preparation, from rabbit muscle	Sigma	T2391
TRIS	Roth	5429
TRIS-HCl	Roth	9090
Triton X-100	Sigma	X100
Trypan blue	Merck	1117320025
Trypsin (1:250) Powder	Gibco	27250-018
Tryptone	BD	211705
Tween® 20	Roth	9127
Uridine 5'diphosphoglucose disodium salt	Sigma	94335
Uridine 5'-triphosphate tris salt, type VI	Sigma	U6875
Uridine 5'-triphosphate trisodium salt hydrate	Sigma	U6625
Water, nuclease-free	Roth	T143
Wizard® SV Gel and PCR Clean-Up System	Promega	A9281
D-Xylulose 5-phosphate sodium salt	Sigma	X0754
D-(+)-Xylose	Sigma	X3877
Zymolase	Seikagaku Biobusiness, Tokyo, Japan	120493
Yeast Extract	BD	212750
Yeast Nitrogen Base (YNB) without amino acids	BD	291940

Table A2: List of Consumables

Name	Manufacturer	Cat. No.
6-well plates (Cellstar, 10 cm ²)	Greiner Bio-One, Solingen, Germany	657165
96-well plates (flat bottom)	Sarstedt, Nümbrecht, Germany	82.1581
96-well plates (flat and round bottom)	Greiner bio-one	655901 and 650101
Aluminum foil (425, core series 591)	3M Scotch, Neuss, Germany	
Amicon Ultra-15 Centrifugal Filter Units (10 kDA)	Millipore, Billerica, MA, USA	UFC901008
Bottle Top Filter	Nalgene, Rochester, NY, USA	595-4520
Centrifuge tubes (15 and 50 mL Cellstar Tubes)	Greiner Bio-One	188261 and 188271
Column, HisTrap™FF (1 mL)	GE Healthcare, München, Germany	17-5319-01
Column, HiTrap™Q HP (1 mL)	GE Healthcare	17-1153-01
Cuvettes (PMMA, 1.5 mL)	Brand, Wertheim, Germany	759085D
Filter Units (0.2 µm)	Nalge Nunc International Corp. (Nalgene)	161-0020
Glass beads (0.5 mm)	Roth	A553
Gloves (Nitrile 3000)	Meditrade, Kiefersfelden, Germany	1280
IMAC Sepharose 6 Fast Flow	GE Healthcare	17-0921-07
Micro pipette tips (10, 100, 200, 1000 and 5000 µL)	Eppendorf, Hamburg, Germany	
Microcentrifuge Tubes	Beckman Coulter, Krefeld, Germany	357448
Multichannel pipette tips (5-100 µL, 20-300 µL)	Eppendorf	
PCR thermo tubes (0.2 mL)	Peqlab, Erlangen, Germany	82-0337
Pipette tips (1, 2, 5, 10, 25, 50 mL)	Eppendorf	
PVDF Transfer Membranes	Millipore	IPVH09120
Reaction tubes (1.5 and 2 mL)	Eppendorf, Corning, VWR	
Syringes (Omnifix® 5, 10, 20, 50 mL)	B. Braun, Melsungen, Germany	
Syringe Filter Holders (Minisart® 0.2 and 0.45 µm)	Sartorius, Göttingen, Germany	16534 and 17824
T-Flasks (Cellstar 75 and 182 cm ²)	Greiner bio-one	658175 and 660175
Tubes, polystyrol	Greiner bio-one	191180

Table A3: List of Equipment

Name	Manufacturer	Model
Äkta™Purifier	GE Healthcare	
Autoclave	Certoclav Steriliser, Traun, Germany	CV-EL 12L
Autoclave	Tuttnauer Systec, Wettenberg, Germany	5075 ELVC Varioklav® 65T
Automatic cell counter	Beckman Coulter	Vi-CELL®
Balance	Mettler Toledo, Giessen, Germany	XS205 Dual Range
Balance	Mettler Toledo	PG5002-S and PG12001-S Delta Range
Balance	Mettler Toledo	XS32001L
Bioreactor	B. Braun Biotech International (Sartorius)	CT5-SK
Bioreactor	Sartorius	Biostat® B plus
Block heater	Grant, Shepreth, UK	QBT
Camera	Herolab, Wiesloch, Germany	Easy 429K
Cell counter	Beckmann Coulter	Vi-Cell™ XR
Centrifuge	Thermo Scientific	Heraeus® Biofuge primo R
Centrifuge	Hettich Lab, Tuttlingen, Germany	Mikro 200
Centrifuge	Beckman Coulter™	Avanti J-20 XP
Centrifuge	GrantBio, Hillsborough, NJ, USA	CV 3000
Centrifuge	Thermo Scientific	Heraeus® Fresco 17
Centrifuge	Thermo Scientific	Heraeus® Multifuge® 1S-R
Clean bench	Thermo Scientific	HERAsafe®
Column	GE Healthcare	XK 16/20
Darkroom	UVP, Upland, CA, USA	EpiChem II (EC2)
Drying Oven	Heraeus (Thermo Scientific)	T 6060
Electroporator	Thermo Electron Corporation, Milford, MA, USA	EquiBio Easyject prima
Electrophoresis System	Biorad, München, Germany	Mini-PROTEAN Tetra
Freeze dryer	Martin Christ, Osterode am Harz, Germany	Alpha 1-2
Freezer	Thermo Scientific	HERRAfreeze
Gel chamber	Biostep, Jahnsdorf, Germany	10 x 11.5 cm
High pressure homogenizer	Avestin, Mannheim, Germany	EmulsiFlex®-C5
Incubator	Heraeus (Thermo Scientific)	HERAcell® 240
Integrity testing of membrane filter systems	Sartorius	Sartocheck Junior BP-Plus
Ion chromatography	Dionex, Sunnyvale, CA, USA	BioLC system with eluent generator, DX320
Magnetic agitator	Mavag, Neunkirch, Switzerland	Type MDB 300
Magnetic Stirrer	IKA, Staufen, Germany	RET basic
Mass flow controller	Bronkhorst High-Tech, Ruurlo, The Netherlands	
Mass spectrometer	Applied Biosystems/MDS SCIEX, Darmstadt, Germany	nanoHPLC-nanoESI-MS/MS (QStar XL)
Metabolite analyzer	Nova Biomedical, Waltham, MA, USA	Bioprofile 100 Plus
Microscope	Zeiss, Göttingen, Germany	Axiovert 40C
Peristaltic pump	Ismatec, Glattbrugg, Switzerland	ISM832A

Peristaltic pump	Watson Marlow, Wilmington, MA, USA	SCI-Q 400
pH meter	WTW, Weilheim, Germany	Inolab pH/Cond level 1
Pipettes	Eppendorf	5, 10, 100, 1000, 5000 μ L
Pipetting aid	Hirschmann Laborgeräte, Eberstadt, Germany	Pipetus®
Power supply system	Biorad	PowerPac 300
Process control system	Siemens, München, Germany	simtec7
Research® pro pipettes, single channel	Eppendorf	0.5-10 μ L, 5-100 μ L
Research® pro pipettes, 8-channel	Eppendorf	5-100 μ L, 20-300 μ L
Scanner	Umax	
Shaker	Kühner, Birsfelden, Germany	ISF-1-W
Software	Herolab, Wiesloch, Germany	EasyWin 32 V.3.01
Software	Biotek, Winooski, VT, USA	Gen5 ver. 1.05.11
Spectrophotometer	Peqlab	NanoDrop ND-1000
Spectrophotometer	Amersham (GE Healthcare)	Ultrospec 500 pro
Spectrophotometer, plate reader	Biotek	ELx 808 and PowerWave XS
Spectrophotometer, plate reader	Tecan, Männedorf, Switzerland	Rainbow Spectra
Superloop™	GE Healthcare	50 and 150 mL
Thermomixer	Eppendorf	comfort
Thermocycler	Biometra, Göttingen, Germany	T3000
Ultrasonic bath	VWR, Darmstadt, Germany	USC600D
Ultrapure Water Purification System	Millipore	Milli-Q-Biocel A10 and Milli-Q-Gradient A10
UV Transilluminator	Life Technologies, Grand Island, NY, USA	TFX-20M
Vacuum pump	Vacuubrand, Wertheim, Germany	MZ2C
Vortexer	Scientific Industries, Bohemia, NY, USA	Vortex-Genie®
Vortexer	Heidolph, Schwabach, Germany	Reax Control

B. Microorganisms, expression vector, primers

E. coli TOP10F' strain (Invitrogen, Carlsbad, CA, USA)

Genotype: F' (proAB, lacIq, lacZΔM15, Tn10 (Tet^R)) mcrA, Δ(mrr-hsdRMS-mcrBC), φ80lacZΔM15, ΔlacX74, deoR, recA1, araD139, Δ(ara-leu)7697, galU, galK, rpsL (Str^R), endA1, nupG λ⁻

P. pastoris GS115 (*his4*; Mut⁺) yeast strain from Invitrogen

Genotype: *his4*, Phenotype: Mut⁺

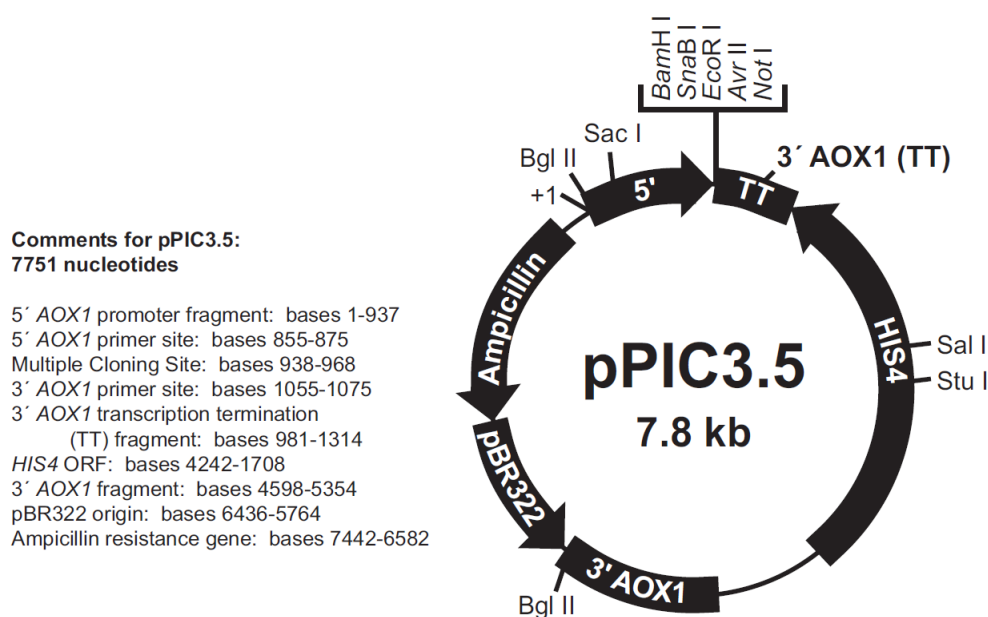


Figure B1: Map of pPIC3.5 (www.invitrogen.com).

Table B1: Overview of the used primers.

Primer name	Base sequence
5' AOX1	5'-GACTGGTTCCAATTGACAAGC-3'
3' AOX1	5'-GCAAATGGCATTCTGACATCC-3'
T7	5'-TAATACGACTCACTATAGGG-3'
GKfor_AvrII	5'-GCTACCTAGGATGAAACATCACCATCACCA-3'
GKrev_NotI	5'-GTCAGCGCCGCTCGAATTCTTAGTCATTGTTCTGA-3'

C. *E. coli* and *P. pastoris* media recipes

Table C1: Media for the cultivation of *P. pastoris*.

Bezeichnung	Komponente	Konzentration
YPD	Yeast extract	1 % (w/v)
	Peptone	2 % (w/v)
	Glucose	2 % (w/v)
	Agar (for solid medium)	2 % (w/v)
MD	YNB*	1.34 % (w/v)
	Glucose	2 % (w/v)
	Biotin	4 x 10 ⁻⁵ % (w/v)
	Agar (for solid medium)	1.5 % (w/v)
MM	YNB*	1.34 % (w/v)
	Methanol	1 % (v/v)
	Biotin	4 x 10 ⁻⁵ % (w/v)
	Agar (for solid medium)	1.5 % (w/v)
BMG	Potassium phosphate buffer, pH 6.0	100 mM
	YNB*	1.34 % (w/v)
	Glycerol	1 % (v/v)
	Biotin	4 x 10 ⁻⁵ % (w/v)
BMM	Potassium phosphate buffer, pH 6.0	100 mM
	YNB*	1.34 % (w/v)
	Methanol	1 % (v/v)
	Biotin	4 x 10 ⁻⁵ % (w/v)
BSM pH 5 (NH ₃)	H ₃ PO ₄ (85 %)	2.67 % (v/v)
	CaSO ₄	0.93 g/L
	K ₂ SO ₄	18.2 g/L
	MgSO ₄ x 7H ₂ O	14.9 g/L
	KOH	4.13 g/L
	Glycerol	40 g/L
	PTM ₁ trace salts	0.435 % (v/v)
PTM₁ Trace salts solution	CuSO ₄	6 g/L
	NaI	0.08 g/L
	MnSO ₄ x H ₂ O	3 g/L
	NaMoO ₄ x 2H ₂ O	0.2 g/L
	H ₃ BO ₃	0.02 g/L
	CoCl ₂	0.5 g/L
	ZnCl ₂	20 g/L
	FeSO ₄ x 7H ₂ O	65 g/L
	Biotin	0.2 g/L
	H ₂ SO ₄ (95-98 %)	0.5 % (v/v)

*YNB - Yeast Nitrogen Base with ammonium sulfate without amino acids. Glycerol, Methanol, Glucose, YNB (each with 10X), biotin (500X), potassium Phosphate (1 M) and PTM₁ were sterile filtered.

Table C2: Media for the cultivation of *E. coli*.

Name	Component	Concentration
LB-Kanamycin pH 7.0 (NaOH)	Tryptone	10 g/L
	NaCl	10 g/L
	Yeast extract	5 g/L
	Kanamycin	25 µg/mL
	Agar (for solid medium)	15 g/L
LB-Ampicillin pH 7.0 (NaOH)	Tryptone	10 g/L
	NaCl	10 g/L
	Yeast extract	5 g/L
	Ampicillin	100 µg/mL
	Agar (for solid medium)	15 g/L

Ampicillin (10 mg/mL in 50 % (v/v) EtOH) and kanamycin (2.5 mg/mL in H₂O) were added separately.

D. Molecular biology: Solutions, preparations and techniques

Table D1: Media and solutions for the transformation of *E. coli*.

Name	Component	Concentration
Psi broth	Yeast extract	5 g/L
	Tryptone	20 g/L
	MgSO ₄	5 g/L
Tfbl pH 5.8 (acetic acid)	KAc	30 mM
	RbCl ₂	100 mM
	CaCl	10 mM
	MnCl ₂ 4 H ₂ O	50 mM
	Glycerin	15 % (v/v)
TfbII pH 6.5 (NaOH)	MOPS	10 mM
	CaCl ₂	75 mM
	RbCl ₂	10 mM
	Glycerin	15 % (v/v)
SOC	Tryptone	20 g/L
	Yeast extract	5 g/L
	NaCl	10 mM
	KCl	2.5 mM
	MgCl ₂	10 mM
	MgSO ₄	10 mM
	D-Glucose	20 mM

SOC: MgCl₂ and MgSO₄ (both 100X), as well as D-Glucose (50X) were sterile filtered.

Table D2: Solutions for agarose gel electrophoresis.

Name	Component	Concentration
10x TPE buffer pH 7.5 (Phosphoric acid)	Tris	108 g/L
	EDTA	0.744 g/L
5x Loading Dye	Glycerin	30 % (v/v)
	Bromphenol blue	0.001 % (w/v)
	Xylencyanol	0.001 % (w/v)
	EDTA	50 mM
Ethidium bromide solution	Ethidium bromide	0.01 % (v/v)

Table D3: Solutions for the plasmid preparation from *E. coli*.

Name	Component	Concentration
AE buffer pH 8.5 (HCl)	Tris	5 mM
Lysispuffer	Tris	50 mM
	EDTA	50 mM
	Saccharose	15 % (w/v)
SDS/NaOH solution	NaOH	200 mM
	SDS	1 % (w/v)
KAc solution	KAc	3 M
	Acetic acid	11.5 % (v/v)
Easyprep-Puffer pH 8.0 (HCl)	Tris	10 mM
	EDTA	1 mM
	Saccharose	15 % (w/v)
	RNase A	0.4 mg/mL
	Lysozyme	2 mg/mL
	BSA	0.1 mg/mL

Table D4: Solutions for the isolation of genomic DNA from *P. pastoris*.

Name	Component	Concentration
SCED pH 7.5	Sorbitol	1 M
	Na-Citrate	10 mM
	EDTA	10 mM
	DTT	10 mM
TE-Puffer pH 7.5 (HCl)	Tris	10 mM
	EDTA	1 mM

DTT (100X) was added freshly.

Table D5: Restriction medium for pPIC3.5.

Components	Volume
AvrII (4 U/μL)	2 μL
NotI (10 U/μL)	2 μL
NEB2 buffer (10x)	3 μL
BSA (10x)	3 μL
Plasmid-DNA (ca. 250 ng/μL)	20 μL

Table D6: Restriction medium for pETM11-GK.

Components	Volume
XbaI (20 U/ μ L)	1 μ L
NotI (10 U/ μ L)	1 μ L
NEB3 buffer (10x)	3 μ L
BSA (10x)	3 μ L
Plasmid-DNA (ca. 100 ng/ μ L)	22 μ L

Table D7: Restriction medium for analysis of plasmid DNA.

Components	Volume
NdeI (20 U/ μ L)	0.25 μ L
Plasmid-DNA (ca. 250 ng/ μ L)	5 μ L
NEB4 buffer (10x)	1 μ L
BSA (10x)	1 μ L
Water	2.75 μ L

Table D8: Optimized PCR medium (50 μ L) for the amplification of GK.

Components	Volume
5x HF Puffer	10 μ L
dNTPs (10 mM)	1 μ L
MgCl ₂ (50 mM)	1.5 μ L
Phusion Polymerase (2 U/ μ L)	0.5 μ L
GKfor_AvrII (15 pmol/ μ L)	7.5 μ L
GKrev_NotI (15 pmol/ μ L)	7.5 μ L
pETM11-GK DNA (9 ng/ μ L)	4 μ L
H ₂ O (sterile, nuclease-free)	22 μ L

Table D9: PCR program used for the amplification of GK.

Step	Temperature	Time	Cycles
Initial denaturation	98 °C	30 s	1
Denaturation	98 °C	10 s	
Hybridization	64 °C	30 s	30
Elongation	72 °C	70 s	
Final elongation	72 °C	10 min	1
Cooling	4 °C	hold	1

Table D10: Optimized PCR medium (20 μ L) for the amplification of pPIC3.5-GK transformants.

Components	Volume
5x Go Taq Puffer	4 μ L
dNTPs (10 mM)	0.5
MgCl ₂ (25 mM)	1.2 μ L
Go Taq Polymerase (5 U/ μ L)	0.1 μ L
GKfor_AvrII (15 pmol/ μ L)	0.7 μ L
GKrev_NotI (15 pmol/ μ L)	0.7 μ L
genomic DNA (100 ng/ μ L) or Plasmid DNA (5 ng/ μ L)	1 μ L
H ₂ O (sterile, nuclease-free)	11.8 μ L

Table D11: Optimized PCR medium (20 μ L) for the amplification of pPIC3.5 transformants.

Components	Volume
5x Go Taq Puffer	4 μ L
dNTPs (10 mM)	0.5
MgCl ₂ (25 mM)	1.2 μ L
Go Taq Polymerase (5 U/ μ L)	0.1 μ L
5' AOX1 (15 pmol/ μ L)	0.7 μ L
3' AOX1 (15 pmol/ μ L)	0.7 μ L
genomic DNA (100 ng/ μ L) or Plasmid DNA (5 ng/ μ L)	1 μ L
H ₂ O (sterile, nuclease-free)	11.8 μ L

Table D12: PCR program used for the analysis of the *Pichia* clones (pPIC3.5-GK).

Step	Temperature	Time	Cycles
Initial denaturation	96 °C	2 min	1
Denaturation	95 °C	30 s	
Hybridization	64 °C	45 s	30
Elongation	72 °C	1.45 min	
Final elongation	72 °C	10 min	1
Cooling	4 °C	hold	1

Table D13: PCR program used for the analysis of the *Pichia* clones (pPIC3.5).

Step	Temperature	Time	Cycles
Initial denaturation	96 °C	2 min	1
Denaturation	95 °C	30 s	
Hybridization	55 °C	45 s	30
Elongation	72 °C	1.45 min	
Final elongation	72 °C	10 min	1
Cooling	4 °C	hold	1

Table D14: Buffers and solutions used for the purification of GK.

Buffer/Solution	Components	Concentration	
Extraction buffer	Sodium phosphate pH 7.4	50	mM
	Benzamidine	1	mM
	ϵ -Aminocaproic acid	1	mM
	Leupeptin	0.02	mM
	DTT	0.5	mM
	PMSF	1	mM
	Triton X-100	1	% (v/v)
	Glycerol	5	% (v/v)
	MgCl ₂	1	mM
Cleaning solution (homogenizer)	Isopropanol	50	% (v/v)
Equilibration buffer (IMAC)	Sodium phosphate pH 7.4	50	mM
	NaCl	0.5	M
	Imidazole	20	mM
Elution buffer (IMAC)	Sodium phosphate pH 7.4	50	mM
	NaCl	0.5	M
	Imidazole	500	mM
Stripping buffer	Sodium phosphate pH 7.4	20	mM
	NaCl	0.5	M
	EDTA	50	mM
CIP (Cleaning-in-Place) solution	NaOH	1	M
Recharging Solution	NiSO ₄	0.1	M
Storage Solution	Ethanol	20	% (v/v)
Equilibration buffer (AAC)	Sodium phosphate pH 6.8	15	mM
Elution buffer (AAC)	Sodium phosphate pH 6.8	15	mM
	NaCl	1	M
Storage buffer	Glycerol	50	% (v/v)
	Sodium phosphate pH 7.4	10	mM

Table D15: Buffers and solutions used for the analysis of protein samples.

Buffer/Solution	Components	Concentration/ Volume	
Reducing buffer (4X)	Tris-HCl pH 6.8	0.25	M
	Glycerol	40	% (v/v)
	SDS	6	% (w/v)
	Bromphenol blue	0.05	% (w/v)
	β -Mercaptoethanol	10	% (w/v)
Non-reducing buffer (4X)	Tris-HCl pH 6.8	0.25	M
	Glycerol	40	% (v/v)
	SDS	6	% (w/v)
	Bromphenol blue	0.05	% (w/v)
Electrophoresis buffer (10X)	SDS	1	% (w/v)
	Glycine	1.92	M
	Tris	0.25	M
Separating gel buffer	Tris-HCl pH 8.8	1.5	M
Stacking gel buffer	Tris-HCl pH 6.8	0.5	M
Separating gel (2X, 10 %)	H ₂ O	3.97	mL
	Acrylamide	3.33	mL
	Separating gel buffer	2.5	mL
	SDS (10 % w/v)	100	μ L
	APS (10 % w/v)	100	μ L
	TEMED	10	μ L
Stacking gel (2X, 3 %)	H ₂ O	6.3	mL
	Acrylamide	1	mL
	Stacking gel buffer	2.5	mL
	SDS (10 % w/v)	100	μ L
	APS (10 % w/v)	100	μ L
	TEMED	10	μ L
Washing buffer	PBS		
	(NaCl	8	g/L
	KCl	0.2	g/L
	KH ₂ PO ₄	0.2	g/L
	Na ₂ HPO ₄	1.15	g/L
	Tween 20	0.05	% (v/v)

E. Vector sequences

(Linear) MAP of: pETM11-PfGK1 check: 2848 from: 1 to: 2113

pETM11/*Pichia farinosa* glycerol kinase 1
 expression of N-terminal His6-tagged **PK98** glycerokinase 1
 CDS 94-2064

A)

September 3, 2007 15:59 ..

```

1  gaaattaatacgaactactataggggaattgtgagcggataacaattccctctagaat
-----+-----+-----+-----+-----+-----+-----+
a  E I N T T H Y R G I V S G * Q F P S R N - a
61  aatthttgatttaactttaagaaggagatataaccATGAACATCACCATCACCATCACCCC
-----+-----+-----+-----+-----+-----+-----+
a  N F D L T L R R R Y T M K H H H H H H H E - a
121  ATGAGCGATTACGACATCCCCACTACTGAGAATCTTTATTTTCAGGGCGCCATGGTAGCT
-----+-----+-----+-----+-----+-----+-----+
a  M S D Y D I P T T E N L Y F Q G A N V R - a
181  CGTCAAAGTAACGCCCTACGCATCCATTAATGCAATCCATGATATTGGAACCACTTCG
-----+-----+-----+-----+-----+-----+-----+
a  F Q S N A P T H E L L A S I D I S T T S - a
241  GCGAGAACCATCTGTTGATGAACATGGAACCGAAATGCCAAGAATCAGATCGAGTAT
-----+-----+-----+-----+-----+-----+-----+
a  R T I L F P D E M G T E I A K N V I E - a
301  TCTACCACGGCCCTCGGAGGCGCGGCTGATCCAAAAATAGGAACAATTTAGAAGAAGS
-----+-----+-----+-----+-----+-----+-----+
a  T T A D E A F A D S K N K P Q S R S R - a
361  TCTTCCTTGATGAGGCATAATGAGCCATTTTCAGTGTGAGGGTATTGCCATTTGCAAT
-----+-----+-----+-----+-----+-----+-----+
a  S L L M K H N E P I T S A E S I A I S I - a
421  ACTGACGATGTTATGATCGAAAACACGCTGCCAGCGTTGGTCCAACTTTGCGTTATCTCT
-----+-----+-----+-----+-----+-----+-----+
a  F E D V H I E N N A A S V S P T L R Y R - a
481  AAGCCAGGTTGGGTTGAGTGTATGCGCTGIGACACATATTGGCAAACGGGTCAGTGTGTTA
-----+-----+-----+-----+-----+-----+-----+
a  F G R V V E C H I V H I L A N A V D S I - a

```

B)

```

41  GCTGCATCCTTGATAACCTTGGTAAGATCAACCAGAATCCCGCTCTCAAGATCAAGTAC
-----+-----+-----+-----+-----+-----+-----+
a  A A S I I T L R K I N Q N P A L K I K -
601  AAGTGAAAGCAATAGGTATTGCTAACATGAGAGAGACCAGCATCGTATGTTCTCGTAAA
-----+-----+-----+-----+-----+-----+-----+
a  V K A I G I A N H P E T T I V W S R -
661  ACAGGAAAGCCATTGAGCAATGGTATGCACCTGGACTGATACGAGAATCCAGAAATCGTG
-----+-----+-----+-----+-----+-----+-----+
a  G E K I L L S N G I L W T D T E T A E -
721  CAGCACTTAGAACGTATGACAGATGACGAGAAAAGGCTGAATGAACCGAAAACCGGT
-----+-----+-----+-----+-----+-----+-----+
a  C H L E R N T D D E K K A E L N Q K T -
781  AATGGAGAAAGTGGATGAAAAGTCGACGGTCAATGCAACCAATATCTATTACTACTA
-----+-----+-----+-----+-----+-----+-----+
a  F L E T V F S A A K L R W I L L E N D -
841  ACAATTAGAGAAGATGATGAGAAGCGAAGGCAATTAATGTTTGAACCTGTTGACACT
-----+-----+-----+-----+-----+-----+-----+
a  I R E D Y E K G E G N I H F G I V D -
901  ACCAATTAGATGTTGACTGCTTCTTTTGAAGAAAACAGCTACAGTGTTCGCGGAT
-----+-----+-----+-----+-----+-----+-----+
a  N I L I Y N M E X E K S E V S E V T N A -
961  AGAACATATTCATGGACTTGAAAACGAAAGATTACGACGATGAGTTATTAGAGTTCTGG
-----+-----+-----+-----+-----+-----+-----+
a  S T Y E M D L E T K D Y D D E L L E E F -
1021  CTGTAGCTAGGATGATCCTAGACAACCGGTTTCAACACAGTTCAAGACTTAAAATACCA
-----+-----+-----+-----+-----+-----+-----+
a  F I D E T R I C L E P K I V S S S E E V Y -
1081  TCGTTTGTACTCCTAECTTACTAECTTAGGATTCCATAATAAGATTGACACCCCTGGG
-----+-----+-----+-----+-----+-----+-----+
a  S P A T P N L S N L G P H R K I H T L -
1140  AGCAAACGATGAGGATTGAATAGATTGAATCCTAAGGTATTATTCTAAGTGGGACCCG

```

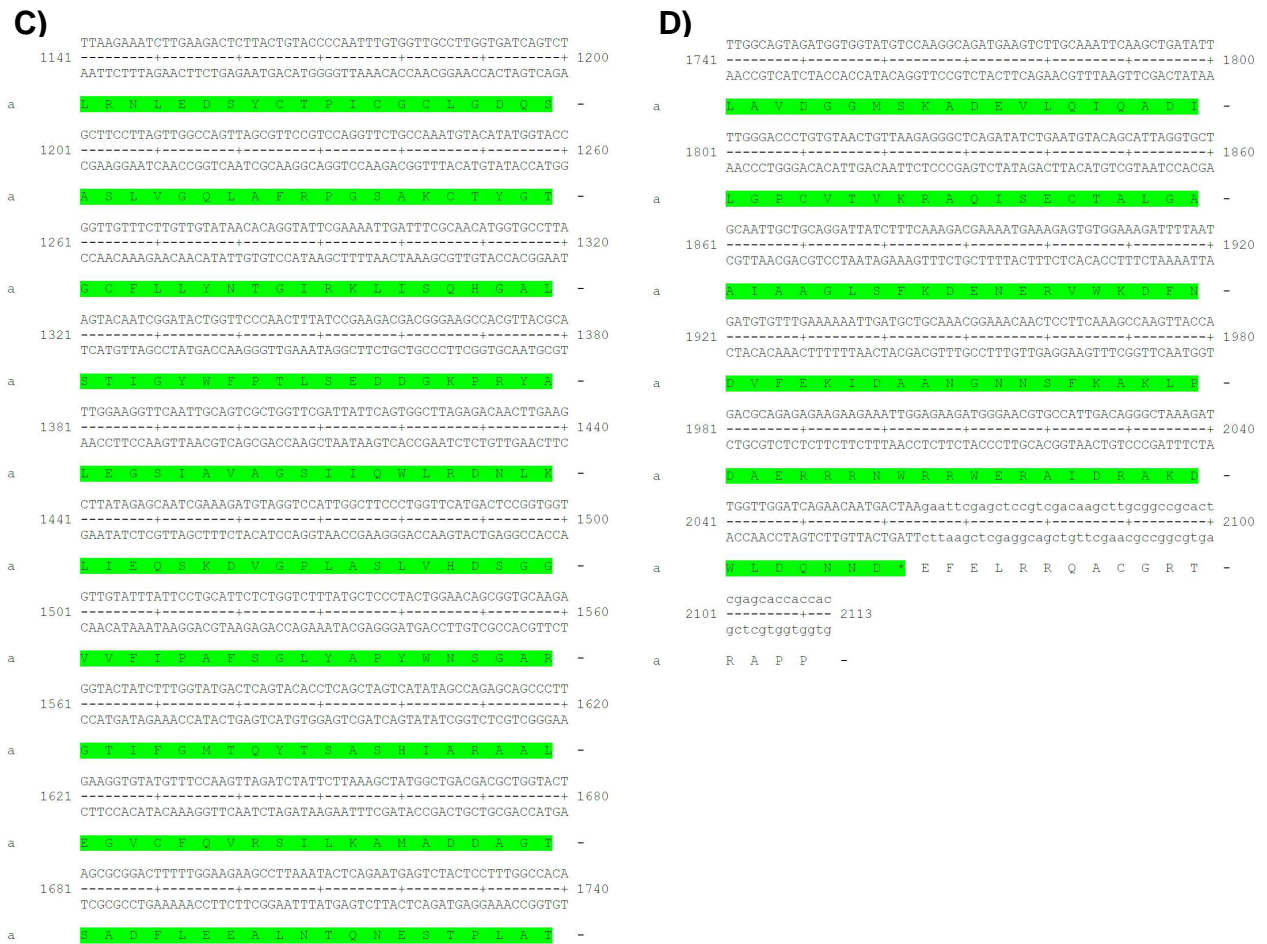


Figure E1: A-D) Sequence of the glycerokinase gene from *P. farinosa* (*GUT1*) in pETM11-GK.

BLAST 2 SEQUENCES RESULTS VERSION BLASTN 2.2.18 [Mar-02-2008]:

Sequence 1: pETM11-GK

Length = 2872 (1 .. 2872)

Sequence 2: pETM11-GK clone 3 - T7 primer

Length = 1002 (1 .. 1002)

Score = 1856 bits (965), Expect = 0.0
 Identities = 976/980 (99%), Gaps = 1/980 (0%)
 Strand=Plus/Plus

```

Query 393 AAATAATTTTGATTAACTTTAAGAAGGAGATATACCATGAAACATCACCATCACCATCA 452
      |||
Sbjct 1 AAATAATTTTG-TTTAACTTTAAGAAGGAGATATACCATGAAACATCACCATCACCATCA 59

Query 453 CCCCATGAGCGATTACGACATCCCCTACTGAGAATCTTTATTTTCAGGGCGCCATGGT 512
      |||
Sbjct 60 CCCCATGAGCGATTACGACATCCCCTACTGAGAATCTTTATTTTCAGGGCGCCATGGT 119

Query 513 ACGTCGTCAAAGTAACGCCCTACGCATCCATTAATGTCATCCATTGATATTGGAACCAC 572
      |||
Sbjct 120 ACGTCGTCAAAGTAACGCCCTACGCATCCATTAATGTCATCCATTGATATTGGAACCAC 179

Query 573 TTCGGCGAGAACCATCTTGTTTGATGAACATGGAACCGAAATGCCAAGAATCAGATCGA 632
      |||
Sbjct 180 TTCGGCGAGAACCATCTTGTTTGATGAACATGGAACCGAAATGCCAAGAATCAGATCGA 239

Query 633 GTATTCTACCACGCCCTCGGAGGCGCGGCTGATTCCAAAAATAAGGAACAATTTAGAAG 692
      |||
Sbjct 240 GTATTCTACCACGCCCTCGGAGGCGCGGCTGATTCCAAAAATAAGGAACAATTTAGAAG 299

Query 693 AAGGTCCTTCTTGATGAGGCATAATGAGCCATTTTCAGTGTGAGGGTATTGCCATTTC 752
      |||
Sbjct 300 AAGGTCCTTCTTGATGAGGCATAATGAGCCATTTTCAGTGTGAGGGTATTGCCATTTC 359

Query 753 GATTACTGACGATGTTATGATCGAAAAACGCTGCCAGCGTTGGTCCAACCTTTCGCTTA 812
      |||
Sbjct 360 GATTACTGACGATGTTATGATCGAAAAACGCTGCCAGCGTTGGTCCAACCTTTCGCTTA 419

Query 813 TCCTAAGCCAGGTTGGGTTGAGTGTATGCCTGTGCACATATTGGCAAACGCGTCCAGTG 872
      |||
Sbjct 420 TCCTAAGCCAGGTTGGGTTGAGTGTATGCCTGTGCACATATTGGCAAACGCGTCCAGTG 479

Query 873 TTTAGCTGCATCCTTGATAACCTTGCGTAAGATCAACCAGAATCCCCTCTCAAGATCAA 932
      |||
Sbjct 480 TTTAGCTGCATCCTTGATAACCTTGCGTAAGATCAACCAGAATCCCCTCTCAAGATCAA 539

Query 933 GTACAAGTGAAAGCAATAGGTATTGCTAACATGAGAGAGACCACGATCGTATGGTCTCG 992
      |||
Sbjct 540 GTACAAGTGAAAGCAATAGGTATTGCTAACATGAGAGAGACCACGATCGTATGGTCTCG 599

Query 993 TAAAACAGGAAAGCCATTGAGCAATGGTATCACCTGGACTGATACGAGAAGTGCAGAAAT 1052
      |||
Sbjct 600 TAAAACAGGAAAGCCATTGAGCAATGGTATCACCTGGACTGATACGAGAAGTGCAGAAAT 659

Query 1053 CGTGCAACCTTAGAACGTATGACAGATGACGAGAAAAAGGCTGAATTGAACCGAAAAAC 1112
      |||
Sbjct 660 CGTGCAACCTTAGAACGTATGACAGATGACGAGAAAAAGGCTGAATTGAACCGAAAAAC 719

Query 1113 CGGTTTACCTCTTTCAACCTACTTTTCAGCTGCCAAGTTACGTTGGTTATTAGATAATGA 1172
      |||
Sbjct 720 CGGTTTACCTCTTTCAACCTACTTTTCAGCTGCCAAGTTACGTTGGTTATTAGATAATGA 779

Query 1173 TGATACAATTAGAGAAGAGTATGAGAAAGGCGAAGGCAATTTAATGTTTGGAACTGTTGA 1232
      |||
Sbjct 780 TGATACAATTAGAGAAGAGTATGAGAAAGGCGAAGGCAATTTAATGTTTGGAACTGTTGA 839

Query 1233 CACTTGGTTAATCTACAACATGACGAAAGAAAAATCTTTTGTTCGGATGTCACAAACGC 1292
      |||
Sbjct 840 CACTTGGTTAATCTACAACATGACGAAAGAAAAATCTTTTGTTCGNATGTCACAAACGC 899

Query 1293 CTCAAGAACATATTTTCATGGACTTGGAACGAAGGATTACGACGATGAGTTATTAGAGTT 1352
      |||
Sbjct 900 CTCAAGAACATATTTTCATGGACTTGGAACGAAGGATTACGACGATGAGTTATTAGAGTT 959

Query 1353 CTGGGACATCGATCCTACTA 1372
      |||
Sbjct 960 CTGGGACNTCGATCCTACTA 979

```

Sequence 1: pPIC3.5-GK

Length = 3012 (1 .. 3012)

Sequence 2: pPIC3.5-GK clone 24 - 5'AOX primer

Length = 986 (1 .. 986)

Score = 1859 bits (967), Expect = 0.0
 Identities = 976/978 (99%), Gaps = 1/978 (0%)
 Strand=Plus/Plus

```

Query 413  ACTTGAGAAGATCAAAAAACAATAATTATTCGAAGGATCCTACGTAGAAATCCCTAGAA 472
          |||
Sbjct 10   ACTTGAGAAGATCAAAAAACAATAATTATTCGAAGGATCCTACGTAGAAATCCCTAGAA 69

Query 473  ATAATTTTGATTTAACTTTAAGAAGGAGATATACCATGAAACATCACCATCACCATCACC 532
          |||
Sbjct 70   ATAATTTTG- TTTAACTTTAAGAAGGAGATATACCATGAAACATCACCATCACCATCACC 128

Query 533  CCATGAGCGATTACGACATCCCCACTACTGAGAATCTTTATTTTCAGGGCGCCATGGTAC 592
          |||
Sbjct 129  CCATGAGCGATTACGACATCCCCACTACTGAGAATCTTTATTTTCAGGGCGCCATGGTAC 188

Query 593  GTCGTCAAAGTAACGCCCTACGCATCCATTAATTGCATCCATTGATATTGGAACCACTT 652
          |||
Sbjct 189  GTCGTCAAAGTAACGCCCTACGCATCCATTAATTGCATCCATTGATATTGGAACCACTT 248

Query 653  CGGCGAGAACCATCTTGTGATGAACATGGAACCGAAATGCCAAGAATCAGATCGAGT 712
          |||
Sbjct 249  CGGCGAGAACCATCTTGTGATGAACATGGAACCGAAATGCCAAGAATCAGATCGAGT 308

Query 713  ATTCTACCACGGCTCGGAGGCGCGGCTGATTCAAAAATAAGGAACAATTTAGAAGAA 772
          |||
Sbjct 309  ATTCCACCACGGCTCGGAGGCGCGGCTGATTCAAAAATAAGGAACAATTTAGAAGAA 368

Query 773  GGTCTTCTTGATGAGGCATAATGAGCCCATTTTCAGTGTGAGGGTATTGCCATTTTGA 832
          |||
Sbjct 369  GGTCTTCTTGATGAGGCATAATGAGCCCATTTTCAGTGTGAGGGTATTGCCATTTTGA 428

Query 833  TTACTGACGATGTTATGATCGAAAAACAACGCTGCCAGCGTTGGTCCAACCTTTGCGTTATC 892
          |||
Sbjct 429  TTACTGACGATGTTATGATCGAAAAACAACGCTGCCAGCGTTGGTCCAACCTTTGCGTTATC 488

Query 893  CTAAGCCAGGTTGGGTTGAGTGTATGCCTGTGCACATATTGGCAAACGCGGTCCAGTGT 952
          |||
Sbjct 489  CTAAGCCAGGTTGGGTTGAGTGTATGCCTGTGCACATATTGGCAAACGCGGTCCAGTGT 548

Query 953  TAGCTGCATCCTTGATAACCTTGCGTAAGATCAACCAGAAATCCCGCTCTCAAGATCAAGT 1012
          |||
Sbjct 549  TAGCTGCATCCTTGATAACCTTGCGTAAGATCAACCAGAAATCCCGCTCTCAAGATCAAGT 608

Query 1013 ACAAGGTGAAAGCAATAGGTATTGCTAACATGAGAGAGACCAGATCGTATGGTCTCGTA 1072
          |||
Sbjct 609  ACAAGGTGAAAGCAATAGGTATTGCTAACATGAGAGAGACCAGATCGTATGGTCTCGTA 668

Query 1073 AAACAGGAAAGCCATTGAGCAATGGTATCACCTGGACTGATACGAGAATCGAGAAATCG 1132
          |||
Sbjct 669  AAACAGGAAAGCCATTGAGCAATGGTATCACCTGGACTGATACGAGAATCGAGAAATCG 728

Query 1133 TGCAGCACTTAGAACGTATGACAGATGACGAGAAAAAGGCTGAATTGAACAGAAAAACCG 1192
          |||
Sbjct 729  TGCAGCACTTAGAACGTATGACAGATGACGAGAAAAAGGCTGAATTGAACAGAAAAACCG 788

Query 1193 GTTTACCTCTTTCAACCTACTTTTCAGCTGCCAAGTTACGTTGGTTATTAGATAATGATG 1252
          |||
Sbjct 789  GTTTACCTCTTTCAACCTACTTTTCAGCTGCCAAGTTACGTTGGTTATTAGATAATGATG 848

Query 1253 ATACAATTAGAGAAGAGTATGAGAAAGCGAAGGCAATTTAATGTTTGGAACTGTTGACA 1312
          |||
Sbjct 849  ATACAATTAGAGAAGAGTATGAGAAAGCGAAGGCAATTTAATGTTTGGAACTGTTGACA 908

Query 1313 CTTGGTTAATCTACAACATGACGAAAGAAAAATCTTTTGTTCGGATGTCACAAACGCCT 1372
          |||
Sbjct 909  CTTGGTTAATCTACAACATGACGAAAGAAAAATCTTTTGTTCGGATGTCACAAACGCCT 968

Query 1373 CAAGAACATATTTTATGG 1390
          |||
Sbjct 969  CAAGAACATATTTTATGG 986

```

Sequence 1: pPIC3.5-GK

Length = 3012 (1 .. 3012)

Sequence 2: pPIC3.5-GK clone 24 - 3'AOX primer

Length = 1021 (1 .. 1021)

```

Score = 1884 bits (980), Expect = 0.0
Identities = 1012/1021 (99%), Gaps = 3/1021 (0%)
Strand=Plus/Minus

Query 1560 AAATCTTGAAGACTCTTACTG-TACCCCAATTTGTGGTTGCC-TTGGTGATCAGTCTGCT 1617
          |||
Sbjct 1021 AAATCTTGAAGACTCTTACTGGTACCCCAATTTGTGGTTGCCNTTGGTGATCAGTCTGCT 962

Query 1618 TCC-TTAGTTGGCCAGTTAGCGTTCGTCAGGTTCTGCCAAATGTACATATGGTACCGG 1676
          |||
Sbjct 961 TCCNTTAGTTGGCCAGTTAGCGTTCGTCAGGTTCTGCCAAATGTACATATGGTACCGG 902

Query 1677 TTGTTTCTTGTGTATAACACAGGTATTCGAAAATTGATTTGCAACATGGTGCCTTAAG 1736
          |||
Sbjct 901 TTGTTTCTTGTGTATAACACAGGTATTCGAAAATTGATTTGCAACATGGTGCCTTAAG 842

Query 1737 TACAATCGGATACTGGTCCCACTTTATCCGAAGACGACGGGAAGCCACGTTACGCATT 1796
          |||
Sbjct 841 TACAATCGGATACTGGTCCCACTTTATCCGAAGACGACGGGAAGCCACATTACGCATT 782

Query 1797 GGAAGGTTCAATTGCAGTCGCTGGTTCGATTATTCAGTGGCTTAGAGACAACCTGAAGCT 1856
          |||
Sbjct 781 GGAAGGTTCAATTGCAGTCGCTGGTTCGATTATTCAGTGGCTTAGAGACAACCTGAAGCT 722

Query 1857 TATAGAGCAATCGAAAGATGTAGGTCCATTGGCTTCCCTGGTTCATGACTCCGGTGGTGT 1916
          |||
Sbjct 721 TATAGAGCAATCGAAAGATGTAGGTCCATTGGCTTCCCTGGTTCATGACTCCGGTGGTGT 662

Query 1917 TGTATTTATTCCTGCATTCTCTGGTCTTTATGCTCCCTACTGGAACAGCGGTGCAAGAGG 1976
          |||
Sbjct 661 TGTATTTATTCCTGCATTCTCTGGTCTTTATGCTCCCTACTGGAACAGCGGTGCAAGAGG 602

Query 1977 TACTATCTTTGGTATGACTCAGTACACCTCAGCTAGTCATATAGCCAGAGCAGCCCTTGA 2036
          |||
Sbjct 601 TACTATCTTTGGTATGACTCAGTACACCTCAGCTAGTCATATAGCCAGAGCAGCCCTTGA 542

Query 2037 AGGTGTATGTTTCCAAGTTAGATCTATTCTTAAAGCTATGGCTGACGACGCTGGTACTAG 2096
          |||
Sbjct 541 AGGTGTATGTTTCCAAGTTAGATCTATTCTTAAAGCTATGGCTGACGACGCTGGTACTAG 482

Query 2097 CGCGGACTTTTTGGAAGAAGCCTTAAATACTCAGAATGAGTCTACTCCTTTGGCCACATT 2156
          |||
Sbjct 481 CGCGGACTTTTTGGAAGAAGCCTTAAATACTCAGAATGAGTCTACTCCTTTGGCCACATT 422

Query 2157 GGCAGTAGATGGTGGTATGTCCAAGGCAGATGAAGTCTTGCAAATTCAGCTGATATTTT 2216
          |||
Sbjct 421 GGCAGTAGATGGTGGTATGTCCAAGGCAGATGAAGTCTTGCAAATTCAGCTGATATTTT 362

Query 2217 GGGACCCTGTGTAAGTGTAAAGAGGCTCAGATATCTGAATGTACAGCATTAGGTGCTGC 2276
          |||
Sbjct 361 GGGACCCTGTGTAAGTGTAAAGAGGCTCGGATATCTGAATGTACAGCATTAGGTGCTGC 302

Query 2277 AATTGCTGCAGGATTATCTTCAAAGACGAAAATGAAAGAGTGTGGAAGATTTTAATGA 2336
          |||
Sbjct 301 AATTGCTGCAGGATTATCTTCAAAGACGAAAATGAAAGAGTGTGGAAGATTTTAATGA 242

Query 2337 TGTGTTTGA AAAAATTTGATGCTGCAAAACGAAACAACCTCCTCAAAGCCAAGTTACCAGA 2396
          |||
Sbjct 241 TGTGTTTGA AAAAATTTGATGCTGCAAAACGAAACAACCTCCTCAAAGCCAAGTTACCAGA 182

Query 2397 CGCAGAGAGAAGAAGAAATTTGGAGAAGATGGGAACGTGCCATTGACAGGGCTAAAGATTG 2456
          |||
Sbjct 181 CGCAGAGAGAAGAAGAAATTTGGAGAAGATGGGAACGTGCCATTGACAGGGCTAAAGATTG 122

Query 2457 GTTGGATCAGAACATGACTAAGAATTCGAGCTCCGTCGACAAGCTTGCAGCCGCGAATT 2516
          |||
Sbjct 121 GTTGGATCAGAACATGACTAAGAATTCGAGCTCCGTCGACAAGCTTGCAGCCGCGAATT 62

Query 2517 AATTGCGCTTAGACATGACTGTTCCCTCAGTTC AAGTTGGGCACTTACGAGAAGACCGGTC 2576
          |||
Sbjct 61 AATTGCGCTTAGACATGACTGTTCCCTCAGTTC AAGTTGGGCACTTACGAGAAGACCGNTC 2

Query 2577 T 2577
          |
Sbjct 1 T 1

```

F. Standard operating procedures (SOPs)

Arbeitsanweisung Nr. M/ 03

Datum: 12.04.2000 Autor: Dr. Annett Kiesel
 ueberarbeitet: 2002 Autor: I. Behrendt
 ueberarbeitet: 23.11.2005 Autor: S.Koenig
 ueberarbeitet: 11.09.2006 Autor: N. Schlawin
 ueberarbeitet: 19.08.2010 Autor: S.Koenig

Herstellung von Glasgow-MEM-Medium aus Pulvermedium (für Gewebekultur und Kultivierung im Bioreaktor)

1.0 Ziel

Herstellung von Glasgow-MEM-Vollmedium zur Kultivierung von MDCK-Zellen in grosseren Mengen. Pulvermedium ist wesentlich preiswerter als Fertigmedium. Da der Sterilfilter aber sehr teuer ist, sollten mindestens 30 L angesetzt werden. Die maximale Menge pro Filtereinsatz betraegt 60L.

2.0 Material

- BHK-21-Medium- (Glasgow-MEM-) Pulvermedium (Fa. Gibco, Best.Nr. 22100-093, für 50 L)
- NaHCO₃ (Fa. Merck, Best.Nr.: 1.06329.1000)
- Glucose (Fa. Roth, Best.Nr.: X997.2)
- Magnetrührer mit Ruehrstab
- Ansatzgefäß (z. B. 5L Becherglas)
- sterile 1–5 L Flaschen (für das sterilfiltrierte Medium)
- 1 N HCl (Fa.Roth, Best.Nr.fuer 37 %: 4625.1 oder Fa. Merck, Best. Nr. fuer 37%: 1.00317.1000)
- 1 N NaOH (Fa. Merck, Best. Nr. fuer Plaetzchen: 1.06482.1000)
- Sterilfiltrieranlage (Sterilfilter Sartobran 300 von Sartorius, Edelstahlruckbehaelter, 2 Druckschlaeuche, 4 Schlauchklemmen, 1 Aterienklemme, Stativ)
- pH-Meter
- Druckluft
- Mikrowelle (zum zuegigen Erhitzen des Milli-Q-Wassers)
- Pepton (Fa. idg / Großbritannien, Best.Nr.: MC 33)
- Schutzbrille

3.0 Methode

3.1 Zusammensetzung des Glasgow-Mediums (4,5 L):

- | | |
|---------------------------------------|--------|
| - Glasgow-MEM-Pulvermedium: | 62,6 g |
| - NaHCO ₃ | 20,0 g |
| - Glucose | 5,00 g |
| - pH-Wert (Einstellung): Sollwert 6,7 | |

3.2 Ansetzen des Glasgow-MEM-Mediums (4,5 L):

- 2,5 L Milli-Q-Wasser in das Ansatzgefassaess auf dem Magnetruerher geben
- 1 L Milli-Q-Wasser auf ca. 90 °C erwaermen (in der Mikrowelle, 10 min bei 1000 W)
- Dann das warme Wasser zu den 2,5 L hinzufuegen, das Milli-Q-Wasser betraegt jetzt ca. 35°C -37°C
- 62,6 g Pulver abwiegen und gleich in das ca. 35°C -37°C warme Wasser einruehren (Pulver ist stark hygroskopisch)

- 20 g NaHCO₃ und 5 g Glucose hinzufuegen und loesen
- pH-Wert mit NaOH oder HCl auf 6,7 einstellen
- Auf 4,5 L mit Milli-Q-Wasser auffuellen und in den Edelstahlbehälter füllen, sofort sterilfiltrieren (in eine oder mehrere sterile Flaschen)
- Da es eine Druckfiltration ist, Schutzbrille tragen. Der Druck betraegt max. 1,5 bar
- Angabe der jeweils verwendeten Chargen (Datum) im Arbeitsblatt eintragen
- Vollstaendige Beschriftung (Datum, Bezeichnung)
- Von dem sterilfiltrierten Medium Sterilkontrollen in CASO-Bouillon anlegen (je 2 am Anfang, 2 in der Mitte und 2 am Ende)

4.0 Lagerung

- Bei 4 °C bis 8°C kann das Medium maximal 6 Monate aufbewahrt werden
Die Stabilitaet von Glutamin und anderen Inhaltsstoffen kann dann abnehmen

5.0 Arbeitsblaetter

M/ 03.1
Z / 07

Arbeitsanweisung Nr. M/ 04

Datum: 14.06.2001 Autor: I. Behrendt
ueberarbeitet: 20.06.2006 Autor: S. Koenig
ueberarbeitet: 30.05.2008 Autor: S. Koenig

Herstellung von Glasgow-MEM-Vollmedium (Z-Medium) aus selbst hergestellten Teilloesungen (GMEM-Medium aus Pulvermedium + FCS + 20 % Lab-M-Peptone) und (V-Medium) aus selbst hergestellten Teilloesungen (GMEM-Medium aus Pulvermedium + 20 % Lab-M-Peptone)

1.0 Ziel

Herstellung von Vollmedium zur Kultivierung von MDCK-Zellen in Kulturflaschen und in Bioreaktoren. Alle Medienbestandteile sind bereits als Loesungen steril vorhanden (FCS) oder steril hergestellt und brauchen nur noch zusammen pipettiert zu werden.

2.0 Material

- foetales Kaelberserum (FCS, Fa. Gibco, Best.Nr. 10270-106): 500 mL-Flasche
- Glasgow-MEM-Medium (BHK21) aus Pulvermedium hergestellt, siehe Arbeitsanweisung Nr. M/03
- Lab-M-Peptone F.M.V. (Fa. idg, Großbritannien, Best. Nr.: MC 33)
- Schottflasche 1 L
- Waage
- sterile Flasche

3.0 Methode

3.1 Ansetzen der 20 %igen Peptonloesung:

- 200 g Lab-M-Peptone in 80 °C warmen Wasser loesen und auf 1 L auffuellen
- in eine 1-L-Flasche fuellen
- Sofort bei 105 °C 30 min autoklavieren

3.2 Zusammensetzung des Vollmediums:

- Die Flasche mit dem FCS wird ueber Nacht im Kuehlschrank aufgetaut
- Alle Teilloesungen auf Zimmertemperatur erwaermen lassen und steril unter der Werkbank auf der Waage in eine sterile Flasche abwiegen

Ansatz für 1 L-Medium Z- Medium:

- 890 mL des Glasgow-MEM-Medium in eine sterile 1 L-Flasche einwiegen
- Zugabe von 100 mL FCS, sowie 10 mL 20 %iges Lab-M-Peptide
- Angabe der jeweils verwendeten Chargen im Arbeitsblatt
- Vollstaendige Beschriftung der Flaschen (Z..., Datum)
- Steriltest anlegen

Ansatz für 1L-Medium V- Medium:

- 990 mL des Glasgow-MEM-Medium in eine sterile 1 L-Flasche einwiegen
- Zugabe von 10 mL 20 %iges Lab-M-Peptide
- Angabe der jeweils verwendeten Chargen im Arbeitsblatt
- Vollstaendige Beschriftung der Flaschen (V..., Datum)
- Steriltest anlegen

4.0 Lagerung

- Das fertige Vollmedium kann im Kuehlschrank ca. 3 Monate aufbewahrt werden (Die Stabilitaet von Glutamin und anderen Inhaltsstoffen kann allerdings nach 4 Wochen schon abnehmen)
- FCS ist aufgetaut 6 Monate bei 6 °C haltbar
- Lab-M-Peptide 20 %ig ist bei 4 °C 6 Monate haltbar

5.0 Arbeitsblaetter

M/ 04.1
M/ 04.2
M/ 04.3
Z/ 07

Arbeitsanweisung Nr. M/ 07

Datum: 8.12.2000	Autor: Ilona Behrendt
überarbeitet: 17.12.03	Autor: Susanne König
überarbeitet: 17.11.05	Autor: Susanne König
überarbeitet: 20.05.10	Autor: Claudia Best

Herstellung der Trypsin-EDTA- Stammlösung (10x) zum Ablösen von Zellkulturen**1.0 Ziel**

Herstellung der Trypsin-EDTA- Stammlösung (10x) für das Ablösen von adhärennten Zellen aus Zellkulturflaschen.

2.0 Material

- Trypsin, 1:250, Pulver (Gibco, Bestellnr.: 27250-018), [befindet sich im Raum N. 1.06 bei 4°C](#)

(bei einer neuen Trypsincharge, von Gibco immer das Analysenzertifikat zuschicken lassen, da dort die Aktivitätsangabe (BAEE- Wert) vermerkt ist!!)

- unsteriles PBS, befindet sich im Raum N. 1.06 bei RT
- EDTA (Sigma, Bestellnr.: ED2SS), befindet sich im Raum N. 1.06 bei RT
- Präzisionswaage
- Spatel, Wägeschälchen
- 250 mL Becherglas
- 250 mL Messzylinder
- Magnetrührer + Rührstäbchen
- Vakuumpumpe, befindet sich im Raum N. 1.07 unter dem Abzug
- 250 mL Nalgene Sterilfilter (gelb, 0,22 µm)
- S2 Sterilbank
- 2 Caso-Bouillons
- Pipettierhilfe Pipettus akku
- sterile Einmalpipetten
- sterile 50 mL Falkonröhrchen

3.0 Methode

Es ist darauf zu achten, dass der BAEE- Wert (Aktivitätsangabe) zwischen 600 – 800 U/mg liegt. Falls dieser kleiner oder höher sein sollte, muss die Einwaagemenge neu berechnet werden.

- für 250 mL werden 1,25 g Trypsin und 0,5 g EDTA auf der Präzisionswaage eingewogen
- diese beiden Substanzen gibt man zusammen mit 250 mL unsterilem PBS in ein Becherglas
- die Lösung wird auf dem Magnetrührer solange gerührt, bis sich die Substanzen vollständig aufgelöst haben
- danach wird die Lösung mit der Vakuumpumpe in ein 250 mL Nalgene Filtersystem steril filtriert
- unter der S2 Sterilbank werden aus dem Nalgene Filtersystem 5 mL als Sterilttest in die 2 Caso-Bouillons pipettiert
- jeweils 50 mL der Trypsinstammlösung werden mit Einmalpipetten in die sterilen Falconröhrchen hinein pipettiert
- zum Schluss werden die Röhrchen gut verschlossen und einzeln beschriftet (Trypsin 10x, Herstellungsdatum, steril)
- das dazugehörige Datenblatt (V/02.1) wird ausgefüllt und im Ordner für Zellkulturlösungen abgeheftet

4.0 Lagerung

Die Lagerung erfolgt bei 4 °C. Die Haltbarkeit beträgt 1 Jahr.

Es ist darauf zu achten, dass trotz der Lagerung bei 4 °C, die Aktivität des Trypsinpulvers abnimmt. Um dies rechtzeitig zu erkennen, wird bei Auffälligkeiten des Ablösevorganges während der Zellpassagierung, wie z.B. längere Ablösedauer, die techn. Assistentin informiert.

Sollten sich die Auffälligkeiten bestätigen, erfolgt somit eine Neubestellung des Trypsinpulvers von der Firma Gibco.

5.0 Verwendung

- diese 10x konzentrierte Trypsinstammlösung wird zum Ablösen der Zellen von Carriern aus dem Bioreaktor, Wavereaktor u.v.m. verwendet
- zum Ablösen der Zellen von T-Flaschen bzw. Rollerflaschen muß diese Lösung noch 1:10 verdünnt werden, da sie sonst dafür zu stark konzentriert ist

6.0 Herstellung von verdünnter Trypsin- EDTA- Lösung (1x)

Material

- 1 Falcon Trypsinstammlösung (10x), [befindet sich im Raum N. 1.06 bei 4°C](#)
- steriles PBS, [befindet sich im Raum N. 1.06 bei RT](#)
- 10 sterile 50 mL Falconröhrchen
- Pipettierhilfe Pipettus akku
- sterile Einmalpipetten
- S2 Sterilbank

Herstellung

- unter der S2 Sterilbank pipettiert man 5 mL von der Trypsinstammlösung in jedes der 10 Falconröhrchen
- danach wird in jedes Falcon noch 45 mL des sterilem PBS dazugegeben
- zum Schluss werden die Falcons gut verschlossen, etwas geschüttelt, und beschriftet (Trypsin 1x, Herstellungsdatum, steril)
- die Lagerung erfolgt ebenfalls bei 4 °C

7.0 Arbeitsblätter

- M / 07.1
- Z / 07
- Z / 04
- V / 02.1

Arbeitsanweisung Nr. Z/ 02

Datum: 25.06.2003

Autor: I. Behrendt

Auftauen von MDCK-Zellen

2.0 Ziel

Schonendes Auftauen von in der Gasphase von flüssigem Stickstoff langzeit-gelagerten MDCK-Zellen.

2.0 Material

- Zellen in Kryoröhrchen im flüssigen Stickstoff
- Stickstoffaufbewahrungsbehälter
- Schutzkleidung: Thermohandschuhe und Schutzschild
- Wasserbad 37 °C
- Kulturgefäß (T25, besser T75)
- Vollmedium (komplett gemischt mit FCS und Tryptosephosphatboullion oder Pepton) oder serumfreies Medium (Episerf, Optipro, Ex-Cell) (auf Raumtemperatur vorgewärmt)
- Werkbank gesäubert
- Pipettierhilfe, Pipetten (steril)
- Desinfektionslösung (Descosept AF / Cleanisept) in Sprühflasche
- Sterillium für Händedesinfektion

3.0 Methode

- Werkbank 15 min vor Arbeitsbeginn einschalten, desinfizieren
- Pipetten, Pipettierhilfe und Medium desinfizieren und in die Sterilbank stellen
- Handschuhe anziehen und desinfizieren
- unter Sterilbank Medium in die Zellkulturflasche pipettieren oder gießen (20 mL in eine T25-Flasche, 50 mL in eine T75-Flasche)
- Zellen aus dem Stickstoffbehälter holen (mit Schutzkleidung!!!) und schnell auftauen

Gefriermittel DMSO ist toxisch. Die Zellen müssen möglichst schnell aufgetaut werden und in das Medium zur Verdünnung überführt werden!! Kryoröhrchen nicht über-Kopf-schütteln – Kontaminationsgefahr!

- Kryoröhrchen sofort nach dem Schmelzen des letzten Eisklumpchen von außen desinfizieren und unter die Werkbank stellen
- den Inhalt mit einer geeigneten Pipette in die Kulturflasche überführen (die Kulturflasche sollte mind. 20 mL Medium enthalten, um das DMSO ausreichend zu verdünnen)
- bei Problemen während der Anzucht:
 1. nach dem Anheften der Zellen (ca. 4 – 12 h) einen Mediumwechsel durchführen, um das DMSO aus der Kultur zu entfernen (siehe Arbeitsanweisung Z/03) oder
 2. gerade aufgetaute Zellen in ein mit 40 mL Medium (37°C) gefülltes 50-mL-Falkongefäß überführen, in der Zentrifuge bei 500 x g Zellen 5 min bei Raumtemperatur abzentrifugieren, Medium abpipettieren und Zellen in einem geeigneten Volumen (Bsp. 50 mL) Medium aufnehmen und in die Zellkulturflasche überführen (Bsp. T75)

Arbeitsanweisung Nr. Z/ 04

Datum: 14.04.2000

Autor: Dr. Annett Kiesel

geändert am: 09.07.2003

Autor: Ilona Behrendt

geändert am: 20.06.2006

Autor: Susanne Koenig

geändert am: 11.09.2006

Autor: Nancy Schlawin

Passagieren von MDCK-Zellen in serumhaltigem Medium

1.0 Ziel

Langzeitkultivierung und Vermehrung von Zellen, zur Beimpfung mit verschiedenen Virusarten und späteren Aufarbeitung.

2.0 Materialien

- Kultur mit konfluent gewachsenen Zellen (25-cm²-, 75-cm²-, 175-cm²-Flasche oder 850-cm²-Rollerflasche); MDCK-Zellen: 4- bis 6-Tage alte, konfluent gewachsene Kultur
- Trypsin/EDTA-Lösung (0,05 % Trypsin/ 0,02 % EDTA, 37 °C), 1:10-Verdünnung aus Stammeslösung, siehe Arbeitsanweisung M/07
- Vollmedium (GlasgowMEM komplett gemischt mit 10 % FCS und Tryptosephosphatbouillon/Pepton), siehe Arbeitsanweisungen M/02 oder M/04
- PBS (Raumtemperatur) siehe Arbeitsanweisung M/01
- foetales Kaelberserum (FCS) (auf Raumtemperatur vorwärmen) Firma:Gibco/Best.Nr.:10270106

3.0 Methode

- Kulturflaschen aus dem Brutschrank nehmen und desinfizieren, unter die Werkbank stellen

- Kulturflaschen aufschrauben, Deckel mit Oeffnungen nach oben legen (Deckel nach hinten legen, so dass man nicht darueber fasst beim Arbeiten)
- altes Medium in eine sterile Abfallflasche abgiessen (nicht den Rand beruehren!)
- die Zellen mit PBS-Loesung 2x waschen (s. Volumentab., I), gebrauchtes PBS in die sterile Abfallflasche abgießen (dazwischen die T-Flaschen immer zuschrauben und schwenken)
- Trypsin/ EDTA-Loesung zupipettieren, ein duenner Fluessigkeitsfilm genuegt (s. Volumentab., II), und die Zellen bei 37 °C für ca. 20 min inkubieren
- in der Zwischenzeit neue Kulturflasche mit entsprechender Menge Medium befuellen (s. Volumentab., IV)
- nach 10 min Trypsininkubation die Flasche zum ersten Mal leicht schuetteln, dann Zellen weiter inkubieren (insgesamt ca. 20 bis 30 min.) bis sich die Zellen nach erneutem kraeftigen Schuetteln vom Boden abloesen (optische Kontrolle und/oder unterm Mikroskop angucken)
- zum Abstoppen der enzymatischen Reaktion FCS (s. Volumentab., III) zu den abgeloeften Zellen geben
- durch mehrmaliges (ca. 2-3x) Aufziehen des Inhaltes der Flasche in eine Pipette erfolgt eine Zellvereinzlung (um Schaum zu vermeiden, Pipetteninhalt am Flaschenboden oder an der Innenseite der Flasche auslaufen lassen!)
- von dieser Zellsuspension entnimmt man 1/3 bis 1/6 (bei Inkubation in Flaschen mit gleichem Volumen) und pipettiert dieses jeweils in eine der vorbereiteten Flaschen (Berechnung der Einsaatdichte siehe unter Punkt 5 oder 6)
- **Beachte!** Fuer Zellkultivierung Deckel mit Membran benutzen (CO₂-durchlaessig), bei Arbeiten mit Virus in den T-Flaschen, geschlossenen Deckel (ohne Membran) nehmen
- Flaschen im Brutschrank bei 37 °C und 5 % CO₂ inkubieren

4.0 Volumentabelle

Kulturgefaeß	PBS zum Waschen (I)	Trypsin/EDTA (II)	FCS (III)	Vollmedium (IV)
25-cm ² -Flasche	5 – 10 mL	1 mL	1 mL	15 - 20 mL
75-cm ² -Flasche	10 – 15 mL	3 mL	3 mL	50 mL
175-cm ² -Flasche	15 – 20 mL	5 mL	5 mL	100 - 125 mL
850-cm ² -Rollerflasche	40 – 50 mL	10 mL	10 mL	250 mL

5.0 „Faustregeln“ für die Anzucht von MDCK-Zellen

- Ausgangskultur: 4- bis 6-Tage alte, konfluent gewachsene Kultur (zu alte Kulturen vermeiden)
- Weiterkultivierung der Zellen in einer Kulturflasche mit gleichem Volumen: 1/3 bis 1/6 der Zellen in die neue Flasche geben
- Vermehrung der Zellen für den Fermenter: Ampulle – T75 – T175 – Rollerflasche: jeweils die gesamten Zellen in das naechst groessere Kulturgefaess ueberfuehren (Ampulle mit 2-5x10⁶ Zellen/mL; wenn weniger Zellen oder alte Zellen: Zwischenstufe über T25)
- Zellen nicht untereinander austauschen (bei Kontaminationsgefahr nicht mehr genau nachvollziehbar, woher diese stammt)
- fuer eine Reaktorkultivierung Zellen aus einer Passagierung kleiner 20 verwenden
- stets eine T 75 Flasche parallel zur Fermentation als Back-up laufen lassen

6.0 Einsaat

6.1 Ermittlung des Einsaatvolumens

- ermittelte Zellzahl der trypsinierten Flasche \underline{Z} (z. B. 1,2 x 10⁶ Zellen/mL)
- Tage, in denen die Zellen bis zur Konfluenz wachsen sollen T (z. B. 4 d)

- empirisch ermittelte Einsaatdichte E , bei der die Zellen nach T Tagen in dem verwendeten Kulturgefaß konfluent sind (z. B. $0,8 \times 10^7$ Zellen pro 175 cm^2 werden benoetigt, um in 4 Tagen eine konfluente Kultur in einer 175-cm^2 -Flasche zu erhalten)
- Rechnung: $E : Z = \text{Volumen [mL]}$

Bsp:

$$(0,8 \times 10^7 \text{ Zellen}) : (1,2 \times 10^6 \text{ Zellen/mL}) = 6,7 \text{ mL}$$

In eine 175-cm^2 -Flasche muessen 6,7 mL einer Zellsuspension, die $1,2 \times 10^6$ Zellen/mL enthaelt, pipettiert werden, um nach 4 Tagen eine konfluente Kultur zu erhalten.

6.2 Bestimmung der Einsaat

- Einsaat = Zellen pro cm^2
= (Einsaatvolumen x Zellzahl) : Oberflaeche

Bsp.:

$$= (6,7 \text{ mL} \times 1,2 \times 10^6 \text{ Zellen/mL}) : 175 \text{ cm}^2 = 4,6 \times 10^4 \text{ Zellen/cm}^2$$

6,7 mL der Zellsuspension (mit $1,2 \times 10^6$ Zellen/ml) ergeben in einer 175-cm^2 -Flasche eine Einsaat von $4,6 \times 10^4$ Zellen/ cm^2 .

- Was ist ein guter Richtwert pro cm^2 ?
z.B. : $3,3 \times 10^4$ cells/ cm^2 fuer Bioreaktor ($\approx 3,0 \times 10^5$ cells/ml)
 $2,9 \times 10^4$ cells / cm^2 fuer Rollerflaschen in 4 Tagen oder
 $1,5 \times 10^4$ cells / cm^2 fuer Rollerflaschen in 7 Tagen
 $7,6 \times 10^4$ cells/ cm^2 fuer T 175 (1:6 gesplittet)
 $4,3 \times 10^4$ cells/ cm^2 fuer T175 (5ml) in Rollerflasche (850 cm^2)

7.0 Lagerung

Zellen wachsen in:

- T-Flaschen bei 37°C im CO_2 -Brutschrank im N1.06
- Rollerflaschen im 37°C Rollerflaschenschrank im N1.06 oder im 37°C Brutraum auf den Rollerflaschengestell
- Spinner bei 37°C im Brutraum auf einen Ruehrer

Die eingefrorenen Zellen werden im Fluessigstickstoffbehaelter im N1.12 gelagert.

Die Dokumentation erfolgt ueber Tabellen mit den jeweiligen Farbcode und Kennnummern, die in einem Ordner im Raum N 1.06 abgeheftet sind.

8.0 Arbeitsblaetter

M / 01

M / 02

M / 04

M / 07

Z / 07

Kurzanleitung G/21 Zellzählgerät ViCell XR

Version 1.5

Erstellt am: 29.03.2006

Aktualisiert am 08.08.2008

Autor: J. Schulze-Horsel

1. Im Vorfeld zu beachten

- Das Gerät darf nur nach Einweisung durch die dafür zuständige Person bzw. nach Absprache durch eine andere eingewiesene Person benutzt werden.
- Die zu messende Probe darf **auf keinen Fall Microcarrier** enthalten, da sonst das Gerät verstopft wird!
- Validierter Messbereich (für Zelltyp „MDCK 100“: $9,6 \cdot 10^4$ bis $1,0 \cdot 10^7$ Zellen/mL (Gesamtzellzahl))

2. Material

Originalprodukte von Beckman Coulter:

Nr. 383260	Single Pack	250 Messungen, Reagenzien plus Probengefäße (ca. 240 Euro)
Nr. 383194	Quad Pack	1000 Messungen (4x Single Pack = ca. 845 Euro)
Nr.		Probengefäße (ViCell Cups)

Die Probengefäße können gespült und mehrmals verwendet werden.

Die Komponenten des Reagenzienpacks sind entweder bereits vorhanden oder können selbst hergestellt werden:

- Trypanblaulösung: 0,4 % w/v Trypanblau und 0,15 mol/L Natriumchlorid in vollentsalztem Wasser (VE-Wasser) mit Papierfilter vorfiltriert, anschliessend 0,45 µm filtriert
- Desinfektionsmittel: Isopropanol (2-Propanol), 90 %
- Reinigungsmittel: Beckman Coulter Clenz (Nr. 8448222, 5 Liter)
- Pufferlösung: dH₂O, z.B. MilliQ-Wasser

Das benötigte Reagenzienvolumen pro 250 Messungen ist:

- Trypanblaulösung ca. 110 mL
- allen anderen Reagenzien ca. 220 mL benötigt

Auffüllen der Reagenzien:

Wenn das aktuelle Reagenzienpack leer ist, im Menü „Instrument“, „Replace reagent pack“ auswählen und den schrittweisen Anweisungen folgen.

Anstelle eines neuen Reagenzienpacks werden die Flaschen des vorhandenen Packs mit dem entsprechend benötigten Volumen (110 bzw. 220 mL) aufgefüllt.

Die Abfallflasche wird in eine Schottflasche umgegossen, autoklaviert und anschließend in den Trypanblau-Abfall entsorgt.

3. Einschalten und Ausschalten der Geräte

Einschalten:

- ViCell einschalten (Schalter auf der Rückseite)
- Computer einschalten

- Software „ViCELL XR 2.03“ starten

Ausschalten:

- Software schließen
- Rechner herunterfahren
- ViCell ausschalten

4. Zellzählung

Anforderungen an die Zellsuspension:

- Probenvolumen: minimal 0,5 mL, maximal 1,5 mL im Probengefäß
- Konzentrationsbereich (Herstellerangaben): $1,0 \cdot 10^4$ bis $1,0 \cdot 10^7$ Zellen/mL
- Proben mit einer Konzentration $> 1,0 \cdot 10^7$ Zellen/mL müssen vorverdünnt werden
- Proben, die Carrier enthalten können, müssen filtriert werden ($< 100 \mu\text{m}$), z.B. mit:
 - Partec Celltrics $100 \mu\text{m}$, Nr. 04-0042-2318)
 - Becton Dickinson Bioscience Discovery Labware, Cell strainer, $70 \mu\text{m}$, Nr. 352235

Messung:

- 5.1. Probe in Original-Probengefäß pipettieren und in das Probenkarussell stellen
- 5.2. „Log in sample“ auswählen, dann im Untermenü eingeben:
 - Probenposition im Karussell angeben
 - falls nötig: Probenbezeichnung eingeben
 - Zelltyp auswählen (Standard: MDCK 50)
 - „Dilution factor“ überprüfen: für unverdünnte Proben: 1.0
 - für sehr wichtige Proben: „Save images“ auswählen (Speicher: 1 MB/Bild)
 - Speichern der Ergebnisse als eigene Excel-Datei oder als Zeile in „Multi-run file“: „bpt_datensammlung.xls“ als Standarddatei auswählen
 - zum Messen: „OK“ oder nächste Probe eingeben („Next sample“)
- 5.3. Start der Messung: „Start queue“, Dauer einer Messung: 3 Minuten
- 5.4. Gerät reinigt sich selbständig, Probengefäß wird ausgeworfen
- 5.5. das Karussell wird nach weiteren Proben durchsucht, die dann mit fortlaufender Nummerierung gemessen werden (sofern nicht anders eingeloggt)
- 5.6. Speicherort für gezählte Proben (in Excel-Dateien): lokal und im Netzwerk
 c:\daten\ViCell\Excell\
 h:\bio\daten\vicellxr\Excell\

Wenn auf der lokalen Festplatte (c:\) kein Speicherplatz mehr vorhanden ist, müssen die lokalen Dateien in den gleichen Ordner auf dem Laufwerk (h:\) kopiert werden. Nach der Sicherung können die lokalen Dateien gelöscht werden. Die Ordner dürfen nicht gelöscht oder umbenannt werden.

Bei Problemen mit dem Speichern auf Spiegellaufwerk Software neu starten.

6. Aufzeichnung von Bioprozessen

Um Zellzählungen verschiedener Proben einer Zeitreihe zusammen zu speichern und auszuwerten, ist es sinnvoll diese als „Bioprocess“ zu sammeln und in einer Datei abzulegen.

- „File“ => „New Bioprocess“
- Bezeichnung für den Prozess vergeben, z.B. Fermentation100

- Zelltyp auswählen
- Speicherdatei auswählen, Daten werden im Unterordner \data\ abgelegt
- in der linken Menüleiste wird ein Icon hinzugefügt (Symbol: Erlenmeyerkolben)
- Messen der Proben des Prozesses: Icon anwählen und Probe eingeben („Log in sample“)

7. Messen von infizierten Zellproben

Mit dem ViCell können auch Zellzählungen von infizierten Kulturen gemacht werden. Dabei sind folgende Besonderheiten zu beachten:

- Vor dem Messen: die Schale mit gebrauchten Probengefäßen (innen) sowie die Abfallflasche entleeren
- Probengefäße unter der Virusbank befüllen
- Nach dem Messen: Schale in den Probengefäß-Virusabfall entleeren und desinfizieren, Inhalt der Abfallflasche in flüssigen Virusabfall geben

8. Entfernen von Microcarriern aus der Flusskammer

Die Flusskammer hat eine Höhe von ca. 100 µm. Daher können sich Microcarrier, die sich in den Proben befinden, in der Kammer festsetzen. Das kann zu veränderten Messwerten führen.

Um Microcarrier aus der Kammer zu entfernen folgende Prozedur durchführen:

- Probengefäß mit 2,5 mL verdünnter Natriumhypochlorid-Lösung (10 %ig, Sigma) füllen und in die erste Position des Probentellers stellen (1:10 verdünnen: 0,250 mL Natriumhypochlorid-Lösung + 2,25 mL Wasser)
- Befehl „Decontaminate“ im Menü „Instrument“ ausführen, dabei Anweisungen befolgen
- Die Reinigung dauert ca. 13 Minuten.
- Anschließend kontrollieren, ob die Flusskammer frei ist („Instrument“ -> „Live-Image“)
- Die Option „Live-Image“ wieder deaktivieren

Arbeitsanweisung Nr. A/02 Version 1.0

Datum: 07.04.2010

Autor: Verena Lohr

Metabolitbestimmung aus Zellkultur

1.0 Ziel

Mithilfe des BioProfile können wichtige Nährstoffe bzw. Stoffwechselprodukte in Zellkulturen schnell bestimmt werden.

Am BioProfile können extrazelluläre Metabolitkonzentrationen von Glucose, Lactat, Ammonium, Glutamin und Glutamat ermittelt werden.

2.0 Material

- Tischzentrifuge Multi-spin PCV-3000, Grant Instruments (N 1.07)
- Zentrifuge Biofuge primo R, Heraeus (N 1.06)
- Heizblock (N 1.06)
- Vortex (N 1.07)
- BioProfile 100Plus (N 1.07)
- 1000 µL-Pipette mit zugehörigen Spitzen
- Standardlösungen für die Kalibriergerade des BioProfile (-80 °C Kühlschrank)

- Glucose in PBS
- Glu, Gln, Lac, Amm in GMEM
(GMEM ohne Glc, Sigma, #G5154)

} Jeweils 3 verschiedene Konzentrationen, gekennzeichnet mit gelben, grünen und blauen Punkten auf dem Deckel, entspricht niedriger, mittlerer und hoher Konzentration

3.0 Methode

3.1 Vorbereitungen der Proben

Für die BioProfile Messung werden mindestens 1,6 mL Probevolumen benötigt.

Für eine gute Analyse sollten Microcarrier (!), Zellreste etc. mittels Zentrifugation vorher entfernt werden.

Adhärente Zellen

Aus Versuchen mit adhärennten Zellen, die in Mikrotiterplatten, T-Flaschen oder Rollerflaschen kultiviert wurden, wird der Zellkulturüberstand direkt verwendet. Aus einer Kultivierung mit adhärennten Zellen auf Microcarriern wird der Überstand verwendet, der nach dem Abzentrifugieren der Microcarrier entsteht (5000xg, 5 min). Dieser wird in ein neues Eppi überführt.

Suspensionszellen

Um den Zellkulturüberstand zu erhalten, wird die Zellsuspension nach der Probenahme bei 1000xg (3500 rpm mit Tischzentrifuge) für 1 min abzentrifugiert und der Überstand in neue Eppis überführt.

Bei Infektionsversuchen sollten die so erhaltenen Überstände sowohl in der Wachstums-, als auch in der Infektionsphase und bei der mock-Infektion 3 Minuten lang im 80°C- Heizblock erhitzt werden (für die Inaktivierung des Virus und aus Gründen der Proben-Gleichbehandlung ebenfalls mit Proben der mock-Infektionen und Wachstumsphase durchführen!). Eine Erhitzung für länger als 3 Minuten könnte Glutamin zerfallen lassen, bei weniger als 3 Minuten ist nicht sicher, ob das Virus inaktiviert wurde, die 3 Minuten sind daher optimal.

Falls für den Versuch mehrere Probenahmen vorgesehen sind, sollten die Proben bei -80° C bis zum Tag der Messung gelagert werden.

3.2 Messung

Die Bedienungsanweisung G_22 für das BioProfile 100Plus ist vor der Benutzung durchzulesen bzw. sollte eine Einweisung an dem Gerät erfolgen.

Vor der Messung

Unter dem Bedienmenü „Status“ sollte nachgesehen werden, ob das Reagenzienpack noch ausreicht, um die gewünschte Probenanzahl zu messen. Richtwert: ein volles Pack reicht für ca. 350 Proben und kann für 2 Wochen nach Einbau verwendet werden. Desweiteren sollte man sich - ebenfalls unter dem Bedienmenü „Status“ - die letzte Flussrate nachsehen (Flussraten von < 3,5 sec sind akzeptabel).

An dem „C“, das hinter jedem Metaboliten auf dem Monitor stehen sollte, erkennt man, dass die letzte automatische Kalibrierung erfolgreich war (falls nicht erscheint hier „NC“). Sollten diese Voraussetzungen nicht erfüllt sein, sollte ein Verantwortlicher angesprochen werden, das sind Claudia Best, Ilona Behrendt und Verena Lohr.

Messung

Am Tag der Messung werden die zu vermessenden Proben und die Standards (Glucosestandard 3x, d.h. gelbes, grünes, blaues Eppi und Standard der restlichen Metabolite, ebenfalls 3x, d.h. gelbes,

grünes, blaues Eppi) aufgetaut, am besten für ca. 6 h im Kühlschrank oder 1-2 h bei Raumtemperatur.

In folgender Reihenfolge werden die aufgetauten Standards und Proben in den Autosampler des BioProfile gestellt (vorher vortexen!!):

1. Glucose-Standards (3x), randomisiert, d.h. egal in welcher Reihenfolge
2. Standards aller anderen Metabolite (3x), randomisiert
3. Proben, randomisiert

Die Anordnung der Proben in randomisierter, d.h. nicht-sortierter Reihenfolge ist wichtig, da es bei sortierter Anordnung zu einem systematischen Fehler kommen kann (Drift). Die Proben eines Versuches werden in einer Einfachbestimmung gemessen, da die Validierung des BioProfile ebenfalls mit einer Einfachbestimmung durchgeführt wurde. *Wichtig: die Eppis müssen vollständig geöffnet werden, d.h. die Deckel ganz runtergeklappt werden, damit der Autosampler sich drehen kann!!*

Pro Probe werden ca. 3 Minuten und 3 Euro benötigt.

Nach der Messung der Proben werden die 6 Standards erneut gemessen (randomisiert!), am besten „per Hand“, da in den Eppis nicht mehr genügend Volumen übrig ist, um sie in den Autosampler zu stellen.

Nach der Messung

Welche Probe an welcher Position stand, sollte beim Rausnehmen der Proben aus dem Autosampler notiert werden, damit die Messwerte richtig zugeordnet werden. Dabei sollte man sich direkt die Werte ansehen und sie mit den validierten Konzentrationsbereichen vergleichen (diese Bereiche sind auf einem Zettel notiert, der am BioProfile hängt). Sollte eine Konzentration über diesem Bereich liegen, so muss die Probe verdünnt und erneut gemessen werden. Dies geschieht ebenfalls in einem Eppi, je nach Konzentration 1:2 oder 1:3 mit PBS. *Wichtig: Vortexen, bevor diese Probe vermessen wird. Bei zu geringer Konzentration sollte man sich dieses notieren.*

3.2 Auswertung

Die Messdaten werden von dem Gerät auf Thermopapier gedruckt. Da dieses im Laufe der Zeit verblasst, sollten die Messwerte in eine Datei geschrieben werden, um die Rohdaten zu sichern.

Die jeweiligen BioProfile-Dateien liegen auf dem BPT-Verzeichnis unter H:/bpt/usp/Labor/Biopprofile_calibration_curves/2010/Quartal_1 (bzw. das entsprechende Jahr und Quartal). Hier werden nun zunächst die Werte der Standards (jeweils zwei) eingetragen, daraus ein Mittelwert gebildet und automatisch in ein Diagramm übertragen. Die Gleichung der Kalibrierkurve wird für Geraden automatisch übernommen, für quadratische Funktionen muss die rechts stehende Gleichung mit den Parametern aus dem Diagramm angepasst werden. In den übrigen Tabs können nun die Messwerte eingetragen werden, in dem Tab „Dokumentation“ muss u.a. eingetragen werden wann und von wem diese Messung durchgeführt wurde und welches Servicepack verwendet wurde (Lot-Nummer und Ablaufdatum stehen auf dem Stecker, der Servicepack und Gerät miteinander verbindet).

4. Anmerkungen

Einfluss von pH-Wert auf die Messung

Da auch der pH-Wert der Probe einen Einfluss auf das Messergebnis haben kann, ist es möglicherweise kritisch, aufgetaute Proben aus der Zellkultur lange offen im Autosampler stehen zu lassen, da bei geöffnetem Eppi CO₂ ausgast und sich der pH möglicherweise signifikant verändert. Bei kritischen Proben sollte entweder auf eine lange Stehzeit verzichtet werden (ohne Autosampler oder kürzere Sequenzen messen) oder zumindest nach der Messung überprüft werden, ob der pH-Wert sich signifikant (um mehr als 1) ändert.

Wiederholungsmessungen

Proben eines Versuches sollten stets in einer Messreihe gemessen werden. Das Nachmessen von einzelnen Proben ist zu vermeiden.

Einfluss von Salzen auf die Messung

Es wurde bisher nur in GMEM getestet, ob Salze einen Einfluss auf die BioProfile-Messung haben. Bei der Auswertung sollte berücksichtigt werden, dass die meisten Kultivierungen nicht in GMEM durchgeführt werden und daher der Salzgehalt der Proben nicht mit dem der Standards übereinstimmt bzw. sich im Laufe der Kultivierung möglicherweise ändert. Theoretisch sollte es zu jedem Medium, das im BioProfile gemessen wird eigene Standards geben, gegen die kalibriert wird. Dies ist allerdings praktisch kaum durchführbar, da sehr aufwändig. Die folgende Tabelle soll daher nur grob zeigen, welche Einflüsse verschiedene Salze auf die Messung von GMEM im BioProfile hatten. Es sei zu beachten, dass bei Zugabe von 20 mM NaHCO₃ zu PBS Glutamat nachzuweisen war, wobei die gemessene Glutamatkonzentration mit steigender NaHCO₃-Konzentration (bis 200 mM) ebenfalls anstieg (auf 1,7 mM), obwohl PBS kein Glutamat enthält.

Salz	Konz. [mM]	Einfluss auf	welcher Einfluss mit steigender Salzkonz.?
NaCl	50-250 mM	Glucose	sinkt deutlich
NaCl	50-250 mM	Osmolalität	steigt deutlich
NaHCO ₃	20-200 mM	Glucose	sinkt deutlich
NaHCO ₃	20-200 mM	Glutamat	steigt deutlich
NaHCO ₃	20-200 mM	pH	steigt
NaHCO ₃	20-200 mM	Osmolalität	steigt deutlich
Mg ₂ SO ₄	0,5-10 mM	Glucose	sinkt
CaCl ₂	0,5-10 mM	Glucose	sinkt
CaCl ₂	0,5-10 mM	Glutamat	sinkt
KCl	0,5-10 mM	Glucose	sinkt
KCl	0,5-10 mM	Ammonium	steigt

Arbeitsanweisung Nr. V/ 03

Datum: 08.05.2000 Autor: Dr. Annett Kiesel
überarbeitet: 08.11.2005 Autor: Claudia Best
überarbeitet: 18.04.2006 Autor: Claudia Best
überarbeitet: 26.09.2007 Autor: Claudia Best

Virenvermehrung in Kulturflaschen

1.0 Ziel

Viren gehören nicht zu den Lebewesen im engeren Sinne, da sie sich u. a. nicht selbständig vermehren können. Zur Vermehrung benötigen Viren einen Wirt, der die Replikation und Proteinbiosynthese der viruseigenen Erbinformation (RNA oder DNA) und der virusspezifischen Proteine übernimmt. Es ist dabei natürlich wichtig, dass der Wirt (z. B. die MDCK-Zelle), noch vital genug ist, um diese StoffwechsellLeistungen zu erbringen.

2.0 Material

- [Virusbeimpungsstandard](#) ([Lagerung: -70 °C, N. 1.11](#))
- [MDCK Zellkultur](#) mit konfluent gewachsenen Zellen **4–6 Tage alt** (T-Flasche, Rollerflasche, Bioreaktor)
- [Trypsinlösung zur Virusinfektion](#) (**500 U/mL oder 5000 U/mL**, [Lagerung -20 °C, N. 1.06](#))
- [V-Medium](#) (Glasgow-MEM mit 1 % Lab-M-Peptide, [Lagerung: 4 °C N. 1.13](#))

- steriles PBS (20 °C, RT, N. 1.06)
- sterile Pipetten, Pipettierhilfe
- S2-Sterilbank
- Meliseptol, MBT oder anderes für behüllte Viren zugelassenes Desinfektionsmittel
- Autoklavierbeutel für den Abfall

3.0 Methode

- unter der S2-Sterilbank, das alte Medium der Zellkultur in eine sterile Abfallflasche abgießen
- die Zellen mit steriler PBS-Lösung 3x waschen, zwischendurch das PBS in die Abfallflasche abgießen
- V-Medium je nach Volumen der Zellkultur dazu geben
- danach die berechnete Menge an Trypsinlösung, als auch vom Virusbeimpfungsstd. dazugeben
- die Verschlusskappen der Zellkulturflaschen werden mit Parafilm abgedeckt, danach für **3 Tage** bei **37 °C** in den CO₂- Brutschrank stellen (N.1.07)
- alles, was mit den Viren in Kontakt kam, muss vor dem Entnehmen aus der S2-Sterilbank von außen mit **MBT** desinfiziert werden (Einwirkzeit des Desinfektionsmittels beachten, i. d. R. ca. 2 min)
- Abfallbeutel nach Gebrauch gründlich verschließen (z. B. zukleben) und sobald wie möglich autoklavieren (20 min bei 121 °C).
- wenn verbrauchte Medien mit Virusmaterial anfallen, diese mit **2 %iger Essigsäure** desinfizieren (10 – 20 mL/L; bei Medium mit **Phenolrot** bis Farbumschlag auf **gelb**)

Kulturgefäß zum Beimpfen	Menge an V-Medium (GMEM+ Lab-M-Pepton)	Menge an Trypsin (500 U/mL)	„Standard“-Menge an Viruslösung
T25 (25 cm ²)	10 mL	0,1 mL	0,04 mL
T75 (75 cm ²)	50 mL	0,5 mL	0,20 mL
T175 (175 cm ²)	125 mL	1,0 mL	0,40 mL
RF (850 cm ²)	250 mL	2,5 mL	1,00 mL
Sixfors (Carrier, Cytodex 1)	500 mL	5,0 mL	2,00 mL
Wavereaktor (Carrier, Cytodex 1)	1,0 L	10,0 mL	variabel, je nach MOI
DasGip Anlage (Carrier, Cytodex 1)	1,0 L	10,0 mL	variabel, je nach MOI
Biostat B-Plus (Carrier, Cytodex 1)	1,0 L	10,0 mL	variabel, je nach MOI
		Trypsin 5000 U/mL	
Bioreaktor 5 L (Carrier, Cytodex 1)	4,50 L	5,0 mL	Std. 10,0 mL
Bioreaktor 15 L (Carrier, Cytodex 1)	15,0 L	15,0 mL	variabel, je nach MOI

4.0 Lagerung

Die Viren können vor der Ernte direkt in den Zellkulturgefäßen eingefroren werden. Sie halten sich bei -70 °C mehrere Jahre, bei -20 °C mehrere Monate. Kurzfristig (max. 8 Wochen) kann Virusmaterial in größeren Volumen bei 2-8 °C gelagert werden, z. B. vor weiteren Aufarbeitungen.

5.0 Arbeitsblatt

V/ 03.1

6.0 Beispielberechnung des MOI's

MOI = Multiplicity of Infection „Anzahl der Viruspartikel pro Zelle“

<u>TCID₅₀ Wert des Virusbeimpungsstd. :</u>	4,30 x 10 ⁷ Viren/ mL
<u>Ermittelte Gesamtzellzahl z. B. von RF:</u>	1,25 x 10 ⁷ Z/mL * 30 mL (15 mL Trypsin + 15 mL FCS)
	= 37,5 x 10 ⁷ Zellen gesamt
	$\frac{4,30 \times 10^7 \text{ Viren}}{37,5 \times 10^7 \text{ Zellen}} = 0,11 \text{ MOI}$

7.0 Beispielberechnung der Trypsinmenge zur Virusinfektion

<u>Trypsinkonzentration der Stammlösung :</u>	5000 Units/ mL
<u>Gewünschte Trypsinkonzentration pro Zelle:</u>	2,0 * 10 ⁻⁶ Units/ Zelle (MDCK)
<u>Zellzahl nach 96 h z.B. im Bioreaktor:</u>	1,0 x 10 ⁶ Z/ mL * 4500 mL = 4,50 * 10 ⁹ Zellen
	$4,50 \times 10^9 \text{ Zellen} * 2,0 \times 10^{-6} \text{ Units/ Zelle} = 9000 \text{ Units}$
	$\frac{9000 \text{ Units}}{5000 \text{ Units}} = \frac{9000 \text{ Units}}{1 \text{ mL}} = \frac{9000 \text{ Units}}{x \text{ mL}} = 1,8 \text{ mL Trypsin}$

8.0 Beispielberechnung der Virusmenge, bei vorgegebenen MOI-Wert

<u>TCID₅₀ Wert des Virusbeimpungsstd. :</u>	4,20 * 10 ⁸ V/mL
<u>Gewünschter MOI – Wert:</u>	0,025
<u>Zellzahl nach 96 h z.B. im Bioreaktor:</u>	1,0 x 10 ⁶ Z/ mL * 4500 mL = 4,50 * 10 ⁹ Zellen
	$\frac{4,50 \times 10^9 \text{ Zellen} * 0,025}{4,20 * 10^8 \text{ V/mL}} = 0,268 \text{ mL} * 1000 = 268 \mu\text{L Viruslösung}$

<u>TCID₅₀ Wert des Virusbeimpungsstd. :</u>	1,59 * 10 ⁷ V/ mL
--	------------------------------

<u>Gewünschter MOI – Wert:</u>	0,025
--------------------------------	-------

<u>Zellzahl nach 96 h z.B. im Sixfors:</u>	1,0 x 10 ⁶ Z/ mL * 500 mL = 5,0 * 10 ⁸ Zellen
--	---

5,0 * 10 ⁸ Zellen	^	MOI 1,00
5,0 * 10 ⁷ Zellen	^	MOI 0,10
5,0 * 10 ⁶ Zellen	^	MOI 0,01
2,5 * 10 ⁷ Zellen	^	MOI 0,05
1,25 * 10 ⁷ Zellen	^	MOI 0,025

$\frac{1,59 \times 10^7 \text{ Viren}}{1 \text{ mL}} = \frac{1,25 \times 10^7 \text{ Zellen}}{x \text{ mL}} = 0,786 \text{ mL} = 786 \mu\text{L Virusmenge zur Beimpung}$

SOP V/05 HA-Assay

Version: 2.2 (20.01.2011)

Author: Verena Lohr

Hemagglutination assay (HA assay)

This SOP is based on the SOP written by Bernd Kalbfuß, Version 2.1 (04.12.2006)

1. Introduction

The HA assay is used to detect influenza virus particles (infectious and non-infectious). Influenza viruses carry the protein hemagglutinin (HA) on their surface which binds to specific glycosylation patterns on proteins which are located on the outer membrane of a cell. Thus, virus particles bind to cells and by using erythrocytes as cell system, influenza virus particles can cross-link erythrocytes with each other. This agglutination of erythrocytes can be observed in wells of a round bottom well plate as agglutinated erythrocytes sediment like a carpet at the bottom of the well instead of a point-like sedimentation.

By titrating the virus containing sample, one can determine a critical concentration of the sample at which this switch in sedimentation behaviour occurs. The negative logarithm of this dilution has been defined as the logarithmic HA titer (or simply log-titer) and is a measure for the concentration of influenza virus particles in the sample. The inverse of the dilution has been termed HA activity with units HAU/100 µL and is also supposed to be proportional to the number of virions in the sample.

There are two ways in which one can analyze the HA assay (procedure of pipetting is the same for both methods):

- i) a classical analysis in which the experimenter visually evaluates the HA titer
- ii) a photometric analysis which uses an automated procedure in order to minimize subjectivity and which includes an additional dilution step that increases sensitivity and reduces the error of the method

2. Materials

- Protective clothing: lab coat, protective gloves (Nitrile)
- Centrifuge (e.g. Primo R, Hera, N1.06)
- Sterile kryotubes
- Influenza virus samples (active or chemically inactivated)
- Internal HA standard (= control which is a chemically inactivated influenza virus sample with defined HA titer, stored at -80°C in N1.11, produced as described in SOP HA assay from Bernd Kalbfuß, Version 2.1 (04.12.2006))
- Erythrocyte suspension (conc. approximately 2.0×10^7 erythrocytes/mL, stored at 4 °C in N1.06, produced as described in SOP V/07 from Claudia Best (07.06.2007))
- Unsterile phosphate buffered saline, PBS (stored in N1.06, produced as described in SOP M/01 from Claudia Best (26.09.2007))
- Unsterile transparent 96well round bottom microtiter plates (stored in N1.06, e.g. Greiner Bio-One, Cat.No. 650101) + transparent disposable lids (stored in N1.06, e.g. Greiner Bio-One, Cat.No. 656101)
- 100 µL micropipette + disposable tips
- 8x100 µL or 8x300 µL multichannel micropipette + disposable tips
- Electronic 8x1200 µL multichannel pipette + 1250 µL disposable tips
- 2 reservoirs for multichannel micropipette (PBS, erythrocyte suspension)
- Plate photometer (e.g. Tecan spectra, Tecan Instruments, N1.07)

3. Sample preparation

Infected cell culture with cells and without microcarrier should be filled directly into sterile kryotubes or other sterile tubes and centrifuged at 300xg for 5 min at 4 °C. If cells can not be settled at this g force, choose an appropriate centrifugation setting. After the centrifugation step transfer the supernatant into a new sterile kryotube and freeze at -80 °C.

4. Assay procedure

It is absolutely necessary to pipet exactly in this assay!!

Active samples have to be handled under S2 work bench! For handling outside the safety hood (e.g. when scanning the microtiter plate with the spectrometer), keep disinfectant or citric acid ready in case of accidental spillage!

4.1 Classical method

The titration of influenza virus by the classical method is based on the method described by Mahy and Kangro [1].

1. Pre-dilute samples which are known to be highly concentrated in PBS (all samples which have a HA activity above 3.0 log HA units/100 µL should be diluted). Typically, a 1:10 pre-dilution is sufficient. Samples from cell culture normally do not require this pre-dilution. However, this has to be decided from the assay performer.
2. Fill the wells of column 2-12 with 100 µL PBS each. Wells B, D, F and H of column 1 and 2 are filled with 29.3 µL PBS.
3. Perform the following steps with a 100 µL pipette under S2 work bench! Don't spray disinfectant onto reservoirs and microtiter plates.

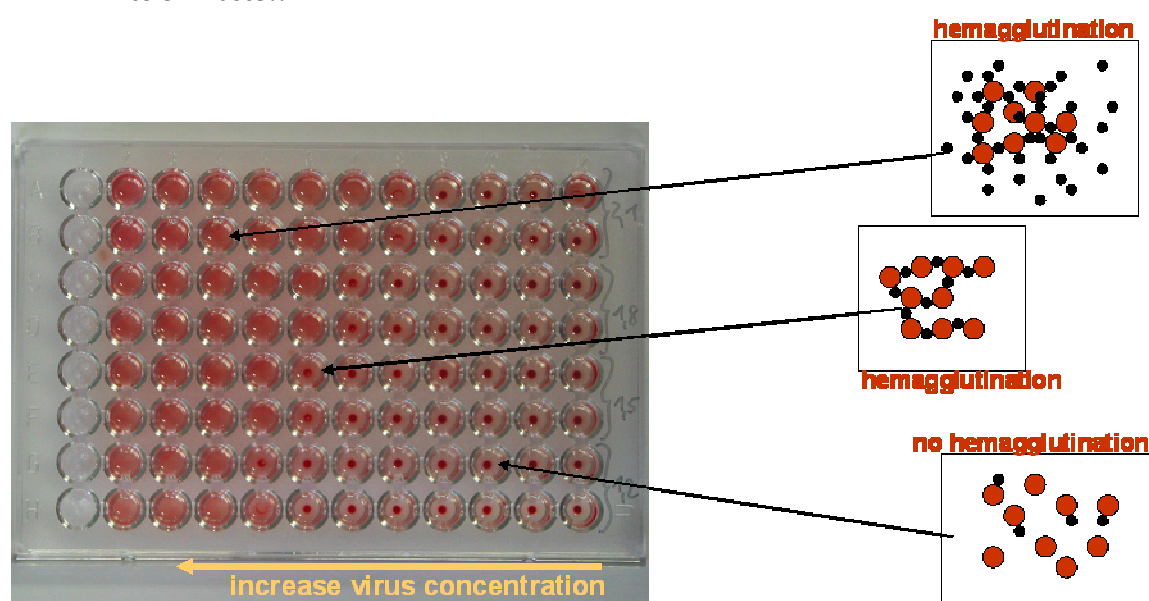
The wells 1 and 2 of row A are filled with 100 µL of internal HA standard. Beneath these, a pre-dilution of internal HA standard is prepared by adding 70.7 µL of HA standard to wells 1 and 2 of row B. These 4 wells are prepared accordingly for the samples in rows 3 to 8. This means that on each plate 3 samples can be prepared. If there are more samples, an additional plate is necessary. Standard is necessary on every second plate.

Pipetting scheme for pipetting internal HA standard and samples onto microtiter plate

	1	2	3
A	100 µL HA standard	100 µL HA standard	...
B	70.7 µL HA standard 29.3 µL PBS	70.7 µL HA standard 29.3 µL PBS	...
C	100 µL sample 1	100 µL sample 1	...
D	70.7 µL sample 1 29.3 µL PBS	70.7 µL sample 1 29.3 µL PBS	...
E

4. Mix column 2 three times with a multichannel pipette and transfer 100 µL of column 2 to column 3. Empty the pipette tips completely once before the transfer. Mix again three times and continue the serial dilution until the end of the plate (column 12). The remaining 100 µL should be disposed. Each well has to be filled with 100 µL after finishing these steps. Add 100 µL of erythrocyte suspension into each well by using an electronic multichannel pipette. Mix the suspension well before you start! Start pipetting at the column with the highest dilution (column 12. *For each plate new tips have to be used!*)
5. Each well which has been pipetted faulty should be marked as the values from these wells need to be eliminated during assay evaluation!
6. Incubate the plates for at least 3 hours under the work bench. If the assay is not analyzable, incubation must be prolonged (over night if necessary).

7. Evaluate the results visually. Therefore, mark every well which shows a perfect erythrocyte dot with a (●) and each imperfect dot with a (○). Record your findings by taking the document "AB-HA_Testauswertung_3.pdf". The last dilution with an imperfect dot is the end point of the titration and is expressed as log HA units per test volume (100 μ L). The inverse of this dilution gives the HA activity [HAU/100 μ L].
8. Compare the measured titer of the internal standard with its nominal titer. The difference (*nominal-measured*) has to be added to the titer of each sample. If two or more standards were analyzed (e.g. because 3 plates were assayed) use the mean difference. If the measured titer of internal standard is more than 0.3 log HAU/100 μ L different from its nominal titer, re-do the whole assay!
9. After evaluation of the titer microtiter plates scan them (see section 4.1) or dispose them into S2 waste!!



Scheme for determination of HA titers in micro titer plate (example shows HA titers from 1.2-2.1 log HA units/100 μ L in double determination)

Overview on dilutions and resulting HA titers (log HA units/100 μ L)

	1	2	3	4	5	6	7	8	9	10	11	12
Dilution	1:1	1:2	1:4	1:8	1:16	1:32	1:64	1:128	1:256	1:512	1:1024	1:2048
HA titer (100 μ L sample)	0	0.3	0.6	0.9	1.2	1.5	1.8	2.1	2.4	2.7	3.0	3.3
HA titer (70.7 μ L sample)	0.15	0.45	0.75	1.05	1.35	1.65	1.95	2.25	2.55	2.85	3.15	3.45

4.1.1 Points to consider

- The detection limit of this assay is 0.15 log HAU/100 μ L. This corresponds to approximately 2.0×10^7 virions/mL; assuming that the number of erythrocytes is proportional to the number of virus particles (each virus particle binds to one erythrocyte).
- The assay has been validated with a standard deviation of ± 0.03 log HAU/100 μ L which is the dilution error.
- The confidence interval for HA activity was determined to be $\pm 15\%$ (with a confidence level of 95 %).

- The validation has been made for the assay procedure which is described here. If you change singular steps in your procedure, be aware that validation is not valid then.
- Before you start with serious analyses, train yourself in pipetting accurately and precisely, e.g. by measuring standard samples several times.
- HA activity may suffer depending on sample treatment and storage conditions. Thus, do not freeze a measured sample and re-thaw it. Probably, HA titer has then been changed.

4.2 Photometric analysis

In order to minimize subjectivity (dependence on the experimenter), the titration result is evaluated photometrically using an automated procedure. However, this evaluation is restricted to samples with titer $>1.0 \log \text{HAU}/100 \mu\text{L}$. Otherwise, sample titers have to be evaluated with the classical method.

4.2.1 Measurement of extinction

1. Perform all steps which are described for the classical method.
2. Cover microtiter plates containing active virus samples with an appropriate lid.
3. Make sure that Tecan photometer is switched on. Open the software “iControl” and choose “HA protocol” from the list of used protocols. The settings should be defined as follows: Messfilter 700 nm, Referenzfilter none, 10 Blitze, Temperatur 0.0 °C, Schüttelmodus none. (Changes can be made by clicking on button “Messparameter definieren”, but should not be done for standard HA protocol.)
4. After having inserted the plate into the reader, click the button “Messung starten”. You will be asked for a file name first and to put your plate onto the tray afterwards. The measurement will be carried out immediately afterwards.

It is of utmost importance to remove either the lid before scanning and to remove any condensed water from the bottom of a microtiter plate before scanning!!

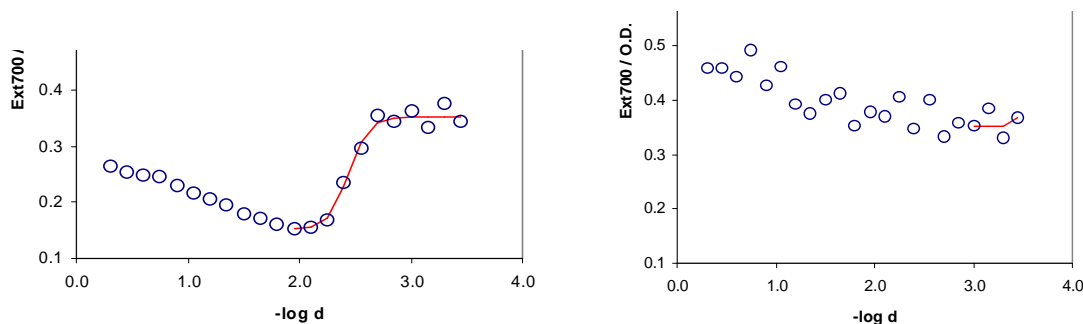
5. Save extinction data as Excel-file in the folder “/bpt/data/Tecan/HA_assay/2010/...” using the file name pattern “<Number>-<Date>_<Experimenter>.xls (e.g. 145_10-03-31_CB). If more than one plate will be measured, let the excel file from the first plate open. Then, the results from the following plate will be saved as a new sheet in this file. You have to rename the sheets after your measurement in order to document which sheet belongs to which plate.
6. Repeat step 4 and 5 for each plate of the assay run.

4.2.2 Evaluation of HA titers

A data evaluation template (Excel-file) has been prepared. The evaluation procedure is described in the following. You have to enable macros for the sheet to work properly!

7. Open the data evaluation template (“/bpt//Labor/HA_neu/Data_Evaluation_Template.xls”) and save a **copy** in the appropriate folder (/bpt/usp/Labor/HA_neu/data/2010/...).
8. Import your extinction data. Therefore, copy all values and paste them into data-sheet. Delete extinction values of all wells that suffered from erroneous pipetting! As long as affected wells are not within the zone of transition, the assay result may be unaffected.
9. Adjust the sample names and dilutions in the “Report” sheet. Fill all empty header fields and transfer the remarks from the run protocol. Specify the internal standard used and the position of the internal standard (normally, position 1 and 9). If only one standard was measured, specify the same position twice.
10. Click “Evaluate” to start HA titer evaluation.

11. Check difference between nominal titer of the standard and the evaluated titer. Re-do the assay if both values differ more than 0.3 log HAU/100 μ L.
12. Check all fitted curves in the "Evaluation" sheet. If fitting of extinction values has not been made by a sigmoidal curve, then re-analyze the sample. Be careful, if this maybe is due to a low titer of the sample. Then take titers evaluated by the classical method.



Evaluation of the transition point by a Boltzmann function. Left: correct fitting, right: erroneous fitting which would lead to high titer evaluation if curve is not checked and rejected

13. Compare the evaluated titers with the results obtained by the classical method. The discrepancy should be less than 0.3 log HAU/100 μ L.
14. Save the document and make at least one hardcopy of the "Report" and "Evaluation" sheets. Documents are collected in a folder located in N1.07 and N0.13.

5. Sample storage

If samples are kept at below -70 °C, they can be stored up to five years without loss of HA activity. Anyway, this holds true for samples which have been prepared as described in this document (see sample preparation). After this period, it cannot be guaranteed that measured HA activities resemble the original values.

[1] Mahy B.W.J., Kangro H.O. "Virology Methods Manual": Academic Press Limited, 1996.

Arbeitsanweisung Nr. V/ 07

Datum: 13.09.2006
geändert: 07.06.2007

Autor: Claudia Best
Autor: Claudia Best

Herstellung einer Erythrocytenlösung mit definierter Zellzahl

1.0 Verwendung

Die Erythrocytenlösung wird bei dem Hämagglutinationstest eingesetzt.

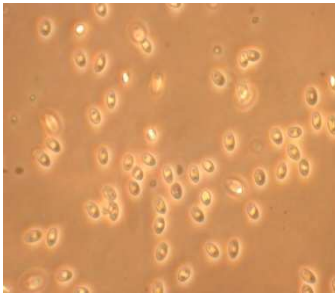
Der Hämagglutinationstest ist ein Nachweis von Influenzaviren. Influenzaviren tragen auf ihrer Oberfläche das Hämagglutinin, das an Erythrocyten bindet und diese verklumpt.

Hämagglutination = Aggregation (Zusammenschluss) von roten Blutkörperchen durch das Hämagglutinin der vorhandenen Virenpartikel. Durch die Aggregation können die Blutkörperchen nicht absinken.

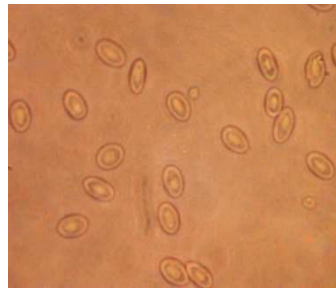
Bei dieser Bestimmungsmethode kann sowohl aktiver als auch inaktiver Virus verwendet werden, da dies keinen Einfluss auf die Messergebnisse hat.

Bilder Hühner-Erythrocyten

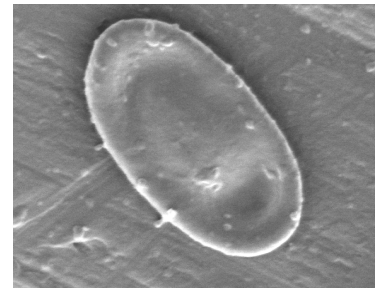
20x Vergrößerung



40x Vergrößerung



10- 20 000x Vergrößerung

**2.0 Material zur Herstellung der Erythrocytengebrauchslösung**

- 15 mL Falconröhrchen mit 5 mL Alseverslösung vorbereiten (liegen in ausreichender Anzahl im Geflügelhof Möckern vor) + 5 mL frisch entnommenes Hühnerblut (**Lösung ist gekühlt zu lagern!!**)
- ca. 3 x 1 L PBS (unsteril), in mit Eis gefüllten Kühlbehältern lagern
- 2 L Becherglas + Magnetrührstäbchen
- 1 L Becherglas als Abfallbehälter
- Zentrifuge Heraeus Biofuge Primo R
- Analysenwaage
- Magnetrührer
- Vi-Cell XR Zellzählgerät
- Vi-Cell Probengefäße zur Zellzahlbestimmung
- 50 mL Falcons (steril)
- 15 mL Falcons
- Pipettus akku
- 50 mL Pipette

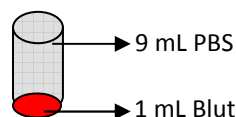
3.0 Vorbereitung der Erythrocytengebrauchslösung

- je 3 mL der Blutsuspension in ein 50 mL Falconröhrchen pipettieren
- danach das Falcon mit unsterilem gekühlten PBS bis ca. 40 mL auffüllen
- die Falconröhrchen mit Blutsuspension bei 500 x g, 4 °C und schwacher Bremse (Stufe 4), 5 min zentrifugieren
- Überstand vorsichtig in ein Becherglas abdekantieren (soviel wie möglich)
- Blutsuspension am Boden des Falconröhrchens mit PBS wieder bis 40 mL auffüllen, kräftig aufschütteln, und erneut zentrifugieren, diesen Waschvorgang noch zweimal wiederholen
- nach dem dritten Waschen füllt man die Falcons wieder bis ca. 40 mL mit PBS auf und schüttelt sie kräftig auf
- die Lösung wird in ein 2 L Becherglas (was vorher, mit einem Magnetrührstäbchen auf einer Analysenwaage ausgewogen und tariert wurde) zusammen gegossen
- die Masse des Becherglases mit der Erythrocytenstammlösung notieren,
- bis zum Abfüllen der Lösung, wird diese mittels eines Magnetrührers gut homogenisiert

4.0 Bestimmung der Erythrocytenanzahl mittels dem Vi-Cell XR Zellzählgerät

- 1 mL der gut durchmischten Erythrocytenstammlösung entnehmen
- für das **Vi-Cell XR Zellzählgerät** wird eine **1:10 Verdünnung** angesetzt

1. **1:10 Verd.** → 1 mL Blut + 9 mL PBS



- aus der 1:10 Verd. entnimmt man 1 mL, und gibt diesen in ein Vi-Cell Probengefäß
- danach erfolgt die Messung am Vi-Cell XR → siehe Kurzanleitung Zellzählgerät (von Josef Schulze-Horsel)

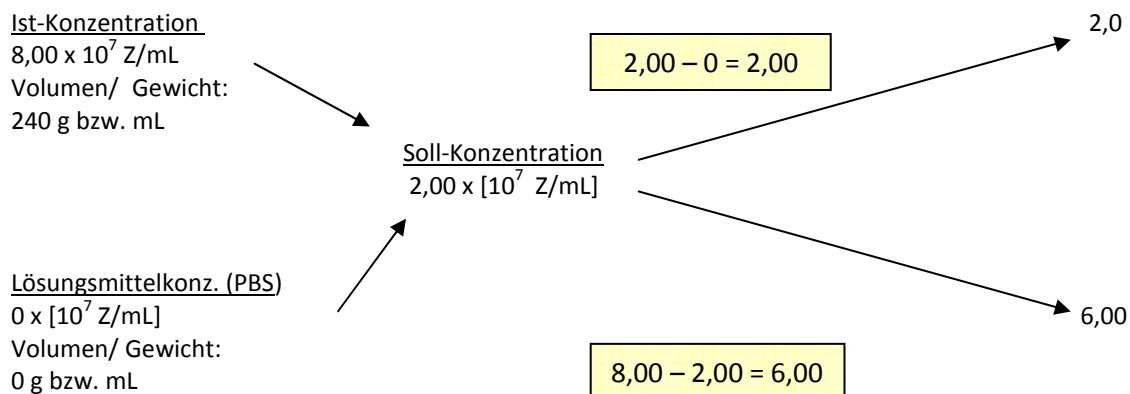
Bei defektem Vi-Cell Gerät bestimmt man die Erythrocytenanzahl mittels der Fuchs-Rosenthalzählkammer.

1 mL der gut durchmischten Erythrocytenstammlösung entnehmen
für die Zählkammer wird eine **1:1000 Verdünnung** angesetzt
mit der Fuchs-Rosenthal Zählkammer werden dann 2x5 Großquadrate (GQ) ausgezählt
z.B. **gezählt 32/ 31 Erythrocyten Mittelwert= 31,5**
 $31,5 * 1000$ (Verd.Blut/ PBS) * 1000 (Zählkammer: $0,2 \mu\text{L}/\text{GQ} * 5 = 1 \mu\text{L} \rightarrow$ in 1 mL , 1000 fache Verd.)
= $3,15 \times 10^7 \text{ Z/mL}$

5.0 Berechnung der Erythrocytengebrauchslösung mit definierter Erythrocytenanzahl ($2,0 \times 10^7 \text{ Z/ mL}$)

Vi-Cell XR gezählte Erythrocyten: z.B. $8,0 \times 10^7 \text{ Z/mL}$

Aufstellen eines Mischungskreuzes



ins Verhältnis setzen: $\frac{240 \text{ mL}}{X} = \frac{2}{8,0}$ $X = \frac{240 \text{ mL} * 8,00}{2} = \frac{960 \text{ mL}}{\text{PBS}} + 240 \text{ mL} = 1200 \text{ mL}$
Erythrocytengebrauchslösung

$1200 \text{ ml} / 45 \text{ ml} = 26,6 \approx 27 \text{ Falcons à } 45 \text{ ml}$

- nun gibt man zu der 240 mL Erythrocytenstammlösung noch 960 mL PBS (4 °C) dazu , und mischt die Lösung noch einmal gut durch
- danach entnimmt man aus der homogenen Lösung (1200 mL) wieder 1 mL Probe, und bestimmt zur Kontrolle die Zellzahl der fertigen Gebrauchslösung
- erhält man wie gefordert die **$2,0 \times 10^7 \text{ Z/mL}$ (Toleranzbereich +/- 5 % → $2,10 - 1,90$)**, so wird die berechnete Falconanzahl mit jeweils 45 mL der Erythrocytengebrauchslösung abgefüllt
- **Achtung:** Während des Abfüllens in die Falcons muss die Lösung im Becherglas mittels des Magnetrührers immer gut durchmischt werden!

6.0 Lagerung

- die Erythrocytengebrauchslösung ist bei 4 °C Lagerung (Kühlschrank, N. 1.06) 14 Tage haltbar.

6.0 Berechnung der Erythrocytengebrauchslösung mit definierter Erythrocytenanzahl ($2,0 \times 10^7 \text{ Z/ mL}$)

- sollte die gezählte Erythrocytenzahl der Gebrauchslösung die +/- 5 % Grenze über- bzw. unterschreiten, so muss man das Volumen mit der Konzentration von $2,0 \times 10^7 \text{ Z/mL}$ neu berechnen

Beispiel: gezählte Erythrocyten/mL (1:10 Verd., Erythrocyten 100 Bilder) = $1,85 \times 10^7 \text{ Z/mL}$

$1,85 \times 10^7 \text{ Z/mL}$ (soll: $2,0 \times 10^7 \text{ Z/mL}$) = 7,5 % Abweichung

- **Berechnung für eine Aufkonzentration:**

$$1,85 \times 10^7 \text{ Z/mL} * 1200 \text{ mL} = 2,00 \times 10^7 * X \quad \left| : 2,00 \times 10^7 \text{ Z/mL} \right.$$

$$1,85 \times 10^7 \text{ Z/mL} * \frac{1200 \text{ mL}}{2,00 \times 10^7 \text{ Z/mL}} = X$$

$$1,85 \times 10^7 \text{ Z/mL} * 6,0 \times 10^{-5} \text{ Z} = X$$

$$\underline{1110,0 \text{ mL}} = X \quad \begin{array}{l} 1200,0 \text{ mL} - 1110,0 \text{ mL} = 90 \text{ mL} \\ \rightarrow 1110,0 \text{ mL} / 45 \text{ mL} = \sim 25 \text{ Falcons} \end{array}$$

- man muss also 90 mL PBS- Lösung aus der Erythrocytegebrauchslösung entfernen
- zunächst zentrifugiert man sie bei 500 x g, 4 °C und schwacher Bremse Stufe 4, 5 min ab und entnimmt soviel PBS aus dem Überstand wie möglich
- nun schüttelt man das restliche Blut wieder auf und gibt es zu den 1110 mL wieder dazu
- danach beginnt man wieder die Lösung mittels des Magnetrührers zu homogenisieren, entnimmt wieder zur Überprüfung 1 mL der Lösung, und bestimmt die Erythrocytenzahl erneut
- liegt sie nun bei den geforderten $2,0 \times 10^7$ Z/mL, so kann man jeweils 45 mL in die entsprechenden Falcons abfüllen und für den Hämagglutinationstest verwenden

Arbeitsanweisung V/08 Version 2.1

Datum: 2.06.08

Autor: Ilona Behrendt

geändert: 26.09.2011

Autor: Britta Isken

Bestimmung des TCID₅₀**3.0 Ziel**

Bestimmung der Virusverdünnung, bei der 50% der adhärennten Zellen infiziert werden.

4.0 Material**2.1. Zellanzucht und Virusvermehrung**

- 4-8 Tage alte konfluente MDCK-Zellen aus Zellkulturflaschen (T175 oder RF)
- PBS steril (Arbeitsanweisung Nr. M/01)
- Trypsin 10000 BAEE / mL in Milli-Q-Wasser, sterilfiltriert (Trypsin, Sigma, Bestell-Nr. T-7409) Lagerung bei -70 °C für Virusinfektion
- Zellkulturmedium (GMEM + 1% Lab-M-Pepton + 10% FCS) siehe Arbeitsanweisung Nr. M/04
- Virusmedium (GMEM + 1% Lab-M-Pepton) siehe Arbeitsanweisung Nr. M/04
- Gentamicin 10 mg / mL (Invitrogen, Bestell-Nr. 11130-036) Lagerung: Raumtemperatur
- 96-Wellplatten 400 µL Inhalt steril mit flachem Boden mit Deckel (für Zellkultur) (Cellstar, Greiner bio-one, Bestell-Nr. 655180) - für jede Probe wird eine Wellplatte benötigt!
- Reaktionsgefäße 1,5 mL, sterilisiert für Verdünnungsreihen
- sterile Pipetten, Pipettierhilfe
- 100 µL Pipette
- Elektronische Einkanalpipette 1 mL (Eppendorf)
- Elektronische Mehrkanalpipette 1250 µL (Eppendorf)
- Pipettenspitzen 100 µL (Plastibrand, steril)
- Pipettenspitzen 1250µL (Eppendorf, steril)
- Multipette mit Combitips 10 ml (Eppendorf, Combitips plus biopure)
- 1 sterile Schottflaschen (250 oder 500 mL)
- 4 Pipettierbehälter, sterilisiert

- 2 kleine Laborschalen, sterilisiert
- Warnhinweisaufkleber: Biogefährdend

2.2. Fixierung und Färbung

- 80%ige Acetonlsg. in Wasser (Aceton, p.A.)
- Primärantikörper entsprechend dem zu testenden Virus
- z.B. - (Equine Influenza A Ziegenserum , final bleed, goat 613, vom 2.08.01, nano Tools)(1:100 mit PBS verdünnt)
- Influenza Anti A/Wisconsin/67/2005 H₃N₂ (HA Serum sheep) von NIBSC
- Influenza Anti B/Malaysia/2506/2004 (HA Serum sheep) von NIBSC
- Influenza Anti A/PR/8/34 H₁N₁ (HA Serum sheep) von NIBSC
- PBS steril (Arbeitsanweisung Nr. M/01)
- konfluent bewachsene Zellkulturflaschen (T75 oder RF)
- Sekundärantikörper (Invitrogen, Bestellnr.: A-11015)
- 100 µL 8-Kanal-Pipette mit Pipettenspitzen
- Laborschale
- 3 Pipettierbehälter
- Entsorgungsbehälter Aceton

5.0 Methode

Anmerkung zur Generierung der Proben: Standardmäßig wird der Infektionsüberstand vor dem Wegfrieren nicht zentrifugiert, in Ausnahmefällen (wie MDCK.SUS2 Zellen) kann eine Zentrifugation bis 5000 x g durchgeführt werden, da sie keinen Einfluss auf den TCID₅₀ Wert hat.

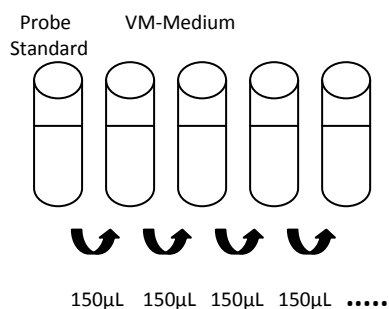
3.1 Zellanzucht und Virusvermehrung

A) Zellanzucht

- konfluente MDCK-Zellen aus Zellkulturflaschen 3-mal mit PBS waschen und mit der vorgeschriebenen Menge Trypsin (1 mg/mL) 20 min bei 37 °C abtrypsinieren, mit Z-Medium abstoppen (siehe Arbeitsanweisung Nr. Z/04)
- Zellkulturmedium mit Gentamicin vermischen (100 mL Zellkulturmedium mit 1 mL Gentamicin)
- abtrypsinisierte Zellen mit angesetztem Zellkulturmedium auf eine Zellzahl von 4-5*10⁵ Zellen/mL verdünnen (siehe Arbeitsanweisung Zellzahlbestimmung)
- 10 mL der Zellsuspension werden ca. für eine Zellkulturplatte benötigt
- je 100 µL der Zellsuspension werden mit der Elektronischen 8-Kanalpipette in jedes Well der Zellkulturplatte pipettiert
- die Zellen 1-2 Tage bei 37 °C mit 5 % CO₂ inkubieren (mikroskopische Beurteilung der Konfluenz der Zellen → müssen dicht bewachsen sein – wenn dies nicht der Fall sein sollte, ist der Versuch hier abubrechen)

B) Herstellen der Virusverdünnung

- Virusmedium mit Trypsin und Gentamicin versetzen, 100 mL Medium + 20 µL Trypsin + 1,0 mL Gentamicin (100 mL VM reichen für ca. 10 Verdünnungsreihen) → VM
- Je 900 µL des Virusmediums in 8–10 Eppendorfcups (je nach benötigter Verdünnungsstufen) pipettieren. Virusverdünnung nach dem folgenden Schema in Eppendorfcups herstellen: mit einer Eppendorfpipette 100 µL aus der zu bestimmenden Probe oder dem Standard entnehmen und in das erste Eppendorfcup geben, 5 mal durch auf- und abpipettieren mischen, mit einer neuen Pipettenspitze 100 µL in das nächste Eppendorfcup geben, fortfahren bis zum Ende.



10^0	10^1	10^2	10^3	10^4	10^5	10^6	10^7	10^8
--------	--------	--------	--------	--------	--------	--------	--------	--------

C) Virusvermehrung

- die Zellkulturplatten 2 mal mit je 100 µL PBS je Well mit der Elektronischen 8-Kanalpipette waschen (entleeren: in Laborschale ausschütten)
- mit einer Eppendorfpipette je 100 µL der Virusverdünnung auf je 8 Wells der Zellkulturplatte geben (mit der höchsten Verdünnungsstufe beginnen)
- in die Reihen 1, 2, 11 und 12 werden nur je 100 µL Virusmedium (mit Trypsin + Gentamicin) je Well gegeben (diese Wells dienen als Nullkontrolle, Randeffekte können dann ausgeschlossen werden)
- einzusetzende Verdünnungsstufen:

bei einem HA über 2,7: $10^3 - 10^{10}$

bei einem HA von 2,1 bis 2,7 (Standard, Saatvirus für Fermentationen) : $10^1 - 10^8$

bei einem HA unter 2,1: $10^0 - 10^7$

	1	2	3	4	5	6	7	8	9	10	11	12
A	Virus-Medium	Virus-Medium	10^1	10^2	10^3	10^4	10^5	10^6	10^7	10^8	Virus-Medium	Virus-Medium
B	Virus-Medium	Virus-Medium	10^1	10^2	10^3	10^4	10^5	10^6	10^7	10^8	Virus-Medium	Virus-Medium
C	Virus-Medium	Virus-Medium	10^1	10^2	10^3	10^4	10^5	10^6	10^7	10^8	Virus-Medium	Virus-Medium
D	Virus-Medium	Virus-Medium	10^1	10^2	10^3	10^4	10^5	10^6	10^7	10^8	Virus-Medium	Virus-Medium
E	Virus-Medium	Virus-Medium	10^1	10^2	10^3	10^4	10^5	10^6	10^7	10^8	Virus-Medium	Virus-Medium
F	Virus-Medium	Virus-Medium	10^1	10^2	10^3	10^4	10^5	10^6	10^7	10^8	Virus-Medium	Virus-Medium
G	Virus-Medium	Virus-Medium	10^1	10^2	10^3	10^4	10^5	10^6	10^7	10^8	Virus-Medium	Virus-Medium
H	Virus-Medium	Virus-Medium	10^1	10^2	10^3	10^4	10^5	10^6	10^7	10^8	Virus-Medium	Virus-Medium

- die Platten mit Virus mit einem Warnhinweis versehen und 1 Tag bei 37 °C mit 5 % CO₂ inkubieren

D) Trypsinzugabe

- Virusmedium mit Trypsin und Gentamicin versetzen (100 mL Medium + 40 µL Trypsin + 1 mL Gentamicin)
- Je 100 µL dieses Mediums in jedes Well pipettieren – Elektronische 8-Kanalpipette, darauf achten dass kein Virus verschleppt wird (von rechts nach links – von der höchsten Verdünnungsstufe zur niedrigsten pipettieren, Reihe für Reihe) nach jeder Platte die Pipettenspitzen werfen
- die Virusplatten nochmals 1 Tag bei 37 °C mit 5 % CO₂ inkubieren

3.2 Fixierung und Färbung

- A) Vorbereitung des Primärantikörpers (nur bei dem Equine Influenza A Ziegen Serum notwendig, wenn kein gereinigter Antikörper mehr vorhanden ist)
- der Primärantikörper für Equine Influenza A Ziegen Serum ist ein polyklonaler Antikörper gegen den Pferdeinfluenza-Virus, aber auch gegen Zellbestandteile, deshalb müssen die Antikörper gegen die Zellen vorher absorbiert werden, sonst überdecken sie die Fluoreszenz der mit Viren infizierten Zellen
 - 1 – 2 Tage alte konfluent bewachsene Zellkulturflasche dreimal mit PBS waschen
 - auf eine T25 – Flasche 1 mL , auf eine T75 – Flasche 3 mL des verdünnten Primärantikörpers geben und 30 min bei 37 °C inkubieren (1 mL 1:100 verdünntes Serum reicht für eine Zellkulturplatte – dementsprechende Menge inkubieren)
 - der gereinigte Primärantikörper kann bei –20 °C eingefroren werden

B) Fixierung

- Medium in Laborschale mit vorgelegter 2%iger Essigsäure in der Sterilbank abgießen und virusgerecht entsorgen
- auf jedes Well 100 µL eiskalte 80 %ige Acetonlösung pipettieren (Acetonlsg.in Eisbehälter stellen – nicht in den Kühlschrank → Kühlschränke sind nicht Ex geschützt)
- die Zellkulturplatten 30 min zum Fixieren auf Eis oder in den Kühlraum stellen → Virus inaktiviert (die weiteren Schritte können außerhalb der Sterilbank durchgeführt werden)
- Zellkulturplatten 2 mal mit PBS spülen – (Aceton-PBS-Gemisch in Abfallbehälter sammeln-zur Entsorgung –Herrn Schäfer geben)

C) Färbung

- gereinigten Primärantikörper für Equine Influenza A Ziegen Serum 1 : 100 mit PBS verdünnen, alle anderen Primärantikörper werden 1 : 200 verdünnt
- je 50 µL davon auf jedes Well mit Elektronischer 8-Kanalpipetten geben und 60 min bei 37 °C inkubieren
- nach dieser Zeit 2-mal mit PBS waschen
- den Sekundärantikörper 1 :500 mit PBS verdünnen
- wieder je 50 µL davon auf jedes Well pipettieren und 60 min bei 37 °C inkubieren
- 2 mal mit PBS waschen, nach dem letzten Waschschrift 100 µL PBS auf jedes Well geben

6.0 Auswertung und Berechnung

- die Auswertung erfolgt an einem Fluoreszenzmikroskop
- jedes Well in dem Virus gefunden wird (fluoreszierende Zellen) wird als positiv gewertet (1), jedes Well ohne fluoreszierende Zellen als negativ (0) und in das Arbeitsblatt eingetragen
- die Berechnung erfolgt nach der Gleichung von Spearman und Kärber:

$$(\log \text{ Virus } 100\%) + (0,5) - \frac{\text{kumulativ } 100 \%}{\text{Anzahl Tests (pro Verdünnung)}} = \log \text{ Virus } / 100 \mu\text{L}$$

Beispiel:

	1	2	3	4	5	6	7	8	9	10	11	12
A	0	0	1	1	1	1	1	1	1	0	0	0
B	0	0	1	1	1	1	1	1	1	0	0	0
C	0	0	1	1	1	1	1	1	0	0	0	0
D	0	0	1	1	1	1	1	1	0	0	0	0
E	0	0	1	1	1	1	1	1	0	0	0	0
F	0	0	1	1	1	1	1	1	1	0	0	0
G	0	0	1	1	1	1	1	0	0	0	0	0
H	0	0	1	1	1	1	1	1	1	0	0	0

0	0	10 ⁻¹	10 ⁻²	10 ⁻³	10 ⁻⁴	10 ⁻⁵	10 ⁻⁶	10 ⁻⁷	10 ⁻⁸	0	0
---	---	------------------	------------------	------------------	------------------	------------------	------------------	------------------	------------------	---	---

0: kein Virus, negatives well; 1: Virus, positives well

Verdünnungsstufe	Anzahl positive wells / Gesamtzahl wells	Anzahl positiver wells kumulativ
10 ⁻⁵	8 / 8	19
10 ⁻⁶	7 / 8	11
10 ⁻⁷	4 / 8	4
10 ⁻⁸	0 / 8	0

Beispielrechnung:

$$(-5) + 0,5 - 19/8 = -6,875 = \gamma; 10^{6,875} \text{ Viren}/100\mu\text{L} = 10^{7,875} \text{ V}/\text{mL} = 7,50 \times 10^7 \text{ Viren}/\text{mL}$$

7.0 Festlegung des Referenzwertes

Für jeden neu hergestellten Standard wird von mindestens 2 Personen je zweimal eine Sechsfachbestimmung durchgeführt. Daraus wird der Mittelwert für den jeweiligen Standard berechnet, der als Referenzwert verwendet wird.

For the 28 established enzyme assays and for the extraction procedure used in this study, a new set of SOPs was created. Please note that due to space limitations, these SOPs are not included in the present appendix but are provided on the CD of this thesis.

Lebenslauf

Persönliche Daten

Name: Robert Paul Janke
Geburtsdatum: 07. März 1983
Geburtsort: Dresden
Familienstand: ledig
Nationalität: deutsch

Schule und Studium

08/1993-06/2001 Abitur am Romain-Rolland-Gymnasium Dresden

08/2001-03/2007 Studium der Bioverfahrenstechnik (Dipl.-Ing.) an der Technischen Universität (TU) Dresden

08/2004-02/2005 Interdisziplinäre Projektarbeit bei der Intervet International GmbH in Unterschleißheim bei München; Abteilung Ingenieurtechnik (Herr J. Niethammer, Herr Dr. K. Kriebitzsch)
Thema: »Mitarbeit im Projektteam zur Planung, Bestellung, Aufbau und Inbetriebnahme eines neuen Produktionsbereiches zur Herstellung von Insulin«

06/2005-11/2005 Große Belegarbeit an der TU Dresden; Institut für Lebensmittel- und Bioverfahrenstechnik (Herr Prof. Dr. rer. nat. habil. T. Bley)
Thema: »Untersuchungen zur Induktion und zur C-Katabolitrepression der Endo-Inulinasebildung unter verfahrenstechnischen Gesichtspunkten«

10/2006-02/2007 Diplomarbeit an der TU Hamburg-Harburg; Institut für Bioprocess- und Biosystemtechnik (Herr Prof. Dr.-Ing. R. Pörtner)
Thema: »Festbettkultivierung von *Lactococcus lactis*«

Berufliche Tätigkeiten

03/2007-01/2012 Wissenschaftlicher Mitarbeiter (Promotion) am Max-Planck-Institut (MPI) für Dynamik komplexer technischer Systeme in Magdeburg; Abteilung Bioprosesstechnik (Leiter: Herr Prof. Dr.-Ing. U. Reichl)
Thema: »Investigation of mammalian cell metabolism by quantification of key metabolic enzyme activities«

09/2007-10/2007 Gastwissenschaftler am MPI für Molekulare Pflanzenphysiologie in Potsdam-Golm; Abteilung Metabolische Netzwerke, Systemregulation (Leiter: Herr Prof. Dr. M. Stitt)

seit 01/2013 Lab Scientist Bioprocess Development, Sandoz GmbH - Werk Schafteuau, Österreich